Energy-based analysis and control of power networks and markets

Stegink, Tjerk Wiebe

Energy-based analysis and control of power networks and markets

Port-Hamiltonian modeling, optimality and game theory

Tjerk Stegink

university of groningen / faculty of science and engineering

The research described in this dissertation has been carried out at the Faculty of Science and Engineering, University of Groningen, the Netherlands.

disc dutch institute of systems and control

The research described in this dissertation is part of the research program of the Dutch Institute of Systems and Control (DISC). The author has succesfully completed the educational programme of the DISC.

Netherlands Organisation for Scientific Research

The research reported in this dissertation is supported by the Netherlands Organisation for Scientific Research (NWO) programme Uncertainty Reduction in Smart Energy Systems (URSES) under the auspices of the project ENBARK.

Cover: Heine Stegink

Printed by: ProefschriftMaken || www.proefschriftmaken.nl

ISBN: 978-94-034-1203-0 (printed version)
ISBN: 978-94-034-1202-3 (electronic version)

rijksuniversiteit
groningen

Energy-based analysis and control of power networks and markets

Port-Hamiltonian modeling, optimality and game theory

Proefschrift

ter verkrijging van de graad van doctor aan de
Rijksuniversiteit Groningen
op gezag van de
rector magnificus prof. dr. E. Sterken
en volgens besluit van het College voor Promoties.

De openbare verdediging zal plaatsvinden op

vrijdag 7 december 2018 om 12.45 uur

door

Tjerk Wiebe Stegink

geboren op 27 februari 1991
te Opsterland

Promotores
Prof. dr. C. De Persis
Prof. dr. A.J. van der Schaft

Beoordelingscommissie
Prof. dr. M.K. Camlibel
Prof. dr. J.W. Bialek
Prof. dr. D.J. Hill

Acknowledgments

Being a PhD candidate has been a wonderful time and this thesis could not be accomplished without the help and support I enjoyed from my colleagues, friends and family. First of all, I would like to thank my supervisors Claudio and Arjan for their invaluable guidance, support, and dedication. I am very grateful for you granting me the opportunity to pursue a PhD in the first place and I really enjoyed working with you on interesting research topics.

Second, I would like to thank Ronald and Junjie for accepting to be my paranymphs. Ronald, knowing you already since high school, and pursuing a PhD as well, it is great to have you as my paranymph. Junjie, it was fun to have you as my office mate during the last years of my PhD.

Also I enjoyed the company of other former office-mates and neighbors at the Bernoulliborg, including Rodolfo, Pooya, Mark, Henk, Jaap and many others. Bart, I liked our talks early in the morning. Hidde-Jan, I am grateful for having you as an office mate during the first years of my PhD, for the honor to be your paranymph and also the great time we had in Japan together with Anneroos.

I would also like to thank Tobias. I enjoyed our fun formal and informal discussions and our collaboration. It was also great to know you better during the Career Course, Martijn. In many aspects, I have learned a lot from your inspiring personality. In addition, I want to thank Danial for our discussions and the time spend in Las Vegas. I wish you all the best for the rest of your career. I would also like to thank all other members of the DTPA/SMS group. I enjoyed the fun group outings with you and it was great to have informal group meetings each week.

Also great thanks to the reading committee, Kanat Camlibel, David Hill, and Janusz Bialek, for their effort and the feedback I received on the thesis. I would like to thank Jorge and Ashish for the opportunity to collaborate with them for three months at the University of California, San Diego. Also I want to give credit to the DISC teachers for the great courses they lectured and I thank NWO for the funding of the project. Furthermore, I would like to thank Jacquelien and the secretaries: Frederika, Ineke, Desiree, Heleen, Wilma and also Karin.

The PhD has also been challenging for me at some moments and I want to express my gratitude to everyone who supported me in difficult times, including my parents Henk and Wyanda. And above all, I would like to thank my wife Marloes for her invaluable support throughout my PhD project. We have said yes to each other to spend the rest of our lives together and I am looking forward to what the future may bring to us.

Tjerk *Groningen, October 31, 2018*

Contents

1 Introduction **1**
- 1.1 Welfare maximization and grid stability . . . 2
- 1.2 Competitive real-time electricity markets . . . 2
- 1.3 Contributions . . . 3
- 1.4 Outline of this thesis . . . 4
- 1.5 List of publications . . . 5
- 1.6 Notation . . . 6
- 1.7 Preliminaries . . . 7
  - 1.7.1 Nonlinear systems . . . 7
  - 1.7.2 Convex optimization and game theory . . . 10

I Modeling of power networks **13**

Introduction **15**

2 Port-Hamiltonian modeling of networked synchronous machines **17**
- 2.1 Introduction . . . 18
- 2.2 Preliminaries . . . 20
  - 2.2.1 Notation . . . 20
  - 2.2.2 The $dq0$-transformation . . . 21
  - 2.2.3 Phasor notation . . . 21
- 2.3 Full-order model of the synchronous machine . . . 22
  - 2.3.1 Port-Hamiltonian representation . . . 24
- 2.4 Model reduction of the synchronous machine . . . 25
  - 2.4.1 Distinction of operation states . . . 26
  - 2.4.2 Synchronous machine equations . . . 27
  - 2.4.3 Synchronous machine models . . . 30
- 2.5 Multi-machine models . . . 33
  - 2.5.1 Sixth-order multi-machine model . . . 34
  - 2.5.2 Third-order multi-machine model . . . 37
  - 2.5.3 The classical multi-machine network . . . 38
- 2.6 Energy functions . . . 39
  - 2.6.1 Synchronous machine . . . 39
  - 2.6.2 Inductive transmission lines . . . 42
  - 2.6.3 Total energy . . . 43
- 2.7 Port-Hamiltonian framework . . . 44

2.7.1 Sixth-order model . . . 44
2.7.2 Third-order model . . . 48
2.7.3 Swing equations . . . 49
2.7.4 Passivity . . . 49
2.8 Conclusions and future research . . . 50
2.8.1 Future research directions . . . 51

II Optimization and frequency regulation in power grids 53

Introduction 55
Contributions . . . 56
Outline . . . 57

3 Primal-dual dynamics for online optimization in power networks 59
3.1 Introduction . . . 60
3.2 Convex optimization . . . 62
3.3 Primal-dual gradient dynamics . . . 62
3.3.1 Brayton-Moser representation . . . 63
3.3.2 Port-Hamiltonian representation . . . 65
3.3.3 Incorporation of inequality constraints . . . 67
3.4 Online optimization in power networks . . . 71
3.4.1 Power network model . . . 71
3.4.2 Social welfare problem . . . 73
3.4.3 Controller design . . . 74
3.4.4 Equilibrium analysis . . . 76
3.4.5 Stability analysis . . . 76
3.5 Conclusions . . . 77

4 Distributed welfare maximizing controllers in power networks 79
4.1 Introduction . . . 80
4.2 Preliminaries . . . 81
4.2.1 Power network model . . . 81
4.2.2 Social welfare problem . . . 82
4.3 Internal-model-based controller . . . 83
4.3.1 Stability . . . 85
4.4 Primal-dual gradient controller . . . 86
4.4.1 Closed-loop equilibria . . . 88
4.4.2 Stability . . . 88
4.5 Numerical results . . . 90
4.6 Conclusions . . . 91

5 Constrained social welfare optimization and frequency regulation 95
5.1 Introduction . . . 96
5.2 Preliminaries . . . 99
5.2.1 Notation . . . 99
5.2.2 Power network model . . . 100

5.2.3 Social welfare problem . . . 103
5.3 Basic primal-dual gradient controller . . . 104
5.4 Variations in the controller design . . . 107
5.4.1 Including nodal power constraints . . . 108
5.4.2 Including line congestion and transmission costs . . . 111
5.4.3 Demand uncertainty . . . 114
5.4.4 Relaxing the strict convexity assumption . . . 116
5.5 Conclusions and possible extensions . . . 117

6 Active power sharing in structure-preserving power networks 119
6.1 Introduction . . . 120
6.2 Preliminaries . . . 122
6.2.1 Notation . . . 122
6.2.2 Differential algebraic equations . . . 122
6.3 Power network model . . . 123
6.4 Dynamic pricing algorithm . . . 125
6.5 Stability of the closed-loop system . . . 127
6.6 Conclusions . . . 130

7 DAPI control of high-dimensional multi-machine models 133
7.1 Introduction . . . 134
7.2 Preliminaries . . . 135
7.3 Multi-machine model . . . 138
7.4 Energy functions . . . 139
7.4.1 Synchronous machine . . . 140
7.4.2 Inductive transmission lines . . . 140
7.4.3 Total energy . . . 141
7.5 Port-Hamiltonian representation . . . 141
7.5.1 Transmission line energy . . . 141
7.5.2 Electrical energy of the synchronous generator . . . 142
7.6 Minimizing generation costs . . . 143
7.7 Conclusions . . . 145

8 Primal-dual dynamics with hard inequality constraints 147
8.1 Introduction . . . 148
8.2 Primal-dual dynamics (hard constraints) . . . 149
8.2.1 Primal-dual dynamics with gains . . . 155
8.2.2 Strict convexity case . . . 155
8.3 Application in data centers . . . 156
8.3.1 Simulation results . . . 158
8.4 Conclusions . . . 160

III Competitive real-time electricity markets 161

Introduction 163
Contributions . . . 164

Outline . . . 165

9 Frequency-aware Bertrand market mechanism 167
9.1 Introduction . . . 168
9.2 Power network model and dynamics . . . 170
9.3 Problem description . . . 171
9.3.1 ISO-generator coordination . . . 171
9.3.2 Inelastic electricity market game . . . 172
9.3.3 Chapter objectives . . . 173
9.4 Existence and uniqueness of Nash equilibria . . . 173
9.5 Interconnection of bid update scheme with power network dynamics 175
9.5.1 Price-bidding mechanism . . . 175
9.5.2 Equilibrium analysis of the interconnected system . . . 177
9.5.3 Convergence analysis . . . 178
9.6 Simulations . . . 181
9.7 Conclusions . . . 182

10 Integrating iterative bidding and frequency regulation 187
10.1 Introduction . . . 188
10.2 Power network frequency dynamics . . . 190
10.3 Problem statement . . . 191
10.4 Robustness of the continuous-time bid and power-setpoint update scheme . . . 193
10.4.1 Bidding process coupled with physical network dynamics . 194
10.4.2 Local input-to-state (LISS) stability . . . 195
10.5 Time-triggered implementation: iterative bid update and market clearing . . . 200
10.5.1 Algorithm description . . . 200
10.5.2 Sufficient condition on triggering times for stability . . . 203
10.6 Simulations . . . 209
10.7 Conclusions . . . 211

11 Conclusions 217
11.1 Discussion . . . 218
11.2 Outlook . . . 219
11.2.1 More realistic physical models . . . 219
11.2.2 Including inflexible loads and generation . . . 220
11.2.3 Robustness . . . 220
11.2.4 Region of attraction . . . 220
11.2.5 The broader perspective . . . 220

Bibliography 223

Summary 233

Samenvatting 235

List of Symbols

Symbol	Name
i, j	node i (or j)
k	transmission line or edge k
A, A_i	asynchronous damping constant(s)
B_{ij}	negative of the susceptance of line $\{i, j\}$
C, C_i	(total) generator cost function
D, D_c	incidence matrix of physical/communication network
E_{fi}	exciter emf/voltage
E'_{qi}, E'_{di}	internal bus transient emfs/voltages
E''_{qi}, E''_{di}	internal bus subtransient emfs/voltages
$\mathcal{E}$	edge set
$\mathcal{G}$	graph of the (power) network
H	Hamiltonian or storage function
I_{qi}, I_{di}	generator currents
$\mathcal{I}_n$	index set $\mathcal{I}_n = \{1, \ldots, n\}$
J	interconnection matrix
K	gain matrix
M, M_i	moment(s) of inertia
P_{gi}, P_{di}	power generation and demand, respectively
R	damping matrix
S	social welfare function
T'_{qoi}, T'_{doi}	open-loop transient time-scales
T''_{qoi}, T''_{doi}	open-loop subtransient time-scales
U, U_i	(total) demand utility function
V_{qi}, V_{di}	external bus voltages
V_i	(external bus) voltage magnitude
$\mathcal{V}$	node set
X_{qi}, X_{di}	synchronous reactances
X'_{qi}, X'_{di}	transient reactances
X''_{di}, X''_{qi}	subtransient reactances
δ_i	rotor angle w.r.t. synchronous reference frame
λ, λ_i	(local) price/Lagrange multiplier
ω_i	local frequency deviation
ω_s	(nominal) synchronous frequency
j	imaginary unit
μ, μ_i	nonnegative Lagrange multiplier

Chapter 1

Introduction

The electrical power network is one the most complex and important technical creations that we know. However, provisioning energy has become increasingly complicated due to several reasons, including the increased share of renewables. For example, in the Irish power grid, which has a high penetration of wind power, "only" up to the 65% of generation is allowed from renewable energy sources based on a comprehensive stability analysis [72]. One of the main challenges presented by significant renewable penetration is their intermittency. Consequently, the large-scale introduction of renewable energy sources will enhance the need for not only the flexibility of conventional power plants but also the flexibility of the demand side. Using the load as an additional degree of freedom is not entirely new but affordable global communication infrastructure and embedded systems make it now possible to add a certain portion of "smart" to the loads. Therefore, demand side management receives increasing attention by research and industry [78]. However, the coordination of both power generation and consumption requires novel control algorithms which enable a fair sharing of respectively costs and utilities, and to keep the system stable. In particular, from a network perspective, capacity management is essential to maintain frequency and voltage stability throughout the system. Furthermore, the design of these new control algorithms to stabilize the network and to let it function near its capacity limits also requires a deep understanding of the physical power network and its components.

In this research, we develop a unifying approach for the modeling, analysis and control of smart grids based on energy functions. Since energy is the main quantity of interest in power networks, this is a natural approach to deal with the problem. The underlying mathematical framework is based on the theory of port-Hamiltonian systems [76, 117]. This approach is based on modeling multi-physical systems by the energy flows between the components (via ports) in the network and utilizes energy functions (also called Hamiltonians) for representing the energy storage in the individual elements. Since energy is the lingua franca between all different physical domains [50], this approach allows us to view different electrical and mechanical components of the smart grid from the same perspective. Furthermore, as energy is a scalar quantity, this provides an insightful starting point for dealing with general stability issues.

1.1 Welfare maximization and grid stability

The flexibility on the demand and supply side has to be coupled with economic criteria. This includes determining how the supply of energy should be allocated between the providers to decrease operation costs and, similarly, how power available from renewables should be shared among the different consumers in such a way that the overall economic utility is maximized. Dynamic pricing has been identified as an effective approach to deal with these aspects and for the power network it was already studied a few decades ago [2]. However, many existing dynamic pricing algorithms neglect the physical constraints and dynamics of the grid. The aim in this thesis is to fill this gap by proposing a unifying framework in which the two aspects (physical modeling based on energy functions on one hand, and dynamic pricing on the other hand) are merged. This provides a natural setting where smart grids can be analyzed and new control algorithms can be designed allowing for economic efficiency and coping with potential instabilities resulting from the intermittency and uncertainty in renewable generation.

Designing control algorithms for power networks modeled in an energy-based port-Hamiltonian form can be guided by intuitive physical considerations. In particular, control algorithms for the grid must be distributed, namely they must use measured quantities that are available locally at the place where the control algorithm is running. Hence, it is important that the mathematical model includes explicitly the topology of the network. Port-Hamiltonian models naturally do so. The aim with dynamic pricing algorithms is to steer the system to an equilibrium that corresponds to the optimal social welfare. This mechanism can be viewed as an "energy-balancing" control which is at the core of many control design techniques for port-Hamiltonian systems [62, 76]. Hence, the port-Hamiltonian framework also lends itself to modeling the economic aspects involved in the control of smart grids.

A large part of the research in this thesis focuses on the use of this integrated physical-economical model of the smart grid to design distributed controllers that achieve stability of the network along with (constrained) social welfare maximization. As a first step, the social welfare will be modeled via the introduction of suitable utility and cost functions. To increase the use of renewable energies despite the uncertainty related with their availability, prices, or related control variables that admit such an interpretation, will be used in real-time to match the demand and supply, and also to route the power flow in an optimal manner.

1.2 Competitive real-time electricity markets

There are also other challenges in the design of real-time market mechanisms for control purposes. For example, as there may be an inherent uncertainty in allowing producers and consumers to react to price signals, stability of the grid may be compromised and can lead to a volatile market [83, 85, 86]. These aspect have to be taking into account in the design of new market architectures. The selfish behavior of market players can also affect the market equilibrium, such as in *Cournot competition* [51], with a loss of global efficiency as a result. Therefore,

we should also bear in mind the competitive nature of electricity markets and thus study this game-theoretic aspect.

For example, what would happen if prosumers do not act as price-takers (which is commonly assumed in the literature) but instead as price-setters? In its simplest form such behavior is analyzed by a model describing the competition in prices which is often termed *Bertrand competition* in the economic literature. For power systems, in [24] a market architecture is proposed where distributed energy resources can cooperate under an aggregator while the aggregators compete among each other in such a price-competition. There it was shown how market players reach a cost efficient equilibrium in which each player is not willing to deviate from (this is often called a *Nash equilibrium*). We proceed along similar lines with the addition that we also take into account the physical frequency deviation, bringing the market close to real-time operation.

1.3 Contributions

In this section we briefly state the main contributions of this thesis, and more details are stated in the introductions of each individual part of this dissertation.

The key contribution in part I of this thesis consists of the port-Hamiltonian modeling of multi-machine systems with varying order of complexity. In particular, by showing that the energy functions of the reduced order models indeed correspond to the first-principle model, port-Hamiltonian representations of the 6th, 3rd and 2nd-order models are obtained, which clearly reveal the nontrivial interconnection and damping structure of these systems. Moreover, by verifying that the models are dissipative, shifted passivity of these systems is shown. This allows these systems to be steered towards a nontrivial equilibrium in a convenient manner as shown in parts II and III.

Part II shows that market dynamics in the form of real-time dynamic pricing can also be cast in the port-Hamiltonian framework. We show that (distributed) dynamic pricing algorithms are obtained by applying a continuous-time gradient algorithm to a social welfare maximization problem. We establish the shifted passivity property of such systems and prove its convergence to an optimizer under milder assumptions compared to the existing literature. One of the key contributions is the interconnection of dynamics pricing algorithms with the physical dynamics in a passivity preserving manner, achieving both frequency regulation and optimal power sharing. For the underlying social welfare problem we consider the power balance, nodal power constraints, line congestion and transmission costs. For the physical system we considered not only the 2nd-order swing equations, but also the 3rd-order (network-reduced and structure-preserving) models and the 6th-order multi-machine model, which are much more complex than what is considered in the current literature.

In Part III we consider the unique intersection of game theory, power network dynamics and optimization (in the form of an economic dispatch problem) which has no precedent in the literature. There we propose novel discrete- and continuous-time frequency-aware bidding mechanisms in which generators are

involved in a price-competition game. We define the notion of an efficient Nash equilibrium and show that such equilibrium exists and corresponds to an optimizer of an economic dispatch problem. By using the frequency as a feedback signal in the negotiation process, the bidding scheme is coupled with the physical swing equations. Our contribution is to show that the closed-loop system is (input-to-state) stable, and that convergence to an efficient Nash equilibrium, economic dispatch and zero frequency deviation is achieved.

1.4 Outline of this thesis

This thesis consists of three parts, studying respectively (i) the modeling of power networks, (ii) its integration with and design of welfare maximizing (market-based) controllers, and (iii) the competitive aspect of electricity markets. The first part of this thesis focuses on the port-Hamiltonian modeling of multi-machine networks, with specific attention to synchronous machine modeling. In particular, the derivation of different synchronous machine models with varying complexity and accuracy is discussed together with the underlying assumptions and limitations. Furthermore, energy characteristics of the different models are discussed and their port-Hamiltonian representations are derived from this. This chapter has partly a tutorial value but mainly highlights the effectiveness of the port-Hamiltonian framework for the analysis of these complex multi-physics models.

The second and main part of this thesis focuses on the optimization and control of power networks. In particular, we consider several variations of the social welfare problem formulated as a mathematical optimization problem. We start with the simplest optimization problem only considering the power balance constraint in Chapter 3, resulting in a centralized control algorithm based on the so-called primal-dual gradient algorithm. In Chapter 4 a distributed version of this controller is designed and a comparison made with an alternative consensus-based control architecture. Later extend the primal-dual based control design in Chapter 5 to include generator limits, line constraints and transmission costs in the optimization problem. On the physical side we also consider several variations including the classical swing equations (Chapter 3) and the 3rd-order model for the power network (Chapter 5). In addition, we consider structure-preserving models where a distinction is made between generator and load nodes (Chapter 6) and we also show that high-order multi-machine models lend themselves for the interconnection with passive (consensus-based) control algorithms (Chapter 7). Finally, Chapter 8 focuses on the stability properties of primal-dual dynamics of general convex optimization problems, while relaxing the strict convexity assumptions for the convergence of the associated projected dynamical system.

The third part of this thesis takes into account the competitive nature of the electricity market. The chapters that are presented in this part have been the result of a fruitful 3-month collaboration with the University of San Diego, California. Here we merged our approach adopted in part II of the thesis with their work on iterative bidding in electricity markets. This allows us to show how frequency-aware iterative bidding leads to optimal power dispatch, a state that corresponds

to a Nash equilibrium and to frequency regulation. In the first chapter of part III (Chapter 9) we focus on continuous-time bid update schemes and frequency dynamics and analyze in more detail the game-theoretic framework. In Chapter 10 we discretize the bidding algorithm resulting in a hybrid system with discrete updates in the bidding mechanism and continuous-time swing dynamics of the physical system. We also establish bounds on the inter-event times that guarantee the convergence of the closed-loop hybrid system.

1.5 List of publications

Journal papers:

- T.W. Stegink, C. De Persis, A.J. van der Schaft. "An energy-based analysis of reduced-order models of (networked) synchronous machines." Mathematical and Computer Modelling of Dynamical Systems, under review. (Chapter 2)
- T.W. Stegink, C. De Persis, A.J. van der Schaft. "A unifying energy-based approach to stability of power grids with market dynamics." IEEE Transactions on Automatic Control 62.6 (2017): 2612-2622. (Chapter 5)
- A.J. van der Schaft, T.W. Stegink. "Perspectives in modeling for control of power networks." Annual Reviews in Control 41 (2016): 119-132.
- T.W. Stegink, A. Cherukuri, C. De Persis, A.J. van der Schaft, J. Cortés. "Frequency-driven market mechanisms for optimal dispatch in power networks." IEEE Transactions on Automatic Control, under review. (Chapter 9)
- T.W. Stegink, A. Cherukuri, C. De Persis, A.J. van der Schaft, J. Cortés. "Hybrid interconnection of iterative bidding and power network dynamics for frequency regulation and optimal dispatch." IEEE Transactions on Control of Network Systems, to be published, 16 July 2018, DOI: 10.1109/TCNS.2018.2856404. (Chapter 10)

Conference papers:

- T.W. Stegink, C. De Persis, A.J. van der Schaft. "Port-Hamiltonian formulation of the gradient method applied to smart grids." IFAC-PapersOnLine 48.13 (2015): 13-18. (Chapter 3)
- T.W. Stegink, C. De Persis, A.J. van der Schaft. "Stabilization of structure-preserving power networks with market dynamics." IFAC-PapersOnLine 50.1 (2017): 6737-6742. (Chapter 6)
- T.W. Stegink, C. De Persis, A.J. van der Schaft. "A port-Hamiltonian approach to optimal frequency regulation in power grids." 54th IEEE Annual Conference on Decision and Control (CDC), 2015. pp. 3224-3229 (Chapter 4)

- T.W. Stegink, C. De Persis, A.J. van der Schaft. "Optimal power dispatch in networks of high-dimensional models of synchronous machines." IEEE 55th Annual Conference on Decision and Control (CDC), 2016. (Chapter 7)
- T.W. Stegink, T. Van Damme, C. De Persis, "Convergence of projected primal-dual dynamics with applications in data centers." 7th IFAC Workshop on Distributed Estimation and Control in Networked Systems (NecSys), 2018. (Chapter 8)
- T.W. Stegink, A. Cherukuri, C. De Persis, A.J. van der Schaft, J. Cortés. "Stable interconnection of continuous-time price-bidding mechanisms with power network dynamics." Proceedings of the 20th Power Systems Computation Conference (PSCC), 2018. (Chapter 9)
- T.W. Stegink, A. Cherukuri, C. De Persis, A.J. van der Schaft, J. Cortés. "Integrating iterative bidding in electricity markets and frequency regulation." American Control Conference (ACC), 2018, pp. 6182-6187. (Chapter 10)
- P. Monshizadeh, C. De Persis, T.W. Stegink, N. Monshizadeh, A.J. van der Schaft. "Stability and Frequency Regulation of Inverters with Capacitive Inertia." IEEE 56th Annual Conference on Decision and Control (CDC), 2017.

1.6 Notation

For $A \in \mathbb{R}^{m\times n}$, we let $\|A\|$ denote the induced 2-norm. Given $v \in \mathbb{R}^n, A = A^T \in \mathbb{R}^{n\times n}$, we denote $\|v\|_A^2 := v^T A v$. Given a symmetric matrix $A \in \mathbb{R}^{n\times n}$, we write $A > 0$ ($A \geq 0$) to indicate that A is a positive (semi-)definite matrix. The set of positive real numbers is denoted by $\mathbb{R}_{>0}$ and likewise the set of vectors in $\mathbb{R}^n$ whose elements are positive by $\mathbb{R}^n_{>0}$. For $u, v \in \mathbb{R}^n$ we write $u \perp v$ if $u^T v = 0$. We use the compact notational form $0 \leq u \perp v \geq 0$ to denote the complementarity conditions $u \geq 0, v \geq 0, u \perp v$. The notation $\mathbb{1} \in \mathbb{R}^n$ is used for the vector whose elements are equal to 1. Given a twice-differentiable function $f : \mathbb{R}^n \to \mathbb{R}^n$ then the Hessian of f evaluated at x is denoted by $\nabla^2 f(x)$. We use the notation $\mathbf{sin}(.), \mathbf{cos}(.)$ for the element-wise sine and cosine functions respectively. Given a differentiable function $f(x_1, \ldots, x_N), x_i \in \mathbb{R}^{n_i}$, then $\nabla f(x_1, \ldots, x_N)$ denotes the gradient of f evaluated at $x_1, \ldots, x_N$ and likewise $\nabla_{x_i} f(x_1, \ldots, x_N) = \frac{\partial f}{\partial x_i}(x_1, \ldots, x_N)$ denotes the gradient of f with respect to x_i. Given a solution x of $\dot{x} = f(x)$, where $f : \mathbb{R}^n \to \mathbb{R}^n$ is a Lebesgue measurable function and locally bounded, the *omega-limit set* (or just *limit set*) $\Omega(x)$ is defined as [26]

$$\Omega(x) := \Big\{ \bar{x} \in \mathbb{R}^n \mid \exists \{t_k\}_{k=1}^{\infty} \subset [0, \infty) \text{ with } \lim_{k\to\infty} t_k = \infty \text{ and } \lim_{k\to\infty} x(t_k) = \bar{x} \Big\}.$$

We use the notation $\mathcal{I}_m$ for the set $\{1, \ldots, m\}$. For vectors $u \in \mathbb{R}^n, v \in \mathbb{R}^m$, we interchangeably write $(u, v) = \text{col}(u, v) = \left[\begin{smallmatrix} u \\ v \end{smallmatrix}\right]$ and likewise for three or more vectors.

1.7 Preliminaries

In this section we state some preliminaries on dynamical systems, convex optimization and game theory that are used in the development of various results appearing in this thesis.

1.7.1 Nonlinear systems

Stability of autonomous systems

Let us consider the system

$$\dot{x} = f(x) \tag{1.1}$$

with $x \in \mathbb{R}^n$ and locally Lipschitz function $f : \mathbb{R}^n \to \mathbb{R}^n$. We assume that $\bar{x}$ is an equilibrium of (1.1), i.e. $f(\bar{x}) = 0 \in \mathbb{R}^n$, unless specified otherwise. Often, we are interested in the stability of such an equilibrium.

Definition 1.7.1 (Lyapunov stability)**.** An equilibrium $\bar{x}$ of system (1.1) is called *Lyapunov stable*, if for any $\epsilon > 0$ there exists a $\delta > 0$ such that given a solution $x(t)$ to the system, $\|x(0) - \bar{x}\| < \delta$ implies that $\|x(t) - \bar{x}\| < \epsilon$ for all $t \geq 0$.

Lyapunov stability of an equilibrium is guaranteed by the existence of a Lyapunov function which we define next.

Definition 1.7.2 ((local) Lyapunov function)**.** Let $0 \in \mathbb{R}^n$ be an equilibrium of (1.1). Let $V : \mathcal{D} \to \mathbb{R}$ be a continuously differentiable function on the domain $\mathcal{D} \subset \mathbb{R}^n, \{0\} \in \mathcal{D}$. Then V is called a *local Lyapunov function* if

1. $V(x) \geq 0$ for all $x \in \mathcal{D}$ where equality holds if and only if $x = 0$.
2. $\frac{d}{dt}V(x) = (\nabla V(x))^T f(x) \leq 0$ for all $x \in \mathcal{D}$.

If $\mathcal{D} = \mathbb{R}^n$, then V is called a *(global) Lyapunov function.* If item 2 holds strictly for all $x \in \mathcal{D}, x \neq 0$, we say that V is a *strict (local) Lyapunov function.*

In many cases, one is also interested in the attractivity of an equilibrium.

Definition 1.7.3 (Asymptotic stability)**.** An equilibrium $\bar{x}$ of system (1.1) is called *asymptotically stable* if it is Lyapunov stable and there exists $\delta > 0$ such that if $\|x(0) - \bar{x}\| < \delta$, then $\lim_{t\to\infty} \|x(t) - \bar{x}\| = 0$.

Next, we state the classical Lyapunov stability theorem.

Theorem 1.7.4 (Lyapunov stability theorem [56])**.** *Let $\bar{x} = 0$ be an equilibrium of (1.1) let V be a Lyapunov function with domain $\mathcal{D} \subset \mathbb{R}^n$, such that $\{0\} \in \mathcal{D}$. Then $\bar{x}$ is (Lyapunov) stable. Moreover, if V is a strict Lyapunov function, then $\bar{x}$ is (locally) asymptotically stable.*

Often it is difficult to find a strict Lyapunov function for a system and one can only construct a (nonstrict) Lyapunov function. The following lemma can help in determining the asymptotic behavior of a nonlinear system.

Proposition 1.7.5 (LaSalle's invariance principle [91])**.** *Let Ψ be a positive invariant set of (1.1), i.e., $x(0) \in \Psi$ implies $x(t) \in \Psi$ for all $t \geq 0$. Suppose that every solution starting in Ψ converges to a set $E \subset \Psi$ and let M be the largest invariant set contained in E. Then, every bounded solution starting in Ψ converges to M as $t \to \infty$.*

When used together with the existence of a Lyapunov function we obtain following stability result.

Proposition 1.7.6 ((Pointwise) asymptotic convergence)**.** *Let $\bar{\mathcal{X}} = f^{-1}(0) \ni 0$ be the set of equilibria of (1.1) and suppose it admits a local Lyapunov function V with domain $\mathcal{D} \ni \{0\}$. Suppose furthermore that there exists a sublevel set $\Upsilon = \{x : V(x) \leq c \in \mathbb{R}_{>0}\} \subset \mathcal{D}$ of V around the origin. Then each trajectory of (1.1) initialized in Υ converges to the largest invariant set M contained in*

$$E := \{x \in \Upsilon \mid (\nabla V(x))^T f(x) = 0\}.$$

If furthermore each point in M is Lyapunov stable, then this trajectory converges to a point in M [42].

(Shifted) passivity of nonlinear systems

Above we considered autonomous systems. Now we will consider dynamical systems with inputs and outputs. These are written in the form

$$\begin{aligned} \dot{x} &= f(x,u) \\ y &= h(x,u) \end{aligned} \tag{1.2}$$

with state $x \in \mathbb{R}^n$, input $u \in \mathbb{R}^m, y \in \mathbb{R}^m$. An important property of such systems is passivity which is closely related to stability.

Definition 1.7.7 (Passivity [117])**.** We say that system (1.2) with $x \in \mathcal{D}$ is *passive* if there exists a differentiable storage function $V : \mathcal{D} \to \mathbb{R}_{\geq 0}$ satisfying the differential dissipation inequality [117]

$$\frac{d}{dt}V(x(t)) = (\nabla V(x(t)))^T f(x(t),u(t)) \leq (u(t))^T y(t) \tag{1.3}$$

along all solutions $x(.)$ corresponding to input functions $u(.)$.

For physical systems, the right-hand side of (1.3) is usually interpreted as the supplied power, and $V(x)$ as the stored energy of the system when being in state x. Most systems considered in this thesis admit another more useful property called *shifted passivity*, sometimes also referred to as *equilibrium-independent passivity* [45].

Definition 1.7.8 (Shifted passivity)**.** The system (1.2), with $x \in \mathcal{D}$, is *shifted passive* if there exists a differentiable storage function $V : \mathcal{D} \to \mathbb{R}_{\geq 0}$ satisfying the

differential dissipation inequality

$$\frac{d}{dt}V(x(t)) = (\nabla V(x(t)))^T f(x(t), u(t)) \leq (u(t) - \bar{u})^T (y(t) - \bar{y})$$

for all $(\bar{x}, \bar{u}, \bar{y})$ such that $f(\bar{x}, \bar{u}) = 0, \bar{y} = h(\bar{x}, \bar{u}), \bar{x} \in \mathcal{D}$ and for all solutions $x(.)$ corresponding to input functions $u(.)$.

Port-Hamiltonian systems

We refer to (1.2) as an *(input-state-output) port-Hamiltonian system* if it can be written in the form

$$\begin{aligned} \dot{x} &= (J(x) - R(x))\nabla H(x) + g(x)u \\ y &= g(x)^T \nabla H(x) \end{aligned}$$

for some skew-symmetric matrix $J(.) \in \mathbb{R}^{n\times n}$, symmetric positive semi-definite matrix $R(.) \in \mathbb{R}^{n\times n}$, matrix $g(.) \in \mathbb{R}^{n\times m}$ and (strictly) convex Hamiltonian $H : \mathbb{R}^n \to \mathbb{R}$. The matrices J, R are often referred to as the interconnection and damping matrix respectively because these reflect the energy routing and energy dissipation structure of a system. By construction, port-Hamiltonian systems are passive using the Hamiltonian as the storage function.

Incrementally port-Hamiltonian systems

In a large part of this thesis, we consider systems that can be written in the form

$$\begin{aligned} \dot{x} &= (J - R)\nabla H(x) + g_1 u + g_2 e_{\mathtt{R}} \\ y &= g_1^T \nabla H(x) \\ f_{\mathtt{R}} &= g_2^T \nabla H(x), \\ e_{\mathtt{R}} &= \nabla S(f_{\mathtt{R}}) \end{aligned} \tag{1.4}$$

with $J = -J^T \in \mathbb{R}^{n\times n}, 0 \leq R = R^T \in \mathbb{R}^{n\times n}, g_1 \in \mathbb{R}^{n\times m}, g_2 \in \mathbb{R}^{n\times p}$ where $S : \mathbb{R}^p \to \mathbb{R}$ is continuously differentiable concave function. We will refer to such a system as an *incrementally port-Hamiltonian system* although the definition adopted in [117] is for systems in a more general form. In particular, (1.4) admits the following maximal monotone relationship (more details are found in [117])

$$(e_{\mathtt{R}_1} - e_{\mathtt{R}_2})^T (f_{\mathtt{R}_1} - f_{\mathtt{R}_2}) \leq 0$$

for all $e_{\mathtt{R}_1}, f_{\mathtt{R}_1}, e_{\mathtt{R}_2}, f_{\mathtt{R}_2} \in \mathbb{R}^p$ that satisfy (1.4). Under some mild assumptions this allows us to show that the system (1.4) is shifted passive.

Proposition 1.7.9 (System (1.4) is shifted passive)**.** *Let* $(\bar{x}, \bar{u}, \bar{y})$ *and* $(\bar{e}_{\mathtt{R}}, \bar{f}_{\mathtt{R}})$ *satisfy* (1.5) *and suppose that* $\nabla^2 H(\bar{x}) > 0$.

$$\begin{aligned} 0 &= (J-R)\nabla H(\bar{x}) + g_1\bar{u} + g_2\bar{e}_{\mathtt{R}} \\ \bar{y} &= g_1^T \nabla H(\bar{x}) \\ \bar{f}_{\mathtt{R}} &= g_2^T \nabla H(\bar{x}), \\ \bar{e}_{\mathtt{R}} &= \nabla S(\bar{f}_{\mathtt{R}}) \end{aligned} \tag{1.5}$$

Then (1.4) *is shifted passive with respect to input-output pair* $(u-\bar{u}, y-\bar{y})$. *In particular, its (local) storage function is given by the* shifted Hamiltonian

$$\bar{H}(\bar{x}) := H(x) - (x-\bar{x})^T \nabla H(\bar{x}) - H(\bar{x}). \tag{1.6}$$

1.7.2 Convex optimization and game theory

Mathematically, an optimization problem is defined by

$$\begin{aligned} &\underset{x}{\text{minimize}} \quad f(x) \\ &\text{subject to} \quad x \in \mathcal{X} \end{aligned} \tag{1.7}$$

where $f : \mathcal{X} \to \mathbb{R}$ is called the *objective function*, $\mathcal{X}$ is the set of feasible solutions and x is often referred to as a *primal variable*. The aim is to find $\bar{x} \in \mathcal{X}$ that minimizes the objective function f, i.e., $f(\bar{x}) \leq f(x), \forall x \in \mathcal{X}$. In this thesis we assume that $\mathcal{X} \subset \mathbb{R}^n$ and $\mathcal{X}$ is a closed and convex set, and that f is a continuously differentiable convex function. In such a case (1.7) is referred to as a *convex* optimization problem. In many applications, the feasibility set has an explicit form given by

$$\mathcal{X} = \{x \in \mathbb{R}^n \mid Ax = b,\ g_i(x) \leq 0,\ i = 1, \ldots, q\},$$

where $A \in \mathbb{R}^{m \times n}, b \in \mathbb{R}^m$, and $g_i : \mathbb{R}^n \to \mathbb{R}, i = 1, \ldots, q$ are continuously differentiable convex functions. Without loss of generality we assume that $\ker(A^T) = \{0\}$, implying that the equality constraints formed by $Ax = b$ are linearly independent. Using this explicit form of the feasibility set, the minimization problem (1.7) can also be written as

$$\underset{x}{\text{minimize}} \quad f(x) \tag{1.8a}$$

$$\text{subject to} \quad Ax = b \tag{1.8b}$$

$$g(x) \leq 0 \tag{1.8c}$$

where we use the notation $g(x) = \text{col}(g_1(x), \ldots, g_q(x))$ and the inequality (1.8c) holds element-wise.

As mentioned before, the quantity x is referred to as the *primal variable* of (1.8). The *dual variables* of (1.8) are often introduced via the Lagrangian function.

Definition 1.7.10 (Lagrangian function)**.** The Lagrangian function of (1.8) is

$$L(x, \lambda, \mu) = f(x) + \lambda^T(Ax - b) + \mu^T g(x)$$

where λ, μ are referred to as *Lagrange multipliers* or *dual variables* of (1.8).

Using the definition of the Lagrangian, we can formulate the so-called *dual problem* associated with (1.8).

Definition 1.7.11 (Dual problem)**.** The dual problem of (1.8) is

$$\text{maximize } g(\lambda, \mu) \tag{1.9a}$$
$$\text{subject to } \mu \geq 0 \tag{1.9b}$$

where

$$g(\lambda, \mu) := \inf_x L(x, \lambda, \mu) = \inf_x (f(x) + \lambda^T(Ax - b) + \mu^T g(x)).$$

Definition 1.7.12 (Primal-dual optimizer)**.** A triple (x^*, λ^*, μ^*) is a *primal-dual optimizer* if x^* is an optimizer of the primal problem (1.8) and (λ^*, μ^*) is an optimizer of the dual problem (1.9).

It is a standard result that for any primal-dual optimizer (x^*, λ^*, μ^*) we have $g(\lambda^*, \mu^*) \leq f(x^*)$ which is often referred to a *weak duality*. In case equality holds, we speak of *strong duality*. This condition is guaranteed by the refined Slater's condition.

Definition 1.7.13 (Refined Slater's condition)**.** There exists $x \in \mathbb{R}^n$ such that

$$\begin{aligned} Ax &= b \\ g_i(x) &\leq 0 \quad \text{if } g_i(.) \text{ is an affine function} \\ g_i(x) &< 0 \quad \text{if } g_i(.) \text{ is not an affine function} \end{aligned}, \qquad i = 1, \ldots, q.$$

Proposition 1.7.14 (Strong duality)**.** *Strong duality holds if (the refined) Slater's condition is satisfied.*

When strong duality holds, optimality of both the primal and dual problem can be verified by the first-order optimality conditions called the Karush-Kuhn-Tucker (KKT) conditions.

Proposition 1.7.15 (KKT optimality conditions [13])**.** *Suppose (the refined) Slater's condition holds. Then (x^*, λ^*, μ^*) is a primal-dual optimizer if and only if it satisfies the KKT optimality conditions*

$$\begin{aligned} \nabla f(x^*) + A^T\lambda^* + (\nabla g(x^*))^T\mu^* &= 0 \\ Ax^* &= b \\ 0 \geq g(x^*) \perp \mu^* &\geq 0. \end{aligned}$$

Game theory

A game is defined as a tuple $(\mathcal{S}, \mathcal{A}, \Pi)$ where [9]

- $\mathcal{S} = \mathcal{I}_n = \{1, \ldots, n\}$ is the set of players
- $\mathcal{A} = \{a \mid a = (a_1, \ldots, a_n), a_i \in \mathcal{A}_i, i \in \mathcal{I}_n\}$ is the set of action profiles
- $\Pi = (\Pi_1, \ldots, \Pi_n), \Pi_i : \mathcal{A} \to \mathbb{R}, i \in \mathcal{I}_n$ is the set of the player payoff functions.

Often, the action profile $(a_1, \ldots, a_n)$ is written as (a_i, a_{-i}) where a_{-i} is the action profile of all players except i. A Nash equilibrium of a game is defined as follows.

Definition 1.7.16 (Nash equilibrium [9])**.** The action profile $(a_1^*, \ldots, a_n^*) \in \mathcal{A}$ is a *Nash equilibrium* if none of the players gain anything by deviating from it, i.e.,

$$\Pi(a_i, a_{-i}^*) \leq \Pi(a_i^*, a_{-i}^*), \qquad \forall a_i \in \mathcal{A}_i, \forall i \in \mathcal{I}_n.$$

In many application the set of action profiles can be further specified. In this thesis, the action space of each player assumed to be a subset of $\mathbb{R}$, i.e. $\mathcal{A}_i \subset \mathbb{R}$.

Part I

Modeling of power networks

Introduction

An electrical power system consists of many individual elements connected together to form a large, complex and dynamic system capable of generating, transmitting and distributing electrical energy over a large geographical area. Because of this interconnection of elements, a large variety of dynamic interactions are possible. Some of these interactions affect only some elements in the network, while others may affect part of the system or the system as a whole. Power system dynamics can be conveniently divided into groups characterized by their cause, consequence, time scale, physical character or the place in the system where they occur [67].

The aim of this part of the thesis is to revisit some of the existing modeling techniques (e.g. from [61, 67]) and develop a comprehensive model structure that reflects the essential features and dynamics of power networks and at the same time is easily extendable to various levels of complexity and accuracy. In particular, our focus will be on different models of synchronous machines and their interconnection with the (transmission) network. Synchronous generators used in coal power plants, gas turbines but also in large hydro power plants still form a principal source of electric energy in power systems. In addition, many large loads are driven by synchronous motors. These devices operate on the same principle and are often referred to as *synchronous machines*. The problem of power system stability is mainly concerned with keeping interconnected synchronous machines in synchronism. In fact, the rotor of a synchronous machine is effectively a flywheel whose inertia is crucial to compensate for fluctuations and disturbances, such as load and generation variations, in a time-scale up to the order of 5 s [72]. In particular this allows synchronous machines to tolerate a temporary power imbalance in the network. Needless to say that an understanding of their characteristics and accurate modeling of their dynamics are of fundamental importance to the study of power system stability [67].

The quantity that all power system components (e.g. synchronous machines, transmission lines etc.) have in common is energy. It is therefore natural to take this quantity as a starting point for modeling the power system components by their main physical and unifying characteristics: energy storage, energy dissipation, energy routing, and energy supply. We will employ the well-established network modeling approach of port-Hamiltonian systems as the starting point for a scalable modeling of power systems. A key property of the mathematical theory of port-Hamiltonian systems is its modularity. This means that the interconnection of port-Hamiltonian systems results in another port-Hamiltonian system with composite energy, dissipation, and interconnection structure. Based on this principle, the power system components are modeled individually the

model of the overall system is constructed by interconnecting the submodels. This naturally allows new components to be locally added or modified without the need for global changes of the model, ensuring easy scalability. A motivating starting point for building up a systematic and scalable port-Hamiltonian framework for the modeling of power systems is the work presented in [37], where a synchronous generator that is interconnected with a resistive load through a transmission line is systematically modeled and studied using the port-Hamiltonian framework. First the models of the individual components are modeled as port-Hamiltonian subsystems and are then combined to yield a global port-Hamiltonian model.

For the generator-line-load system studied in [37], a Lyapunov stability analysis based on the energy flow is performed. This simplified stability analysis already provides valuable insights into the main difficulties of a general stability analysis. Also other works, for example [122], show that proving stability considering a first-principle model for the synchronous generator can be challenging, in particular for multi-machine networks [21]. On the other hand, for many stability studies one is only interested in particular aspect of the electromechanical dynamics, for example the operation around the synchronous frequency. This allows to make simplifications to the more complicated multi-machine models presented in e.g. [21, 37, 122] while still capturing the essential nonlinear behavior of power networks.

However, many frequency stability studies use the classical model described by the so-called *swing equations* for which the dynamics at each bus is described by a second-order model, see e.g. [19, 64, 131], and is often considered to be a oversimplified model of the power network dynamics [22, 73]. Therefore, we will focus on dynamical models that are much more complex and accurate than the swing equations. For example, we will consider models in which also (high order) voltage dynamics are explicitly considered. However, this points to the need for a thorough study of the relation between different port-Hamiltonian models at different levels of abstraction. In particular, this raises the question what the relation of the energy characteristics is between the swing equations and the available higher-order generator models, like the one studied in [21, 37]. This will be the focus of Chapter 2.

Chapter 2

Port-Hamiltonian modeling of networked synchronous machines

Abstract: *Stability of power networks is an increasingly important topic because of the high penetration of renewable distributed generation units. This requires the development of advanced (typically model-based) techniques for the analysis and controller design of power networks. Although there are widely accepted reduced-order models to describe the dynamic behavior of power networks, they are commonly presented without details about the reduction procedure, hampering the understanding of the physical phenomena behind them. The present chapter aims to provide a modular model derivation of multi-machine power networks. Starting from first-principle fundamental physics, we present detailed dynamical models of synchronous machines and clearly state the underlying assumptions which lead to some of the standard reduced-order multi-machine models, including the classical second-order swing equations. In addition, the energy functions for the reduced-order multi-machine models are derived from the full-order model. We show that, for purely inductive networks, these energy functions can be used to represent the multi-machine systems as port-Hamiltonian systems. Moreover, the systems are proven to be passive with respect to their steady states, which allows for a power-preserving interconnection with other passive components, including passive controllers. As a result, the corresponding energy function or Hamiltonian can be used to provide a rigorous stability analysis of advanced models for the power network without having to linearize the system.*

2.1 Introduction

The control and stability of power networks has become increasingly challenging over the last decades. As renewable energy sources penetrate the grid, the conventional power plants have more difficulty in keeping the frequency around the nominal value, e.g. 50 Hz, leading to an increased chance of network failures or, in the worst case, even blackouts.

The current developments require a sophisticated stability analysis of more advanced models for the power network as the grid is operating more frequently near its capacity constraints. For example, using high-order models of synchronous machines that better approximate the actual system allows us to establish results on the stability of power networks that are more reliable and accurate.

However, in much of the recent literature, a rigorous stability analysis has been carried out only for low-order models of the power network which have a limited accuracy. For models of intermediate complexity the stability analysis has merely been done for the linearized system [3, 67]. Hence, a novel approach is required to make a profound stability analysis of these more complicated models possible.

In this chapter, we propose a unifying energy-based approach for the modeling and analysis of multi-machine power networks which is based on the theory of port-Hamiltonian systems. Since energy is the main quantity of interest, the port-Hamiltonian framework is a natural approach to deal with the problem [117]. Moreover, it lends itself to deal with large-scale nonlinear multi-physics systems like power networks [37, 105–107].

Literature review

The emphasis in the present chapter lies on the modeling and analysis of (networked) synchronous machines since they have a crucial role in the stability of power networks as they are the most flexible and have to compensate for the increased fluctuation of both the supply and demand of power. An advanced model of the synchronous machine is the first-principles model which is derived in many power-engineering books [4, 61, 67], see in particular [67, Chapter 11] for a detailed derivation of the model.

Modeling the first-principles synchronous (multi-)machine model using the theory of port-Hamiltonian systems has been done previously in [37]. However, in this work, stabilization of the synchronous machine to the synchronous frequency could not be proven. In [21] a similar model for the synchronous machine is used, but with the damper windings neglected. Under some additional assumptions, asymptotic stability of a single machine is proven using a shifted energy function. However, such a stability result could not be proven for multi-machine systems.

Summarizing, the complexity of the full-order model of the synchronous machine makes a rigorous stability analysis troublesome, especially when considering multi-machine networks, see also [75]. Moreover, it is often not necessary to consider the full-order model when studying a particular aspect of the electromechanical dynamics such as the operation around the synchronous frequency [67].

On the other side of the spectrum, much of the literature using Lyapunov stability techniques rely on the second-order (non)linear swing equations as the model for the power network [38, 64, 67, 71, 77, 92, 131, 135] or the third-order model as e.g. in [113]. For microgrids similar models are considered in which a Lyapunov stability analysis is carried out [32, 33]. However, the models are often presented without stating the details on the model reduction procedure or the validity of the model. For example, the swing equations are inaccurate and only valid on a specific time scale up to the order of a few seconds so that asymptotic stability results have a limited value for the actual system [4, 22, 61, 67].

Hence, it is appropriate to make simplifying assumptions for the full-order model and to focus on multi-machine models with intermediate complexity which provide a more accurate description of the network compared to the second- and third-order models [4, 61, 67]. However, in the present literature the stability analysis of intermediate-order multi-machine models is only carried out for the linearized system [3, 4, 61, 67]. In particular, in [3] a fourth-order model for the synchronous machine is considered which is coupled with market dynamics and the stability is analyzed by examining the eigenvalues of the linearized system. Consequently, the stability results are only valid around a specific operating point. This highlights the need for new analytical tools to make it possible to state more general rigorous statements regarding the stability of complex models of power networks.

Contributions

The main contribution of this chapter is establishing a unifying energy-based analysis of intermediate-order models of (networked) synchronous machines. In doing so, we first explain how these intermediate-order models are obtained from the first-principles model and highlight what the underlying assumptions are, and then how these synchronous machine are coupled through inductive lines. This part has a tutorial value where we follow the lines of [67], in which a detailed derivation of the reduced-order models is given. This forms the foundation of our second contribution which is the systematic procedure to obtain the energy functions of the reduced order multi-models. In particular, we show how the energy functions of the reduced order models are obtained from the first-principles model, which is represented in a very different a coordinate system, and that these energy functions contain a common factor which is often ignored in power system stability studies.

Another key contribution is that, building on the expression of the energy functions (or Hamiltonians), port-Hamiltonian representations of various synchronous machine models are obtained which include the full-order model as well as the 6th, 3rd, and classical 2nd order models. In particular, this reveals the sparse but nontrivial interconnection and damping structures of these systems, having the complexity mainly appearing in the expression of the Hamiltonian. Specifically for the 6th order model, we show that the system is dissipative by explicitly proving that the dissipation matrix is positive definite which is far from trivial.

Finally, by exploiting the specific structure of the port-Hamiltonian systems (state-independent interconnection and damping structure), shifted passivity of the reduced order multi-machine models is proven. To the author's best knowledge, such shifted passivity has not been established for these intermediate (4,5,6-)order models. In particular, this allows to consider a nonlinear sixth-order multi-machine model, having a quite accurate description of the power network dynamics, while permitting a rigorous (Lyapunov-based) stability analysis of nontrivial equilibria. This is in contrast with the current literature which mainly relies on linearization techniques for the stability analysis of such complex systems.

Outline

The remainder of the chapter is structured as follows. First we state the preliminaries in Section 2.2. Then in Section 2.3 the full-order first-principles model is presented and its port-Hamiltonian form is given. The model reduction procedure is discussed in Section 2.4 in which synchronous machine models of intermediate order are obtained. In Section 2.5 these models are used to establish multi-machine models, including the sixth, third and classical second-order model. Then in Section 2.6 energy functions of the reduced order models are derived, which in Section 2.7 are used to put the multi-machine models in port-Hamiltonian form. Finally, Section 2.8 discusses the conclusions and possible directions for future research.

2.2 Preliminaries

2.2.1 Notation

The set of real numbers and the set of complex numbers are respectively defined by $\mathbb{R}, \mathbb{C}$. Given a complex number $\alpha \in \mathbb{C}$, the real and imaginary part of are denoted by $\Re(\alpha), \Im(\alpha)$ respectively. The imaginary unit is denoted by $\mathrm{j} = \sqrt{-1}$. Let $\{v_1, v_2, \ldots, v_n\}$ be a set of real numbers, then $\mathrm{diag}(v_1, v_2, \ldots, v_n)$ denotes the $n \times n$ diagonal matrix with the entries $v_1, v_2, \ldots, v_n$ on the diagonal and likewise $\mathrm{col}(v_1, v_2, \ldots, v_n)$ denotes the column vector with the entries $v_1, v_2, \ldots, v_n$. Let $f : \mathbb{R}^n \to \mathbb{R}$ be a twice differentiable function, then $\nabla f(x)$ denotes the gradient of f evaluated at x and $\nabla^2 f(x)$ denotes the Hessian of f evaluated at x. Given a symmetric matrix $A \in \mathbb{R}^{n \times n}$, we write $A > 0$ ($A \geq 0$) to indicate that A is a positive (semi-)definite matrix.

Power network

We consider a power grid consisting of n buses. The network is represented by a connected and undirected graph $\mathcal{G} = (\mathcal{V}, \mathcal{E})$, where the set of nodes, $\mathcal{V} = \{1, \ldots, n\}$, is the set of buses representing the synchronous machines and the set of edges, $\mathcal{E} \subset \mathcal{V} \times \mathcal{V}$, is the set of transmission lines connecting the buses where each edge $\{i, j\} \in \mathcal{E}$ is an unordered pair of two vertices $i, j \in \mathcal{V}$. Given a node i, then the set of neigboring nodes is denoted by $\mathcal{N}_i := \{j \mid \{i, j\}) \in \mathcal{E}\}$. Let m denote the

number of edges, arbitrarily labeled with a unique identifier in $\{1, \ldots, m\}$. For a complete list of symbols used in the power network model, we refer to the list of symbols of this thesis.

2.2.2 The $dq0$-transformation

An important coordinate transformation used in the literature on power systems is the $dq0$-transformation [37, 67] or *Park transformation* [79] which is defined by

$$T_{dq0}(\gamma) = \sqrt{\frac{3}{2}} \begin{bmatrix} \cos(\gamma) & \cos(\gamma - \frac{2\pi}{3}) & \cos(\gamma + \frac{2\pi}{3}) \\ \sin(\gamma) & \sin(\gamma - \frac{2\pi}{3}) & \sin(\gamma + \frac{2\pi}{3}) \\ \frac{1}{\sqrt{2}} & \frac{1}{\sqrt{2}} & \frac{1}{\sqrt{2}} \end{bmatrix}. \tag{2.1}$$

Observe that the mapping (2.1) is orthogonal, i.e., $T_{dq0}^{-1}(\gamma) = T_{dq0}^{T}(\gamma)$. The $dq0$-transformation offers various advantages when analyzing power system dynamics and is therefore widely used in applications. In particular, the $dq0$-transformation maps *symmetric* or *balanced* three-phase AC signals (see [90, Section 2] for the definition) to constant signals. This significantly simplifies the modeling and analysis of power systems, which is the main reason why the transformation (2.1) is used in the present case. In addition, the transformation (2.1) exploits the fact that, in a power system operated under symmetric conditions, a three-phase signal can be represented by two quantities [90].

For example, for a synchronous machine with AC voltage given by $V^{\mathrm{ABC}} = \mathrm{col}(V^A, V^B, V^C)$ in the static ABC-reference frame, see Figure 2.1, the $dq0$-transformation is used to map this AC voltage to the (local) $dq0$-coordinates as $V^{dq0} = \mathrm{col}(V_d, V_q, V_0) = T_{dq0}(\gamma)V^{\mathrm{ABC}}$. Note that the local $dq0$-reference is aligned with the rotor of the machine which has angle γ with respect to the static ABC-reference frame, see again Figure 2.1. In case more that one synchronous machine is considered, then the voltage V^{dq0^j} in local $dq0$-coordinates of machine j can be expressed in the local $dq0$-coordinates of machine i as

$$V^{dq0^i} = T_{dq0}(\gamma_i)V^{ABC^i} = T_{dq0}(\gamma_i)V^{ABC^j} = T_{dq0}(\gamma_i)T_{dq0}(\gamma_j)^T V^{dq0^j}. \tag{2.2}$$

An analogous expression can be obtained for relation between the currents I^{dq0^i}, and I^{dq0^j}. Here we can verify that

$$T_{dq0}(\gamma_i)T_{dq0}(\gamma_j)^T = \begin{bmatrix} \cos\gamma_{ij} & -\sin\gamma_{ij} & 0 \\ \sin\gamma_{ij} & \cos\gamma_{ij} & 0 \\ 0 & 0 & 1 \end{bmatrix}$$

where $\gamma_{ij} := \gamma_i - \gamma_j$ represents the rotor angle difference between synchronous machines i and j respectively.

2.2.3 Phasor notation

When considering operation around the synchronous frequency, the voltages and currents can be represented as phasors in the dq-coordinates rotating at the

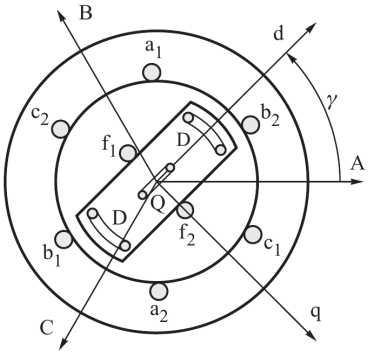

Figure 2.1: Schematic illustration of a (salient-pole) synchronous machine [67].

synchronous frequency. We use the following notation for the phasor[1] [67]:

$$\overline{V} = \sqrt{V_q^2 + V_d^2}\exp\left(\mathrm{j}\arctan\left(\frac{V_d}{V_q}\right)\right) = \overline{V}_q + \overline{V}_d = V_q + \mathrm{j}V_d,$$
$$\overline{I} = \sqrt{I_q^2 + I_d^2}\exp\left(\mathrm{j}\arctan\left(\frac{I_d}{I_q}\right)\right) = \overline{I}_q + \overline{I}_d = I_q + \mathrm{j}I_d,$$

which is commonly used in the power system literature [67, 90]. Here the bar-notation is used to represent the complex phasor and we define $\overline{V}_q = V_q, \overline{V}_d = \mathrm{j}V_d$ and likewise $\overline{I}_q = I_q, \overline{I}_d = \mathrm{j}I_d$ for the currents. In this notation, the mapping between the voltages (and current) from one dq-reference frame to another is given by

$$\begin{aligned}\overline{V}^{dq^i} &= e^{-\mathrm{j}\gamma_{ij}}\overline{V}^{dq^j} = (\cos\gamma_{ij} - \mathrm{j}\sin\gamma_{ij})(V_q^{dq^j} + \mathrm{j}V_d^{dq^j}) \\ &= V_q^{dq^j}\cos\gamma_{ij} + V_d^{dq^j}\sin\gamma_{ij} + \mathrm{j}(V_d^{dq^j}\cos\gamma_{ij} - V_q^{dq^j}\sin\gamma_{ij}).\end{aligned} \tag{2.3}$$

By equating the real and imaginary parts, this exactly corresponds to the transformation (2.2) as expected.

2.3 Full-order model of the synchronous machine

A synchronous machine is a multi-physics system characterized by both mechanical and electrical variables, i.e., an electromechanical system. Derived from physical first-principles laws, the dynamics can be described in terms of certain specific physical quantities such as the magnetic flux, voltages, angles, momenta and torques. The complete model can be described by a system of ordinary differential equations (ODE's) where the flux-current relations are represented by algebraic constraints. The generator rotor circuit is formed by a field circuit and three amortisseur circuits, which is divided in one d-axis circuit and two q-axis circuits.

[1] This is in contrast to [61, 89] where the convention $\overline{V} = V_d + \mathrm{j}V_q$ is used.

The stator is formed by 3-phase windings which are spatially distributed in order to generate 3-phase voltages at machine terminals. For convenience magnetic saturation effects are neglected in the model of the synchronous machine. After applying the $dq0$-transformation $T_{dq0}(\gamma)$ on the ABC-variables with respect to the rotor angle γ, its dynamics in the $dq0$-reference frame is governed by the following 9th-order system of differential equations [37, 61, 67][2]:

$$\dot{\Psi}_d = -RI_d - \Psi_q\omega - V_d \tag{2.4a}$$
$$\dot{\Psi}_q = -RI_q + \Psi_d\omega - V_q \tag{2.4b}$$
$$\dot{\Psi}_0 = -RI_0 - V_0 \tag{2.4c}$$
$$\dot{\Psi}_f = -R_f I_f + V_f \tag{2.4d}$$
$$\dot{\Psi}_g = -R_g I_g \tag{2.4e}$$
$$\dot{\Psi}_D = -R_D I_D \tag{2.4f}$$
$$\dot{\Psi}_Q = -R_Q I_Q \tag{2.4g}$$
$$\dot{\gamma} = \omega \tag{2.4h}$$
$$J\dot{\omega} = \Psi_q I_d - \Psi_d I_q - d\omega + \tau. \tag{2.4i}$$

Here V_d, V_q, V_0 are instantaneous external voltages, τ is the external mechanical torque and V_f is the excitation voltage. The rotor angle γ, governed by (2.4h), is taken with respect to the static ABC-reference frame, see also Figure 2.1. The quantities Ψ_d, Ψ_q, Ψ_0 are stator winding flux linkages and $\Psi_f, \Psi_g, \Psi_D, \Psi_Q$ are the rotor flux linkages respectively and are related to the currents as [67]

$$\begin{bmatrix} \Psi_d \\ \Psi_f \\ \Psi_D \end{bmatrix} = \overbrace{\begin{bmatrix} L_d & \kappa M_f & \kappa M_D \\ \kappa M_f & L_f & L_{fD} \\ \kappa M_D & L_{fD} & L_D \end{bmatrix}}^{\mathcal{L}_d} \begin{bmatrix} I_d \\ I_f \\ I_D \end{bmatrix} \tag{2.5}$$

$$\begin{bmatrix} \Psi_q \\ \Psi_g \\ \Psi_Q \end{bmatrix} = \underbrace{\begin{bmatrix} L_q & \kappa M_g & \kappa M_Q \\ \kappa M_g & L_g & L_{gQ} \\ \kappa M_Q & L_{gQ} & L_Q \end{bmatrix}}_{\mathcal{L}_q} \begin{bmatrix} I_q \\ I_g \\ I_Q \end{bmatrix} \tag{2.6}$$

$$\Psi_0 = L_0 I_0, \tag{2.7}$$

where $\kappa = \sqrt{\frac{3}{2}}$, see also the list of symbols at the start of this thesis. Note that in the $dq0$-coordinates, the inductor equations can be split up in each of the three axes, resulting into the three completely independent equations (2.5)-(2.7). For a physically relevant model, the inductance matrices $\mathcal{L}_d, \mathcal{L}_q \in \mathbb{R}^{3\times 3}$ are assumed to be positive definite. An immediate observation from (2.4c) and (2.7) is that the dynamics associated to the 0-axis is fully decoupled from the rest of the system. Therefore, without loss of generality, we omit this differential equation in the sequel and focus solely on the dynamics in the d- and q-axes.

[2]See in particular [67, Chapter 11] for a detailed derivation of the model (2.4).

Remark 2.3.1 (Additional damper winding). Many generators, and in particular turbogenerators, have a solid-steel rotor body which acts as a screen in the q-axis [67]. It is convenient to represent this by the additional winding in the q-axis represented by the symbol g, see (2.4e). However, for salient-pole synchronous generators, this winding is absent. For completeness, both cases are considered in this chapter.

2.3.1 Port-Hamiltonian representation

Inspired by the work [37], it can be shown that full-order model (2.4) admits a port-Hamiltonian representation, see [117] for a survey. More specifically, by defining the state vector $x = (\Psi_d, \Psi_q, \Psi_f, \Psi_g, \Psi_D, \Psi_Q, \gamma, p), p = J\omega$, the dq-dynamics of a single synchronous machine can be written in port-Hamiltonian form as

$$\begin{bmatrix} \dot{\Psi}_d \\ \dot{\Psi}_q \\ \dot{\Psi}_f \\ \dot{\Psi}_g \\ \dot{\Psi}_D \\ \dot{\Psi}_Q \\ \dot{\gamma} \\ \dot{p} \end{bmatrix} = \begin{bmatrix} -R & 0 & 0 & 0 & 0 & 0 & 0 & -\Psi_q \\ 0 & -R & 0 & 0 & 0 & 0 & 0 & \Psi_d \\ 0 & 0 & -R_f & 0 & 0 & 0 & 0 & 0 \\ 0 & 0 & 0 & -R_g & 0 & 0 & 0 & 0 \\ 0 & 0 & 0 & 0 & -R_D & 0 & 0 & 0 \\ 0 & 0 & 0 & 0 & 0 & -R_Q & 0 & 0 \\ 0 & 0 & 0 & 0 & 0 & 0 & 0 & 1 \\ \Psi_q & -\Psi_d & 0 & 0 & 0 & 0 & -1 & -d \end{bmatrix} \nabla H(x) + Gu$$

$$y = G^T \nabla H(x) = \begin{bmatrix} I_d \\ I_q \\ I_f \\ \omega \end{bmatrix}, \quad G^T = \begin{bmatrix} 1 & 0 & 0 & 0 & 0 & 0 & 0 & 0 \\ 0 & 1 & 0 & 0 & 0 & 0 & 0 & 0 \\ 0 & 0 & 1 & 0 & 0 & 0 & 0 & 0 \\ 0 & 0 & 0 & 0 & 0 & 0 & 0 & 1 \end{bmatrix}, \quad u = \begin{bmatrix} V_d \\ V_q \\ V_f \\ \tau \end{bmatrix}. \tag{2.8}$$

where the Hamiltonian is given by the sum of the electrical and mechanical energy:

$$H(x) = H_d(x) + H_q(x) + H_m(x) = \frac{1}{2} \begin{bmatrix} \Psi_d \\ \Psi_f \\ \Psi_D \end{bmatrix}^T \begin{bmatrix} L_d & \kappa M_f & \kappa M_D \\ \kappa M_f & L_f & L_{fD} \\ \kappa M_D & L_{fD} & L_D \end{bmatrix}^{-1} \begin{bmatrix} \Psi_d \\ \Psi_f \\ \Psi_D \end{bmatrix}$$
$$+ \frac{1}{2} \begin{bmatrix} \Psi_q \\ \Psi_g \\ \Psi_Q \end{bmatrix}^T \begin{bmatrix} L_q & \kappa M_g & \kappa M_Q \\ \kappa M_g & L_g & L_{gQ} \\ \kappa M_Q & L_{gQ} & L_Q \end{bmatrix}^{-1} \begin{bmatrix} \Psi_q \\ \Psi_g \\ \Psi_Q \end{bmatrix} + \frac{1}{2} J^{-1} p^2.$$

Here the power-pairs $(V_d, I_d), (V_q, I_q)$ correspond to the external electrical power supplied by the generator. In addition, the power-pair (V_f, I_f) corresponds to the power supplied by the exciter to the synchronous machine. Finally, the pair (τ, ω) is associated with the mechanical power injected into the synchronous machine. As noted from the port-Hamiltonian structure of the system (2.8), it naturally follows that the system is *passive* with respect to the previously mentioned input/output pairs, i.e.,

$$\dot{H} \leq V_d I_d + V_q I_q + V_f I_f + \tau\omega.$$

A crucial observation is that the interconnection structure of the port-Hamiltonian system (2.8) depends on the state x. This property significantly increases the complexity of a Lyapunov-based stability analysis of equilibria that are different from the origin, see [21, 37, 70, 119] for more details on this challenge.

2.4 Model reduction of the synchronous machine

To simplify the analysis of (networked) synchronous machines, it is preferable to consider reduced-order models with decreasing complexity [61, 67, 89]. In this section we, following the exposition of [67], discuss briefly how several well-known lower order models are obtained from the first-principles model (2.4). In each reduction step the underlying assumptions and validity of the reduced-order model is discussed.

The main assumptions rely on time-scale separation implying that singular perturbation techniques can be used to obtain reduced-order models [1]. In particular, in the initial reduction step, this allows the stator windings of the synchronous machine to be considered in quasi steady state. In [59] this quasi steady state assumption is validated by the use of iterative time-scale separation. In doing so, it is assumed that the frequency is around the synchronous frequency[3] ω_s and that $\dot{\Psi}_d, \dot{\Psi}_q$ are assumed to be small [67].

Assumption 2.4.1 (Operation around $\omega \approx \omega_s$)**.** The synchronous machine is operating around synchronous frequency ($\omega \approx \omega_s$) and in addition $\dot{\Psi}_d$ and $\dot{\Psi}_q$ are small compared to $-\omega\Psi_q$ and $\omega\Psi_d$ which implies

$$\begin{bmatrix} V_d \\ V_q \end{bmatrix} \approx -\begin{bmatrix} R & 0 \\ 0 & R \end{bmatrix} \begin{bmatrix} I_d \\ I_q \end{bmatrix} + \omega_s \begin{bmatrix} -\Psi_q \\ \Psi_d \end{bmatrix}. \tag{2.9}$$

Remark 2.4.2 (Singular perturbation process). It is known that during transients Ψ_d, Ψ_q oscillate with high frequency equal to $\omega \approx \omega_s$ implying that $\dot{\Psi}_d, \dot{\Psi}_q$ become very large. The validation of the contradicting Assumption 2.4.1 is part of a singular perturbation process where the slow variables are approximated by taking the averaging effect of the fast oscillatory variables Ψ_d, Ψ_q, see also [1, 59].

By Assumption 2.4.1, the two differential equations (2.4a), (2.4b) corresponding to Ψ_d, Ψ_q are replaced by algebraic equations (2.9), so that a system of differential-algebraic equations (DAE's) is obtained [67]. For many power system studies it is desirable to rephrase and further simplify the model (2.4d)-(2.4h) together with the algebraic equations (2.9) so that they are in a more acceptable form and easier to interface to the power system network equations. In the following sections, under some additional assumptions based on time-scale separation, we eliminate the two algebraic constraints obtained by putting an equality in (2.9). Before examining how this is done, it is necessary to relate the circuit equations to the flux conditions inside the synchronous machine when it is in the steady state, transient state or the subtransient state.

[3] For example, in Europe the synchronous frequency is 50 Hz and in the United States it is 60 Hz.

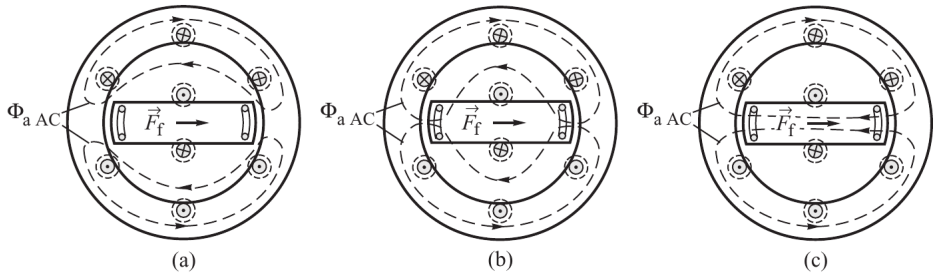

Figure 2.2: The path of the armature flux in: (a) the subtransient state (screening effect of the damper windings and the field winding); (b) the transient state (screening effect of the field and g-damper winding only); (c) the steady state [67].

2.4.1 Distinction of operation states

Following the established literature on power systems [4, 61, 67, 89], a distinction between 3 different operation states of the synchronous machine is made. Each of the 3 characteristic operation states correspond to different stages of rotor screening and a different time-scale [1, 59], see Figure 2.2.

Immediately after a fault, the current induced in both the rotor field and damper windings forces the armature reaction flux completely out of the rotor to keep the rotor flux linkages constant (this is also referred to as the *Lenz effect*), see Figure 2.2a, and the generator is said to be in the *subtransient state* [61, 67].

As energy is dissipated in the resistance of the rotor windings, the currents maintaining constant rotor flux linkages decay with time allowing flux to enter the windings. As for typical generators the rotor DQ-damper winding resistances are the largest, the DQ-damper currents are the first to decay, allowing the armature flux to enter the rotor pole face. However, it is still forced out of the field winding and the g-damper winding itself, see Figure 2.2b. Then the generator is said to be in the *transient state*.

The field and g-winding currents then decay with time to their steady state values allowing the armature reaction flux eventually to enter the whole rotor and assume the minimum reluctance path. Then the generator is in *steady state* as illustrated in Figure 2.2c [67].

Remark 2.4.3 (Properties of the g-damper winding). Since the field winding and g-damper winding resistances are comparable and are typically much smaller compared to the DQ-damper winding resistances, the field winding f and the g-damper winding have similar properties in the different operation states.

Synchronous machine parameters

Depending on which state the synchronous machine is operating in, the effective impedance of the armature coil to any current change will depend on the parameters of the different circuits, their mutual coupling and whether or not the circuits are closed or not [67]. The (positive scalar) inductances and timescales associated

with transient and subtransient operation are defined by [67]

$$
\begin{aligned}
L'_d &= L_d - \frac{\kappa^2 M_f^2}{L_f}, \qquad T'_{do} = \frac{L_f}{R_f}, \\
L'_q &= L_q - \frac{\kappa^2 M_g^2}{L_g}, \qquad T'_{qo} = \frac{L_g}{R_g}, \\
L''_d &= L_d - \kappa^2 \left[\frac{M_f^2 L_D + M_D^2 L_f - 2 M_f M_D L_{fD}}{L_f L_D - L_{fD}^2} \right], \\
L''_q &= L_q - \kappa^2 \left[\frac{M_g^2 L_Q + M_Q^2 L_g - 2 M_g M_Q L_{gQ}}{L_g L_Q - L_{gQ}^2} \right], \\
T''_{do} &= \frac{1}{R_D} \left(L_D - \frac{L_{fD}^2}{L_f} \right), \quad T''_{qo} = \frac{1}{R_Q} \left(L_Q - \frac{L_{gQ}^2}{L_g} \right).
\end{aligned}
\tag{2.10}
$$

Based on the two-reaction theory of [79], the corresponding d- and q-axis reactances for steady state operation ($X_d = \omega_s L_d, X_q = \omega_s L_q$), transient operation ($X'_d = \omega_s L'_d, X'_q = \omega_s L'_q$) and subtransient operation ($X''_d = \omega_s L''_d, X''_q = \omega_s L''_q$) are defined.

Remark 2.4.4 (Relation between (sub)transient reactances). For realistic synchronous machines it holds that $X_d > X'_d > X''_d > 0$ and $X_q \geq X'_q > X''_q > 0$, where $X_q = X'_q$ holds only for a salient-pole synchronous machine (where the g-damper winding is absent), see also [67, Table 4.3] and [61, Table 4.2] for typical values of these reactances.

Definition 2.4.5 (Saliency)**.** The *(sub)transient saliency* is defined as the difference between the (sub)transient reactances, i.e. $X'_d - X'_q; (X''_d - X''_q)$. We say that the (sub)transient saliency is negligible if $X'_d = X'_q; (X''_d = X''_q)$.

For both transient and subtransient state of the machine, different assumptions can be made to obtain the corresponding (differential) equations of the synchronous machine.

2.4.2 Synchronous machine equations

Transient operation

In transient operation state the armature flux has penetrated the damper circuits and the field and g windings screen the rotor body from the armature flux. The damper windings are no more effective ($\dot{\Psi}_D = \dot{\Psi}_Q = 0$) and thus the damper currents are zero.

Assumption 2.4.6 (Transient operation)**.** During transient operation $I_D = I_Q = 0$.

From (2.5), Ψ_d can be expressed in terms of I_d, Ψ_f from which it follows that the internal (transient) and external emfs are related by

$$\begin{aligned} V_q &= -RI_q + \omega_s \left[I_d \left(L_d - \frac{\kappa^2 M_f^2}{L_f} \right) + \frac{\kappa M_f}{L_f} \Psi_f \right] \\ &= -RI_q + \omega_s L'_d I_d + E'_q = -RI_q + X'_d I_d + E'_q \end{aligned} \tag{2.11}$$

where the internal emf E'_q is defined by $E'_q := \omega_s \left(\frac{\kappa M_f}{L_f} \right) \Psi_f$. Similarly, from (2.6) we can express Ψ_q in terms of I_q, Ψ_g to obtain

$$V_d = -RI_d - X'_q I_q + E'_d \tag{2.12}$$

where $E'_d := -\omega_s \left(\frac{\kappa M_g}{L_g} \right) \Psi_g$. However, the flux linkages Ψ_f, Ψ_g do not remain constant during transient operation but change slowly as the armature flux penetrates through the windings [67]. By substituting (2.4d), the differential equation for E'_q is derived as

$$\begin{aligned} \dot{E}'_q &= \omega_s \frac{\kappa M_f}{L_f} \dot{\Psi}_f = \omega_s \frac{\kappa M_f}{L_f} (V_f - R_f I_f) = \omega_s \frac{\kappa M_f}{L_f} (V_f + R_f \frac{\kappa M_f I_d}{L_f}) - \frac{R_f}{L_f} E'_q \\ &= \frac{E_f + (X_d - X'_d) I_d - E'_q}{T'_{do}}, \end{aligned} \tag{2.13}$$

where we used that $I_D = 0$, $T'_{do} = L_f / R_f$, and the definition $E_f := \omega_s \kappa M_f V_f / R_f$ for the scaled excitation voltage. In a similar fashion the differential equation of E'_q is derived to obtain

$$\dot{E}'_d = \frac{-(X_q - X'_q) I_q - E'_d}{T'_{qo}}. \tag{2.14}$$

Subtransient operation

During the subtransient period the rotor damper coils screens both the field winding and the rotor body from changes in the armature flux. The field and g flux linkages Ψ_f, Ψ_g remain constant during this period while the damper winding flux linkages decay with time as the generator moves towards the transient state [67]. Therefore, we make here a different assumption compared to Section 2.4.2.

Assumption 2.4.7 (Subtransient operation)**.** During subtransient operation the flux linkages Ψ_f, Ψ_g are constant.

Using equation (2.5) one can express Ψ_d in terms of i_d, Ψ_f, Ψ_D to obtain [67]

$$\begin{aligned} &\Psi_d = L''_d I_d + k_1 \Psi_f + k_2 \Psi_D, \\ &k_1 = \kappa \cdot \frac{M_f L_D - M_D L_{fD}}{L_f L_D - L_{fD}^2}, \quad k_2 = \kappa \cdot \frac{M_D L_f - M_f L_{fD}}{L_f L_D - L_{fD}^2}. \end{aligned}$$

Together with Assumption 2.4.1 this implies

$$\begin{aligned} V_q &= -RI_q + \omega_s \Psi_d = -RI_q + \omega_s L''_d I_d + \omega_s k_1 \Psi_f + \omega_s k_2 \Psi_D \\ &= -RI_q + X''_d I_d + E''_q \end{aligned} \tag{2.15}$$

where $E''_q := \omega_s(k_1\Psi_f + k_2\Psi_D)$. Similarly for the q-axis we obtain

$$\begin{aligned} \Psi_q &= L''_q I_q + k_3 \Psi_g + k_4 \Psi_Q, \\ k_3 &= \kappa \cdot \frac{M_g L_Q - M_Q L_{gQ}}{L_g L_Q - L_{gQ}^2}, \quad k_4 = \kappa \cdot \frac{M_Q L_g - M_g L_{gQ}}{L_g L_Q - L_{gQ}^2} \end{aligned}$$

and

$$\begin{aligned} V_d &= -RI_q - \omega_s \Psi_q = -RI_d - \omega_s L''_q I_q - \omega_s k_3 \Psi_g - \omega_s k_4 \Psi_Q \\ &= -RI_d - X''_q I_q + E''_d \end{aligned} \tag{2.16}$$

where $E''_d := -\omega_s(k_3\Psi_g + k_4\Psi_Q)$. By eliminating the I_f, Ψ_d from (2.5) and I_g, Ψ_q from (2.6) we obtain respectively

$$\begin{aligned} I_D &= \frac{\kappa L_{fD} M_f I_d - \kappa L_f M_D I_d - L_{fD} \Psi_f + L_f \Psi_D}{L_D L_f - L_{fD}^2} \\ I_Q &= \frac{\kappa L_{gQ} M_g I_q - \kappa L_g M_Q I_q - L_{gQ} \Psi_g + L_g \Psi_Q}{L_Q L_g - L_{gQ}^2}. \end{aligned}$$

Using Assumption 2.4.7 we find that

$$\dot{E}''_q = \omega_s k_2 \dot{\Psi}_D = -\omega_s k_2 R_D I_D, \qquad \dot{E}''_d = -\omega_s k_4 \dot{\Psi}_Q = \omega_s k_4 R_Q I_Q, \tag{2.17}$$

which can be rewritten as

$$T''_{do} \dot{E}''_q = E'_q - E''_q + (X'_d - X''_d) I_d, \tag{2.18}$$

$$T''_{qo} \dot{E}''_d = E'_d - E''_d - (X'_q - X''_q) I_q. \tag{2.19}$$

Frequency dynamics

Recall that the frequency dynamics of the full-order model is described by (2.4i):

$$J\dot{\omega} = \Psi_q I_d - \Psi_d I_q - d\omega + \tau.$$

By Assumption 2.4.1, the latter differential equation is rewritten as

$$J\dot{\omega} = -\frac{1}{\omega_s}\left(V_d I_d + V_q I_q + R(I_d^2 + I_q^2)\right) - d\omega + \tau.$$

Since the mechanical damping force $F_d = -d\omega$ is often very small in large machines, it is neglected in many synchronous machine models [61, 67].

Assumption 2.4.8 (Negligible mechanical damping)**.** The mechanical damping of the synchronous machine is negligible, i.e., $d = 0$.

It is convenient to express the frequency dynamics in terms of the *frequency deviation* with respect to the synchronous frequency ω_s. By Assumption 2.4.8, the frequency deviation $\Delta\omega := \omega - \omega_s$ is governed by the differential equation

$$J\Delta\dot{\omega} = -\frac{1}{\omega_s}\left(V_d I_d + V_q I_q + R(I_d^2 + I_q^2)\right) + \tau. \tag{2.20}$$

After multiplying (2.20) by the synchronous frequency ω_s one obtains

$$M\Delta\dot{\omega} = -\left(V_d I_d + V_q I_q + R(I_d^2 + I_q^2)\right) + \omega_s\tau = -P_e + P_m, \tag{2.21}$$

where it is common practice to define the quantity $M := \omega_s J$ [61, 67]. Here the mechanical power injection is denoted by $P_m = \omega_s\tau$ and the electrical power P_e produced by the synchronous generator is equal to

$$P_e = V_d I_d + V_q I_q + R(I_d^2 + I_q^2).$$

Remark 2.4.9 (Alternative formulation of frequency dynamics). Note that by equations (2.15) and (2.16) the electrical power P_e produced by the synchronous generator alternatively takes the form

$$P_e = E_d'' I_d + E_q'' I_q + (X_d'' - X_q'')I_d I_q \tag{2.22}$$

such that the differential equation (2.21) can be rewritten as

$$M\Delta\dot{\omega} = -E_d'' I_d - E_q'' I_q - (X_d'' - X_q'')I_d I_q + P_m. \tag{2.23}$$

2.4.3 Synchronous machine models

Based on the results established in Section 2.4.2, several generator models with decreasing complexity and accuracy are developed. In each model reduction step, the validity and assumptions made in the corresponding model are discussed.

Sixth-order model

By combining the equations derived in Section 2.4.2, a sixth-order model describing the synchronous generator is obtained. In particular, by (2.13), (2.14), (2.18), (2.19) and (2.23) we obtain the following system of ordinary differential equations

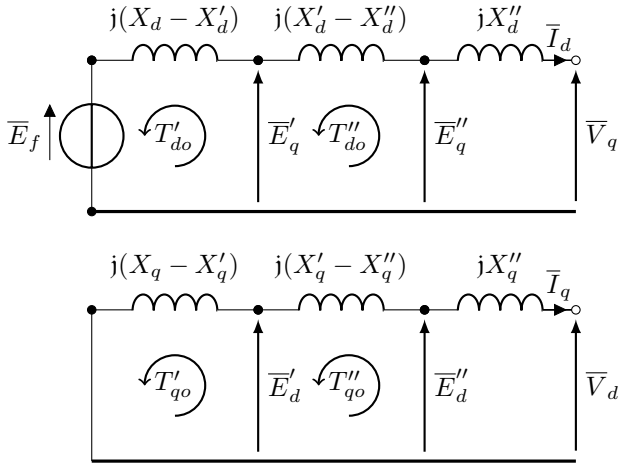

Figure 2.3: The generator equivalent circuits for both dq-axes in case the stator winding resistance R is neglected [67].

describing the generator dynamics [67]:

$$\dot{\delta} = \Delta\omega \tag{2.24a}$$
$$M\Delta\dot{\omega} = P_m - E''_d I_d - E''_q I_q - (X''_d - X''_q) I_d I_q \tag{2.24b}$$
$$T'_{do}\dot{E}'_q = E_f - E'_q + I_d(X_d - X'_d) \tag{2.24c}$$
$$T'_{qo}\dot{E}'_d = -E'_d - I_q(X_q - X'_q) \tag{2.24d}$$
$$T''_{do}\dot{E}''_q = E'_q - E''_q + I_d(X'_d - X''_d) \tag{2.24e}$$
$$T''_{qo}\dot{E}''_d = E'_d - E''_d - I_q(X'_q - X''_q), \tag{2.24f}$$

where $\delta(t) := \gamma(t) - \omega_s t$ represents the rotor angle with respect to the synchronous rotating reference frame. By equations (2.15) and (2.16) the internal and external voltages of the synchronous generator are related by

$$\begin{bmatrix} V_d \\ V_q \end{bmatrix} = \begin{bmatrix} E''_d \\ E''_q \end{bmatrix} - \begin{bmatrix} R & X''_q \\ -X''_d & R \end{bmatrix} \begin{bmatrix} I_d \\ I_q \end{bmatrix}. \tag{2.25}$$

It is worth noting the similar structure of these (differential) equations. The equation (2.25) and the right hand side of (2.24c)-(2.24f) relates to the equivalent d- or q-axis generator circuits, with the resistances neglected, as shown in Figure 2.3. In particular, the algebraic equation (2.25) corresponds to the right-hand side of Figure 2.3. In addition, the subtransient dynamics (2.24e), (2.24f) corresponds to the center reactances $X'_d - X''_d$, $X'_q - X''_q$ illustrated in Figure 2.3 and the transient dynamics (2.24c), (2.24d) corresponds to the left-hand side of Figure 2.3. Observe that there is no additional voltage in the q-axis due to the absence of a field winding on this axis.

Fifth-order model

In a salient-pole generator the laminated rotor construction prevent eddy currents flowing in the rotor body such that there is no screening in the q-axis implying that $X_q = X'_q$ [67]. In that case the g-winding is absent in the full-order model (2.4). Consequently, E'_d is absent so that the fifth-order model becomes

$$\begin{aligned}
\dot{\delta} &= \Delta\omega \\
M\Delta\dot{\omega} &= P_m - E''_d I_d - E''_q I_q - (X''_d - X''_q) I_d I_q \\
T'_{do}\dot{E}'_q &= E_f - E'_q + I_d(X_d - X'_d) \\
T''_{do}\dot{E}''_q &= E'_q - E''_q + I_d(X'_d - X''_d) \\
T''_{qo}\dot{E}''_d &= -E''_d - I_q(X'_q - X''_q).
\end{aligned} \tag{2.26}$$

Fourth-order model

In this model the subtransient dynamics of the sixth-order model induced by the damper windings is neglected. This is motivated by the fact that $T''_{do} \ll T'_{do}, T''_{qo} \ll T'_{qo}$. Therefore the dynamics corresponding with E''_q, E''_d is at much faster time scale compared to the E'_q, E'_d dynamics. As a result, at the slower time-scale we obtain the quasi steady state condition [1]:

$$\begin{aligned}
E''_q &= E'_q + I_d(X'_d - X''_d) \\
E''_d &= E'_d - I_q(X'_q - X''_q).
\end{aligned} \tag{2.27}$$

Substitution of the latter algebraic equations in the remaining four differential equations yields the fourth-order model

$$\begin{aligned}
\dot{\delta} &= \Delta\omega \\
M\Delta\dot{\omega} &= P_m - D\Delta\omega - E'_d I_d - E'_q I_q - (X'_d - X'_q) I_d I_q \\
T'_{do}\dot{E}'_q &= E_f - E'_q + I_d(X_d - X'_d) \\
T'_{qo}\dot{E}'_d &= -E'_d - I_q(X_q - X'_q).
\end{aligned} \tag{2.28}$$

Remark 2.4.10 (Transient operation). Note that (2.27) together with (2.25) also implies (2.11) and (2.12) as expected since the subtransient dynamics is neglected.

As the damper windings are ignored, the air-gap power appearing in the frequency dynamics neglects the asynchronous torque produced by the damper windings. To compensate the effects of the damper windings a linear asynchronous damping power $D\Delta\omega$ with damping constant $D > 0$ is introduced [67]. However, more accurate nonlinear approximations of the damping power exist as well, see [67, Chapter 5.2].

Third-order model

Starting from the fourth-order model, we make here the same assumptions as done in the transition from the sixth-order model to the fifth-order model ($E'_d = 0$) so

that the third-order model, which also referred to as the *flux-decay model* or *one-axis model* [61], is given by

$$\dot{\delta} = \Delta\omega \tag{2.29a}$$
$$M\Delta\dot{\omega} = -D\Delta\omega + P_m - E'_q I_q - (X'_d - X'_q) I_d I_q \tag{2.29b}$$
$$T'_{do}\dot{E}'_q = E_f - E'_q + I_d(X_d - X'_d). \tag{2.29c}$$

Second-order classical model

The second-order model is derived from the fourth-order (or third-order) model by assuming that the internal emfs E'_q, E'_d are constant [4, 61, 67]. This can be validated if the timescales T'_{qo}, T'_{do} are large (of the order of a few seconds) so that the internal emfs E'_q, E'_d can be approximated by a constant (on a bounded time interval) provided that E_f, I_d, I_q do not change much. From this assumption, a constant voltage behind transient reactance model is obtained which is commonly referred to as the *constant flux linkage model* or *classical model* [4, 61, 67]:

$$\begin{aligned} \dot{\delta} &= \Delta\omega \\ M\Delta\dot{\omega} &= -D\Delta\omega + P_m - E'_q I_q - E'_d I_d - (X'_d - X'_q) I_d I_q \end{aligned} \tag{2.30}$$

The assumption that the changes in dq-currents and the internal emfs are small implies that only generators located a long way from the point of the disturbance should be represented by the classical model [67]. In addition, since the assumption that E'_d, E'_q are constant is only valid on a limited time-interval, the classical model is only valid for analyzing the *first swing stability* [4]. Indeed, in for example [22] it was shown that the second-order swing equations (2.30) are not valid for asymptotic stability analyses.

2.5 Multi-machine models

To obtain a representation of the power grid, we consider a multi-machine network. For simplicity we consider the case that each node in the network represents a synchronous machine, that is, each node represents either a synchronous generator, or a synchronous motor. In addition, we assume that the stator winding resistances and the resistances in the network are negligible. This assumption is valid for networks with high voltage transmission lines where the line resistances are negligible.

Assumption 2.5.1 (Inductive lines)**.** The network is considered to be purely inductive and the stator winding resistances are negligible, i.e., $R = 0$.

In this section the multi-machine models starting from the sixth-, third-, and second-order models for the synchronous generator are established. The derivations of the fourth- and fifth-order multi-machine models are omitted as these are very similar to ones presented in this section. To obtain reduced-order multi-machine models, the equations for the nodal currents in the network are

derived which are then substituted in the single generator models reformulated in Section 2.4.3.

2.5.1 Sixth-order multi-machine model

For the sixth (and fifth) order model(s) it is convenient to make the following assumption which is valid for synchronous generators with damper windings in both d- and q-axes [67].

Assumption 2.5.2 ($X''_{di} = X''_{qi}$)**.** For each synchronous machine in the network, the subtransient saliency is negligible, i.e., $X''_{di} = X''_{qi} \ \ \forall i \in \mathcal{V}$.

By Assumption 2.5.2, the second term of the electrical power (2.22) appearing in the frequency dynamics (2.24b) vanishes. Moreover, the assumption of $X''_d = X''_q$ allows the two individual d- and q-axis circuits in Figure 2.3 to be replaced by one equivalent circuit, see Figure 2.4. As a result, all the voltages, emfs and currents are phasors in the synchronous rotating reference frame of rather than their components resolved along the d- and q-axes. An important advantage of this is that the generator reactance may be treated in a similar way as the reactance of a transmission line, as we will show later. This has particular importance for multi-machine systems when combining the algebraic equations describing the generators and the network [67].

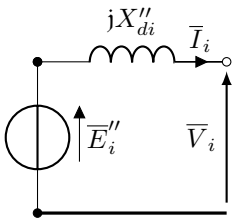

Figure 2.4: Subtransient emf behind a subtransient reactance.

As illustrated in Figure 2.4, the internal and external voltages are related to each other by

$$\overline{E}''_i = \overline{V}_i + \mathrm{j}X''_{di}\overline{I}_i, \qquad \forall i \in \mathcal{V}. \tag{2.31}$$

Consider a power network where each node $i \in \mathcal{V} = \{1, 2, \ldots, n\}$ represents a synchronous machine and each edge $\{i, j\} \in \mathcal{E}$ a transmission line, see Figure 2.5 for a two-node case. To derive the algebraic equations associated with the network, we assume that the network operates at steady state. Under this assumption, the network equations take the form

$$\overline{I}_s = Y\overline{V}_s = \mathcal{Y}\overline{E}''_s$$

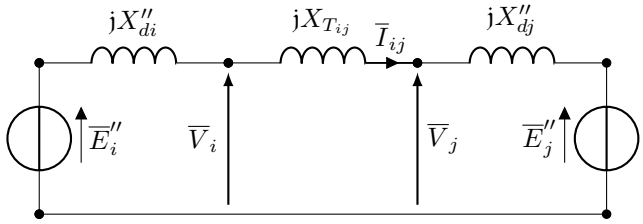

Figure 2.5: Interconnection of two synchronous machines governed by the 5th or 6th order model by a purely inductive transmission line with reactance $X_{T_{ij}}$.

where $\overline{I}_s, \overline{V}_s, \overline{E}''_s \in \mathbb{C}^n$ represent the nodal current and external/internal voltage phasors with respect to the synchronous rotating reference frame and $Y \in \mathbb{C}^{n\times n}$ is the admittance matrix of the network. The admittance matrix $\mathcal{Y} \in \mathbb{C}^{n\times n}$ is obtained by adding the reactances $X''_{di}, i \in \mathcal{V}$ to the transmission line reactances, i.e., $\mathcal{Y}$ takes the form $\mathcal{Y}_{ii} = G_{ii} - \mathrm{j}B_{ii}, \mathcal{Y}_{ij} = -G_{ij} + \mathrm{j}B_{ij}, i \neq j$ where B_{ij} is defined as[4] are given by [90]

$$\begin{aligned} B_{ij} &= \begin{cases} 0 & \text{if nodes } i \text{ and } j \text{ are not connected} \\ \frac{1}{X_{ij}} & \text{if nodes } i \text{ and } j \text{ are connected} \end{cases} \\ B_{ii} &= \sum_{j\in\mathcal{N}_i} B_{ij} \end{aligned} \tag{2.32}$$

and where $X_{ij} := X_{T_{ij}} + X''_{di} + X''_{dj}$ is the total reactance between the subtransient voltage sources as illustrated in Figure 2.5. As we assumed purely inductive lines, see Assumption 2.5.1, the conductance matrix equals the zero matrix and thus $G_{ij} = 0\ \forall i, j \in \mathcal{V}$. We note that in the derivations in Section 2.4 the currents $\overline{I} = V_q + \mathrm{j}V_d$ and internal voltages $\overline{E}'' = E''_q + \mathrm{j}E''_d$ are expressed with respect to the *local* $dq0$-reference frame of the synchronous machine. Thus, according to (2.3), $\overline{I}_s = \mathrm{diag}(e^{-\mathrm{j}(\omega_s t - \gamma_i)})\overline{I} = \mathrm{diag}(e^{\mathrm{j}\delta_i})\overline{I}$ and similarly $\overline{E}''_s = \mathrm{diag}(e^{\mathrm{j}\delta_i})\overline{E}''$. Consequently,

$$\overline{I} = \mathrm{diag}(e^{-\mathrm{j}\delta_i})\mathcal{Y}\,\mathrm{diag}(e^{\mathrm{j}\delta_i})\overline{E}'', \tag{2.33}$$

where $\overline{I} = \mathrm{col}(\overline{I}_1, \ldots, \overline{I}_n), \overline{E}'' = \mathrm{col}(\overline{E}''_1, \ldots, \overline{E}''_n)$. Then the dq-current phasor at node i takes the form

$$\overline{I}_i = \mathcal{Y}_{ii}\overline{E}''_i + \sum_{j\in\mathcal{N}_i} \mathcal{Y}_{ij} e^{-\mathrm{j}\delta_{ij}} \overline{E}''_j. \tag{2.34}$$

[4]Note that we use a different sign convention than used in [90], which is consistent with the rest of this thesis. With this sign convention, $B_{ii}, B_{ij} \geq 0$ are the negatives of the susceptances.

Using the phasor representation $\overline{E}_i'' = E_{qi}'' + \mathrm{j}E_{di}'', \overline{I}_i = I_{qi} + \mathrm{j}I_{di}$, and equating both the real and imaginary part of equation (2.34), we obtain after rewriting

$$\begin{aligned} I_{di} &= -B_{ii}E_{qi}'' + \sum_{j\in\mathcal{N}_i}\left[B_{ij}(E_{dj}''\sin\delta_{ij} + E_{qj}''\cos\delta_{ij})\right], \\ I_{qi} &= B_{ii}E_{di}'' + \sum_{j\in\mathcal{N}_i}\left[B_{ij}(E_{qj}''\sin\delta_{ij} - E_{dj}''\cos\delta_{ij})\right]. \end{aligned} \tag{2.35}$$

Remark 2.5.3 (Nonzero transfer conductances). Compared to (2.35), a slightly more complicated expression for the *dq*-currents can be derived in the more general case where the transfer conductances are nonzero, see e.g. [90].

By substituting the network equations (2.35) into the sixth-order model of the synchronous machine derived in Section 2.4.3, the multi-machine model (2.36) is obtained. A subscript i is added to the model (2.24) to indicate that this is the model of synchronous machine $i \in \mathcal{V}$.

$$\begin{aligned} \dot{\delta}_i &= \Delta\omega_i \\ M_i\Delta\dot{\omega}_i &= P_{mi} - \sum_{j\in\mathcal{N}_i} B_{ij}\Big[(E_{di}''E_{dj}'' + E_{qi}''E_{qj}'')\sin\delta_{ij} + (E_{di}''E_{qj}'' - E_{qi}''E_{dj}'')\cos\delta_{ij}\Big] \\ T_{doi}'\dot{E}_{qi}' &= E_{fi} - E_{qi}' - (X_{di} - X_{di}')(B_{ii}E_{qi}'' - \sum_{j\in\mathcal{N}_i}\left[B_{ij}(E_{dj}''\sin\delta_{ij} + E_{qj}''\cos\delta_{ij})\right]) \\ T_{qoi}'\dot{E}_{di}' &= -E_{di}' - (X_{qi} - X_{qi}')(B_{ii}E_{di}'' - \sum_{j\in\mathcal{N}_i}\left[B_{ij}(E_{dj}''\cos\delta_{ij} - E_{qj}''\sin\delta_{ij})\right]) \\ T_{doi}''\dot{E}_{qi}'' &= E_{qi}' - E_{qi}'' - (X_{di}' - X_{di}'')(B_{ii}E_{qi}'' - \sum_{j\in\mathcal{N}_i}\left[B_{ij}(E_{dj}''\sin\delta_{ij} + E_{qj}''\cos\delta_{ij})\right]) \\ T_{qoi}''\dot{E}_{di}'' &= E_{di}' - E_{di}'' - (X_{qi}' - X_{qi}'')(B_{ii}E_{di}'' - \sum_{j\in\mathcal{N}_i}\left[B_{ij}(E_{dj}''\cos\delta_{ij} - E_{qj}''\sin\delta_{ij})\right]) \end{aligned} \tag{2.36}$$

The electrical power P_{ei} produced by synchronous machine i is obtained from (2.22) and (2.35), and is given by

$$\begin{aligned} P_{ei} &= E_{di}''I_{di} + E_{qi}''I_{qi} \\ &= \sum_{j\in\mathcal{N}_i} \underbrace{B_{ij}\Big[(E_{di}''E_{dj}'' + E_{qi}''E_{qj}'')\sin\delta_{ij} + (E_{di}''E_{qj}'' - E_{qi}''E_{dj}'')\cos\delta_{ij}\Big]}_{P_{ij}}. \end{aligned} \tag{2.37}$$

Remark 2.5.4 (Energy conservation). Since the transmission lines are purely inductive by assumption, there are no energy losses in the transmission lines implying that the following energy conservation law holds: $P_{ij} = -P_{ji}$ where P_{ij} given in (2.37) represents the power transmission from node i to node j. In particular, we also have $\sum_{i\in\mathcal{V}} P_{ei} = 0$ with P_{ei} is given by (2.37).

Remark 2.5.5 (Including resistances). While in the above model the resistances of the network and the stator windings are neglected, the model easily extends to

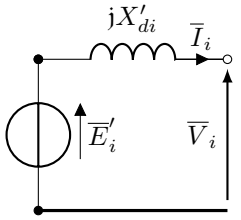

Figure 2.6: Single generator equivalent circuit in case the transient saliency is neglected [67]

the case of nonzero resistances. This can be done following the same procedure as before but instead substituting the more complicated expression for the currents I_{di}, I_{qi}, see Remark 2.5.3.

2.5.2 Third-order multi-machine model

The derivation of the third-order multi-machine models proceeds along the same lines as for the sixth-order model. For similar reasons as for the sixth- and fifth-order models, it is convenient for the 2nd, 3rd and 4th order multi-machine models to assume that the transient saliency is negligible.

Assumption 2.5.6 ($X'_{di} = X'_{qi}$)**.** The transient saliency is negligible: $X'_{di} = X'_{qi} \quad \forall i \in \mathcal{V}$.

By making the *classical assumption* that $X'_d = X'_q$, the second term of the electrical power appearing in the frequency dynamics (2.29b) vanishes [67]. In addition, the assumption of $X'_d = X'_q$ allows the separate d and q-axis circuits shown in Figure 2.3 to be replaced by one simple equivalent circuit, see Figure 2.6, representing a transient voltage source behind a transient reactance.

Remark 2.5.7 (Negligible transient saliency). Although there is always some degree of transient saliency implying that $X'_{di} \neq X'_{qi}$, it should be noted that if the network reactances are relatively large, then the effect of the transient saliency on the power network dynamics is negligible making Assumption 2.5.6 acceptable [67].

Similar as before, the interconnection of two synchronous machines can be represented as in Figure 2.7. As illustrated in this figure, the internal and external voltages are related to each other by [67]

$$\overline{E}'_i = \overline{V}_i + \mathrm{j}X'_{di}\overline{I}_i, \qquad \forall i \in \mathcal{V}. \tag{2.38}$$

The algebraic equations associated with the network amount to [90]

$$\overline{I} = \mathrm{diag}(e^{-\mathrm{j}\delta_i})\mathcal{Y}\,\mathrm{diag}(e^{\mathrm{j}\delta_i})\overline{E}', \tag{2.39}$$

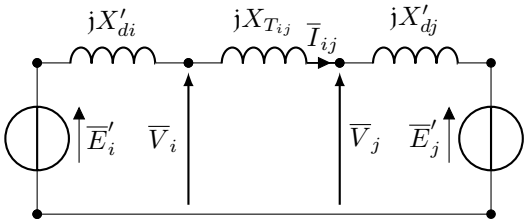

Figure 2.7: Interconnection of two synchronous machines governed by the 2nd, 3rd or 4th order model by a purely inductive transmission line with reactance $X_{T_{ij}}$.

resulting in a similar expression for the dq-currents as for the sixth-order model:

$$\begin{aligned} I_{di} &= -B_{ii}E'_{qi} + \sum_{j\in\mathcal{N}_i}\left[B_{ij}(E'_{dj}\sin\delta_{ij} + E'_{qj}\cos\delta_{ij})\right], \\ I_{qi} &= B_{ii}E'_{di} + \sum_{j\in\mathcal{N}_i}\left[B_{ij}(E'_{qj}\sin\delta_{ij} - E'_{dj}\cos\delta_{ij})\right]. \end{aligned} \tag{2.40}$$

By using the third-order model of the synchronous machine (2.29), the network equations (2.40), and the fact that that $E'_{di} = 0$ for the third-order model, the flux-decay (or one-axis) multi-machine model is obtained.

$$\begin{aligned} \dot{\delta}_i &= \Delta\omega_i \\ M_i\Delta\dot{\omega}_i &= P_{mi} - D_i\Delta\omega_i - \sum_{j\in\mathcal{N}_i} B_{ij}E'_{qi}E'_{qj}\sin\delta_{ij} \\ T'_{doi}\dot{E}'_{qi} &= E_{fi} - E'_{qi} - (X_{di} - X'_{di})(B_{ii}E'_{qi} - \sum_{j\in\mathcal{N}_i} B_{ij}E'_{qj}\cos\delta_{ij})) \end{aligned} \tag{2.41}$$

It is observed that, similar as for the sixth-order multi-machine model (2.36), Remark 2.5.4 and Remark 2.5.5 also hold for the third-order model (2.41).

2.5.3 The classical multi-machine network

The derivation of the classical second-order swing equations takes a slightly different approach compared to the multi-machine models obtained previously. For completeness, the derivation of the second-order multi-machine model with RL-transmission lines is given in this section.

Suppose that Assumption 2.5.6 holds. Let the transient voltage phasor be represented as $\overline{E}'_i = e^{\mathrm{j}\alpha_i}|\overline{E}'_i|$, then by (2.39) we have

$$\overline{I}_i = \mathcal{Y}_{ii}e^{\mathrm{j}\alpha_i}|\overline{E}'_i| + \sum_{j\in\mathcal{N}_i}\mathcal{Y}_{ij}e^{-\mathrm{j}\delta_{ij}}e^{\mathrm{j}\alpha_j}|\overline{E}'_j|, \qquad \forall i\in\mathcal{V}.$$

By defining the angles[5] $\theta_i := \delta_i + \alpha_i$ it can be shown that the electrical power supplied by the synchronous machine amounts to

$$\begin{aligned} P_{ei} &= \Re(\overline{E}_i' \overline{I}_i^*) = \Re(\overline{E}_i'^* \overline{I}_i) = \Re\Big(\mathcal{Y}_{ii}|\overline{E}_i'|^2 + \sum_{j\in\mathcal{N}_i} \mathcal{Y}_{ij} e^{-\mathrm{j}(\delta_{ij}+\alpha_{ij})} |\overline{E}_i'||\overline{E}_j'|\Big) \\ &= G_{ii}|\overline{E}_i'|^2 - \sum_{j\in\mathcal{N}_i} (G_{ij}\cos\theta_{ij} - B_{ij}\sin\theta_{ij})|\overline{E}_i'||\overline{E}_j'|. \end{aligned}$$

It is convenient to express the system dynamics in terms of the voltage angles θ_i. By noting that α_i is constant[6] it follows that $\dot{\theta}_i = \dot{\delta}_i = \Delta\omega_i$. Hence, the multi-machine classical model with nonzero transfer conductances is described by

$$\begin{aligned} \dot{\theta}_i &= \Delta\omega_i \\ M_i\Delta\dot{\omega}_i &= -D_i\Delta\omega_i + P_{mi} - G_{ii}|\overline{E}_i'|^2 \\ &\quad + \sum_{j\in\mathcal{N}_i} (G_{ij}\cos\theta_{ij} - B_{ij}\sin\theta_{ij})|\overline{E}_i'||\overline{E}_j'|, \qquad i \in \mathcal{V}. \end{aligned} \tag{2.42}$$

Remark 2.5.8 (Purely inductive network). Note that in a purely inductive network $G = 0$ and $B_{ij} \leq 0$ for all i, j. The resulting multi-machine network, commonly referred to as the *swing equations*, is often used in power network stability studies, see e.g. [19, 64, 105, 131].

Remark 2.5.9 (Load nodes). In the multi-machine models constructed in this section it is assumed that each node in the network represents a synchronous machine. However, a more realistic model of a power network can be obtained by making a distinction between generator and load nodes [3, 10]. This is beyond the scope of the present chapter. Instead, we assume that some synchronous machines act as *synchronous motors* for which the injected mechanical power is *negative*.

2.6 Energy functions

When analyzing the stability of a synchronous machine (or a multi-machine network) it is desired to search for a suitable Lyapunov function. Often the physical energy stored in the system can be used as a Lyapunov function for the zero-input case. In this section we derive the energy functions of the reduced order models of the synchronous machine. In addition, the energy functions corresponding to the transmission lines are obtained.

2.6.1 Synchronous machine

The physical energy stored in a synchronous machine consists of both an electrical part and a mechanical part. We first derive the electrical energy of the synchronous

[5] Note that the angle θ_i represents the *voltage angle* of generator i with respect to the synchronous rotating reference frame.

[6] Note that for the third-order model $\alpha_i = 0$ implying that in this case θ_i is equal to the rotor angle δ_i with respect to the synchronous rotating reference frame.

machine. For notational convenience the subscript i for synchronous machine $i \in \mathcal{V}$ is dropped.

Electrical energy

In this section we search for an expression for the electrical energy of the reduced order models for the synchronous machine. A natural starting point is to look at the electrical energy of the full-order system and rewrite this in terms of the state variables of the reduced order system. Recall that the electrical energy in the d- and q-axis of the full-order system is respectively given by[7]

$$H_{dq} = H_d + H_q = \frac{1}{2}\begin{bmatrix}\Psi_d\\ \Psi_f\\ \Psi_D\end{bmatrix}^T \begin{bmatrix} L_d & \kappa M_f & \kappa M_D\\ \kappa M_f & L_f & L_{fD}\\ \kappa M_D & L_{fD} & L_D\end{bmatrix}^{-1} \begin{bmatrix}\Psi_d\\ \Psi_f\\ \Psi_D\end{bmatrix} + \frac{1}{2}\begin{bmatrix}\Psi_q\\ \Psi_g\\ \Psi_Q\end{bmatrix}^T \begin{bmatrix} L_q & \kappa M_g & \kappa M_Q\\ \kappa M_g & L_g & L_{gQ}\\ \kappa M_Q & L_{gQ} & L_Q\end{bmatrix}^{-1} \begin{bmatrix}\Psi_q\\ \Psi_g\\ \Psi_Q\end{bmatrix}.$$

Using the definitions of E'_q, E''_q and the reactances X_d, X'_d, X''_d we can express the electrical energy in the d-axis as

$$H_d = \frac{1}{2}\begin{bmatrix}\Psi_d\\ E'_q\\ E''_q\end{bmatrix}^T \begin{bmatrix} \frac{\omega_s}{X''_d} & 0 & -\frac{1}{X''_d}\\ 0 & \frac{1}{\omega_s(X_d - X'_d)} + \frac{1}{\omega_s(X'_d - X''_d)} & -\frac{1}{\omega_s(X'_d - X''_d)}\\ -\frac{1}{X''_d} & -\frac{1}{\omega_s(X'_d - X''_d)} & \frac{X'_d}{\omega_s(X'_d - X''_d)X''_d}\end{bmatrix} \begin{bmatrix}\Psi_d\\ E'_q\\ E''_q\end{bmatrix} \tag{2.43}$$

and a similar expression for the energy H_q can be derived for the q-axis.

Remark 2.6.1 (Complexity in derivating (2.43)). To obtain (2.43) requires not only computing the inverse of the inductance matrices $\mathcal{L}_d, \mathcal{L}_q$ but also to eliminate the appropriate parameters and variables used in the model (2.4). Interestingly, we obtain the relatively sparse expression (2.43) where we verified the correctness by the computer algebra program Mathematica 11.

Sixth-order model We can also express the electrical energy (2.43) in term of the currents I_d, I_q as follows. First, by Assumption 2.4.1 we eliminate Ψ_d, Ψ_q by substituting $\Psi_q = -\omega_s^{-1}(V_d + RI_d), \Psi_d = \omega_s^{-1}(V_q + RI_q)$. Then V_d, V_q can be eliminated by substituting (2.25), that is, $V_d = E''_d - RI_d - X''_q I_q, V_q = E''_q - RI_q + X''_d I_d$. Consequently, for the sixth-order model the electrical energy stored in the machine given by (2.43) takes the alternative form

$$H_d = \frac{1}{2\omega_s}\begin{bmatrix}I_d\\ E'_q\\ E''_q\end{bmatrix}^T \begin{bmatrix} X''_d & 0 & 0\\ 0 & \frac{1}{X_d - X'_d} + \frac{1}{X'_d - X''_d} & -\frac{1}{X'_d - X''_d}\\ 0 & -\frac{1}{X'_d - X''_d} & \frac{1}{X'_d - X''_d}\end{bmatrix} \begin{bmatrix}I_d\\ E'_q\\ E''_q\end{bmatrix}, \tag{2.44}$$

[7] For notational convenience the subscript i is omitted in this section.

which interestingly is even simpler than (2.43). As before, a similar expression is obtained for the q-axis by exchanging the dq-subscripts.

Remark 2.6.2 (Energy storage in generator circuits). One interesting observation is that (2.44) is identical to the energy stored in the generator equivalent circuits illustrated in Figure 2.3 in the zero input case ($E_f = 0$). Here we observe that the energy stored in the center reactances as in Figure 2.3 is given by

$$\begin{aligned}\frac{1}{2}LI_d^2 &= \frac{1}{2\omega_s}(X'_d - X''_d)I_d^2 = \frac{1}{2\omega_s}(X'_d - X''_d)(\frac{1}{X'_d - X''_d}(E'_q - E''_q))^2 \\ &= \frac{1}{2\omega_s}\frac{1}{X'_d - X''_d}\begin{bmatrix}E'_q & E''_q\end{bmatrix}\begin{bmatrix}1 & -1\\ -1 & 1\end{bmatrix}\begin{bmatrix}E'_q\\ E''_q\end{bmatrix}.\end{aligned} \tag{2.45}$$

Fifth-order model For the fifth-order model we have that $E'_d = 0$ implying that the electrical energy in the q-axis modifies to

$$H_q = \frac{1}{2\omega_s}\begin{bmatrix}I_q\\ E''_d\end{bmatrix}^T\begin{bmatrix}X''_q & 0\\ 0 & \frac{1}{X'_q - X''_q}\end{bmatrix}\begin{bmatrix}I_q\\ E''_d\end{bmatrix}, \tag{2.46}$$

while the expression for H_d remains identical to the one for the sixth-order model, see equation (2.44).

Lower-order models Since for the fourth, third and second-order model the subtransient dynamics is neglected, we can substitute (2.27) into (2.44) such that the electrical energy $H_{dq} := H_d + H_q$ can be written as

$$H_{dq} = \frac{1}{2\omega_s}\begin{bmatrix}I_d\\ E'_q\end{bmatrix}^T\begin{bmatrix}X'_d & 0\\ 0 & \frac{1}{X_d - X'_d}\end{bmatrix}\begin{bmatrix}I_d\\ E'_q\end{bmatrix} + \frac{1}{2\omega_s}\begin{bmatrix}I_q\\ E'_d\end{bmatrix}^T\begin{bmatrix}X'_q & 0\\ 0 & \frac{1}{X_q - X'_q}\end{bmatrix}\begin{bmatrix}I_q\\ E'_d\end{bmatrix} \tag{2.47}$$

and for the third-order model we have $E'_d = 0$.

Remark 2.6.3 (Synchronous machines reactances as part of line reactances). If the (sub)transient saliency is neglected then the reactance X'_d (X''_d) can considered as part the (transmission) network, see Section 2.5. Therefore, the energy stored in this reactance will be part of the energy stored in the transmission lines which will be discussed in Section 2.6.2. As a result, the part of the energy (2.47) corresponding with I_d, I_q can be disregarded here. For example, for the fourth-, third- and second-order model the energy function associated to the electrical energy stored in the generator circuit is given by

$$H_{dq} = \frac{1}{2\omega_s}\frac{(E'_q)^2}{X_d - X'_d} + \frac{1}{2\omega_s}\frac{(E'_d)^2}{X_q - X'_q}, \tag{2.48}$$

where $E'_d = 0$ for the third-order model.

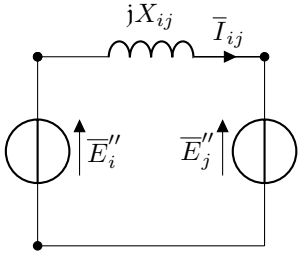

Figure 2.8: An inductive transmission line at steady state. The internal voltages $\overline{E}_i'', \overline{E}_j''$ are expressed in the corresponding local $dq0$-reference frame.

Bearing in mind Remark 2.6.3 and noting that for the second-order model the voltages E_q', E_d' are constant, it follows that the electrical energy (2.48) is constant as well.

Mechanical energy

The rotational kinetic energy of the synchronous machine is given by

$$H_m = \frac{1}{2} J\omega^2 = \frac{1}{2\omega_s} M(\Delta\omega + \omega_s)^2 \tag{2.49}$$

where we recall that M is defined as $M = \omega_s J$ as discussed in Section 2.4.2.

2.6.2 Inductive transmission lines

Sixth- and fifth-order models

Consider an inductive transmission line between nodes i and j at steady state, see Figure 2.8. When expressed in the local dq-reference frame of synchronous machine i, we observe from Figure 2.8 that

$$\mathrm{j}X_{ij}\overline{I}_{ij} = \overline{E}_i'' - e^{-\mathrm{j}\delta_{ij}}\overline{E}_j''. \tag{2.50}$$

By equating the real and imaginary part of (2.50) we obtain

$$X_{ij}\begin{bmatrix} I_{qij} \\ -I_{dij} \end{bmatrix} = \begin{bmatrix} E_{di}'' - E_{dj}'' \cos\delta_{ij} + E_{qj}'' \sin\delta_{ij} \\ E_{qi}'' - E_{dj}'' \sin\delta_{ij} - E_{qj}'' \cos\delta_{ij} \end{bmatrix}. \tag{2.51}$$

Note that the energy of the inductive transmission line between nodes i and j is given by

$$H_{ij} = \frac{1}{2} L_{ij} \overline{I}_{ij}^* \overline{I}_{ij} = \frac{X_{ij}}{2\omega_s}(I_{dij}^2 + I_{qij}^2)$$

which by (2.51) can be written as

$$\begin{aligned} H_{ij} =& \frac{B_{ij}}{\omega_s}\Big[\left(E''_{di}E''_{qj} - E''_{dj}E''_{qi}\right)\sin\delta_{ij} - \left(E''_{di}E''_{dj} + E''_{qi}E''_{qj}\right)\cos\delta_{ij} \\ &+ \tfrac{1}{2}E''^2_{di} + \tfrac{1}{2}E''^2_{dj} + \tfrac{1}{2}E''^2_{qi} + \tfrac{1}{2}E''^2_{qj}\Big] \end{aligned} \tag{2.52}$$

where $B_{ij} = \frac{1}{X_{ij}} < 0$ is the negative of the susceptance of transmission line $\{i,j\} \in \mathcal{E}$ [90].

Fourth- and third-order models

For the fourth- and third-order model the transient reactances[8] X'_{di} can be considered as part of the network implying that the energy in the transmission lines can be obtained by replacing the subtransient voltages by the transient voltages in (2.52). For the third-order model $E'_{di} = 0$ for all $i \in \mathcal{V}$ so that the energy function associated to the transmission line between node i and j simplifies to

$$H_{ij} = \frac{B_{ij}}{\omega_s}\left(\tfrac{1}{2}E'^2_{qi} + \tfrac{1}{2}E'^2_{qj} - E'_{qi}E'_{qj}\cos\delta_{ij}\right). \tag{2.53}$$

Second-order model

For the second-order model it is convenient to represent transient voltages as $\overline{E}'_i = |\overline{E}'_i|e^{\mathrm{j}\alpha_i}$ where α_i is the voltage angle of $\overline{E}'_i$ with respect to the rotor angle. Then, by defining the voltages angles $\theta_i = \delta_i + \alpha_i$ as in Section 2.5.3, the energy in the transmission line[9] (2.52) takes the much simpler form

$$\begin{aligned} H_{ij} &= \frac{B_{ij}}{2\omega_s}(\overline{E}'_i - \overline{E}'_j e^{-\mathrm{j}\delta_{ij}})^*(\overline{E}'_i - \overline{E}'_j e^{-\mathrm{j}\delta_{ij}}) \\ &= \frac{B_{ij}}{2\omega_s}(|\overline{E}'_i|^2 - 2|\overline{E}'_i||\overline{E}'_j|\cos\theta_{ij} + |\overline{E}'_j|^2). \end{aligned} \tag{2.54}$$

2.6.3 Total energy

The total energy of the multi-machine system is equal to the sum of the previously mentioned energy functions

$$H = \sum_{i\in\mathcal{V}}(H_{di} + H_{qi} + H_{mi}) + \sum_{\{i,j\}\in\mathcal{E}} H_{ij}, \tag{2.55}$$

where the expressions for each individual energy function depends on the order of the model. The resulting energy function H could serve as a candidate Lyaponuv function for the stability analysis of the multi-machine power network (with zero inputs).

[8] Provided that the transient saliency is neglected, i.e., $X'_{di} = X'_{qi}$ for all $i \in \mathcal{V}$.

[9] Where the subtransient voltages are replaced by the transient voltages.

Remark 2.6.4 (Common factor ω_s^{-1} in energy function). It is observed that each of the individual energy functions appearing in (2.55) contains a factor ω_s^{-1}. Therefore, a modified version of the energy function defined by $U = \omega_s H$ can also be used as a Lyapunov function for the multi-machine system. However, the function U does not have the dimension of energy anymore, but has the dimension of power instead. In fact, in most of the literature these modified energy functions[10] (without the factor ω_s^{-1}) are (part of) the collection of Lyapunov functions used to analyze the stability of the power network, see e.g. [64, 77, 105, 113, 131, 132].

2.7 Port-Hamiltonian framework

By using the energy function established in the previous section, a convenient representation of the multi-machine models of Section 2.5 can be obtained. This is based on the theory of port-Hamiltonian systems, which yields a systematic framework for network modeling of multi-physics systems. In particular, we show in this section that the complex multi-machine systems (2.36), (2.41), (2.42) admit a simple port-Hamiltonian representation. Finally, some important passivity properties are proven for the resulting systems.

2.7.1 Sixth-order model

Energy in the transmission lines

Recall from (2.52) that the energy stored in the inductive transmission line between node i and j is given by

$$\begin{aligned} H_{ij} = \frac{B_{ij}}{\omega_s}\Big[&\left(E''_{di}E''_{qj} - E''_{dj}E''_{qi}\right)\sin\delta_{ij} - \left(E''_{di}E''_{dj} + E''_{qi}E''_{qj}\right)\cos\delta_{ij} \\ &+ \tfrac{1}{2}E''^2_{di} + \tfrac{1}{2}E''^2_{dj} + \tfrac{1}{2}E''^2_{qi} + \tfrac{1}{2}E''^2_{qj}\Big] \end{aligned} \tag{2.56}$$

where $B_{ij} = \frac{1}{X_{ij}} > 0$. Observe that the gradient of H_{ij} takes the form

$$\begin{bmatrix} \frac{\partial H_{ij}}{\partial \delta_i} \\ \frac{\partial H_{ij}}{\partial E''_{qi}} \\ \frac{\partial H_{ij}}{\partial E''_{di}} \end{bmatrix} = -\frac{B_{ij}}{\omega_s} \begin{bmatrix} (E''_{qi}E''_{dj} - E''_{di}E''_{qj})\cos\delta_{ij} - (E''_{di}E''_{dj} + E''_{qi}E''_{qj})\sin\delta_{ij} \\ -E''_{qi} + E''_{qj}\cos\delta_{ij} - E''_{dj}\sin\delta_{ij} \\ -E''_{di} + E''_{dj}\cos\delta_{ij} + E''_{qj}\sin\delta_{ij} \end{bmatrix}.$$

[10] Which are sometimes incorrectly called *energy functions* as well.

After defining the total energy stored in the transmission lines by $H_T = \sum_{\{i,j\}\in\mathcal{E}} H_{ij}$, we obtain likewise

$$\begin{bmatrix} \frac{\partial H_T}{\partial \delta_i} \\ \frac{\partial H_T}{\partial E''_{qi}} \\ \frac{\partial H_T}{\partial E''_{di}} \end{bmatrix} = -\frac{1}{\omega_s} \begin{bmatrix} \sum_{j\in\mathcal{N}_i} B_{ij}[(E''_{qi}E''_{dj} - E''_{di}E''_{qj})\cos\delta_{ij} - (E''_{di}E''_{dj} + E''_{qi}E''_{qj})\sin\delta_{ij}] \\ -B_{ii}E''_{qi} + \sum_{j\in\mathcal{N}_i} B_{ij}(E''_{qj}\cos\delta_{ij} + E''_{dj}\sin\delta_{ij}) \\ -B_{ii}E''_{di} + \sum_{j\in\mathcal{N}_i} B_{ij}(E''_{dj}\cos\delta_{ij} + E''_{qj}\sin\delta_{ij}) \end{bmatrix}$$
$$= \frac{1}{\omega_s} \begin{bmatrix} P_{ei} \\ -I_{di} \\ I_{qi} \end{bmatrix}$$

where we have used the fact that $B_{ii} = \sum_{j\in\mathcal{N}_i} B_{ij}$ and equations (2.35), (2.37).

Electrical energy synchronous machine

Further notice that the electrical energy stored in the d-axis in machine i is given by

$$H_{di} = \frac{1}{2\omega_s} \begin{bmatrix} E'_{qi} & E''_{qi} \end{bmatrix} \begin{bmatrix} \frac{1}{X_{di}-X'_{di}} + \frac{1}{X'_{di}-X''_{di}} & -\frac{1}{X'_{di}-X''_{di}} \\ -\frac{1}{X'_{di}-X''_{di}} & \frac{1}{X'_{di}-X''_{di}} \end{bmatrix} \begin{bmatrix} E'_{qi} \\ E''_{qi} \end{bmatrix}$$

and satisfies

$$\begin{bmatrix} X_{di} - X'_{di} & X_{di} - X'_{di} \end{bmatrix} \begin{bmatrix} \frac{\partial H_{di}}{\partial E'_{qi}} \\ \frac{\partial H_{di}}{\partial E''_{qi}} \end{bmatrix} = \frac{1}{\omega_s} E'_{qi}$$
$$\begin{bmatrix} 0 & X'_{di} - X''_{di} \end{bmatrix} \begin{bmatrix} \frac{\partial H_{di}}{\partial E'_{qi}} \\ \frac{\partial H_{di}}{\partial E''_{qi}} \end{bmatrix} = \frac{1}{\omega_s}(E''_{qi} - E'_{qi}).$$

Observe that a similar result can be established for the energy function H_{qi} by exchanging the d- and q-subscripts.

Mechanical energy

To obtain a port-Hamiltonian representation of the multi-machine models, it is convenient to shift the (kinetic) energy function (2.49) with respect to the synchronous frequency to obtain

$$\bar{H}_{mi} = \frac{1}{2} J_i \Delta\omega_i^2 = \frac{1}{2\omega_s} M_i \Delta\omega_i^2 = \frac{1}{2\omega_s} M_i^{-1} \mathtt{p}_i^2,$$

where $M_i = \omega_s J_i$ and we define the variable $\mathtt{p}_i = M_i \Delta\omega_i$.

Remark 2.7.1 (Modified 'moment of inertia'). Note that the quantity $\mathtt{p}_i$ does not represent the angular momentum of the synchronous machine but instead it is equal to $\mathtt{p}_i = \omega_s J \Delta\omega_i$ so it has a different physical dimension. In addition, it is shifted with respect to the synchronous frequency.

Using this definition of the Hamiltonian $\bar{H}_{mi}(\mathtt{p}_i)$, it follows that its gradient satisfies

$$\frac{\partial \bar{H}_{mi}}{\partial \mathtt{p}_i}(\mathtt{p}_i) = \frac{1}{\omega_s} M_i^{-1} \mathtt{p}_i = \frac{\Delta\omega_i}{\omega_s}.$$

Port-Hamiltonian representation

By the previous observations, the dynamics of a single synchronous machine in a multi-machine system (2.36) can be written in the form

$$\begin{aligned}
\begin{bmatrix} \dot{\delta}_i \\ \dot{\mathtt{p}}_i \\ \dot{E}'_{qi} \\ \dot{E}'_{di} \\ \dot{E}''_{qi} \\ \dot{E}''_{di} \end{bmatrix} &= \omega_s \begin{bmatrix} 0 & 1 & 0 & 0 & 0 & 0 \\ -1 & 0 & 0 & 0 & 0 & 0 \\ 0 & 0 & -\frac{\hat{X}_{di}}{T'_{doi}} & 0 & -\frac{\hat{X}_{di}}{T'_{doi}} & 0 \\ 0 & 0 & 0 & -\frac{\hat{X}_{qi}}{T'_{qoi}} & 0 & -\frac{\hat{X}_{qi}}{T'_{qoi}} \\ 0 & 0 & 0 & 0 & -\frac{\hat{X}'_{di}}{T''_{doi}} & 0 \\ 0 & 0 & 0 & 0 & 0 & -\frac{\hat{X}'_{qi}}{T''_{qoi}} \end{bmatrix} \nabla_i H + \begin{bmatrix} 0 & 0 \\ 1 & 0 \\ 0 & \frac{1}{T'_{doi}} \\ 0 & 0 \\ 0 & 0 \\ 0 & 0 \end{bmatrix} \begin{bmatrix} P_{mi} \\ E_{fi} \end{bmatrix} \\
y_i &= \begin{bmatrix} 0 & 1 & 0 & 0 & 0 & 0 \\ 0 & 0 & \frac{1}{T'_{doi}} & 0 & 0 & 0 \end{bmatrix} \nabla_i H
\end{aligned} \tag{2.57}$$

where

$$H = \sum_{i \in \mathcal{V}} \Big(\bar{H}_{mi} + H_{di} + H_{qi} \Big) + \sum_{\{i,j\} \in \mathcal{E}} H_{ij}$$

and $\hat{X}_{di} := X_{di} - X'_{di}, \hat{X}'_{di} := X'_{di} - X''_{di}, \hat{X}_{qi} := X_{qi} - X'_{qi}, \hat{X}'_{qi} := X'_{qi} - X''_{qi}$ and $\nabla_i H$ denotes the gradient of H with respect to the variables $\mathrm{col}(\delta_i, \mathtt{p}_i, E'_{qi}, E'_{di}, E''_{qi}, E''_{di})$. By aggregating the states of the synchronous machines, i.e. $\delta = \mathrm{col}(\delta_1, \ldots, \delta_n)$ etc., the multi-machine system is described by

$$\begin{aligned}
\begin{bmatrix} \dot{\delta} \\ \dot{\mathtt{p}} \\ \dot{E}'_q \\ \dot{E}'_d \\ \dot{E}''_q \\ \dot{E}''_d \end{bmatrix} &= \underbrace{\omega_s \begin{bmatrix} 0 & I & 0 & 0 & 0 & 0 \\ -I & 0 & 0 & 0 & 0 & 0 \\ 0 & 0 & -(T'_{do})^{-1}\hat{X}_d & 0 & -(T'_{do})^{-1}\hat{X}_d & 0 \\ 0 & 0 & 0 & -(T'_{qo})^{-1}\hat{X}_q & 0 & -(T'_{qo})^{-1}\hat{X}_q \\ 0 & 0 & 0 & 0 & -(T''_{do})^{-1}\hat{X}'_d & 0 \\ 0 & 0 & 0 & 0 & 0 & -(T''_{qo})^{-1}\hat{X}'_q \end{bmatrix}}_{J-R} \nabla H \\
&\quad + g \begin{bmatrix} P_m \\ E_f \end{bmatrix}, \qquad y = g^T \nabla H, \qquad g = \begin{bmatrix} 0 & I & 0 & 0 & 0 & 0 \\ 0 & 0 & (T'_{do})^{-1} & 0 & 0 & 0 \end{bmatrix}^T,
\end{aligned} \tag{2.58}$$

where $\hat{X}_d = \mathrm{diag}(\hat{X}_{d1}, \ldots, \hat{X}_{dn}), T'_{do} = \mathrm{diag}(T'_{do1}, \ldots, T'_{don})$ and likewise definitions are used for the quantities $\hat{X}'_d, \hat{X}_q, \hat{X}'_q, T'_{qo}, T''_{do}, T''_{qo}$. The matrix $J - R$ depicted in equation (2.58) consists of a skew-symmetric matrix $J = -J^T$ and a symmetric matrix $R = R^T$ often called the *dissipation matrix* [117]. Provided that

dissipation matrix is positive semi-definite, i.e. $R \geq 0$, the system (2.58) is indeed a port-Hamiltonian representation of the sixth-order multi-machine network (2.36).

Proposition 2.7.2 (Positive semi-definite dissipation matrix R)**.** (2.58) *defines a port-Hamiltonian representation of the 6-order multi-machine network* (2.36)*. In particular, the matrix R is positive semi-definite.*

Proof. The dissipation matrix of the system (2.58) is equal to the symmetric part of the matrix in (2.58) and amounts to

$$R = \omega_s \begin{bmatrix} 0 & 0 & 0 & 0 & 0 & 0 \\ 0 & 0 & 0 & 0 & 0 & 0 \\ 0 & 0 & (T'_{do})^{-1}\hat{X}_d & 0 & \frac{1}{2}(T'_{do})^{-1}\hat{X}_d & 0 \\ 0 & 0 & 0 & (T'_{qo})^{-1}\hat{X}_q & 0 & \frac{1}{2}(T'_{qo})^{-1}\hat{X}_q \\ 0 & 0 & \frac{1}{2}(T'_{do})^{-1}\hat{X}_d & 0 & (T''_{do})^{-1}\hat{X}'_d & 0 \\ 0 & 0 & 0 & \frac{1}{2}(T'_{qo})^{-1}\hat{X}_q & 0 & (T''_{qo})^{-1}\hat{X}'_q \end{bmatrix}.$$

By invoking the Schur complement, $R = R^T \geq 0$ if and only if

$$\begin{bmatrix} 2\frac{X_{di}-X'_{di}}{T'_{doi}} & \frac{X_{di}-X'_{di}}{T'_{doi}} \\ \frac{X_{di}-X'_{di}}{T'_{doi}} & 2\frac{X'_{di}-X''_{di}}{T''_{doi}} \end{bmatrix} \geq 0 \quad \text{and} \quad \begin{bmatrix} 2\frac{X_{qi}-X'_{qi}}{T'_{qoi}} & \frac{X_{qi}-X'_{qi}}{T'_{qoi}} \\ \frac{X_{qi}-X'_{qi}}{T'_{qoi}} & 2\frac{X'_{qi}-X''_{qi}}{T''_{qoi}} \end{bmatrix} \geq 0, \quad \forall i \in \mathcal{V},$$

which holds if and only if

$$4(X'_{di} - X''_{di})T'_{doi} - (X_{di} - X'_{di})T''_{doi} \geq 0, \tag{2.59a}$$
$$4(X'_{qi} - X''_{qi})T'_{qoi} - (X_{qi} - X'_{qi})T''_{qoi} \geq 0, \tag{2.59b}$$

holds for all $i \in \mathcal{V}$. By substituting the quantities from (2.10) and simplying the equations using computer algebra program Mathematica 11, we obtain

$$\begin{aligned} &4(X'_{di} - X''_{di})T'_{doi} - (X_{di} - X'_{di})T''_{doi} \\ &\quad = \kappa^2\omega_s \cdot \left.\frac{4L_f^2(L_fM_D - L_{fD}M_f)^2R_D + (L_DL_f - L_{fD}^2)^2M_f^2R_f}{L_f^2(L_DL_f - L_{fD}^2)R_DR_f}\right|_i > 0 \\ &4(X'_{qi} - X''_{qi})T'_{qoi} - (X_{qi} - X'_{qi})T''_{qoi} \\ &\quad = \kappa^2\omega_s \cdot \left.\frac{4L_g^2(L_gM_Q - L_{gQ}M_g)^2R_Q + (L_QL_g - L_{gQ}^2)^2M_g^2R_g}{L_g^2(L_QL_g - L_{gQ}^2)R_QR_g}\right|_i > 0 \end{aligned} \tag{2.60}$$

where by $|_i$ we mean the constants (e.g. L_f, L_g) associated to machine $i \in \mathcal{V}$. We claim that the inequality holds in (2.60). This follows from the fact for a realistic synchronous machine we have that $R_D, R_Q, R_f, R_g, L_f, L_g, L_D, L_Q > 0$ and, since $X_d - X'_d > 0, X_d - X'_d > 0$ (see Remark 2.4.4), we have that $M_f \neq 0, M_g \neq 0$. In addition, $L_DL_f - L_{fD}^2 > 0, L_QL_g - L_{fQ}^2 > 0$ as the inductance matrices $\mathcal{L}_d, \mathcal{L}_q$ defined in (2.5), (2.6) are positive definite. Hence, (2.59) holds in the strict sense and consequently R is positive semi-definite and therefore (2.58) defines a port-Hamiltonian system. □

Remark 2.7.3 (Fifth- and fourth-order models). It can be shown that similar (but slightly simpler) port-Hamiltonian structures appear for the fifth- and fourth-order multi-machine networks using the corresponding (shifted) energy functions derived in Section 2.6 and Section 2.7.1 as the Hamiltonian.

2.7.2 Third-order model

Recall from (2.53) that the energy stored in the inductive transmission line between node i and j is given by

$$H_{ij} = \frac{B_{ij}}{\omega_s}\left(\tfrac{1}{2}E_{qi}'^2 + \tfrac{1}{2}E_{qj}'^2 - E_{qi}'E_{qj}'\cos\delta_{ij}\right). \tag{2.61}$$

Observe that the gradient of H_{ij} is given by

$$\begin{bmatrix} \frac{\partial H_{ij}}{\partial \delta_i} \\ \frac{\partial H_{ij}}{\partial E_{qi}'} \end{bmatrix} = -\frac{B_{ij}}{\omega_s}\begin{bmatrix} -E_{qi}'E_{qj}'\sin\delta_{ij} \\ -E_{qi}' + E_{qj}'\cos\delta_{ij} \end{bmatrix}.$$

Define now the total energy stored in the transmission lines by $H_T = \sum_{\{i,j\}\in\mathcal{E}} H_{ij}$. Then we obtain likewise

$$\begin{bmatrix} \frac{\partial H_T}{\partial \delta_i} \\ \frac{\partial H_T}{\partial E_{qi}'} \end{bmatrix} = -\frac{1}{\omega_s}\begin{bmatrix} \sum_{j\in\mathcal{N}_i} B_{ij} - E_{qi}'E_{qj}'\sin\delta_{ij} \\ -B_{ii}E_{qi}' + \sum_{j\in\mathcal{N}_i} B_{ij}E_{qj}'\cos\delta_{ij} \end{bmatrix} = \frac{1}{\omega_s}\begin{bmatrix} P_{ei} \\ -I_{di} \end{bmatrix}.$$

Further notice that the electrical energy stored in machine i is given by

$$H_{dqi} = \frac{1}{2\omega_s}\frac{(E_{qi}')^2}{X_{di} - X_{di}'}$$

and satisfies

$$(X_{di} - X_{di}')\frac{\partial H_{dqi}}{\partial E_{qi}'} = \frac{1}{\omega_s}E_{qi}'.$$

By the previous observations and aggregating the states, the dynamics of the third-order multi-machine system (2.41) can now be written in port-Hamiltonian form as

$$\begin{aligned} \begin{bmatrix} \dot{\delta} \\ \dot{\mathrm{p}} \\ \dot{E}_q' \end{bmatrix} &= \omega_s \begin{bmatrix} 0 & I & 0 \\ -I & -D & 0 \\ 0 & 0 & -(T_{do}')^{-1}(X_d - X_d') \end{bmatrix} \nabla H + g\begin{bmatrix} P_m \\ E_f \end{bmatrix}, \\ y &= g^T\nabla H, \quad g^T = \begin{bmatrix} 0 & I & 0 \\ 0 & 0 & (T_{do}')^{-1} \end{bmatrix}, \quad H = \sum_{i\in\mathcal{V}}\left(\bar{H}_{mi} + H_{dqi}\right) + \sum_{\{i,j\}\in\mathcal{E}} H_{ij} \end{aligned} \tag{2.62}$$

where $X_d = \mathrm{diag}(X_{d1},\ldots,X_{dn}), X_d' = \mathrm{diag}(X_{d1}',\ldots,X_{dn}')$, and in addition $T_{do}' = \mathrm{diag}(T_{do1}',\ldots,T_{don}')$.

2.7.3 Swing equations

Recall from (2.54) that the energy stored in the inductive transmission line between node i and j is given by

$$H_{ij} = \quad = \frac{B_{ij}}{2\omega_s}(|\overline{E}_i'|^2 - 2|\overline{E}_i'||\overline{E}_j'|\cos\theta_{ij} + |\overline{E}_j'|^2). \tag{2.63}$$

Define now the total energy stored in the transmission lines by $H_T = \sum_{\{i,j\}\in\mathcal{E}} H_{ij}$ and observe that the gradient of H_T with respect to the transformed angle θ is given by

$$\frac{\partial H_T}{\partial \theta_i} = \sum_{j\in\mathcal{N}_i} \frac{B_{ij}}{\omega_s}|\overline{E}_i'||\overline{E}_j'|\sin\theta_{ij}.$$

For the second-order model the electrical energy stored in the generator circuits is constant and can therefore be omitted from the Hamiltonian without loss of generality. By the previous observations and aggregating the states, the dynamics of the second-order multi-machine system (2.42) with $G = 0$ can be written in port-Hamiltonian form as

$$\begin{aligned} \begin{bmatrix}\dot{\delta}\\ \dot{\mathfrak{p}}\end{bmatrix} &= \omega_s \begin{bmatrix}0 & I\\ -I & -D\end{bmatrix}\nabla H + \begin{bmatrix}0\\ I\end{bmatrix} P_m \\ y &= \begin{bmatrix}0 & I\end{bmatrix}\nabla H = \frac{\Delta\omega}{\omega_s}, \qquad H = \sum_{i\in\mathcal{V}} \bar{H}_{mi} + \sum_{\{i,j\}\in\mathcal{E}} H_{ij}. \end{aligned} \tag{2.64}$$

2.7.4 Passivity

Since the multi-machine systems (2.58), (2.62), (2.64) are in the port-Hamiltonian form

$$\begin{aligned} \dot{x} &= (J-R)\nabla H(x) + gu \\ y &= g^T\nabla H(x) \end{aligned} \tag{2.65}$$

with constant matrices $J = -J^T, R = R^T \geq 0, g$, they satisfy the following shifted passivity property.

Proposition 2.7.4 (Shifted passivity)**.** *Let $(\bar{x}, \bar{u}, \bar{y})$ correspond to a steady state of (2.65) and satisfy $\nabla^2 H(\bar{x}) > 0$, $\bar{y} = g^T\nabla H(\bar{x})$. Then the system (2.65) is passive with respect to the shifted external port-variables $(u-\bar{u}, y-\bar{y})$, and the local storage function is given by $\bar{H}(x) := H(x) - (x-\bar{x})^T\nabla H(\bar{x}) - H(\bar{x})$.*

Proof. By defining the *shifted Hamiltonian* (see e.g. [117]) as $\bar{H}(x) = H(x) - (x - \bar{x})^T \nabla H(\bar{x}) - H(\bar{x})$, the system (2.65) can be rewritten as

$$\begin{aligned} \dot{x} &= (J - R)\nabla H(x) + gu \\ &= (J - R)(\nabla \bar{H}(x) + \nabla H(\bar{x})) + gu \\ &= (J - R)\nabla \bar{H}(x) + g(u - \bar{u}) \\ y - \bar{y} &= g^T(\nabla H(x) - \nabla H(\bar{x})) = g^T \nabla \bar{H}(x). \end{aligned}$$

The passivity follows by taking the time-derivative of the shifted Hamiltonian $\bar{H}$ which yields

$$\dot{\bar{H}} = -(\nabla \bar{H}(x))^T R \nabla \bar{H}(x) + (u - \bar{u})^T (y - \bar{y}) \leq (u - \bar{u})^T (y - \bar{y}).$$

Since in addition $\nabla^2 \bar{H}(\bar{x}) = \nabla^2 H(\bar{x}) > 0$, it follows that $\bar{H}$ acts as a suitable local storage function. □

Remark 2.7.5 (Hessian condition). To use Proposition 2.7.4 one must verify that the Hessian of the Hamiltonian evaluated at the (desired) equilibrium is positive definite. For the second and third-order multi-machine models a sufficient condition is established for guaranteeing that the Hessian is positive definite, see [19, 32] respectively. It can be verified that these conditions hold for a typical operation point of the power network, i.e., for which the voltage (angle) differences are small. However, further research is required to establish similar conditions for the higher-order multi-machine models, which preferably can be checked in a distributed fashion.

The passivity property mentioned in Proposition 2.7.4 that the previously derived multi-machine models (2.58), (2.62), (2.64) admit proves to be very useful when interconnection with (passive and optimal) controllers, see Chapters 5 and 7 for an analysis of the third- and sixth-order models respectively.

2.8 Conclusions and future research

In this chapter we provided a unifying energy-based approach to the modeling of multi-machine power networks. Starting from the first-principles model of the synchronous machine, reduced order models are obtained and the underlying assumptions are explained. After determining the energy functions of the reduced-order models, port-Hamiltonian representations of the multi-machine systems are established. In particular, it is shown that advanced multi-machine models that are much more advanced can be analyzed using the port-Hamiltonian framework. Moreover, the resulting port-Hamiltonian systems are proven to be shifted passive with respect to its steady states. The latter property has turned out to be crucial in many contexts, in particular for the stability analysis of the (optimal) equilibria of the closed-loop system [32, 107, 113].

2.8.1 Future research directions

The results established in this chapter can be extended in many possible ways. We elaborate on the main research directions in the following.

Control

One natural extension of the work established in the present chapter is to consider (distributed) control of multi-machine networks. For frequency control, this can be done following the lines of [95, 108, 113]. Since in the present chapter we established a systematic way for obtaining the energy functions and proved (shifted) passivity of the system, we conjecture that the same kind of (distributed averaging) controllers established in these references can be applied to (purely inductive) multi-machine models where each synchronous machine is described by a 2,3,4,5 or 6th-order model. In fact, the control of 6th-order multi-machine networks will be discussed in Chapter 7 of this thesis. Alternatively, one can continue along the lines of [64, 105, 107, 130] and consider controllers based on the primal-dual gradient method. In addition, further effort is required to investigate the possibilities of (optimal) voltage control using passive controllers. One possibility is to extend the work of [32, 33] to high-dimensional multi-machine models.

Nonzero transfer conductances

Another possible extension to this work is to include transmission line resistances in the network. However, in [14, 75] and references therein it is observed that in the case of nonzero transfer conductances, a Lyapunov-based stability analysis can be cumbersome and involves adding nontrivial cross terms in the Lyapunov function. Even then, the stability analysis relies on a 'sufficiently small transfer conductances' assumption [14, 75]. On the other hand, one approach that could be adopted in future research is to assume the resistive transmission lines are uniform such that the R/X ratios are identical for all transmission lines. This simplifies the analysis and possibly the present work could be extended to this case (and keeping the port-Hamiltonian structure intact), for example by following the lines of [32] and references therein.

More extensive power network models

In the present chapter we considered the case that each node in the network represents a synchronous machine. A natural extension is to generalize the established results to the case where some of the nodes represent inverters or (frequency-dependent) loads instead. In addition, while advanced models of the synchronous generator are considered in this chapter, there are many possible extensions to these models. For example, models for the turbine and speed governor as considered in e.g. [3, 114, 130] could also be taken into account. Finally, the model can be expanded such that the excitation system and the automatic voltage regulator (AVR) are included as well [67].

Part II

Optimization and frequency regulation in power grids

Introduction

As argued in Chapter 1, a major problem in future smart grids is the management of demand and supply, due to a more active role of both producers and consumers (or a combination of both, commonly called *prosumers*). Because of new market architectures [124] and increased communication (e.g. with the use of smart meters [57]), these players make choices about their production and consumption more according to market-driven considerations. However, these purely economic considerations cannot be detached from physical factors. In fact, demand-supply imbalance of the active power can lead to sustained frequency deviations from the desired reference value which can only be tolerated for a limited amount of time. A natural approach to deal with this problem is to adjust power production and consumption taking the measured frequency deviation as an output signal which should be fed back to suitable control devices.

Within this approach, this raises the question to which set point the actual production and consumption should be adjusted. An answer to this problem comes from taking into account economic factors. A common approach in economic modeling and analysis is to assume the existence of utility functions for each prosumer, which measure the benefit that each prosumer is gaining from producing/consuming a certain amount of power. The optimal allocation of power consumption, production and distribution within the grid can then be computed by maximizing the overall societal benefit, which is given by the sum of the individual utilities minus the total generation costs. Of course, this is subject to the physical constraints imposed by the grid which include the power balance (demanded and supplied power should be in balance), capacity constraints and thermal limits of the transmission lines. Under appropriate assumptions on the utility functions (smoothness, concavity), one can compute the optimal solution to the problem by the so-called dual-Lagrangian technique [12], which moreover allows to solve the problem in a distributed fashion [62]. In fact, the dual formulation leads to the optimal solution to the original problem, while the Lagrangian multipliers associated with the dual formulation can be interpreted as price variables associated with consumers and producers.

Once the optimal solution is found, control algorithms that guarantee the convergence to such optimal solution must be designed. At each bus, corresponding to consumers and producers, local measurements (such as frequency deviation, power flows at the buses, etc.) are processed by the control algorithms to deliver the optimal consumption/production. In our approach such rates are adjusted dynamically depending on the measurements, thus leading to an increased adaptive and flexible smart grid.

Contributions

A solution we propose is to consider for the generation/consumption rates of each producer/consumer a control algorithm driven by two factors. The first factor models the selfish behavior of each agent that aims at maximizing its own utility disregarding the other agents in the grid. This selfish behavior causes a departure from the good operating regime of the grid, resulting e.g. in a deviation from the reference frequency. This selfish behavior must be penalized by the second factor that aims at regulating the production/consumption and depends on the local frequency deviation. From a mathematical point of view, the 'selfish' term coincides with the gradient of the concave/convex functions modeling respectively the utilities and costs of the prosumers.

In this part of the thesis, we show that these algorithms are (shifted) passive dynamical systems [118], which in fact can be written in port-Hamiltonian form. Since the feedback interconnection of port-Hamiltonian systems is still a port-Hamiltonian system, the overall dynamical system resulting from combining the physical dynamics of the grid with the behavior of the prosumers defines a port-Hamiltonian system. Hence, we are able to treat the 'physical' dynamics of the grid and the 'economic' dynamics of the prosumers on an equal footing. Furthermore, we exploit the modular character of port-Hamiltonian and passive systems. In particular, we show that for the smart-grid/dynamic pricing interconnection we can easily consider more complex models for the physical system and more sophisticated (market-driven) control algorithms. Thus on the physical side we do not restrict ourselves only to the well-known swing equations, that indeed feature port-Hamiltonian and passivity properties [5]. Specifically, we consider network-preserving and network-reduced models of the physical power grid that include voltage dynamics, reactive power flows and high-dimensional synchronous machine models. Compared to the existing literature these models are much more complex and difficult to analyze.

On the economic side, we show that the dynamic pricing algorithms can be constructed from the primal-dual gradient dynamics of a constrained social welfare optimization problem. We consider several variations of this problem, which include considering line congestion and power transmission costs for a cyclic networks, and nodal generation and load limits for general graph topologies. Moreover, the information exchange of (price-based) control variables occurs over an connected communication graph, allowing for a distributed implementation of the control mechanism. We show that shifted passivity plays a key role in establishing local asymptotic stability of the physical/economical system to the set of desired points (optimal power sharing and zero frequency deviation). This in particular allows us to guarantee convergence without relying on small/large gain arguments as seen in some other existing works (e.g. [131]).

We also study the passivity and convergence properties of general continuous-time primal-dual dynamics, considering convex optimization problems with a general class of constraints. In particular, we show that the equilibria of such dynamics coincide with the primal-dual optimizers of the optimization problem and, by exploiting shifted passivity, we establish global asymptotic convergence

under the assumption of strict convexity of the objective function. We also study primal-dual dynamics that are subject to hard constraints, that is, constraints that may not be violated throughout the execution of the algorithm. A key contribution to the existing literature is that we weaken the strict convexity assumption while establishing pointwise asymptotic stability of such dynamics.

Finally, we compare the primal-dual based control algorithms with an alternative control scheme adopted throughout the literature, and often referred to as distributed averaging integral (DAI) control [95]. Our contribution is that, we consider simultaneously cost minimization and utility maximization as defined by the social welfare problem. This is in contrast with the DAI control scheme where only cost efficiency is considered. We consider the advantages and limitations of each of the two control designs for social welfare maximization and their performance is compared by simulations.

Outline

Chapter 3: In this chapter we introduce the primal-dual dynamics associated to a general optimization problem. There we first consider the case that only affine constraints are considered. For that case it is shown, that the primal-dual dynamics admits a Brayton-Moser as well as a port-Hamiltonian representation. By introducing suitable discontinuous passive subsystems and their interconnection with this port-Hamiltonian system, we are able to incorporate inequality constraints in the underlying optimization problem. These results are then applied to power networks by first introduction a simple social welfare problem and writing the equations for the associated primal-dual dynamics, which can be interpreted as a dynamic pricing algorithm. By interconnection with the swing dynamics of the power network, local asymptotic stability of the closed-loop system is proven and steady-state optimality is achieved.

Chapter 4: This chapter presents various extensions to the results of Chapter 3 on the application on power networks. In particular, a more advanced physical power network model is adopted which includes both frequency and voltage dynamics. In addition, after stating a distributed version of the dynamics pricing scheme, numerous variations and extensions to the basic design are proposed. These consist of including constraints on the power generation and consumption for power grids with a general network topology. Also, thermal constraints on the transmission lines and power transmission costs are considered in the social welfare problem for acyclic networks. Furthermore, an alternative control scheme is proposed to deal with the uncertainty of both power generation and demand. By exploiting the passivity properties of the physical dynamics and the dynamic pricing mechanism, we establish (voltage) stability and convergence to a state of optimal social welfare and also zero frequency.

Chapter 5: Here we present market-driven controllers for structure-preserving power networks, i.e., a distinction is made between generator and load nodes.

First, we formulate the power network dynamics as a system differential-algebraic equations (DAE's) that considers both active and reactive power flows. Then a dynamic pricing algorithm is constructed from the associated social welfare problem that assigns possibly different prices at the generator and load nodes. We show that the interconnection with the physical system result in a closed-loop DAE-system, whose algebraic constraints can eliminated to obtain a system of ordinary differential equations. By constructing a suitable energy-inspired Lyapunov function, the equilibrium set corresponding to optimal active power sharing and zero frequency deviation is proven to be locally asymptotically stable.

Chapter 6: In this chapter we propose an alternative control scheme inspired by the popular distributed averaging integral (DAI) controller and a comparison is made with the primal-dual gradient based controller design. We start with defining a simple optimization problem involving aiming at the trade-off between maximizing the consumer utility and minimizing generation costs. Then the two different controllers are constructed for this social welfare problem and are interconnected with the power network swing equations. We discuss the advantages and limitations of each approach and prove the closed-loop convergence and optimality in each case. Finally, we show with simulations the different performance of the two controllers for the same scenario.

Chapter 7: We show here that optimal power sharing can also be achieved for high-dimensional models of power network. Specifically, a sixth order model is used to describe dynamics of each synchronous machine. By defining the energy functions of the system, we obtain a port-Hamiltonian representation of the multi-machine network. Then a consensus based control architecture is proposed in port-Hamiltonian form to obtain frequency regulation and optimal power sharing in the presence of an unknown demand. By utilizing the (sparse) interconnection and damping structure of the closed-loop port-Hamiltonian system, local asymptotic stability is guaranteed under some equilibrium condition.

Chapter 8: This final chapter in this part focuses on general primal-dual dynamic that deal with hard inequality constraints. We consider a general convex optimization problem with affine equality constraint and convex inequality constraints. For such an optimization, a primal-dual gradient dynamics is constructed that includes a projection of the primal variables onto the feasible set defined by the inequality constraints. For the resulting complementarity system global pointwise convergence to the set of primal-dual optimizers is proven without requiring strict convexity of the objective function. As an application outside power networks, we consider a job scheduling problem in data centers and show the effectiveness of our approach.

Chapter 3

Primal-dual dynamics for online optimization in power networks

Abstract: *Primal-dual gradient methods are well-known for solving constrained convex optimization problems. In this chapter, we study the passivity and stability properties of its continuous-time counterpart. We show for convex optimization problems with affine equality constraints that the primal-dual dynamics admits a Brayton-Moser and a port-Hamiltonian representation. In fact, its dynamics can be interpreted as a interconnection of multiple (incrementally port-Hamiltonian) passive systems, a property that also holds when considering inequality constraints in the optimization problem. This passivity property plays a key role in proving asymptotic stability of the method to the set of optimizers, which invokes a suitable invariance principle. As an application to smart grids, we study the problem of frequency regulation in power grids while allocating the power generation and consumption to maximize the total social welfare. By constructing its associated primal-dual dynamics, we obtain a real-time dynamic pricing model in port-Hamiltonian form. By coupling with the port-Hamiltonian description of the physical network we obtain a closed-loop port-Hamiltonian system, whose properties are exploited to prove local asymptotic stability of the interconnected system.*

Published as:

T.W. Stegink, C. De Persis, A.J. van der Schaft. "Port-Hamiltonian formulation of the gradient method applied to smart grids." IFAC-PapersOnLine 48.13 (2015): 13-18.

3.1 Introduction

Constrained optimization problems arise in various domains, including optimal resource allocation, network flow control and welfare maximization. One of the well-known algorithms for determining the (primal-dual) optimizers of such a constrained optimization problem is the primal-dual gradient method [6]. To make such algorithms more flexible, there is an increasing body of research that looked at ways to apply the primal-dual gradient method in dynamic environments, see e.g. [120, 125, 136]. For example, a common approach to flow control is to decompose the problem into a static optimization problem and a dynamic stabilization problem [55, 66]. The static optimization incorporates capacity constraints and utilization and/or cost efficiency, and its solution provides the desired steady state operating point (equilibrium of the closed loop system). The update laws of the dynamic system are then designed to guarantee asymptotic stability of the equilibrium.

Recently, such dynamic optimization algorithms are also interconnected with physical systems. The motivation for having the interconnection with other (physical) systems are applications where there is the need to have online (real-time) optimization. Examples of such online optimization methods can be found for energy efficient buildings [28, 43], job scheduling in data centers [116], network flow control [126] and power networks [131, 136]. A natural starting point to analyze these coupled systems is to start from comprehensive modeling frameworks for physical systems. Two of these are the closely-related Brayton-Moser and the port-Hamiltonian frameworks, see [49, 50] and [76, 117] respectively, which lend themselves for multi-domain modeling. For example, in [28] a Brayton-Moser framework is adopted in the control of energy-efficient buildings and in [37] a complex large scale power network is modeled using the port-Hamiltonian framework. In this chapter, we show that the primal-dual gradient dynamics associated to an optimization problem also admit Brayton-Moser and port-Hamiltonian representations. This enables them to be interconnected with physical systems using the same perspective, and analyzing them by considering the same tools as utilized in these frameworks. A key property property of many physical systems is passivity, i.e. the rate of change of energy is equal to the power supplied to the system minus the energy dissipation rate. In this work, we show the primal-dual dynamics naturally admits such passivity property, which allows for a two-way power-preserving interconnection with a physical system. In this way, the primal-dual dynamics can be used as feedback controller for the physical system.

This is particularly useful for power networks where it is desired to quickly restore operation to the optimal point after a change in the (physical) system has occurred. In power networks, this optimal point often corresponds to a fair sharing of resources among generators and consumers. The problem of allocating of power generation and demand in an optimal manner while respecting the physical constraints is called the *social welfare problem*. We show in this research that the primal-dual dynamics associated to the social welfare problem can in fact be interpreted as a simple market model for real-time dynamic pricing. In this way, we are able to analyze the economic and physical aspects in an unifying manner.

Contributions

The key contributions of this chapter are the following. First, we show that for convex optimization problems with affine equality constraints, the dynamics of the associated gradient method can be represented as a Brayton-Moser or a port-Hamiltonian system. A main advantage of the latter representation is that the system can then easily be interconnected to other port-Hamiltonian systems. For the case of smart grids, it is possible to formulate the market dynamics as a port-Hamiltonian system which can be interconnected with the physical model to obtain a closed-loop port-Hamiltonian system. Using this formulation, the stability analysis is straightforward where the (shifted) Hamiltonian naturally acts as a Lyapunov function.

Secondly, in case of a general convex minimization problems with inequality constraints, we show that the dynamics of the gradient method can be interpreted as an interconnection of multiple (shifted) passive systems corresponding to the equality and inequality constraints respectively. By interconnecting them via power-ports the shifted passivity of the coupled system follows, for which we show that it is a useful property in the stability analysis of the gradient method and the interconnection with external (shifted) passive systems.

Finally, we apply this general theory on the gradient method to a physical model of the power network. We consider the social welfare maximization problem with the constraint of zero frequency deviation and design a controller based on the gradient method that achieves these goals. The energy-based design method we propose is fundamentally different from the methods in the existing literature and enables the coupling of the market and physical dynamics in smart grids. This in particular allows us to rigorously prove the asymptotic stability of the nonlinear physical-economical system and its convergence to a point of optimal social welfare and zero frequency deviation.

Outline: The outline of this chapter is as follows. Section 3.2 states some preliminaries regarding with convex optimization problems and the associated optimality conditions. The results on the primal-dual gradient method are discussed in Section 3.3. Here we first consider the case of only affine equality constraints in the optimization problem and explain how the primal-dual dynamics are constructed and can be represented as a Brayton-Moser or a port-Hamiltonian system. Thereafter, convex inequality constraints are included as well and a passivity-based proof will be given on the convergence to the set of optimal points. In Section 3.4 the gradient method is applied to the social welfare problem appearing power networks. First, a model describing the power network dynamics is given in the form of the swing equations. Then the physical model of the power network is coupled with the primal-dual dynamics to obtain a asymptotically stable closed-loop port-Hamiltonian system, whose equilibria corresponds to maximal social welfare and zero frequency deviation.

3.2 Convex optimization

In this chapter we consider optimization problems of the form

$$\underset{x}{\text{minimize}} \quad f(x) \tag{3.1a}$$

$$\text{subject to} \quad Ax = b \tag{3.1b}$$

$$g(x) \leq 0 \tag{3.1c}$$

where $A \in \mathbb{R}^{m\times n}, b \in \mathbb{R}^m$. We use the notation $g(x) = \text{col}(g_1(x), \dots, g_q(x))$ and the inequality (3.1c) holds element-wise. The function $f : \mathbb{R}^n \to \mathbb{R}$ is called the *objective function*, and $x \in \mathbb{R}^n$ is often referred to as a *primal variable*. We assume that $f, g_i : \mathbb{R}^n \to \mathbb{R}, i = 1, \dots, q$, are continuous differentiable convex functions. In such a case (3.1) is referred to as a *convex optimization problem*.

We assume that there exists $x \in \mathbb{R}^n$ such that $Ax = b$ and $g(x) < 0$. This condition is also referred to as *Slater's condition*. (And a weaker version exists if some g_i's are affine functions, see also [12].) Under this assumption, using the fact that the problem (3.1) is convex, we know that $\bar{x}$ is an optimal solution to (3.1) if and only if there exist so called *dual variables* $\bar{\lambda} \in \mathbb{R}^m, \bar{\mu} \in \mathbb{R}^q$ such that the Karush-Kuhn-Tucker (KKT) optimality conditions

$$\nabla f(\bar{x}) + \sum_{i\in\mathcal{I}_q} \nabla g_i(\bar{x})\bar{\mu}_i + A^T\bar{\lambda} = 0 \tag{3.2a}$$

$$A\bar{x} - b = 0 \tag{3.2b}$$

$$0 \geq g(\bar{x}) \perp \bar{\mu} \geq 0 \tag{3.2c}$$

are satisfied [12]. Here we use the compact notation (3.2c) for the conditions $g(x) \leq 0, (g(x))^T\mu = 0$, and $\mu \geq 0$ where the inequalities hold element-wise. Define $\bar{\mathcal{Z}}$ as the set of all solutions to the KKT conditions, i.e.

$$\bar{\mathcal{Z}} := \{(\bar{x}, \bar{\lambda}, \bar{\mu}) \mid (\bar{x}, \bar{\lambda}, \bar{\mu}) \text{ is a solution to (3.2)}\} \tag{3.3}$$

and suppose that $\bar{\mathcal{Z}} \neq \emptyset$ so that the minimization problem is feasible. The aim is to find $(\bar{x}, \bar{\lambda}, \bar{\mu}) \in \bar{\mathcal{Z}}$, but typically it is hard to construct such a point using the KKT conditions (3.2) directly. Instead, there is a broad range of literature that proposes (iterative) algorithms to find such a primal-dual optimizer. In the next section we consider a few variants of such algorithms in the continuous-time domain, and discuss in more detail their passivity properties and conditions for asymptotic stability. We refer to such algorithms as *primal-dual (gradient) dynamics*, since the associated dynamical system describes the evolution of both the primal and dual variables.

3.3 Primal-dual gradient dynamics

In this section we introduce a continuous-time gradient algorithm for solving a general convex optimization problem. We start with a simpler case where only

affine equality constraints are considered and thereafter discuss how inequality constraints can be added. We show that in the former case the associated primal-dual dynamics can be represented in several ways. Our first observation is that it can be represented as a Brayton-Moser system where the Lagrangian acts naturally as the potential function. Then we show that by transitioning from co-energy to energy variables it is possible to rewrite the Brayton-Moser equations as an incrementally port-Hamiltonian system, which lends itself for a straightforward stability analysis.

3.3.1 Brayton-Moser representation

Let us consider the following minimization problem with affine equality constraints

$$\begin{aligned} &\underset{x}{\text{minimize}} \quad f(x) \\ &\text{subject to} \quad Ax - b = 0, \end{aligned} \tag{3.4}$$

where f is assumed to be a strictly convex function and $A \in \mathbb{R}^{m\times n}$ satisfies $\ker(A^T) = \{0\}$. The corresponding Lagrangian is given by

$$L(x, \lambda) = f(x) + \lambda^T(Ax - b)$$

From the first-order optimality conditions of (3.4), see also (3.2), we observe that the gradient of L satisfies

$$\nabla L(\bar{x}, \bar{\lambda}) = \begin{bmatrix} \nabla f(\bar{x}) + A^T\bar{\lambda} \\ A\bar{x} - b \end{bmatrix} = 0. \tag{3.5}$$

We assume that (3.4) is feasible and, as a result, there is a unique $(\bar{x}, \bar{\lambda})$ satisfying (3.5). Then the associated primal-dual gradient dynamics is described by

$$\begin{aligned} K_x\dot{x} &= -\nabla f(x) - A^T\lambda \\ K_\lambda\dot{\lambda} &= Ax - b. \end{aligned} \tag{3.6}$$

where $K_x \in \mathbb{R}^{n\times n}, K_\lambda \in \mathbb{R}^{m\times m}$ are symmetric positive definite matrices representing the gains of the dynamics. An interesting observation we make is that the latter system can be written in Brayton-Moser form (see e.g. [117] for more details)

$$\begin{bmatrix} \frac{\partial^2 H^*}{\partial x^2}(x, \lambda) & 0 \\ 0 & -\frac{\partial^2 H^*}{\partial \lambda^2}(x, \lambda) \end{bmatrix} \begin{bmatrix} \dot{x} \\ \dot{\lambda} \end{bmatrix} = - \begin{bmatrix} \frac{\partial L}{\partial x}(x, \lambda) \\ \frac{\partial L}{\partial \lambda}(x, \lambda) \end{bmatrix}. \tag{3.7}$$

Here the co-energy variables are $\mathtt{z} = (x, \lambda)$ and the co-Hamiltonian amounts to

$$H^*(\mathtt{z}) = H_1^*(x) + H_2^*(\lambda) = \frac{1}{2}x^T K_x x + \frac{1}{2}\lambda^T K_\lambda \lambda.$$

Interestingly, the Lagrangian function acts as the mixed-potential function of the system (3.7). The pseudo-Riemannian metric is in this case given by

$$Q = \begin{bmatrix} \frac{\partial^2 H_1^*}{\partial x^2}(x) & 0 \\ 0 & -\frac{\partial^2 H_2^*}{\partial \lambda^2}(\lambda) \end{bmatrix} = \begin{bmatrix} K_x & 0 \\ 0 & -K_\lambda \end{bmatrix}.$$

Note that since Q is indefinite, L cannot be used as a Lyapunov function to prove asymptotic stability of the system. However, we can make use of the fact that the Lagrangian is a saddle function, i.e. $L(x, \lambda)$ is (strictly) convex in x and concave in λ. In particular, we note that $(\bar{x}, \bar{\lambda})$ is a saddle-point meaning that [6]

$$L(\bar{x}, \lambda) \leq L(\bar{x}, \bar{\lambda}) \leq L(x, \bar{\lambda}), \qquad \forall x \in \mathbb{R}^n, \forall \lambda \in \mathbb{R}^m. \tag{3.8}$$

As a result, the function

$$V(\mathtt{z}) = \frac{1}{2}(x - \bar{x})^T K_x (x - \bar{x}) + \frac{1}{2}(\lambda - \bar{\lambda})^T K_\lambda (\lambda - \bar{\lambda}) \tag{3.9}$$

qualifies for a Lyapunov function as we show now.

Proposition 3.3.1 (Asymptotic convergence of (3.6))**.** *Consider system* (3.6) *and assume f is strictly convex. Then the saddle-point $(\bar{x}, \bar{\lambda})$ is globally asymptotically stable.*

Proof. By taking the time-derivative of V we obtain

$$\begin{aligned} \dot{V} &= -(x - \bar{x})^T \frac{\partial L}{\partial x}(x, \lambda) + (\lambda - \bar{\lambda})^T \frac{\partial L}{\partial \lambda}(x, \lambda) \\ &\leq L(\bar{x}, \lambda) - L(x, \lambda) + L(x, \lambda) - L(x, \bar{\lambda}) = L(\bar{x}, \lambda) - L(x, \bar{\lambda}) \leq 0 \end{aligned}$$

Since f is strictly convex and by (3.8) equality holds only if $x = \bar{x}$. On the largest invariant set where $\dot{V} = 0$ we have that

$$\dot{x} = -\nabla f(\bar{x}) - A^T \lambda = -A^T(\lambda - \bar{\lambda}) = 0$$

and thus $\lambda = \bar{\lambda}$ as $\ker(A^T) = \{0\}$ by assumption. By LaSalle's invariance principle [56] it then follows that each trajectory satisfying (3.6) converges to the unique saddle-point $(\bar{x}, \bar{\lambda})$. □

Augmentation

In the result of Proposition 3.3.1 we assumed that the objective function f is strictly convex. We show now that by a slight modification of the primal-dual dynamics (3.5), we only require convexity of f for the convergence. To this end, consider the optimization problem

$$\begin{aligned} \underset{x}{\text{minimize}} \quad & f(x) - \|Ax - b\|_\Xi^2 \\ \text{subject to} \quad & Ax - b = 0, \end{aligned} \tag{3.10}$$

with positive definite matrix $\Xi \in \mathbb{R}^{m\times m}$ and note that the set of optimizers if identical with the set of optimizers of (3.4). We refer to now to a set of optimizer since if f is assumed to be convex only, then there may be a continuum of optimal solutions to (3.4). The corresponding Lagrangian is of the form

$$L(x,\lambda) = f(x) + \lambda^T(Ax-b) + \frac{1}{2}\|Ax-b\|_\Xi^2, \tag{3.11}$$

and is often referred to as the *augmented Lagrangian*. The primal-dual dynamics is now given by

$$\begin{aligned} K_x\dot{x} &= -\nabla f(x) - A^T\lambda - A^T\Xi(Ax-b) \\ K_\lambda\dot{\lambda} &= Ax-b. \end{aligned} \tag{3.12}$$

and can again be written in the Brayton-Moser form (3.7) but now with L being the augmented Lagrangian defined by (3.11). We observe that the set of equilibria

$$\bar{\mathcal{Z}} = \{(\bar{x},\bar{\lambda}) \mid -\nabla f(\bar{x}) - A^T\bar{\lambda} = 0, A\bar{x} = b\} \tag{3.13}$$

of (3.12) is identical to the set of primal-dual optimizer of (3.10) or equivalently (3.4). The next result states the convergence of the dynamics.

Proposition 3.3.2 (Asymptotic convergence of (3.6))**.** *Consider system* (3.12)*. Assume f is convex and $\Xi > 0$. Then the set of primal-dual optimizers $\bar{\mathcal{Z}}$ is globally asymptotically stable.*

Proof. Consider again the function V defined by (3.9). Its time-derivative takes the form

$$\begin{aligned} \dot{V} &= -(x-\bar{x})^T(-\nabla f(x) - A^T\lambda - A^T\Xi(Ax-b)) + (\lambda-\bar{\lambda})^T(Ax-b) \\ &= -(x-\bar{x})^T(\nabla f(x) - \nabla f(\bar{x})) - \|Ax-b\|_\Xi^2 \leq 0 \end{aligned} \tag{3.14}$$

Since f is convex equality holds only if $\nabla f(x) = \nabla f(\bar{x})$ and $Ax = b$. On the largest invariant set where $\dot{V} = 0$ we then have that

$$\begin{aligned} \dot{x} &= -\nabla f(\bar{x}) - A^T\lambda = -A^T(\lambda-\bar{\lambda}) \\ \dot{\lambda} &= 0 \end{aligned}$$

where λ is constant. By (3.14) the trajectories are bounded and therefore $\dot{x} = 0$. Thus $\lambda = \bar{\lambda}$ follows as before. By LaSalle's invariance principle [56] it then follows that each trajectory satisfying (3.6) converges to the set $\bar{\mathcal{Z}}$. □

3.3.2 Port-Hamiltonian representation

In this section we show that the primal-dual dynamics (3.12) also admits a port-Hamiltonian representation. To capture both cases considered in Section 3.3.1, i.e. the primal-dual dynamics with and without augmentation, we consider the general case where $\Xi \geq 0$ is a positive semi-definite matrix.

In the Brayton-Moser formulation (3.7) x and λ are co-energy variables. We perform the transition to energy variables $\mathtt{x}$ as

$$\mathtt{x} = \begin{bmatrix} \mathtt{x}_x \\ \mathtt{x}_\lambda \end{bmatrix} = \frac{\partial H^*}{\partial \mathtt{z}}(\mathtt{z}) = \begin{bmatrix} K_x x \\ K_\lambda \lambda \end{bmatrix} = \begin{bmatrix} K_x x \\ K_\lambda \lambda \end{bmatrix}.$$

Note that, in the sequel, we will interchangeably write the system dynamics in terms of either energy or co-energy variables for ease of notation. The Hamiltonian is given by the Legendre transform of $H*$ given as

$$H(\mathtt{x}) = \mathtt{x}^T \mathtt{z}(\mathtt{x}) - H^*(\mathtt{z}(\mathtt{x})) = \frac{1}{2} \mathtt{x}^T K^{-1} \mathtt{x}$$

with $K := \text{blockdiag}(K_x, K_\lambda)$. We can now rewrite system (3.12) as

$$\begin{aligned} \dot{\mathtt{x}} &= \begin{bmatrix} -A^T \Xi A & -A^T \\ A & 0 \end{bmatrix} \nabla H(\mathtt{x}) - \nabla \mathtt{f}(e_{\mathtt{R}}) \\ e_{\mathtt{R}} &= \nabla H(\mathtt{x}) = \mathtt{z} = \begin{bmatrix} x \\ \lambda \end{bmatrix} \end{aligned} \tag{3.15}$$

with $\mathtt{f} : \mathbb{R}^{n+m} \to \mathbb{R}, \mathtt{f}(\mathtt{x}) = \mathtt{f}(x, \lambda) = f(x) - \lambda^T b$. Since f is convex, $\mathtt{f}$ is also convex and, as a result, (3.15) satisfies the monotone relationship

$$(e_{R1} - e_{R2})^T (\nabla \mathtt{f}(e_{R1}) - \nabla \mathtt{f}(e_{R2})) \geq 0 \tag{3.16}$$

for all $e_{R1}, e_{R2} \in \mathbb{R}^{n+m}$, and thus (3.15) defines an incrementally port-Hamiltonian system. Recall that any $(\bar{x}, \bar{\lambda})$ satisfying (3.5) is an equilibrium of the latter system and vice versa. Given such primal-dual optimizer $(\bar{x}, \bar{\lambda})$ we can then define the *shifted Hamiltonian* by $\bar{H}(\mathtt{x}) = \frac{1}{2}(\mathtt{x} - \bar{\mathtt{x}})^T K^{-1} (\mathtt{x} - \bar{\mathtt{x}})$ with $\bar{\mathtt{x}} = (K_x \bar{x}, K_\lambda \bar{\lambda})$ such that we obtain the equivalent system description

$$\begin{aligned} \dot{\mathtt{x}} &= \begin{bmatrix} -A^T \Xi A & -A^T \\ A & 0 \end{bmatrix} \nabla \bar{H}(\mathtt{x}) - \nabla \mathtt{f}(e_{\mathtt{R}}) + \nabla \mathtt{f}(\bar{e}_{\mathtt{R}}) \\ e_{\mathtt{R}} &= \nabla H(\mathtt{x}) = \begin{bmatrix} x \\ \lambda \end{bmatrix}, \qquad \bar{e}_{\mathtt{R}} = \nabla H(\bar{\mathtt{x}}) = \begin{bmatrix} \bar{x} \\ \bar{\lambda} \end{bmatrix} \\ e_{\mathtt{R}} - \bar{e}_{\mathtt{R}} &= \nabla \bar{H}(x), \end{aligned} \tag{3.17}$$

Using this form of the system, it is straightforward to establish the same asymptotic stability results as derived in Section 3.3.1, i.e. asymptotic stability to the set of optimal points is guaranteed provided that either (i) f is a *strictly* convex function or (ii) Ξ is a positive definite matrix. In particular, we observe that by exploiting the structure of the system (3.17) that

$$\begin{aligned} \dot{\bar{H}}(\mathtt{x}) &= -(\nabla \bar{H}(\mathtt{x}))^T \begin{bmatrix} A^T \Xi A & 0 \\ 0 & 0 \end{bmatrix} \nabla \bar{H}(\mathtt{x}) - (e_{R1} - e_{R2})^T (\nabla \mathtt{f}(e_{R1}) - \nabla \mathtt{f}(e_{R2})) \\ &= -\|Ax - b\|_\Xi^2 - (x - \bar{x})^T (\nabla f(x) - \nabla f(\bar{x})) \leq 0 \end{aligned} \tag{3.18}$$

which is similar as what we derived in (3.14).

Remark 3.3.3 (Benefits of using the port-Hamiltonian framework). One of the benefits of using the port-Hamiltonian form of the system (3.6) is that even if the the number of variables and equalities in the optimization problem increases, the interconnection and damping structure is easily observed and an explicit form the the monotone relationship can be given. Moreover, the (shifted) Hamiltionian naturally is a canditate Lyapunov function candidate. This makes the stability analysis of the system straightforward, in particular when interconnecting it with other systems in port-Hamiltonian form, as we will show in Section 3.4.

3.3.3 Incorporation of inequality constraints

In this section we extend some of the previous convergence results to the case where also inequality constraints in the minimization problem (which are of the form (3.1c)) are considered. We restrict ourselves to the case where the Lagrangian is not augmented, i.e. $\Xi = 0$, see also Section 3.3.1. To deal with the inequality constraints, we introduce the following input-output systems

$$\begin{aligned} \dot{\mathtt{x}}_{\mu_i} &= (g_i(w_i))^+_{\mu_i} := \begin{cases} g_i(w_i) & \text{if } \mu_i > 0 \\ \max\{0, g_i(w_i)\} & \text{if } \mu_i = 0 \end{cases} \\ y_{\mu_i} &= \nabla g_i(w_i) \nabla H_{\mu_i}(\mathtt{x}_{\mu_i}), \qquad i \in \mathcal{I}_q = \{1, \dots, q\} \end{aligned} \tag{3.19}$$

where $\mathtt{x}_{\mu_i} := K_{\mu_i}\mu_i, \mu_i : \mathbb{R}_{\geq 0} \to \mathbb{R}_{\geq 0}, K_{\mu_i} > 0, H_{\mu_i}(\mu_i) = \frac{1}{2}K^{-1}_{\mu_i}\mathtt{x}^2_{\mu_i}$ and $g_i : \mathbb{R}^n \to \mathbb{R}$ are convex continuously differentiable functions for $i \in \mathcal{I}_q$. Here $w_i \in \mathbb{R}^n$ is the input and $y_{\mu_i} \in \mathbb{R}^n$ is output of system $i \in \mathcal{I}_q$. One important observation we make is that $(\bar{\mu}_i, \bar{w}_i)$ corresponds to an equilibrium of (3.19) if and only if it satisfies the complementarity conditions

$$g_i(\bar{w}_i) \leq 0, \quad g_i(\bar{w}_i)\bar{\mu}_i = 0, \quad \bar{\mu}_i \geq 0. \tag{3.20}$$

The following proposition states the shifted passivity property of the subsystems (3.19).

Proposition 3.3.4. *Let $i \in \mathcal{I}_q$ and suppose $(\bar{\mu}_i, \bar{w}_i)$ satisfies* (3.20)*. Then* (3.19) *is passive with respect to the shifted external port-variables $\tilde{w}_i := w_i - \bar{w}_i, \tilde{y}_{\mu_i} := y_{\mu_i} - \bar{y}_{\mu_i}$ with $\bar{y}_{\mu_i} = \nabla g_i(\bar{w}_i)\bar{\mu}_i$. In addition, for constant input signal $w(t) = \bar{w}_i$, $\mu_i(t)$ converges in finite time an equilibrium of* (3.19)*.*

Proof. Let $i \in \mathcal{I}_q$ and let $(\bar{\mu}_i, \bar{w}_i)$ satisfy (3.20). Define the shifted state variable $\tilde{\mu}_i := \mu_i - \bar{\mu}_i$. We first observe that for all $\omega_i \in \mathbb{R}^n$ the following inequalities hold.

$$\tilde{\mu}_i(g_i(w_i))^+_{\mu_i} \leq \tilde{\mu}_i g_i(w_i) \tag{3.21a}$$

$$g_i(w_i) \leq g_i(\bar{w}_i) + (w_i - \bar{w}_i)^T \nabla g_i(w_i) \tag{3.21b}$$

$$g_i(w_i) \geq g_i(\bar{w}_i) + (w_i - \bar{w}_i)^T \nabla g_i(\bar{w}_i) \tag{3.21c}$$

$$\tilde{\mu}_i g_i(\bar{w}_i) \leq 0 \tag{3.21d}$$

The first inequality holds since if $\mu_i > 0$ it trivially holds and if $\mu_i = 0$ then

$$\begin{aligned}\tilde{\mu}_i(g_i(w_i))^+_{\mu_i} &= -\bar{\mu}_i \max\{0, g_i(w_i)\} = \min\{0, -\bar{\mu}_i g_i(w_i)\} \\ &\leq -\bar{\mu}_i g_i(w_i) = \tilde{\mu}_i g_i(w_i).\end{aligned}$$

Inequalities (3.21b),(3.21c) follow from the convexity of the function g_i. Finally, (3.21d) holds because

$$\tilde{\mu}_i g_i(\bar{w}_i) = \mu_i g_i(\bar{w}_i) \leq 0$$

since $\mu_i \geq 0, g_i(\bar{w}_i) \leq 0$ and $\bar{\mu}_i g_i(\bar{w}_i) = 0$. Next, consider the shifted storage function $\bar{H}_{\mu_i} = \frac{1}{2} K^{-1}_{\mu_i} \tilde{r}^2_{\mu_i} = \frac{1}{2} K_{\mu_i} \tilde{\mu}_i^2$ and suppose that $\tilde{\mu}_i \geq 0$ for the moment. Then by the previous observations (3.21) we obtain

$$\begin{aligned}\dot{\bar{H}}_{\mu_i} &= \tilde{\mu}_i(g_i(w_i))^+_{\mu_i} \leq \tilde{\mu}_i g_i(w_i) \leq \tilde{\mu}_i(g_i(\bar{w}_i) + \tilde{w}_i^T \nabla g_i(w_i)) \\ &\leq \tilde{w}_i^T \nabla g_i(w_i)\tilde{\mu}_i \\ &\leq \tilde{w}_i^T \nabla g_i(w_i)\tilde{\mu}_i + \tilde{w}_i^T(\nabla g_i(w_i) - \nabla g_i(\bar{w}_i))\bar{\mu}_i \\ &= \tilde{w}_i^T \left[\nabla g_i(w_i)\mu_i - \nabla g_i(w_i)\bar{\mu}_i + \nabla g_i(w_i)\bar{\mu}_i - \nabla g_i(\bar{w}_i)\bar{\mu}_i\right] \\ &= \tilde{w}_i^T(\nabla g_i(w_i)\mu_i - \nabla g_i(\bar{w}_i)\bar{\mu}_i) = \tilde{w}_i^T \tilde{y}_{\mu_i}.\end{aligned}$$

Suppose now that $\tilde{\mu}_i < 0$, then we obtain similarly

$$\begin{aligned}\dot{\bar{H}}_{\mu_i} &= \tilde{\mu}_i(g_i(w_i))^+_{\mu_i} \leq \tilde{\mu}_i g_i(w_i) \leq \tilde{\mu}_i(g_i(\bar{w}_i) + \tilde{w}_i^T \nabla g_i(\bar{w}_i)) \\ &\leq \tilde{w}_i^T \nabla g_i(\bar{w}_i)\tilde{\mu}_i \\ &\leq \tilde{w}_i^T \nabla g_i(\bar{w}_i)\tilde{\mu}_i + \tilde{w}_i^T(\nabla g_i(w_i) - \nabla g_i(\bar{w}_i))\mu_i \\ &= \tilde{w}_i^T \left[\nabla g_i(\bar{w}_i)\mu_i - \nabla g_i(\bar{w}_i)\bar{\mu}_i + \nabla g_i(w_i)\mu_i - \nabla g_i(\bar{w}_i)\mu_i\right] \\ &= \tilde{w}_i^T(\nabla g_i(w_i)\mu_i - \nabla g_i(\bar{w}_i)\bar{\mu}_i) = \tilde{w}_i^T \tilde{y}_{\mu_i}.\end{aligned}$$

Hence, for all $\mu_i \geq 0$ we have $\dot{\bar{H}}_{\mu_i} \leq \tilde{w}_i^T \tilde{y}_{\mu_i}$, so (3.19) is passive with respect to the shifted external port-variables $\tilde{w}_i, \tilde{y}_{\mu_i}$. Now we will prove the second statement. Let $i \in \mathcal{I}_q$ and suppose that $w_i(t) = \bar{w}_i$ for all time $t \geq 0$, then in particular $g_i(w_i) = g_i(\bar{w}_i) \leq 0$. If $g_i(\bar{w}_i) = 0$ it is immediately obtained that $\mu_i : \mathbb{R}_{\geq 0} \to \mathbb{R}_{\geq 0}$ satisfies

$$g_i(\bar{w}) \leq 0, \qquad g_i(\bar{w})\mu_i = 0, \qquad \mu_i \geq 0 \tag{3.22}$$

Hence, $\mu_i(t)$ satisfying (3.19) is at steady state for all $t \geq 0$. If $g_i(\bar{w}_i) < 0$ then there exists a finite time $T = -\mu(0)/g_i(w_i)$ such that $\mu_i(T)$ satisfies equation (3.22). In fact, $\mu_i(t) = 0$ for all $t \geq T$ in that case and thus $u(t)$ convergences to an equilibrium of (3.19) in finite time. This concludes the proof of Proposition 3.3.4. □

To be able to interconnect the subsystems (3.19) to (3.15) we introduce additional inputs and outputs to obtain the incrementally port-Hamiltonian system

$$\begin{aligned} \dot{\mathtt{x}} &= \begin{bmatrix} 0 & -A^T \\ A & 0 \end{bmatrix} \nabla H(\mathtt{x}) - \nabla \mathtt{f}(e_{\mathtt{R}}) + \begin{bmatrix} I \\ 0 \end{bmatrix} u \\ y &= \begin{bmatrix} I & 0 \end{bmatrix} \nabla H(\mathtt{x}) = x \\ e_{\mathtt{R}} &= \nabla H(\mathtt{x}) = \mathtt{z} = \begin{bmatrix} x \\ \lambda \end{bmatrix} \end{aligned} \tag{3.23}$$

with $\mathtt{f}$ as defined before. In particular, the following shifted passivity property is satisfied.

Proposition 3.3.5 (Shifted passivity of (3.23))**.** *Let $\bar{x}, \bar{e}_{\mathtt{R}}, \bar{y}$ be such that*

$$\begin{aligned} 0 &= \begin{bmatrix} 0 & -A^T \\ A & 0 \end{bmatrix} \nabla H(\bar{\mathtt{x}}) - \nabla \mathtt{f}(\bar{e}_{\mathtt{R}}) + \begin{bmatrix} I \\ 0 \end{bmatrix} \bar{u} \\ \bar{y} &= \begin{bmatrix} I & 0 \end{bmatrix} \nabla H(\bar{\mathtt{x}}) \\ \bar{e}_{\mathtt{R}} &= \nabla H(\bar{\mathtt{x}}) \end{aligned} \tag{3.24}$$

Then (3.23) *is passive with respect to the shifted input-output variables $(u-\bar{u}, y-\bar{y})$ using storage function $\bar{H}(\mathtt{x}) = \frac{1}{2}(\mathtt{x}-\bar{\mathtt{x}})^T K^{-1}(\mathtt{x}-\bar{\mathtt{x}})$.*

Proof. The proof of this lemma follows the lines of Section 3.3.2 with the addition that also the shifted inputs and outputs appear in the system (3.17) and the dissipation inequality (3.18). □

Having established the shifted passivity property of subsystems (3.19) and (3.24), we are now able to interconnect them by introducing the following interconnection structure given by

$$w_i = y \quad \forall i \in \mathcal{I}_q, \quad u = -\sum_{i \in \mathcal{I}_q} y_{\mu_i}, \tag{3.25}$$

which defines a power-preserving coupling between the systems (3.19) and (3.23). In this way, the closed-loop dynamics can be written as

$$\begin{aligned} K_x \dot{x} &= -\nabla f(x) - A^T \lambda - A^T \Xi (Ax - b) - \nabla g(x) \mu \\ K_\lambda \dot{\lambda} &= Ax - b. \\ K_{\mu_i} \dot{\mu}_i &= (g_i(x)))^+_{\mu_i}, \qquad i \in \mathcal{I}_q \end{aligned} \tag{3.26}$$

or in the partial port-Hamiltonian form as

$$\begin{aligned} \dot{\mathtt{x}} &= \begin{bmatrix} 0 & -A^T \\ A & 0 \end{bmatrix} \nabla H(\mathtt{x}) - \nabla \mathtt{f}(e_{\mathtt{R}}) - \begin{bmatrix} \nabla g(x) \mu \\ 0 \end{bmatrix} \\ \dot{\mathtt{x}}_{\mu_i} &= (g_i(x))^+_{\mu_i}, \qquad i \in \mathcal{I}_q, \\ e_{\mathtt{R}} &= \nabla H(\mathtt{x}) \end{aligned} \tag{3.27}$$

Here the total storage function is $H_e(\mathtt{x}, \mathtt{x}_\mu) := H(\mathtt{x}) + \sum_{i\in\mathcal{I}_q} H_{\mu_i}(\mathtt{x}_{\mu_i})$ and we use the convention $\nabla g(x) = \begin{bmatrix}\nabla g_1(x) & \cdots & \nabla g_q(x)\end{bmatrix}, \mu = (\mu_1, \ldots, \mu_q) \in \mathbb{R}^q_{\geq 0}$. The set of equilibria $\bar{\mathcal{Z}}_e$ of the latter system is characterized by

$$\begin{aligned} -\nabla f(\bar{x}) - A^T\bar{\lambda} - \nabla g(\bar{x})\bar{\mu} &= 0, \\ A\bar{x} &= b, \\ 0 \geq g(\bar{x}) \perp \bar{\mu} &\geq 0 \end{aligned} \tag{3.28}$$

i.e. $(\bar{x}, \bar{\lambda}, \bar{\mu}) \in \bar{\mathcal{Z}}_e$ if and only if it satisfies (3.28). The important observation we make is that the equilibrium set $\bar{\mathcal{Z}}_e$ is identical to the set of solutions of the KKT optimality conditions corresponding to the minimization problem (3.1). Moreover, provided that f is strictly convex, the solutions of (3.29), (3.27) or equivalently (3.26) converge asymptotically to the set of optimal points of the latter minimization problem, as we show in the next theorem.

Theorem 3.3.6. *Suppose that $\bar{\mathcal{Z}}_e \neq \emptyset$ and that f is strictly convex. Then all trajectories (x, λ, μ) of (3.26) converge to the set $\bar{\mathcal{Z}}_e$.*

Proof. Let $(\bar{x}, \bar{\lambda}, \bar{\mu}) \in \bar{\mathcal{Z}}_e$ and define $\bar{\mathtt{x}} = (K_x\bar{x}, K_\lambda\bar{\lambda}), \bar{\mathtt{x}}_\mu = (\bar{\mathtt{x}}_{\mu_1}, \ldots, \bar{\mathtt{x}}_{\mu_m}) = (K_{\mu_1}\bar{\mu}_1, \ldots, K_{\mu_m}\bar{\mu}_m) = K_\mu\bar{\mu}$ and $\bar{e}_{\mathtt{R}} = \nabla H(\bar{\mathtt{x}})$. Consider the shifted storage function

$$\bar{H}_e(\mathtt{x}, \mathtt{x}_\mu) = \bar{H}(\mathtt{x}) + \sum_{i\in\mathcal{I}_q} \bar{H}_{\mu_i}(\mathtt{x}_{\mu_i})$$

then (3.27) can equivalently be written as

$$\begin{aligned} \dot{\mathtt{x}} &= \begin{bmatrix} 0 & -A^T \\ A & 0 \end{bmatrix} \nabla\bar{H}(\mathtt{x}) - \nabla\mathtt{f}(e_{\mathtt{R}}) - \nabla\mathtt{f}(\bar{e}_{\mathtt{R}}) - \begin{bmatrix} \nabla g(x)\mu - \nabla g(\bar{x})\bar{\mu}) \\ 0 \end{bmatrix} \\ \dot{\mathtt{x}}_{\mu_i} &= (g_i(x))^+_{\mu_i}, \qquad i \in \mathcal{I}_q \\ e_{\mathtt{R}} - \bar{e}_{\mathtt{R}} &= \nabla\bar{H}(\mathtt{x}) \end{aligned} \tag{3.29}$$

By exploiting the shifted passivity properties of the subsystems (see Propositions 3.3.4 and 3.3.5), we note that the time-derivative of $\bar{H}_e$ satisfies

$$\dot{\bar{H}}_e(\mathtt{x}, \mathtt{x}_{\mu_i}) = \dot{\bar{H}}(\mathtt{x}) + \sum_{i\in\mathcal{I}_q} \dot{\bar{H}}_{\mu_i}(\mathtt{x}_{\mu_i}) \leq \tilde{u}^T\tilde{y} + \sum_{i\in\mathcal{I}_q} \tilde{w}_i^T\tilde{y}_{\mu_i} \overset{(3.25)}{=} \tilde{u}^T\tilde{y} - \tilde{u}^T\tilde{y} = 0.$$

where $\tilde{u} = u - \bar{u}$ and $\tilde{w}_i, \tilde{y}, \tilde{y}_{\mu_i}, i \in \mathcal{I}_q$ are define likewise. Observe that $\dot{\bar{H}}_e = 0$ only if $x = \bar{x}$ by the proof of Proposition 3.3.1. On this invariant set we have that $\dot{\lambda} = 0$ and, by the second statement of Proposition 3.3.4, $\mu_i, i \in \mathcal{I}_q$ are also at equilibrium. By applying a Caratheodory variant of LaSalle's invariance principle (as stated in [26]) we conclude that $(x, \lambda, \mu) \to \bar{\mathcal{Z}}_e$ as $t \to \infty$. □

3.4 Online optimization in power networks

In this section we consider an application of the primal-dual gradient method for power networks. We start with introducing the model describing the frequency evolution of the network and then define the social welfare maximization problem. Thereafter, we use its associated primal-dual dynamics to design an online controller which maximizes the social welfare while regulating the physical frequency.

3.4.1 Power network model

Consider a power grid consisting of n buses. The network is represented by a connected, undirected graph $\mathcal{G} = (\mathcal{V}, \mathcal{E})$, where nodes $\mathcal{V} = \mathcal{I}_n := \{1, \dots, n\}$ represent buses and edges $\mathcal{E} \subset \mathcal{V} \times \mathcal{V}$ are the transmission lines connecting the buses. Let m denote the number of edges, arbitrarily labeled with a unique identifier in $\mathcal{I}_m$. The ends of edge $k \sim \{i, j\}$, with $i, j \in \mathcal{V}$ are arbitrary labeled with a '+' and a '-', so that the incidence matrix D of the network is given by

$$D_{ik} = \begin{cases} +1 & \text{if } i \text{ is the positive end of } k \\ -1 & \text{if } i \text{ is the negative end of } k \\ 0 & \text{otherwise.} \end{cases}$$

Each bus represents a control area and is assumed to have controllable power generation and a controllable load. The dynamics at each bus is given by [67]

$$\begin{aligned} \dot{\delta}_i &= \omega_i \\ M_i \dot{\omega}_i &= -\sum_{j \in \mathcal{N}_i} V_i V_j B_{ij} \sin(\delta_i - \delta_j) - A_i \omega_i + P_{gi} - P_{di}, \end{aligned} \tag{3.30}$$

which are commonly known as the *swing equations*. A list of variables and parameters used in model (3.30) is given in Table 3.1. By using the power network

δ_i	voltage angle at bus i
ω_i	frequency deviation at bus i
V_i	voltage at bus i
M_i	moment of inertia at bus i
A_i	damping constant at bus i
$\mathcal{N}_i$	set of buses connected to bus i
B_{ij}	susceptance of the line between buses i and j
P_{di}	power demand at bus i
P_{gi}	power generation at bus i

Table 3.1: Variables and parameters of the system (3.30).

model (3.30) the following assumptions are made, which are standard in a broad range of literature on power network dynamics.

Assumption 3.4.1 (swing equation model)**.** For (3.30) we assume the following:

- Lines are lossless, i.e. the conductance is zero. This assumption is generally valid for the case of high voltage lines connecting different control areas.
- Nodal voltages V_i are constant.
- Reactive power flows are ignored.
- A balanced load condition is assumed, such that the three phase network can be analyzed by a single phase.

More details regarding the derivation of (3.30) and the underlying assumptions can be found in Chapter 2. We define the voltage angle differences between the buses by $\eta = D^T\delta \in \mathbb{R}^m$ where $\delta = (\delta_1, \dots, \delta_n) \in \mathbb{R}^n$. Further define the angular momenta of the moments of inertia $M = \mathrm{diag}(M_1, \dots, M_n)$ by $p := M\omega$, where $\omega = (\omega_1, \dots, \omega_n)$ is the frequency deviation with respect to the nominal frequency. In addition, $A = \mathrm{diag}(A_1, \dots, A_n) > 0$. Let $\Gamma = \mathrm{diag}(\gamma_1, \dots, \gamma_m) > 0$ where $\gamma_k = V_i V_j B_{ij}$ for each edge $k \sim \{i, j\}$ between nodes $i, j \in \mathcal{V}$. Finally, we define the Hamiltonian $H_p(\eta, p)$ by

$$H_p(\eta, p) = \frac{1}{2} p^T M^{-1} p - \mathbb{1}^T \Gamma \cos \eta$$

then the swing equations (3.30) are represented in port-Hamiltonian form as

$$\begin{aligned} \begin{bmatrix} \dot{\eta} \\ \dot{p} \end{bmatrix} &= \begin{bmatrix} 0 & D^T \\ -D & -A \end{bmatrix} \nabla H_p(\eta, p) + \begin{bmatrix} 0 & 0 \\ I & -I \end{bmatrix} u_1 \\ y_1 &= \begin{bmatrix} 0 & I \\ 0 & -I \end{bmatrix} \nabla H_p(\eta, p) = \begin{bmatrix} M^{-1} p \\ -M^{-1} p \end{bmatrix} = \begin{bmatrix} \omega \\ -\omega \end{bmatrix} \end{aligned} \tag{3.31}$$

with inputs $u_1 = (P_g, P_d) \in \mathbb{R}^{2n}$. We assume the initial condition of the system satisfies $\eta(0) = D^T\delta(0)$. An immediate observation is that that the system (3.31) is passive with storage function H_p. In particular, it satisfies the passivity property $\dot{H}_p \leq u_1^T y_1$. We also note that (3.31) is passive with respect to the steady states of the system. However, since the potential energy of the system is bounded, this passivity property only holds locally.

Proposition 3.4.2 (Local shifted passivity of (3.31))**.** *Consider system* (3.31)*. Let* $\bar{\eta}, \bar{p}, \bar{u}_1, \bar{y}_1$ *correspond to an equilibrium of* (3.31)*, i.e.,*

$$0 = \begin{bmatrix} 0 & D^T \\ -D & -A \end{bmatrix} \nabla H_p(\bar{\eta}, \bar{p}) + \begin{bmatrix} 0 & 0 \\ I & -I \end{bmatrix} \bar{u}_1, \tag{3.32}$$

$$\bar{y}_1 = \begin{bmatrix} 0 & I \\ 0 & -I \end{bmatrix} \nabla H_p(\bar{\eta}, \bar{p}). \tag{3.33}$$

Suppose furthermore that $\bar{\eta}_k \in (-\frac{\pi}{2}, \frac{\pi}{2})$ *for all* $k \in \mathcal{E}$*. Then* (3.31) *is passive with respect to the shifted input-output variables* $\tilde{u}_1 := u_1 - \bar{u}_1, \tilde{y}_1 := y_1 - \bar{y}_1$ *where the*

local storage function takes the form

$$\bar{H}_p(\eta,p) := H(\eta,p) - \begin{bmatrix}(\eta-\bar{\eta})^T & (p-\bar{p})^T\end{bmatrix}\begin{bmatrix}\frac{\partial H_p}{\partial \eta}(\bar{\eta},\bar{p})\\ \frac{\partial H_p}{\partial p}(\bar{\eta},\bar{p})\end{bmatrix} - H(\bar{\eta},\bar{p}). \tag{3.34}$$

Proof. Consider the storage function defined in (3.34). We first observe that $\bar{H}(\bar{\eta},\bar{p}) = 0, \nabla\bar{H}_p(\bar{\eta},\bar{p}) = 0$ and the Hessian of $\bar{H}_p$ evaluated at $(\bar{\eta},\bar{p})$ is given by

$$\nabla^2 H_p(\bar{\eta},\bar{p}) = \begin{bmatrix}\Gamma\,\mathrm{diag}(\cos\bar{\eta}) & 0\\ 0 & M^{-1}\end{bmatrix}.$$

By assumption $\bar{\eta}_k \in (-\frac{\pi}{2},\frac{\pi}{2})$ for all $k \in \mathcal{E}$ and therefore $\mathrm{diag}(\cos\bar{\eta}) > 0$ and $\nabla^2 H(\bar{\eta},\bar{p}) > 0$. As a result, $(\bar{\eta},\bar{p})$ is a local strict minimum of $\bar{H}_p$ and there exists a neighborhood around $(\bar{\eta},\bar{p})$ for which H_p is strictly convex. In addition, the time-derivative of $\bar{H}_p$ amounts to

$$\begin{aligned}\dot{\bar{H}}_p &= (\nabla\bar{H}_p)^T\left(\begin{bmatrix}0 & D^T\\ -D & -A\end{bmatrix}\nabla H_p + \begin{bmatrix}0 & 0\\ I & -I\end{bmatrix}u_1\right)\\ &= (\nabla\bar{H}_p)^T\left(\begin{bmatrix}0 & D^T\\ -D & -A\end{bmatrix}\nabla\bar{H}_p + \begin{bmatrix}0 & 0\\ I & -I\end{bmatrix}(u_1-\bar{u}_1)\right)\\ &= (\nabla\bar{H}_p)^T\begin{bmatrix}0 & 0\\ 0 & -A\end{bmatrix}\nabla\bar{H}_p + (u_1-\bar{u}_1)^T(y_1-\bar{y}_1) \le (u_1-\bar{u}_1)^T(y_1-\bar{y}_1)\end{aligned}$$

where the second equality follows from (3.32) and the fact that $\nabla\bar{H}_p(\eta,p) = \nabla H_p(\eta,p) - \nabla H_p(\bar{\eta},\bar{p})$. Hence, the system (3.31) is passive with respect to the shifted input-output variables where $\bar{H}_p$ qualifies as a local storage function. □

This shifted passivity property proves to be crucial in the interconnection with the primal-dual dynamics associated with the social welfare optimization problem, which we introduce next.

3.4.2 Social welfare problem

The social welfare function $S : \mathbb{R}^{2n} \to \mathbb{R}$ is defined as $S(P_g,P_d) := U(P_d) - C(P_g)$, where $U : \mathbb{R}^n \to \mathbb{R}$ represents the total utility of the consumers and $C : \mathbb{R}^n \to \mathbb{R}$ the total cost of the generators. We assume that U, C are strictly concave and strictly convex functions respectively.[1] The objective is to maximize the social welfare under the constraint of balancing the total supply and demand. Mathematically,

[1]Typically, U, C are of the additive form $U(P_d) = \sum_{i\in\mathcal{V}} U_i(P_{di}), C(P_d) = \sum_{i\in\mathcal{V}} C_i(P_{di})$ with U_i, C_i being the individual strictly concave/convex utility/cost functions of respectively the consumers and producers at each node. However, the following results continue to hold for general $C(.), U(.)$ that are strictly convex and strictly concave functions respectively.

we consider the following optimization problem

$$\begin{aligned} \underset{P_g, P_d \in \mathbb{R}^n}{\text{maximize}} \quad & U(P_d) - C(P_g) \\ \text{subject to} \quad & \mathbb{1}^T P_g = \mathbb{1}^T P_d, \end{aligned} \tag{3.35}$$

which we assume to be feasible. The corresponding Lagrangian is given by

$$L(P_g, P_d, \lambda) = U(P_d) - C(P_g) + \lambda(\mathbb{1}^T P_g - \mathbb{1}^T P_d),$$

with scalar Lagrange multiplier $\lambda \in \mathbb{R}$. The first-order optimality conditions of (3.35) are given by $\nabla L = 0$:

$$\begin{aligned} \nabla U(\bar{P}_d) &= \mathbb{1}\bar{\lambda} \\ \nabla C(\bar{P}_g) &= \mathbb{1}\bar{\lambda} \\ \mathbb{1}^T \bar{P}_g &= \mathbb{1}^T \bar{P}_d. \end{aligned} \tag{3.36}$$

Since C, U are strictly convex and concave respectively it follows that $(\bar{P}_g, \bar{P}_d, \bar{\lambda})$ satisfying (3.36) is unique.

Remark 3.4.3 (Economic interpretation of optimality conditions). The optimality condition (3.36) can be explained in economic terms as follows. These state that the social welfare is maximized if the marginal utility of each consumer and the marginal cost of each producer is identical to $\bar{\lambda}$, which can be interpreted as the (market clearing) price.

3.4.3 Controller design

By applying the method described in Section 3.3, we can formulate the primal-dual dynamics associated to the social welfare problem (3.35). These dynamics take the form

$$\begin{aligned} K_g \dot{P}_g &= -\nabla C(P_g) + \mathbb{1}\lambda \\ K_d \dot{P}_d &= \nabla U(P_d) - \mathbb{1}\lambda \\ K_\lambda \dot{\lambda} &= \mathbb{1}^T P_d - \mathbb{1}^T P_g \end{aligned} \tag{3.37}$$

where $K_g, K_d \in \mathbb{R}^{n \times n}, K_\lambda \in \mathbb{R}_{>0}$ are positive definite matrices representing the gains of the system. The dynamics (3.37) has an economic interpretation [2]: each producer aims a maximizing their profit by updating their production by comparing its marginal cost with the quantity λ. Likewise, each consumer aims at maximizing its utility but is penalized by λ. Here λ can be interpreted as a time-varying common electricity price in all control areas which changes accordingly when the total supply and demand are not matched.

As in Section 3.3.2 we can write the dynamics (3.37) in port-Hamiltonian form as

$$\begin{aligned}\dot{x}_c &= \begin{bmatrix} 0 & 0 & \mathbb{1} \\ 0 & 0 & -\mathbb{1} \\ -\mathbb{1}^T & \mathbb{1}^T & 0 \end{bmatrix} \nabla H_c(x_c) + \begin{bmatrix} I & 0 \\ 0 & I \\ 0 & 0 \end{bmatrix} (\nabla S(y_2) + u_2) \\ y_2 &= \begin{bmatrix} I & 0 & 0 \\ 0 & I & 0 \end{bmatrix} \nabla H_c(x_c) = \begin{bmatrix} P_g \\ P_d \end{bmatrix}. \end{aligned} \tag{3.38}$$

Here we added the inputs $u_2 \in \mathbb{R}^{2n}$ and outputs $y_2 \in \mathbb{R}^{2n}$ to the system (3.37) and we explain later the interpretation of these additional inputs. The energy and co-energy variables of the system are respectively given by $x_c = (x_g, x_d, x_\lambda) = (K_g P_g, K_d P_d, K_\lambda \lambda)$, $z_c = (P_g, P_d, \lambda)$. The controller Hamiltonian is defined by the quadratic function

$$H_c(x_c) = \frac{1}{2} x_c^T K_c^{-1} x_c$$

with $K_c := \text{blockdiag}(K_g, K_d, K_\lambda)$. Since the market dynamics is represented as a port-Hamiltonian system with properly chosen inputs and outputs, it is possible to couple the primal-dual dynamics with the port-Hamiltonian form of the physical dynamics by a power-preserving interconnection. Such an interconnection between (3.38) and (3.31) is given by $u_1 = y_2$, $u_2 = -y_1$. As a result, the closed-loop dynamics can be written in terms of the co-energy variables as

$$\dot{\eta} = D^T \omega \tag{3.39a}$$

$$M\dot{\omega} = -D\Gamma \sin \eta - A\omega + P_g - P_d \tag{3.39b}$$

$$K_g \dot{P}_g = -\nabla C(P_g) + \mathbb{1}\lambda - \omega \tag{3.39c}$$

$$K_d \dot{P}_d = \nabla U(P_g) - \mathbb{1}\lambda + \omega \tag{3.39d}$$

$$K_\lambda \dot{\lambda} = \mathbb{1}^T P_d - \mathbb{1}^T P_g. \tag{3.39e}$$

In this way, the change of power generation and demand does not only depend on the quantity λ but also depends on the physical frequency of the network. By defining the energy variable $x = (\eta, p, x_g, x_d, x_\lambda)$, the port-Hamiltonian form of (3.39) is given by

$$\begin{aligned}\dot{x} &= \begin{bmatrix} 0 & D^T & 0 & 0 & 0 \\ -D & -A & I & -I & 0 \\ 0 & -I & 0 & 0 & \mathbb{1} \\ 0 & I & 0 & 0 & -\mathbb{1} \\ 0 & 0 & -\mathbb{1}^T & \mathbb{1}^T & 0 \end{bmatrix} \nabla H(x) + \begin{bmatrix} 0 & 0 \\ 0 & 0 \\ I & 0 \\ 0 & I \\ 0 & 0 \end{bmatrix} \nabla S(y) \\ y &= \begin{bmatrix} 0 & 0 & I & 0 & 0 \\ 0 & 0 & 0 & I & 0 \end{bmatrix} \nabla H(x) = \begin{bmatrix} P_g \\ P_d \end{bmatrix} \end{aligned} \tag{3.40}$$

with Hamiltonian $H(x) = H_p(\eta, p) + H_c(x_g, x_d, x_\lambda)$ and S is the social welfare function defined in (3.35). Since S is a strictly concave function, it satisfies the

following monotone relationship:

$$(y - \bar{y})^T(\nabla S(y) - \nabla S(\bar{y})) \leq 0$$

for all $y, \bar{y} \in \mathbb{R}^{2n}$ where equality holds if and only if $y = \bar{y}$.

3.4.4 Equilibrium analysis

In this section we determine the equilibrium points of the interconnected system and show that these corresponds to zero frequency deviation and maximal social welfare. To see this, it is convenient to express the equilibrium in the co-energy variables. Let $\bar{z} = (\bar{\eta}, \bar{\omega}, \bar{P}_g, \bar{P}_d, \bar{\lambda})$ be an equilibrium of (3.39) and note that it satisfies

$$0 = D^T\bar{\omega} \tag{3.41a}$$
$$0 = -D\Gamma \sin\bar{\eta} - A\bar{\omega} + \bar{P}_g - \bar{P}_d \tag{3.41b}$$
$$0 = -\nabla C(\bar{P}_g) + \mathbb{1}\bar{\lambda} - \bar{\omega} \tag{3.41c}$$
$$0 = \nabla U(\bar{P}_g) - \mathbb{1}\bar{\lambda} + \bar{\omega} \tag{3.41d}$$
$$0 = \mathbb{1}^T\bar{P}_d - \mathbb{1}^T\bar{P}_g \tag{3.41e}$$

Then from (3.41a) it follows that $\bar{\omega} = \mathbb{1}^T\alpha$ for some $\alpha \in \mathbb{R}$. As the rows of an incidence matrix sum to zero we have $\mathbb{1}^T D = 0$. Thus by premultiplying (3.41b) with $\mathbb{1}^T$ we obtain $\mathbb{1}^T A\mathbb{1}\alpha = 0$ and since $A > 0$ it thus follows that $\alpha = 0$ and in turn $\bar{\omega} = 0$. Then we conclude from conditions (3.41c)-(3.41e) and (3.36) that $(\bar{P}_g, \bar{P}_d, \bar{\lambda})$ is a primal-dual optimizer of (3.35).

3.4.5 Stability analysis

We are now in the position to state the main result of this section which is the local asymptotic stability of (3.39). To this end, we define the set of equilibria of (3.39) as

$$\bar{\mathcal{Z}} = \{(\bar{\eta}, \bar{\omega}, \bar{P}_g, \bar{P}_d, \bar{\lambda}) \mid (\bar{\eta}, \bar{\omega}, \bar{P}_g, \bar{P}_d, \bar{\lambda}) \text{ satisfies (3.41)}\}.$$

Theorem 3.4.4. *Consider system* (3.39) *and let* $\bar{z} \in \bar{\mathcal{Z}}$ *be such that* $\bar{\eta} \in (-\frac{\pi}{2}, \frac{\pi}{2})^m$ *and* $\bar{\eta} \in \mathrm{im}(D^T)$. *Then* $\bar{z}$ *is locally asymptotically stable.*

Proof. Let $\bar{z} \in \bar{\mathcal{Z}}$ satisfy the hypothesis and define $\bar{x} = (\bar{\eta}, 0, K_g\bar{P}_g, K_d\bar{P}_d, K_\lambda\bar{\lambda})$. We define the shifted Hamiltonian $\bar{H}$ of the closed-loop system by [117]

$$\begin{aligned}\bar{H}(x) &= H(x) - (x - \bar{x})^T\nabla H(\bar{x}) - H(\bar{x}) \\ &= \frac{1}{2}(p - \bar{p})^T M^{-1}(p - \bar{p}) + \frac{1}{2}(x_c - \bar{x}_c)^T K_c^{-1}(x_c - \bar{x}_c) \\ &- \mathbb{1}^T\Gamma\cos\eta - (\eta - \bar{\eta})^T\Gamma\sin\bar{\eta} + \mathbb{1}^T\Gamma\cos\bar{\eta}.\end{aligned}$$

Then we can rewrite the closed-loop system (3.40) as

$$\dot{x} = \begin{bmatrix} 0 & D^T & 0 & 0 & 0 \\ -D & -A & I & -I & 0 \\ 0 & -I & 0 & 0 & \mathbb{1} \\ 0 & I & 0 & 0 & -\mathbb{1} \\ 0 & 0 & -\mathbb{1}^T & \mathbb{1}^T & 0 \end{bmatrix} \nabla \bar{H}(x) + \begin{bmatrix} I & 0 \\ 0 & I \\ 0 & 0 \\ 0 & 0 \\ 0 & 0 \end{bmatrix} (\nabla S(y) - \nabla S(\bar{y}))$$
$$y - \bar{y} = \begin{bmatrix} I & 0 & 0 & 0 & 0 \\ 0 & I & 0 & 0 & 0 \end{bmatrix} \nabla \bar{H}(x) = \begin{bmatrix} P_g - \bar{P}_g \\ P_d - \bar{P}_d \end{bmatrix}$$

Similar as in Section 3.4.4 it can be shown that $\bar{H}(\bar{x}) = 0$ and $\bar{H}(x) > 0$ for all $x \neq \bar{x}$ in a sufficiently small open neighborhood $\mathcal{O}$ of $\bar{x}$, see also [17]. Moreover, the shifted Hamiltonian $\bar{H}$ satisfies the dissipation inequality

$$\begin{aligned} \dot{\bar{H}} =& - p^T M^{-1} A M^{-1} p + (y - \bar{y})^T (\nabla S(y) - \nabla S(\bar{y})) \\ =& - \omega^T A \omega - (P_g - \bar{P}_g)^T (\nabla C(P_g) - \nabla C(\bar{P}_g)) \\ & + (P_d - \bar{P}_d)^T (\nabla U(P_d) - \nabla U(\bar{P}_d)) \leq 0 \end{aligned}$$

where equality holds if and only if $\omega = 0, P_g = \bar{P}_g, P_d = \bar{P}_d$ since U, C are strictly concave/convex in P_d, P_g respectively. As $\dot{\bar{H}} \leq 0$ there exists a compact sublevel set $\Upsilon \subset \mathcal{O}$ of $\bar{H}$ around $\bar{x}$, which is forward invariant. By LaSalle's principle any trajectory initialized in (3.39)[2] converges to the largest invariant set where $\dot{\bar{H}} = 0$. On this invariant set S we have $\lambda = \bar{\lambda}$ and $D\Gamma \sin \eta = D\Gamma \sin \bar{\eta} = \bar{P}_g - \bar{P}_d$. Since $\eta, \bar{\eta} \in \mathrm{im}(D^T)$ and the fact that the trajectory is initialized close to the equilibrium there exists $\delta, \bar{\delta} \in \mathbb{R}^n$ such that $\eta = D^T \delta \in (-\frac{\pi}{2}, \frac{\pi}{2})^m, \bar{\eta} = D^T \bar{\delta} \in (-\frac{\pi}{2}, \frac{\pi}{2})^m$. As a result,

$$\begin{aligned} 0 &= (\delta - \bar{\delta})^T D\Gamma \sin \eta - D\Gamma \sin \bar{\eta} \\ &= (\delta - \bar{\delta})^T D\Gamma (\sin(D^T \delta) - \sin(D^T \bar{\delta})) \\ &= (\delta - \bar{\delta})^T D \int_0^1 \Gamma \, \mathrm{diag}(\cos(\tau D^T \delta + (1 - \tau) D^T \bar{\delta})) d\tau D^T (\delta - \bar{\delta}) \geq 0. \end{aligned}$$

Since the matrix within the integral is positive definite it follows that $D^T(\delta - \bar{\delta}) = \eta - \bar{\eta} = 0$. We can now conclude that $\bar{z}$ is locally asymptotically stable. □

3.5 Conclusions

In this chapter we have considered several variations of the primal-dual dynamics for convex constrained optimization. In case the optimization problem only contains affine constraints, we have shown that its dynamics can be represented in Brayton-Moser form or as an (incrementally) port-Hamiltonian system. The latter formulation clearly reveals the interconnection and damping structure of the system. We have seen that these characteristics allow for a straightforward

[2] We recall here that we assumed that the initial condition satisfies $\eta(0) \in \mathrm{im}(D^T)$.

stability analysis of the system to the set of optimal points. By using passivity-based arguments we have extended the previous convergence result to the case where inequality constraints are included as well.

For the case of power networks, we have seen an example how we can design real-time applications of the algorithm in dynamic environments. There we have formulated the social welfare maximization problem under the constraint that the total generation must meet the total demand. By constructing the associated primal-dual dynamics we obtained a controller which can be interpreted as a real-time dynamic pricing model. We have shown that both the frequency dynamics governed by the swing equations as well as the economic dynamics of the power network can be represented as port-Hamiltonian systems, which are interconnected in a power-preserving manner. In addition, we established convergence of the closed-loop system to the set of optimal points. For this example, the dynamic pricing model we proposed uses a common price in all control areas. In the following chapters, we will propose a distributed version of the proposed control scheme, to obtain a time-varying price which may differ in each control area. We also show how inequality constraints such as congestion on the power supply and demand can be included in the social welfare problem.

Chapter 4

Distributed welfare maximizing controllers in power networks

Abstract: *This chapter studies the problem of frequency regulation in power grids, while maximizing the social welfare. It extends Chapter 3 in the following aspects. First, two price-based controllers are proposed; the first one an internal-model-based controller and the second one based on a continuous-time gradient method for optimization. Secondly, both controllers are be implemented in a fully distributed fashion, with freedom in choosing a controller communication network. As a result, two real-time dynamic pricing models described by port-Hamiltonian systems are obtained. By coupling with the port-Hamiltonian description of the physical network we obtain a closed-loop port-Hamiltonian system, whose properties are exploited to prove asymptotic stability of the set of optimal points. Numerical results show the performance of both controllers in an academic case study.*

Published as:

T.W. Stegink, C. De Persis, A.J. van der Schaft. "A port-Hamiltonian approach to optimal frequency regulation in power grids." 54th IEEE Conference on Decision and Control (CDC), 2015.

4.1 Introduction

Stability of power networks is becoming an increasingly important topic in recent years. In particular, with the growth of renewable energy sources there is an increasing fluctuation in the supply of power. As a result, it is more difficult for traditional energy sources to match the supply with the demand. To alleviate some of these problems, we may introduce a feedback mechanism that encourages the consumers to change their usage when it is difficult for the generators and the network to match demand. One approach is by using real-time dynamic pricing as a control method.

The idea of using dynamic pricing to achieve optimal supply-demand matching is not new in the literature on power networks. A historical paper on dynamic pricing and market stability for example [2]. See e.g. also the works [57, 84] for more recent papers on real-time dynamic pricing, which mainly focus on the economic part of optimal supply-demand matching. However, the coupling between the solution of the optimization problem and the physical dynamics of the network should not be ignored as this could result in instability of the grid [132]. This coupling between the physics of the power network with the market dynamics has previously been studied in e.g. [3, 64, 132].

In this chapter, we propose a new approach for the modeling, analysis and control of smart grids based on using energy functions, both for the physical network as well as for the dynamic pricing algorithm. The underlying framework is based on the theory of port-Hamiltonian systems, which lends itself to the integration of dynamic pricing algorithms that allow to consider economical factors in the control of smart grids. The objective is to have producers and consumers to fairly share utilities and costs associated with the generation and consumption of energy. The challenge of achieving this in an optimal manner is called the *social welfare problem*. At the same time, the goal is to regulate the frequency of the power network to its nominal value (e.g. 50 Hz or 60 Hz).

One of the approaches to solve an optimal frequency regulation problem is by using a internal-model-based controller as in [17, 19], sometimes referred to as *distributed averaging integral control* [123]. We will continue along the same lines as in [19] which, among other things, treated optimal frequency regulation in case of quadratic power production cost functions and constant unknown demand.

The first main contribution of this chapter is that we extend the results of [19] to the case of a quadratic consumer utility function. The internal-model-based controller proposed in [19] is modified accordingly so that it steers the trajectories to the points of maximal social welfare while regulating the frequency. Moreover, this is all achieved in the port-Hamiltonian framework. In particular, we will show that the dynamics of the physical model of the power network can be represented as a port-Hamiltonian system, as well as the real-time dynamic pricing model.

Another well-known controller design method for solving a (social welfare) optimization problem is primal-dual gradient method based control. The literature on the gradient method has become quite extensive over the last decades, starting with the monograph [6]. Also in power grids this method is often applied to design distributed controllers, see for example [64, 132] and [36]. Our contribution

to the existing literature consists in showing that the real-time dynamic pricing model obtained when applying the gradient method can be represented as a port-Hamiltonian system, which demonstrates that the port-Hamiltonian framework can be extended from physical system modeling to markets dynamics as well.

The outline of this chapter is as follows. In Section 4.2 we first state the preliminaries on the power network model and the social welfare problem. Next, we introduce an internal-model-based controller in Section 4.3, and discuss its asymptotic stability. Thereafter in Section 4.4, we propose a gradient method based controller in port-Hamiltonian form and we perform a similar stability analysis. Numerical results on both controllers will be discussed subsequently in Section 4.5. Finally, we state suggestions for future research.

4.2 Preliminaries

4.2.1 Power network model

Consider a power grid consisting of n buses. The network is represented by a connected, undirected graph $\mathcal{G} = (\mathcal{V}, \mathcal{E})$, where nodes $\mathcal{V} = \mathcal{I}_n := \{1, \dots, n\}$ represent buses and edges $\mathcal{E} \subset \mathcal{V} \times \mathcal{V}$ are the transmission lines connecting the buses. Let m denote the number of edges, arbitrarily labeled with a unique identifier in $\mathcal{I}_m$. The ends of edge $k \sim \{i, j\}$, with $i, j \in \mathcal{V}$ are arbitrary labeled with a '+' and a '-', so that the incidence matrix D of the network is given by

$$D_{ik} = \begin{cases} +1 & \text{if } i \text{ is the postive end of } k \\ -1 & \text{if } i \text{ is the negative end of } k \\ 0 & \text{otherwise.} \end{cases} \tag{4.1}$$

Each bus represents a control area and is assumed to have controllable power generation and a price-controllable load. The dynamics at each bus $i \in \mathcal{V}$ are assumed to be given by [19, 67]

$$\begin{aligned} \dot{\delta}_i &= \omega_i \\ M_i \dot{\omega}_i &= P_{gi} - P_{di} - \sum_{j \in \mathcal{N}_i} V_i V_j B_{ij} \sin(\delta_i - \delta_j) - A_i \omega_i \end{aligned} \tag{4.2}$$

commonly known as the *swing equations*.

Assumption 4.2.1 (Swing equation model)**.** By using the power network model (4.2) the following assumptions are made, which are standard in a broad range of literature on power network dynamics.

- Lines are lossless, i.e. the conductance is zero. This assumption is generally valid for the case of high voltage lines connecting different control areas.
- Nodal voltages V_i are constant.

- Reactive power flows are ignored.
- A balanced load condition is assumed, such that the three phase network can be analyzed by a single phase.

Define the voltage angle differences between the buses by $\eta = D^T\omega$, where $\omega = \omega^b - \omega^n$ are the (aggregated) frequency deviations. Further define the angular momenta of the moments of inertia $M = \text{diag}(M_1, \ldots, M_n)$ by $p := M\omega$. Let $\Gamma = \text{diag}(\gamma_1, \ldots, \gamma_k)$ and $\gamma_k = V_i V_j B_{ij}$ where k corresponds to edge $(i,j) \in \mathcal{E}$. Finally, define the Hamiltonian $H_p(\eta, p)$ by

$$H_p(\eta, p) = \frac{1}{2} p^T M^{-1} p - \mathbb{1}^T \Gamma \cos \eta \tag{4.3}$$

which consists of a kinetic energy and a pendulum like potential energy. Here $\cos(.)$ denotes the element-wise cosine function and a similar convention will be used for the function $\sin(.)$. The swing equations (4.2) are then represented by the port-Hamiltonian system

$$\begin{aligned} \begin{bmatrix} \dot{\eta} \\ \dot{p} \end{bmatrix} &= \begin{bmatrix} 0 & D^T \\ -D & -A \end{bmatrix} \nabla H_p(\eta, p) + \begin{bmatrix} 0 & 0 \\ I & -I \end{bmatrix} u_p \\ y_p &= \begin{bmatrix} 0 & I \\ 0 & -I \end{bmatrix} \nabla H_p(\eta, p) = \begin{bmatrix} M^{-1} p \\ -M^{-1} p \end{bmatrix} = \begin{bmatrix} \omega \\ -\omega \end{bmatrix} \end{aligned} \tag{4.4}$$

where $u_p = (P_g, P_d)$. Note that system (4.4) satisfies the passivity property

$$\begin{aligned} \dot{H}_p &= p^T M^{-1} \dot{p} + (\Gamma \sin \eta)^T \dot{\eta} \\ &= p^T M^{-1}(-D\Gamma \sin \eta - A M^{-1} p + P_g - P_d) + (\Gamma \sin \eta)^T D^T M^{-1} p \\ &= -\omega^T A \omega + \omega^T (P_g - P_d) \leq u_p^T y_p. \end{aligned}$$

For an extensive study on the stability and equilibria of the swing equations based on the Hamiltonian function (4.3), we refer to [19].

4.2.2 Social welfare problem

We define the social welfare by $U(P_d) - C(P_g)$, which consists of a utility function $U(P_d)$ of the consumers P_d and the total power generation cost $C(P_g)$ associated to the producers P_g. The objective is to maximize the social welfare under the constraint of zero frequency deviation, which can be formulated as an optimization problem. We assume that $C(P_g)$ is a strictly convex function and $U(P_d)$ is a strictly concave function so that we will obtain an optimization problem which is convex. By analyzing the equilibria of (4.2), it follows that a necessary condition for zero frequency deviation is $\mathbb{1}^T P_d = \mathbb{1}^T P_g$ [19], i.e. the total supply must match the total demand. It can be noted that (P_g, P_d) is a solution to the latter equation if and only if there exists a vector $v \in \mathbb{R}^{m_c}$ such that $D_c v - P_g + P_d = 0$ where $D_c \in \mathbb{R}^{n \times m_c}$ is the incidence matrix (defined similarly as in (4.1)) of some connected *communication graph* with m_c edges and n nodes. This communication

graph may be different from the physical network topology and will play a central role in the controllers proposed in Sections 4.3 and 4.4. Because of the latter equivalence, we consider the following convex minimization problem:

$$\begin{aligned} \underset{P_g,P_d,v}{\text{maximize}} \quad & S(P_g,P_d) := U(P_d) - C(P_g) \\ \text{subject to} \quad & D_c v - P_g + P_d = 0. \end{aligned} \tag{4.5}$$

The corresponding Lagrangian is given by

$$L = U(P_d) - C(P_g) - \lambda^T (D_c v - P_g + P_d)$$

with Lagrange multipliers $\lambda \in \mathbb{R}^n$. The resulting first-order optimality conditions ($\nabla L = 0$) are given by

$$\begin{aligned} \nabla C(\bar{P}_g) - \bar{\lambda} &= 0 \\ -\nabla U(\bar{P}_d) + \bar{\lambda} &= 0 \\ D_c^T \bar{\lambda} &= 0 \\ D_c \bar{v} - \bar{P}_g + \bar{P}_d &= 0. \end{aligned} \tag{4.6}$$

Since the minimization problem is convex it follows that $(\bar{P}_g, \bar{P}_d, \bar{v})$ is an optimal solution to (4.5) if and only if there exists a $\bar{\lambda} \in \mathbb{R}^n$ such that (4.6) holds [12].

4.3 Internal-model-based controller

In this section we extend the results of [19] in which we include a utility function for the demand. We assume that the utility functions are quadratic and given by $C(P_g) = \frac{1}{2} P_g^T Q_g P_g + c^T P_g, U(P_d) = -\frac{1}{2} P_d^T Q_d P_d + b^T P_d$ where $Q_d, Q_g \in \mathbb{R}^{n \times n}$ are symmetric positive definite matrices and $c, b \in \mathbb{R}^n$. Consider minimization problem (4.5), then the first-order optimally conditions (4.6) take the form

$$\begin{aligned} Q_g \bar{P}_g + c - \bar{\lambda} &= 0 \\ Q_d \bar{P}_d - b + \bar{\lambda} &= 0 \\ D_c^T \bar{\lambda} &= 0 \\ D_c \bar{v} - \bar{P}_g + \bar{P}_d &= 0. \end{aligned} \tag{4.7}$$

Note that $Q_g P_g + c$ are the (aggregated) marginal costs of the producers and likewise $-Q_d P_d + b$ are the marginal utilities of the consumers. Observe from (4.7) that the prosumers (combined producers and consumers) achieve maximal welfare if their marginal costs and utilities respectively are equal to the price λ, which is a standard result in economics. The optimal production and demand are therefore given by

$$\begin{aligned} \bar{P}_g &= Q_g^{-1}(\bar{\lambda} - c) \\ \bar{P}_d &= Q_d^{-1}(b - \bar{\lambda}). \end{aligned} \tag{4.8}$$

From the third equation of (4.7) it follows that the prices must be identical in each control area, i.e. $\bar{\lambda} = \mathbb{1}\lambda^*$ where the common price λ^* is computed as

$$\begin{aligned} &\mathbb{1}^T \bar{P}_g = \mathbb{1}^T Q_g^{-1}(\mathbb{1}\lambda^* - c) = \mathbb{1}^T Q_d^{-1}(b - \mathbb{1}\lambda^*) = \mathbb{1}^T \bar{P}_d \\ &\Rightarrow \bar{\lambda} = \mathbb{1}\lambda^*, \qquad \lambda^* = \frac{\mathbb{1}^T(Q_g^{-1}c + Q_d^{-1}b)}{\mathbb{1}^T(Q_g^{-1} + Q_d^{-1})\mathbb{1}}. \end{aligned} \tag{4.9}$$

Based on the controller design proposed in [19], we consider the following price-based controller dynamics in port-Hamiltonian form with inputs u_λ and outputs y_λ:

$$\begin{aligned} \dot{\lambda} &= -L_c \nabla H_c(\lambda) + \begin{bmatrix} Q_g^{-1} & -Q_d^{-1} \end{bmatrix} u_\lambda \\ y_\lambda &= \begin{bmatrix} Q_g^{-1} \\ -Q_d^{-1} \end{bmatrix} \nabla H_c(\lambda) + \begin{bmatrix} -Q_g^{-1}c \\ Q_d^{-1}b \end{bmatrix}. \end{aligned} \tag{4.10}$$

The controller Hamiltonian is given by $H_c(\lambda) = \frac{1}{2}\lambda^T\lambda$ and $L_c = D_c D_c^T$ is the Laplacian matrix of the communication graph. We interconnect systems (4.4) and (4.10) in a power-preserving way by $u_\lambda = -y_p, u_p = y_\lambda$. Then we obtain the closed-loop port-Hamiltonian system

$$\begin{bmatrix} \dot{\eta} \\ \dot{p} \\ \dot{\lambda} \end{bmatrix} = \begin{bmatrix} 0 & D^T & 0 \\ -D & -A & Q_g^{-1} + Q_d^{-1} \\ 0 & -Q_g^{-1} - Q_c^{-1} & -L_c \end{bmatrix} \nabla H(x) - \begin{bmatrix} 0 \\ Q_g^{-1}c + Q_d^{-1}b \\ 0 \end{bmatrix} \tag{4.11}$$

where $x = (\eta, p, \lambda)$ and the Hamiltonian is given by

$$H(x) = H_p(\eta, p) + H_c(\lambda) = \frac{1}{2}p^T M^{-1} p - \mathbb{1}^T \Gamma \cos \eta + \frac{1}{2}\lambda^T\lambda.$$

It is noticed that all equilibria of (4.11) are characterized by $(\bar{\eta}, \bar{p}, \bar{\lambda})$ satisfying

$$\begin{aligned} &\bar{p} = 0 \\ &0 = -D\Gamma \sin \bar{\eta} + (Q_g^{-1} + Q_d^{-1})\bar{\lambda} - Q_g^{-1}c - Q_d^{-1}b \\ &\bar{\lambda} = \mathbb{1}\lambda^*, \qquad \lambda^* = \frac{\mathbb{1}^T(Q_g^{-1}c + Q_d^{-1}b)}{\mathbb{1}^T(Q_g^{-1} + Q_d^{-1})\mathbb{1}}. \end{aligned} \tag{4.12}$$

We define $\bar{\mathcal{Z}}_1$ as the solution set of (4.12), i.e.

$$\bar{\mathcal{Z}}_1 = \{(\bar{\eta}, \bar{p}, \bar{\lambda}) \mid (\bar{\eta}, \bar{p}, \bar{\lambda}) \text{ is a solution to (4.12)}\}.$$

For proving asymptotic stability of the closed-loop system (4.11) an additional assumption is required.

Assumption 4.3.1. There exists a $(\bar{\eta}, \bar{p}, \bar{\lambda}) \in \bar{\mathcal{Z}}_1$ such that $\bar{\eta}_k \in (-\pi/2, \pi/2)$ for all $k \in \mathcal{E}$.

This assumption is standard in studies on power grid stability and is also referred to as a security constraint [113].

4.3.1 Stability

We will show that trajectories (η, p, λ) satisfying (4.11) and initializing sufficiently close to an equilibrium point of (4.11) converge to the set $\bar{\mathcal{Z}}_1$. Moreover, we show that this set corresponds to the optimal points of the social welfare problem.

Theorem 4.3.2. *For every $\bar{x} \in \bar{\mathcal{Z}}_1$ satisfying Assumption 4.3.1 there exists an open neighborhood $\mathcal{O}$ around $\bar{x}$ such that all trajectories x satisfying* (4.11) *with initial conditions in $\mathcal{O}$ converge to the set $\bar{\mathcal{Z}}_1$. Moreover, the power generations and demands converge to the optimal value given by* (4.8) *and* (4.9)*.*

Proof. Since the system (4.11) is not centered around the origin we introduce a shifted Hamiltonian $\bar{H}$ w.r.t. $\bar{x} \in \bar{\mathcal{Z}}_1$ (see e.g. [19, 117]), which will act as a Lyapunov function:

$$\begin{aligned}\bar{H}(x) &= H(x) - (x-\bar{x})^T \nabla H(\bar{x}) - H(\bar{x}) = \frac{1}{2} p^T M^{-1} p - \mathbb{1}^T \Gamma \cos \eta + \frac{1}{2} \lambda^T \lambda \\ &\quad - \begin{bmatrix} \eta^T - \bar{\eta}^T & 0 & \lambda^T - \bar{\lambda}^T \end{bmatrix} \begin{bmatrix} \Gamma \sin \bar{\eta} \\ 0 \\ \bar{\lambda} \end{bmatrix} - \mathbb{1}^T \Gamma \cos \bar{\eta} + \frac{1}{2} \bar{\lambda}^T \bar{\lambda} \\ &= \frac{1}{2} p^T M^{-1} p + \frac{1}{2} \|\lambda - \bar{\lambda}\|^2 - \mathbb{1}^T \Gamma \cos \eta - (\eta - \bar{\eta})^T \Gamma \sin \bar{\eta} + \mathbb{1}^T \Gamma \cos \bar{\eta}.\end{aligned} \tag{4.13}$$

Bearing in mind Assumption 4.3.1 and [18], the shifted Hamiltonian satisfies $\bar{H}(\bar{x}) = 0$ and $\bar{H}(x) > 0$ for all $x \neq \bar{x}$ in an sufficiently small open neighborhood around $\bar{x}$. Moreover, the shifted Hamiltonian satisfies $\nabla \bar{H}(x) = \nabla H(x) - \nabla H(\bar{x})$ so that (4.11) can be rewritten as

$$\begin{aligned}\dot{x} &= \begin{bmatrix} 0 & D^T & 0 \\ -D & -A & Q_g^{-1} + Q_d^{-1} \\ 0 & -Q_g^{-1} - Q_c^{-1} & -L_c \end{bmatrix} \nabla \bar{H}(x) \\ &\quad + \begin{bmatrix} 0 \\ -D\Gamma \sin \bar{\eta} + (Q_g^{-1} + Q_d^{-1})\bar{\lambda} - Q_g^{-1} c - Q_d^{-1} b \\ -L_c \bar{\lambda} \end{bmatrix} \\ &= \begin{bmatrix} 0 & D^T & 0 \\ -D & -A & Q_g^{-1} + Q_d^{-1} \\ 0 & -Q_g^{-1} - Q_c^{-1} & -L_c \end{bmatrix} \nabla \bar{H}(x).\end{aligned}$$

Because of the port-Hamiltonian structure of the system it is convenient to show that the shifted Hamiltonian satisfies

$$\dot{\bar{H}} = -\omega^T A \omega - (\lambda - \bar{\lambda})^T L_c (\lambda - \bar{\lambda}) \leq 0 \tag{4.14}$$

where equality holds if and only if $\omega = 0$ and $\lambda = \bar{\lambda} + \mathbb{1}\alpha$ for some scalar function α. On the set $\dot{\bar{H}} = 0$ we have

$$\begin{aligned}\dot{\eta} &= 0\\ \dot{p} &= -D\Gamma\,\mathbf{sin}\,\eta + D\Gamma\,\mathbf{sin}\,\bar{\eta} + (Q_g^{-1} + Q_d^{-1})\mathbb{1}\alpha = 0\\ \dot{\lambda} &= 0\end{aligned}$$

Obviously, in the largest invariant set where $\dot{H} = 0$ we must have that $\alpha \equiv 0$, which follows from the premultiplication by $\mathbb{1}^T$ of the second equation. Hence, by LaSalle's invariance principle $p \to 0, \lambda \to \bar{\lambda}, \eta \to \hat{\eta}$ as $t \to \infty$ for some constant $\hat{\eta}$ satisfying

$$D\Gamma\,\mathbf{sin}\,\hat{\eta} = D\Gamma\,\mathbf{sin}\,\bar{\eta} = (Q_g^{-1} + Q_d^{-1})\bar{\lambda} - Q_g^{-1}c - Q_d^{-1}b.$$

hence $x \to \bar{\mathcal{Z}}_1$ as $t \to \infty$. Moreover, since interconnection between the controller and the swing equations is given by

$$\begin{bmatrix} P_g \\ P_d \end{bmatrix} = u_p = y_\lambda = \begin{bmatrix} Q_g^{-1}(\lambda - c) \\ Q_d^{-1}(b - \lambda) \end{bmatrix}$$

it follows that the power generations and demands converge to the optimal value given by (4.8) and (4.9) as $t \to \infty$. □

4.4 Primal-dual gradient controller

By applying the primal-dual gradient method [6, 64, 120, 132] to the minimization problem (4.5) we obtain the real-time dynamic pricing model

$$\begin{aligned} K_g\dot{P}_g &= -\nabla C(P_g) + \lambda + w_g\\ K_d\dot{P}_d &= \nabla U(P_d) - \lambda + w_d\\ K_v\dot{v} &= -D_c^T\lambda\\ K_\lambda\dot{\lambda} &= D_c v - P_g + P_d \end{aligned} \tag{4.15}$$

where we introduce additional inputs $w = (w_g, w_d)$ which are to be specified later on. Here $K_c = \text{blockdiag}(K_g, K_d, K_v, K_\lambda) > 0$ are the gains of the controller. Note that we have constructed a distributed controller where λ_i acts as a price in control area $i \in \mathcal{V}$ and v represents the information exchange of the differences of the prices λ along the edges the communication graph. We define the energy variables as

$$x_c = (x_g, x_d, x_v, x_\lambda) = (K_g P_g, K_d P_d, K_v v, K_\lambda \lambda) = K_c z_c$$

and notice that in the sequel, we interchangeably write the system characteristics in terms of energy variables (often denoted by x) and co-energy variables (often denoted by z) for ease of notation.

An interesting fact is that the market dynamics (4.15) admits an incremental port-Hamiltonian representation which is given by

$$\begin{aligned}\dot{x}_c &= \begin{bmatrix} 0 & 0 & 0 & I \\ 0 & 0 & 0 & -I \\ 0 & 0 & 0 & -D_c^T \\ -I & I & D_c & 0 \end{bmatrix} \nabla H(x_c) + \begin{bmatrix} I & 0 \\ 0 & I \\ 0 & 0 \\ 0 & 0 \end{bmatrix} (w + \nabla S(y_c)) \\ y_c &= \begin{bmatrix} I & 0 & 0 & 0 \\ 0 & I & 0 & 0 \end{bmatrix} \nabla H(x_c) = \begin{bmatrix} P_g \\ P_d \end{bmatrix}.\end{aligned} \tag{4.16}$$

with the quadratic controller Hamiltonian

$$H_c(x_c) = \frac{1}{2} x_c^T K_c^{-1} x_c. \tag{4.17}$$

Note that the latter system is indeed a incrementally port-Hamiltonian system since S is concave and therefore satisfies the property

$$(y_{c1} - y_{c2})^T (\nabla S(y_{c1}) - \nabla S(y_{c2})) \leq 0, \qquad \forall y_{c1}, y_{c2} \in \mathbb{R}^{2n}.$$

We obtain a power-preserving interconnection between (4.4) and (4.16) by choosing $w = -y_p, u_p = y_c$. Define the extended (co-)energy variables by $x = (\eta, p, x_c), z = (\eta, \omega, z_c)$ then the closed-loop system becomes

$$\begin{aligned} \dot{\eta} &= D^T \omega \\ M\dot{\omega} &= -D^T \Gamma \, \mathbf{sin}\, \eta - A\omega + P_g - P_d \\ K_g \dot{P}_g &= -\nabla C(P_g) + \lambda - \omega \\ K_d \dot{P}_d &= \nabla U(P_d) - \lambda + \omega \\ K_v \dot{v} &= -D_c^T \lambda \\ K_\lambda \dot{\lambda} &= D_c v - P_g + P_d \end{aligned} \tag{4.18}$$

which can be written in port-Hamiltonian form as

$$\dot{x} = \begin{bmatrix} 0 & D^T & 0 & 0 & 0 & 0 \\ -D & -A & I & -I & 0 & 0 \\ 0 & -I & 0 & 0 & 0 & I \\ 0 & I & 0 & 0 & 0 & -I \\ 0 & 0 & 0 & 0 & 0 & -D_c^T \\ 0 & 0 & -I & I & D_c & 0 \end{bmatrix} \nabla H(x) + \underbrace{\begin{bmatrix} 0 & 0 \\ 0 & 0 \\ I & 0 \\ 0 & I \\ 0 & 0 \\ 0 & 0 \end{bmatrix}}_{G} \nabla S(y) \tag{4.19}$$

$$y = G^T \nabla H(x) = \begin{bmatrix} P_g \\ P_d \end{bmatrix} \tag{4.20}$$

with H as the sum of the energy function (4.3) corresponding to the physical model, and the controller Hamiltonian (4.17).

4.4.1 Closed-loop equilibria

We define the equilibrium set of (4.19), expressed in the co-energy variables, by

$$\bar{\mathcal{Z}}_2 = \{\bar{z} = (\bar{\eta}, \bar{\omega}, \bar{P}_g, \bar{P}_d, \bar{v}, \bar{\lambda}) \mid \bar{z} \text{ satisfies (4.22)}\}. \tag{4.21}$$

where

$$0 = D^T \bar{\omega} \tag{4.22a}$$
$$0 = -D^T \Gamma \sin \bar{\eta} - A\bar{\omega} + \bar{P}_g - \bar{P}_d \tag{4.22b}$$
$$0 = -\nabla C(\bar{P}_g) + \bar{\lambda} - \bar{\omega} \tag{4.22c}$$
$$0 = \nabla U(\bar{P}_d) - \bar{\lambda} + \bar{\omega} \tag{4.22d}$$
$$0 = -D_c^T \bar{\lambda} \tag{4.22e}$$
$$0 = D_c \bar{v} - \bar{P}_g + \bar{P}_d \tag{4.22f}$$

By (4.22a) we observe that $\bar{\omega} = \mathbb{1}\omega_*$ for some $\omega_* \in \mathbb{R}$. Then by premultiplying (4.22b), and (4.22f) by $\mathbb{1}^T$ it follows that $\omega_* = 0$ and thus zero frequency is achieved at steady state. Hence, $\bar{\mathcal{Z}}_2$ is equal to the set of $\bar{z}$ satisfying the KKT optimality conditions (4.6) and the zero frequency constraints

$$-D\Gamma \sin \bar{\eta} + \bar{P}_g - \bar{P}_d = 0, \quad \bar{\omega} = 0$$

of the physical network and therefore corresponds to the desired optimal points.

4.4.2 Stability

We now state the main stability result of the coupled system (4.18).

Theorem 4.4.1. *For every $\bar{z} \in \bar{\mathcal{Z}}_2$, with $\bar{\mathcal{Z}}_2$ defined in* (4.21)*, there exists an open neighborhood $\mathcal{O}$ around $\bar{z}$ such that all trajectories z satisfying* (4.19) *with initial conditions in $\mathcal{O}$ converge to the set $\bar{\mathcal{Z}}_2$.*

Proof. Let $\bar{z} \in \bar{\mathcal{Z}}_2$ and let this equilibrium be expressed in the energy variables by defining the vectors $\bar{x} = (\bar{\eta}, 0, K_g\bar{P}_g, K_d\bar{P}_d, K_v\bar{v}, K_\lambda\bar{\lambda}), \bar{y} = G^T\nabla H(\bar{x})$. Let the shifted Hamiltonian $\bar{H}$ around $\bar{x}$ be given by

$$\begin{aligned}\bar{H}(x) &= H(x) - (x-\bar{x})^T \nabla H(\bar{x}) - H(\bar{x}) \\ &= \frac{1}{2}(p-\bar{p})^T M^{-1}(p-\bar{p}) + \frac{1}{2}(x_c - \bar{x}_c)^T K_c^{-1}(x_c - \bar{x}_c) \\ &- \mathbb{1}^T \Gamma \cos \eta - (\eta - \bar{\eta})^T \Gamma \sin \bar{\eta} + \mathbb{1}^T \Gamma \cos \bar{\eta}.\end{aligned}$$

As in mentioned in the proof of Theorem 4.3.2, it can be shown that $\bar{H}(\bar{x}) = 0$ and $\bar{H}(x) > 0$ for all $x \neq \bar{x}$ in a sufficiently small open neighborhood around $\bar{x}$. After rewriting, the closed loop port-Hamiltonian system (4.19) is equivalently

described by

$$\dot{x} = \begin{bmatrix} 0 & D^T & 0 & 0 & 0 & 0 \\ -D & -A & I & -I & 0 & 0 \\ 0 & -I & 0 & 0 & 0 & I \\ 0 & I & 0 & 0 & 0 & -I \\ 0 & 0 & 0 & 0 & 0 & -D_c^T \\ 0 & 0 & -I & I & D_c & 0 \end{bmatrix} \nabla \bar{H}(x) + G(\nabla S(y) - \nabla S(\bar{y}))$$
$$y - \bar{y} = G^T \nabla \bar{H}(x)$$

Then time-derivative of the shifted Hamiltonian $\bar{H}$ satisfies

$$\dot{\bar{H}} = -\omega^T A \omega + (y - \bar{y})^T (\nabla S(y) - \nabla S(\bar{y})) \leq 0$$

where equality holds if and only if $\omega = 0, P_g = \bar{P}_g, P_d = \bar{P}_d$ since $S(.)$ is a strictly concave function. On the largest invariant set M where $\dot{\bar{H}} = 0$ we have $\lambda = \bar{\lambda}$ and therefore v is constant. We conclude that $M \subset \bar{\mathcal{Z}}_2$ and by LaSalle's invariance principle it follows that $z \to M \subset \bar{\mathcal{Z}}_2$ as $t \to \infty$ for trajectories initialized sufficiently close to $\bar{x}$. □

Comparison of both controllers

When comparing both controllers it is noticed that the internal-model-based controller requires that the utility and cost functions are quadratic. Since the matrices Q_g, Q_d appear in the closed-loop interconnection structure (4.11), it would be challenging to generalize the internal-model-based controller to the case where general strictly convex utility functions are considered. On the other hand, by applying the primal-dual gradient method to the optimization problem (4.5) it is possible to construct a distributed controller that can deal with general convex utility functions.

Remark 4.4.2 (Economic interpretation of controllers (4.10), (4.15)). The controller variables λ of both controllers are interpreted as the electricity prices, where we may have different prices in each of the control areas initially. However, the controllers differ in the way they compensate for the price differences. On the one hand, the v dynamics of the gradient method based controller *integrates* the differences between the prices λ. On the other hand, in the internal-model-based controller these differences are *dissipated* through the Laplacian matrix L_c, by noting from (4.14) that as long as λ is not in the range of $\mathbb{1}$, energy will be dissipated from the system. This has a stabilizing effect on the overall dynamics of the closed-loop system in case the internal-model-based controller is applied, see also Section 4.5.

What both controllers have in common is that in the design of the distributed controllers there is freedom of choosing any communication graph, where the only requirement is that the graph is connected. Another remark is that, if we would

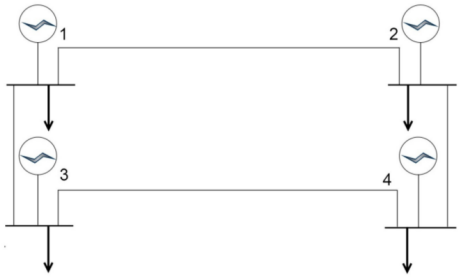

Figure 4.1: A power grid consisting of 4 control areas [19].

assume that

$$C(P_g) = \sum_{i=1}^{n} C_i(P_{gi}), \quad U(P_d) = \sum_{i=1}^{n} U_i(P_{di}),$$

both distributed controllers in each control area require only information about their individual utility and cost functions, which beneficial is for privacy reasons and communication purposes.

4.5 Numerical results

We illustrate the performance of both proposed controllers, when applied to an academic test case, where we consider of 4 control areas[1], see Figure 4.1. To compare both controllers we use identical quadratic utility and cost functions in the social welfare problem. The parameters we use for both cases are given by $Q_g = \text{diag}(1, 2, 3, 4), M = \Gamma = Q_d = \frac{1}{2}A = I, c = 0, b = \text{col}(1, 1.25, 1.5, 1.75), D_c = D, K_c = I$.

We initialize at (optimal) steady operation and at time $t = 1$ we introduce a change in the utility function of the demand corresponding to area 4 by changing b into $b = \text{col}(1, 1.25, 1.5, 2)$, i.e. the consumption of electricity becomes more attractive in this area. The dynamics of the closed-loop systems are plotted in Figure 4.2 and 4.3 on page 91. At steady state we observe that the power production is higher in the control areas with lower costs functions and similar conclusions can be drawn for the power consumption. Hence at steady state, the social welfare is maximized.

When the consumers utility function is changed, we observe that indeed the consumption increases in control area 4, as we would expect. As a consequence, the common electricity price rises so that the power demands in the other control areas decrease. Simultaneously, the power production is increased to match the total supply and demand. It follows that, after finite time, the closed-loop dynamics is operating at maximal social welfare again. It is noted that both controllers

[1]This example is based on the 4 control area case study discussed in [19].

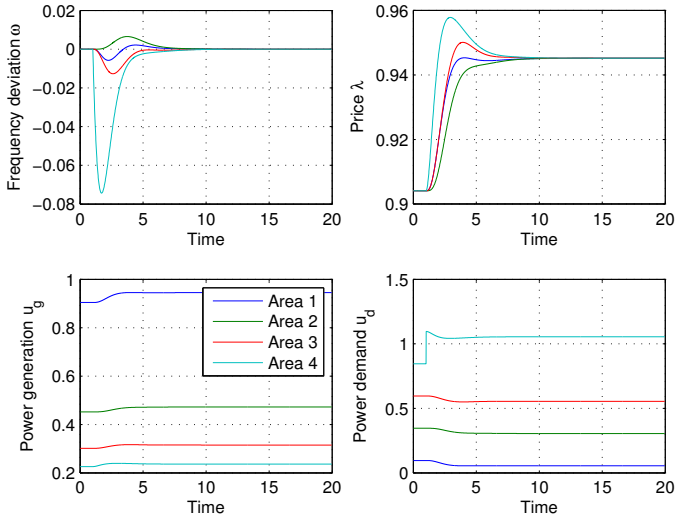

Figure 4.2: Performance of the internal-model-based controller. At time $t = 1$ the consumers utility function corresponding to control area 4 is changed, so that consumption of electricity becomes more attractive in this area.

show comparable performance with the gradient method based controller showing a slightly more oscillatory behavior, which can be explained by Remark 4.4.2.

4.6 Conclusions

In this chapter we proposed a novel way of modeling, analysis and control of smart grids based on the port-Hamiltonian framework. We have proposed two different types of distributed real-time price-based controllers that achieve frequency regulation while maximizing the social welfare, which are internal-model-based and gradient method based. In the design there is freedom in choosing any connected communication graph. An important result is that the market dynamics, obtained from applying the two proposed price-based controllers, can be represented in a port-Hamiltonian form. By coupling this with the port-Hamiltonian representation of the physical power network, a closed-loop port-Hamiltonian system is obtained whose properties are exploited to prove asymptotic stability to the set of optimal points. By applying the real-time dynamic pricing models to an identical academic test case, numerical results have shown the performance of both controllers in case of quadratic utility functions, and show convergence to the point where the social welfare is maximized, even after a change in the consumers utility function.

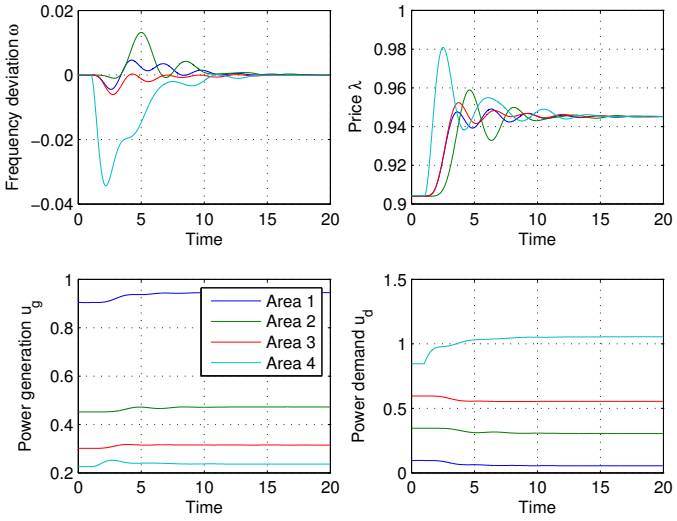

Figure 4.3: Performance of the gradient method based controller. The same parameters and change in the utility function are considered as in the results shown in Figure 4.2. Note that the gradient method based controller shows a slightly more oscillatory behavior, since it contains additional layers of integrators compared to the internal-model-based controller.

Possible extensions

In this chapter we only considered the total supply-demand matching constraints in the social welfare problem. An natural extension is to consider both non-quadratic utility/cost functions and to include additional inequality constraints which for example correspond to congestion. This is possible (only) for the primal-dual gradient based controller and is investigated in the next chapter. Furthermore, although the model for the power network used here is relatively simple, this chapter established a good starting point for considering more complex physical systems of the power grid in the port-Hamiltonian framework. In these models one may for example include reactive power and voltage dynamics as we show in Chapters 5,6,7. In addition to the proposed controller design methods, one would also like to develop distributed controllers that can deal with uncertainties, for example, in the (demand) utility functions.

Chapter 5

Constrained social welfare optimization and frequency regulation

Abstract: *In this chapter a unifying energy-based approach is provided to the modeling and stability analysis of power systems coupled with market dynamics. We consider a standard model of the power network with a third-order model for the synchronous generators involving voltage dynamics. By applying the primal-dual gradient method to a social welfare optimization, a distributed dynamic pricing algorithm is obtained, which can naturally be formulated in port-Hamiltonian form. By interconnection with the physical model a closed-loop port-Hamiltonian system is obtained, whose properties are exploited to prove asymptotic stability to the set of optimal points. Then we provide several variations and extensions to the basic controller design. This includes extension to the case that also general constraints on the nodal power generation and demand are considered in the social welfare problem. Additionally, the case of line congestion and power transmission costs in acyclic networks is covered. Also a dynamic pricing algorithm is proposed that does not require knowledge about the power supply and demand for the implementation.*

Published as:

T.W. Stegink, C. De Persis, A.J. van der Schaft. "A unifying energy-based approach to stability of power grids with market dynamics." IEEE Transactions on Automatic Control 62.6 (2017): 2612-2622.

5.1 Introduction

Provisioning energy has become increasingly complicated due to several reasons, including the increased share of renewables. As a result, the generators operate more often near their capacity limits and transmission line congestion occurs more frequently. One effective approach to alleviate some of these challenges is to use real-time dynamic pricing as a control method [2]. This feedback mechanism can be used to encourage the consumers to change their usage when in some parts of the grid it is difficult for the generators and the network to match the demand. Real-time dynamic pricing also allows producers and consumers to fairly share utilities and costs associated with the generation and consumption of energy among the different control areas. The challenge of achieving this in an optimal manner while the grid operates within its capacity limits, is called the *social welfare problem* [57, 58].

Many of the existing dynamic pricing algorithms focus on the economic part of optimal supply-demand matching [57, 84]. However, if market mechanisms are used to determine the optimal power dispatch (with near real-time updates of the dispatch commands) dynamic coupling occurs between the market update process and the physical response of the physical power network dynamics [3]. Consequently, under the assumption of market-based dispatch, it is essential to consider the stability of the coupled system incorporating both market operation and electromechanical power system dynamics simultaneously.

While on this subject a vast literature is already available, the aim of this chapter is to provide a rigorous and unifying passivity-based stability analysis. We focus on a more accurate and higher order model for the physical power network than conventionally used in the literature. In particular, we use a third-order model for the synchronous generators including voltage dynamics. As a result, market dynamics, frequency dynamics and voltage dynamics are considered simultaneously.

Finally, we propose variations of the basic controller design that, among other things, allow the incorporation of capacity constraints on the generation and demand of power and on the transmission lines, and enhance the transient dynamics of the closed-loop system. The approach taken in this chapter is to model both the dynamic pricing controller as well as the physical network in a port-Hamiltonian way, emphasizing energy storage and power flow. This provides a unified framework for the modeling, analysis and control of power networks with market dynamics, with possible extensions to more refined models of the physical power network, including for example turbine dynamics but also higher order models of the synchronous machine (see also Chapter 7).

Literature review

The coupling between a high-order dynamic power network and market dynamics has been studied before in [3]. Here a fourth-order model of the synchronous generator is used in conjunction with turbine and exciter dynamics, which is

coupled to a simple model describing the market dynamics. The results established in [3] are based on an eigenvalue analysis of the linearized system.

It is shown in [113] that the third-order model (often called the *flux-decay model*) for describing the power network, as used in the present chapter, admits a useful passivity property that allows for a rigorous stability analysis of the interconnection with optimal power dispatch controllers, even in the presence of time-varying demand.

A common way to solve a general optimization problem like the social welfare problem is by applying the primal-dual gradient method [6, 36, 52]. Also in power grids this is a commonly used approach to design optimal distributed controllers, see e.g. [64, 68, 92, 130–132]. The problem formulations vary in these papers, with the focus being on either the generation side [64, 92], the load side [68, 69, 135] or both [130–133]. We will elaborate on these references in the following two paragraphs.

A vast literature focuses on linear power system models coupled with gradient-method-based controllers [64, 68, 69, 92, 130, 137]. In these references the property that the linear power system dynamics can be formulated as a gradient method applied to a certain optimization problem is exploited. This is commonly referred to as *reverse-engineering* of the power system dynamics [64, 92, 130]. However, this approach falls short in dealing with models involving nonlinear power flows.

Nevertheless, [131–133, 135] show the possibility to achieve optimal power dispatch in power networks with nonlinear power flows using gradient-method-based controllers. On the other hand, the controllers proposed in [131–133] have restrictions in assigning the controller parameters and in addition require that the topology of the physical network is a tree.

Main contributions

The contribution of this chapter is to propose a novel energy-based approach to the problem that differs substantially from the aforementioned works. We proceed along the lines of [105, 106], where a port-Hamiltonian approach to the design of gradient-method-based controllers in power networks is proposed. In those papers it is shown that both the power network as well as the controller designs admit a port-Hamiltonian representation which are then interconnected to obtain a closed-loop port-Hamiltonian system.

After showing that the third-order dynamical model describing the power network admits a port-Hamiltonian representation, we provide a systematic method to design gradient-method-based controllers that is able to balance power supply and demand while maximizing the social welfare at steady state. This design is carried out first by establishing the optimality conditions associated with the social welfare problem. Then the continuous-time gradient method is applied to obtain the port-Hamiltonian form of the dynamic pricing controller. Then, following [105, 106], the market dynamics is coupled to the physical power network in a *power-preserving* manner so that all the trajectories of the closed-loop system converge to the desired synchronous solution and to optimal power dispatch.

Although the proposed controllers share similarities with others presented in the literature, the way in which they are interconnected to the physical network, which is based on passivity, is to the best of our knowledge new. Moreover, they show several advantages.

Physical model: Since our approach is based on passivity and does not require to reverse-engineer the power system dynamics as a primal-dual gradient dynamics, it allows to deal with more complex nonlinear models of the power network. More specifically, the physical model for describing the power network in this chapter admits nonlinear power flows and time-varying voltages, and is more accurate and reliable than the classical second-order model [61, 67, 89].

In addition, most of the results that are established in the present chapter are valid for the case of nonlinear power flows and cyclic networks, in contrast to e.g. [64, 92, 130, 137], where the power flows are linearized and e.g. [131–133] where the physical network topology is a tree. Moreover, in the aforementioned references the voltages are assumed to be constant. While the third-order model for the power network as considered in this chapter has been studied before using passivity based techniques [113], the combination with gradient method based controllers is novel. In addition, the stability analysis does not rely on linearization and is based on energy functions which allow us to establish rigorous stability results.

State transformation: In [64, 92] it is shown how a state transformation of the closed-loop system can be used to eliminate the information about the demand from the controller dynamics, which improves implementation of the resulting controller. We pursue this idea and show that the same kind of state transformation can also be used for more complex physical models as considered in this chapter. This avoids the requirement of knowing the demand to determine the market price.

Controller parameters: In the present chapter we show that both the physical power network as well as the dynamic pricing controllers admit a port-Hamiltonian representation, and in particular are passive systems. As a result, the interconnection between the controller and the nonlinear power system is *power-preserving*, implying passivity of the closed-loop system as well. Consequently, we do not have to impose any condition on controller design parameters for guaranteeing asymptotic stability, contrary to [131–133].

Port-Hamiltonian framework: Because of the use of the port-Hamiltonian framework, the proposed controller designs have the potential to deal with more complex models for the power network compared to the model described in this chapter. As long as the more complex model remains port-Hamiltonian, the results continue to be valid. This may lead to inclusion of, for example, turbine dynamics or automatic voltage regulators in the analysis, although this is beyond the scope of the present chapter. Furthermore, higher order models for the synchronous generator could be considered.

In addition, we propose various extensions to the basic controller design that have not been investigated in the aforementioned references.

Transmission costs: In addition to nodal power constraints and line congestion, we also consider the possibility of including power transmission costs into the social welfare problem. Including such costs may in particular be useful in reducing energy losses or the risk of a breakdown of certain transmission lines.

Non-strict convex objective functions: By relaxing the conditions on the objective function, we show that also non-strict convex/concave cost/utility functions can be considered respectively. In addition, the proposed technique allows to add damping in the gradient method based controller which may improve the convergence rate of the closed-loop system.

Barrier functions: We highlight the possibility to use barrier functions to enforce the trajectories to stay withing the feasible region, which allows operation within the capacity constraints for all time, even during transients. This permits a more realistic application of the proposed controller design.

Outline: The remainder of this chapter is organized as follows. In Section 5.2 the preliminaries are stated. Then the basic dynamic pricing algorithm is discussed in Section 5.3 and convergence of the closed-loop system is proven. Variations of the basic controller design are discussed in Section 5.4 where in Section 5.4.1 nodal power congestion is included into the social welfare problem, and in Section 5.4.2 the case line congestion for the acyclic power networks is discussed. A dynamic pricing algorithm is proposed in Section 5.4.3 which does not require knowledge about the power supply and demand. In Section 5.4.4 the possibility to relax the convexity assumption and to improve the transient dynamics of the basic controller is discussed. Finally, the conclusions and suggestions for future research are discussed in Section 5.5.

5.2 Preliminaries

5.2.1 Notation

Given a symmetric matrix $A \in \mathbb{R}^{n\times n}$, we write $A > 0$ ($A \geq 0$) to indicate that A is a positive (semi-)definite matrix. The set of positive real numbers is denoted by $\mathbb{R}_{>0}$ and likewise the set of vectors in $\mathbb{R}^n$ whose elements are positive by $\mathbb{R}^n_{>0}$. For $u, v \in \mathbb{R}^n$ we write $u \perp v$ if $u^T v = 0$. We use the compact notational form $0 \leq u \perp v \geq 0$ to denote the complementarity conditions $u \geq 0, v \geq 0, u \perp v$. The notation $\mathbb{1} \in \mathbb{R}^n$ is used for the vector whose elements are equal to 1. Given a twice-differentiable function $f : \mathbb{R}^n \to \mathbb{R}^n$ then the Hessian of f evaluated at x is denoted by $\nabla^2 f(x)$. Given a vector $\eta \in \mathbb{R}^m$, we denote by $\mathbf{sin}(.)$ the element-wise sine function. Given a differentiable function $f(x_1, x_2), x_1 \in \mathbb{R}^{n_1}, x_2 \in \mathbb{R}^{n_2}$ then $\nabla f(x_1, x_2)$ denotes the gradient of f with respect to x_1, x_2 evaluated at x_1, x_2

and likewise $\nabla_{x_1} f(x_1, x_2)$ denotes the gradient of f with respect to x_1. Given a solution x of $\dot{x} = f(x)$, where $f : \mathbb{R}^n \to \mathbb{R}^n$ is a Lebesgue measurable function and locally bounded, the *omega-limit set* $\Omega(x)$ is defined as [26]

$$\Omega(x) := \Big\{ \bar{x} \in \mathbb{R}^n \mid \exists \{t_k\}_{k=1}^{\infty} \subset [0, \infty) \text{ with } \lim_{k\to\infty} t_k = \infty \text{ and } \lim_{k\to\infty} x(t_k) = \bar{x} \Big\}.$$

5.2.2 Power network model

Consider a power grid consisting of n buses. The network is represented by a connected and undirected $\mathcal{R}$ graph $\mathcal{G} = (\mathcal{V}, \mathcal{E})$, where the nodes, $\mathcal{V} = \mathcal{I}_n := \{1, \ldots, n\}$, is the set of buses and the edges, $\mathcal{E} \subset \mathcal{V} \times \mathcal{V}$, is the set of transmission lines connecting the buses. The edges are arbitrarily labeled with a unique identifier in $\mathcal{I}_m = \{1, \ldots, m\}$ where the k-th edge connecting nodes i and j is denoted as $k \sim \{i, j\}$. The ends of edge $k \sim \{i, j\}$ are arbitrary labeled with a '+' and a '-', so that the incidence matrix D of the resulting directed graph is given by

$$D_{ik} = \begin{cases} +1 & \text{if } i \text{ is the positive end of edge } k \\ -1 & \text{if } i \text{ is the negative end of edge } k \\ 0 & \text{otherwise.} \end{cases}$$

Each bus represents a control area and is assumed to have a controllable power supply and demand. The dynamics at each bus $i \in \mathcal{I}_n$ is assumed to be given by [67, 113]

$$\begin{aligned} \dot{\delta}_i &= \omega_i \\ M_i \dot{\omega}_i &= -\sum_{j \in \mathcal{N}_i} B_{ij} E'_{qi} E'_{qj} \sin \delta_{ij} - A_i \omega_i + P_{gi} - P_{di} \\ T'_{doi} \dot{E}'_{qi} &= E_{fi} - (1 - (X_{di} - X'_{di}) B_{ii}) E'_{qi} - (X_{di} - X'_{di}) \sum_{j \in \mathcal{N}_i} B_{ij} E'_{qj} \cos \delta_{ij}, \end{aligned} \tag{5.1}$$

which is commonly referred to as the *flux-decay model*. Here we use a similar notation as used in established literature on power systems [4, 61, 67, 89]. See Table 5.1 for a list of symbols used in the model (5.1) and throughout the chapter.

δ_i	voltage angle
ω_i^b	frequency
ω_s	nominal synchronous frequency
ω_i	frequency deviation $\omega_i := \omega_i^b - \omega_s$
E'_{qi}	q-axis transient internal voltage
E_{fi}	excitation voltage
P_{di}	power demand
P_{gi}	power generation
M_i	moment of inertia
$\mathcal{N}_i$	set of buses connected to bus i
A_i	asynchronous damping constant
B_{ij}	negative of the susceptance of transmission line (i, j)
B_{ii}	self-susceptance
X_{di}	d-axis synchronous reactance of generator i
X'_{di}	d-axis transient reactance of generator i
T'_{doi}	d-axis open-circuit transient time constant

Table 5.1: Parameters and state variables of model (5.1).

Assumption 5.2.1 (Physical power network model)**.** By using the power network model (5.1) the following assumptions are made, which are standard in a broad range of literature on power network dynamics [67].

- Lines are purely inductive, i.e., the conductance is zero. This assumption is generally valid for the case of high voltage lines connecting different control areas.
- The grid is operating around the synchronous frequency which implies $\omega_i^b \approx \omega_s$ for each $i \in \mathcal{V}$.
- In addition, we assume for simplicity that the excitation voltage E_{fi} is constant for all $i \in \mathcal{V}$.

Define the voltage angle differences between the buses by $\eta = D^T\delta$. Further define the angular momenta by $p := M\omega$, where $\omega = \omega^b - \mathbb{1}\omega_s$ are the (aggregated) frequency deviations and $M = \mathrm{diag}_{i\in\mathcal{V}}\{M_i\}$ are the moments of inertia. Let $\Gamma(E'_q) = \mathrm{diag}_{k\in\mathcal{E}}\{\gamma_k\}$ and $\gamma_k = B_{ij}E'_{qi}E'_{qj} = B_{ji}E'_{qi}E'_{qj}$ where $k \sim \{i, j\}$ corresponds to the edge between node i and j. Then we can write (5.1) more compactly as [113]

$$\begin{aligned} \dot{\eta} &= D^T\omega \\ M\dot{\omega} &= -D\Gamma(E'_q)\,\mathbf{sin}\,\eta - A\omega + P_g - P_d \\ T'_{do}\dot{E}'_q &= -F(\eta)E'_q + E_f \end{aligned} \tag{5.2}$$

where $A = \text{diag}_{i\in\mathcal{V}}\{A_i\}, P_g = \text{col}_{i\in\mathcal{V}}\{P_{gi}\}, P_d = \text{col}_{i\in\mathcal{V}}\{P_{di}\}, T'_d = \text{diag}_{i\in\mathcal{V}}\{T'_{doi}\}, E'_q = \text{col}_{i\in\mathcal{V}}\{E'_{qi}\}, E_f = \text{col}_{i\in\mathcal{V}}\{E_{fi}\}$. For a given η, the components of the matrix $F(\eta) \in \mathbb{R}^{n\times n}$ are defined as

$$\begin{aligned} F_{ii}(\eta) &= \frac{1}{X_{di} - X'_{di}} + B_{ii}, \qquad\qquad i \in \mathcal{V} \\ F_{ij}(\eta) &= -B_{ij}\cos\eta_k = F_{ji}(\eta), \quad \text{if } k \sim \{i,j\} \in \mathcal{E} \end{aligned} \tag{5.3}$$

and $F_{ij}(\eta) = 0$ otherwise. Since for realistic power networks $X_{di} > X'_{di}$, and $B_{ii} = \sum_{j\in\mathcal{N}_i} B_{ij} > 0$ for all $i \in \mathcal{V}$, it follows that $F(\eta) > 0$ for all $\eta \in \mathbb{R}^m$ [61, 67].

Considering the physical energy[1] stored in the generator and the transmission lines respectively, we define the Hamiltonian as

$$\begin{aligned} H_p = \frac{1}{2}\sum_{i\in\mathcal{V}} \left(M_i^{-1} p_i^2 + \frac{(E'_{qi} - E_{fi})^2}{X_{di} - X'_{di}} \right) \\ + \frac{1}{2} \sum_{k\sim\{i,j\}\in\mathcal{E}} B_{ij} \left((E'_{qi})^2 + (E'_{qj})^2 - 2E'_{qi}E'_{qj}\cos\eta_k \right) \end{aligned} \tag{5.4}$$

where $\eta_k = \delta_i - \delta_j$. The first term of the Hamiltonian H_p represents the shifted kinetic energy stored in the rotors of the generators and the second term corresponds to the (shifted) magnetic energy stored in the generator circuits. Finally, the last term of H_p corresponds to the magnetic energy stored in the inductive transmission lines.

By (5.4), the system (5.2) can be written in port-Hamiltonian form [117] as

$$\begin{aligned} \dot{x}_p &= \begin{bmatrix} 0 & D^T & 0 \\ -D & -A & 0 \\ 0 & 0 & -R_q \end{bmatrix} \nabla H_p + \begin{bmatrix} 0 & 0 \\ I & -I \\ 0 & 0 \end{bmatrix} u_p \\ y_p &= \begin{bmatrix} 0 & I & 0 \\ 0 & -I & 0 \end{bmatrix} \nabla H_p = \begin{bmatrix} \omega \\ -\omega \end{bmatrix} \end{aligned} \tag{5.5}$$

where $x_p = (\eta, p, E'_q)$, $u_p = (P_g, P_d)$ and

$$\begin{aligned} R_q &= (T'_{do})^{-1}(X_d - X'_d) > 0, \\ T'_{do} &= \text{diag}_{i\in\mathcal{V}}\{T'_{doi}\} > 0, \\ X_d - X'_d &= \text{diag}_{i\in\mathcal{V}}\{X_{di} - X'_{di}\} > 0. \end{aligned}$$

For a study on the stability and equilibria of the flux-decay model (5.5), based on the Hamiltonian function (5.4), we refer to [113]. The stability results established in [113] rely on the following assumption.

[1] For aesthetic reasons we define the Hamiltonian H_p as ω_s times the physical energy as the factor $1/\omega_s$ appears in each of the energy functions. As a result, H_p has the dimension of power instead of energy.

Assumption 5.2.2 (Security constraint)**.** Given constant optimal input $u_p = \bar{u}_p = (\bar{P}_g, \bar{P}_d)$. There exists an equilibrium $(\bar{\eta}, \bar{p}, \bar{E}'_q)$ of (5.5) that satisfies $\bar{\eta} \in \operatorname{im} D^T$, $\bar{\eta} \in (-\pi/2, \pi/2)^m$ and $\nabla^2 H(\bar{\eta}, \bar{p}, \bar{E}'_q) > 0$.

What we mean with an *optimal* input will be discussed in the next section. The assumption $\bar{\eta} \in (-\pi/2, \pi/2)^m$ is standard in studies on power grid stability and is also referred to as a security constraint [113]. In addition, the Hessian condition guarantees the existence of a local storage function around the equilibrium. The following result, which establishes decentralized conditions for checking the positive definiteness of the Hessian, was proven in [31]:

Proposition 5.2.3 (Sufficient condition for positive definite Hessian)**.** *Let* $\bar{E}'_{qi} \in \mathbb{R}^n_{>0}$ *and* $\bar{\eta} \in (-\pi/2, \pi/2)^m$*. If for all* $i \in \mathcal{V}$ *we have*

$$\frac{1}{X_{di} - X'_{di}} + B_{ii} - \sum_{k \sim \{i,j\} \in \mathcal{E}} B_{ij} \frac{\bar{E}_{qi} + \bar{E}_{qj} \sin^2 \bar{\eta}_k}{\bar{E}_{qi} \cos \bar{\eta}_k} > 0,$$

then $\nabla^2 H_p(\bar{x}_p) > 0$.

It can be verified that the condition stated in Proposition 5.2.3 is satisfied if the following holds [31]:

- the generator reactances are small compared to the transmission line reactances
- the voltage (angle) differences are small.

Remarkably, these conditions hold for a typical operation point in power transmission networks.

5.2.3 Social welfare problem

We define the social welfare by $S(P_g, P_d) := U(P_d) - C(P_g)$, which consists of a utility function $U(P_d)$ of the power consumption P_d and the cost $C(P_g)$ associated to the power production P_g. We assume that $C(P_g), U(P_d)$ are strictly convex and strictly concave functions respectively.[2] The objective is to maximize the social welfare while achieving zero frequency deviation. By analyzing the equilibria of (5.1), it follows that a necessary condition for zero frequency deviation is $\mathbb{1}^T P_d = \mathbb{1}^T P_g$, i.e., the total supply must match the total demand [113]. It can be noted that (P_g, P_d) is a solution to the latter equation if and only if there exists a vector $v \in \mathbb{R}^{m_c}$ satisfying $D_c v - P_g + P_d = 0$ where $D_c \in \mathbb{R}^{n \times m_c}$ is the incidence matrix of some connected *communication* graph with m_c edges and n nodes. Because of the latter equivalence, we consider the following convex minimization problem:

$$\underset{P_g, P_d, v}{\text{minimize}} \quad -S(P_g, P_d) = C(P_g) - U(P_d) \tag{5.6a}$$

$$\text{subject to} \quad D_c v - P_g + P_d = 0. \tag{5.6b}$$

[2] Typically, C, U are in the additive form $C(P_g) = \sum_{i \in \mathcal{V}} C_i(P_g), U(P_d) = \sum_{i \in \mathcal{V}} U_i(P_d)$ but in our results it is also possible to include mutual costs and utilities among the different control areas, provided that the convexity/concavity assumptions on C, U are satisfied.

Remark 5.2.4 (Reactive power sharing). Although this chapter focuses on optimal *active* power sharing, we stress that it is also possible to consider (optimal) *reactive* power sharing simultaneously, see e.g. [31] for more details.

The Lagrangian corresponding to (5.6) is given by

$$\mathcal{L} = C(P_g) - U(P_d) + \lambda^T(D_c v - P_g + P_d) \tag{5.7}$$

with Lagrange multipliers $\lambda \in \mathbb{R}^n$. The resulting first-order optimality conditions are given by the Karush–Kuhn–Tucker (KKT) conditions

$$\begin{aligned} \nabla C(\bar{P}_g) - \bar{\lambda} &= 0, \\ -\nabla U(\bar{P}_d) + \bar{\lambda} &= 0, \\ D_c^T \bar{\lambda} &= 0, \\ D_c \bar{v} - \bar{P}_g + \bar{P}_d &= 0. \end{aligned} \tag{5.8}$$

Since the minimization problem is convex, strong duality holds and it follows that $(\bar{P}_g, \bar{P}_d, \bar{v})$ is an optimal solution to (5.6) if and only if there exists an $\bar{\lambda} \in \mathbb{R}^n$ that satisfies (5.8) [12].

5.3 Basic primal-dual gradient controller

In this section we design the basic dynamic pricing algorithm which will be used as the starting point for the controllers designs discussed in Section 5.4. Its dynamics is obtained by applying the primal-dual gradient method [6, 64, 132] to the minimization problem (5.6), resulting in

$$K_g \dot{P}_g = -\nabla C(P_g) + \lambda + u_c^g \tag{5.9a}$$

$$K_d \dot{P}_d = \nabla U(P_d) - \lambda + u_c^d \tag{5.9b}$$

$$K_v \dot{v} = -D_c^T \lambda \tag{5.9c}$$

$$K_\lambda \dot{\lambda} = D_c v - P_g + P_d. \tag{5.9d}$$

Here we introduce additional inputs $u_c = (u_c^g, u_c^d)$ which are to be specified later on, and $K_c := \text{blockdiag}(K_g, K_d, K_v, K_\lambda) > 0$ are controller design parameters. Recall from Section 5.2.3 that there is freedom in choosing a communication network and the associated incidence matrix. Depending on the application, one may prefer all-to-all communication where the underlying graph is complete, or communication networks where its associated graph is a star, line or cycle graph. In addition, K_c determines the converge rate of the dynamics (5.9); a large K_c gives a slow convergence rate whereas a small K_c gives a fast convergence rate.

Observe that the dynamics (5.9) has a clear economic interpretation [2, 3, 57]: each power producer aims at maximizing their own profit, which occurs whenever their individual marginal cost is equal to the local price $\lambda_i + u_{ci}^g$. At the same time, each consumer maximizes its own utility but is penalized by the local price $\lambda_i - u_{ci}^d$. The equations (5.9c), (5.9d) represent the distributed dynamic pricing

mechanism where the quantity v represents a *virtual* power flow along the edges of the communication graph with incidence matrix D_c. We emphasize *virtual*, since v may not correspond to the real physical power flow as the communication graph may be different than the physical network topology. Equation (5.9d) shows that the local price λ_i rises if the power demand plus power outflow at node $i \in \mathcal{V}$ is greater than the local power supply plus power inflow of power at node i and vice versa. The inputs u_c^g, u_c^d are interpreted as additional penalties or prices that are assigned to the power producers and consumers respectively. These inputs can be chosen appropriately to compensate for the frequency deviation in the physical power network as we will show now.

To this end, define the variables $x_c = (x_g, x_d, x_v, x_\lambda) = (K_g P_g, K_d P_d, K_v v, K_\lambda \lambda) = K_c z_c$ and note that, in the sequel, we interchangeably write the system dynamics in terms of both x_c and z_c for ease of notation. In these new variables the dynamics (5.9) admits a natural port-Hamiltonian representation [105], which is given by

$$\dot{x}_c = \begin{bmatrix} 0 & 0 & 0 & I \\ 0 & 0 & 0 & -I \\ 0 & 0 & 0 & -D_c^T \\ -I & I & D_c & 0 \end{bmatrix} \nabla H_c(x_c) + \begin{bmatrix} I & 0 \\ 0 & I \\ 0 & 0 \\ 0 & 0 \end{bmatrix} (\nabla S(y_c) + u_c) \tag{5.10}$$

$$y_c = \begin{bmatrix} I & 0 & 0 & 0 \\ 0 & I & 0 & 0 \end{bmatrix} \nabla H_c(x_c) = \begin{bmatrix} P_g \\ P_d \end{bmatrix},$$

$$H_c(x_c) = \frac{1}{2} x_c^T K_c^{-1} x_c. \tag{5.11}$$

Note that the system (5.10) is indeed an incrementally port-Hamiltonian system since S is concave and therefore satisfies the incremental passivity property

$$(y_1 - y_2)^T (\nabla S(y_1) - \nabla S(y_2)) \leq 0, \ \forall y_1, y_2 \in \mathbb{R}^{2n}.$$

The port-Hamiltonian controller (5.10) is interconnected to the physical network (5.5) by taking $u_c = -y_p, u_p = y_c$. In z-coordinates the closed-loop system is then described by

$$\dot{\eta} = D^T \omega \tag{5.12a}$$

$$M\dot{\omega} = -D\Gamma(E_q') \sin \eta - A\omega + P_g - P_d \tag{5.12b}$$

$$T_{do}' \dot{E}_q' = -F(\eta) E_q' + E_f \tag{5.12c}$$

$$K_g \dot{P}_g = -\nabla C(P_g) + \lambda - \omega \tag{5.12d}$$

$$K_d \dot{P}_d = \nabla U(P_d) - \lambda + \omega \tag{5.12e}$$

$$K_v \dot{v} = -\nabla C_T(v) - D^T \lambda \tag{5.12f}$$

$$K_\lambda \dot{\lambda} = Dv - P_g + P_d. \tag{5.12g}$$

We define the equilibrium set of (5.12) by

$$\bar{\mathcal{Z}}_1 = \{\bar{z} = (\bar{\eta}, \bar{\omega}, \bar{E}_q', \bar{P}_g, \bar{P}_d, \bar{v}, \bar{\lambda}) \mid \bar{z} \text{ is an equilibrium of (5.12)}\}. \tag{5.13}$$

We note that $\bar{\mathcal{Z}}_1$ corresponds to maximal social welfare and zero frequency deviation in the physical network. To see this, let $\bar{z} = (\bar{\eta}, \bar{\omega}, \bar{E}'_q, \bar{P}_g, \bar{P}_d, \bar{v}, \bar{\lambda}) \in \bar{\mathcal{Z}}_1$ be an equilibrium of (5.12). Then by premultiplying (5.12g) by $\mathbb{1}^T$ we have the power balance $\mathbb{1}^T \bar{P}_g = \mathbb{1}^T \bar{P}_d$. From (5.12a) it follows that $\omega = \mathbb{1} w_s$ for some $\omega_s \in \mathbb{R}$. As a result, premultiplication of (5.12b) by $\mathbb{1}^T$ gives $\mathbb{1}^T A \mathbb{1} \omega_s = 0$ and thus $\bar{\omega} = \mathbb{1}\omega_s = 0$. Finally, since $\bar{\omega} = 0$ we have that the optimality conditions (5.8) are satisfied by (5.12d)-(5.12g) at the equilibrium condition.

For the stability analysis of (5.12) it is convenient to write the system in port-Hamiltonian form. To this end, define the extended vectors of variables by

$$x := \begin{bmatrix} I & 0 & 0 & 0 & 0 & 0 & 0 \\ 0 & M & 0 & 0 & 0 & 0 & 0 \\ 0 & 0 & I & 0 & 0 & 0 & 0 \\ 0 & 0 & 0 & K_g & 0 & 0 & 0 \\ 0 & 0 & 0 & 0 & K_d & 0 & 0 \\ 0 & 0 & 0 & 0 & 0 & K_v & 0 \\ 0 & 0 & 0 & 0 & 0 & 0 & K_\lambda \end{bmatrix} \begin{bmatrix} \eta \\ \omega \\ E'_q \\ P_g \\ P_d \\ v \\ \lambda \end{bmatrix} =: Kz. \tag{5.14}$$

Then the closed-loop port-Hamiltonian system takes the form

$$\begin{aligned} \dot{x} &= \begin{bmatrix} 0 & D^T & 0 & 0 & 0 & 0 & 0 \\ -D & -A & 0 & I & -I & 0 & 0 \\ 0 & 0 & -R_q & 0 & 0 & 0 & 0 \\ 0 & -I & 0 & 0 & 0 & 0 & I \\ 0 & I & 0 & 0 & 0 & 0 & -I \\ 0 & 0 & 0 & 0 & 0 & 0 & -D_c^T \\ 0 & 0 & 0 & -I & I & D_c & 0 \end{bmatrix} \nabla H(x) + \begin{bmatrix} 0 & 0 \\ 0 & 0 \\ 0 & 0 \\ I & 0 \\ 0 & I \\ 0 & 0 \\ 0 & 0 \end{bmatrix} \nabla S(y), \\ y &= \begin{bmatrix} 0 & 0 & 0 & I & 0 & 0 & 0 \\ 0 & 0 & 0 & 0 & I & 0 & 0 \end{bmatrix} \nabla H(x) \end{aligned} \tag{5.15}$$

where $H = H_p + H_c$ is equal to the sum of the energy function (5.4) corresponding to the physical model, and the controller Hamiltonian (5.11). We note that this form of the coupled dynamics clearly reveals the damping and interconnection structure of the system. In particular, we can write (5.15) as the incrementally port-Hamiltonian system

$$\begin{aligned} \dot{x} &= (J - R)\nabla H(x) + G \nabla S(y), \\ y &= G^T \nabla H(x) \end{aligned} \tag{5.16}$$

where $R = R^T \geq 0, J = -J^T$ are formed by taking the symmetric, respectively anti-symmetric part of the square matrix depicted in (5.15). Having established the port-Hamiltonian form of the interconnected system, we now state the main result of this section which is the local asymptotic stability of (5.12).

Theorem 5.3.1 (Local asymptotic of (5.12))**.** *For every $\bar{z} \in \bar{\mathcal{Z}}_1$ satisfying Assumption 5.2.2 there exists a neighborhood Υ around $\bar{z}$ where all trajectories*

z satisfying (5.12) *with initial conditions in* Υ *converge to the set* $\bar{\mathcal{Z}}_1$*. In addition, the convergence of each such trajectory is to a point.*

Proof. Let $\bar{z} \in \bar{\mathcal{Z}}_1$ and consider the equivalent port-Hamiltonian form of the system given by (5.15). Define the shifted Hamiltonian $\bar{H}$ around $\bar{x} := K\bar{z}$ as [117]

$$\bar{H}(x) = H(x) - (x - \bar{x})^T \nabla H(\bar{x}) - H(\bar{x}). \tag{5.17}$$

By (5.15), the time-derivative of the shifted Hamiltonian $\bar{H}$ satisfies

$$\dot{\bar{H}} = -\omega^T A \omega + (y - \bar{y})^T (\nabla S(y) - \nabla S(\bar{y})) - (\nabla_{E_q'} \bar{H})^T R_q \nabla_{E_q'} \bar{H} \leq 0, \tag{5.18}$$

where equality holds if and only if $\nabla_{E_q'} \bar{H}(x) = \nabla_{E_q'} H(x) = 0, \omega = 0, P_g = \bar{P}_g, P_d = \bar{P}_d$ since $S(.)$ is strictly concave. Bearing in mind Assumption 5.2.2, it is observed that $\nabla^2 H(x) = \nabla^2 \bar{H}(x) > 0$ for all x in a sufficiently small open neighborhood around $\bar{x}$. Hence, as $\dot{\bar{H}} \leq 0$, there exists a compact sublevel set Υ of $\bar{H}$ around $\bar{z}$ contained in such neighborhood, which is forward invariant. By LaSalle's invariance principle, each the solution with initial conditions in Υ converges to the largest invariant set $\mathcal{S}$ contained in $\Upsilon \cap \{z \mid \nabla_{E_q'} H(x) = 0, \omega = 0,\ P_g = \bar{P}_g,\ P_d = \bar{P}_d\}$. On such invariant set λ, η, v, E_q' are constant and thus $\mathcal{S}$ in contained in the set of equilibria. As a result, for system (5.12), z converges to $\mathcal{S} \subset \bar{\mathcal{Z}}_1$ as $t \to \infty$.

Finally, we prove that the convergence of each solution of (5.15) initializing in Υ is to a point. This is equivalent to proving that its omega-limit set $\Omega(x)$ is a singleton. Since the solution x is bounded, $\Omega(x) \neq \emptyset$ by the Bolzano-Weierstrass theorem [88]. By contradiction, suppose now that there exist two distinct point in $\Omega(x)$, say $\bar{x}_1, \bar{x}_2 \in \Omega(x), \bar{x}_1 \neq \bar{x}_2$. Then there exists $\bar{H}_1(x), \bar{H}_2(x)$ defined by (5.17) with respect to $\bar{x}_1, \bar{x}_2$ respectively and scalars $c_1, c_2 \in \mathbb{R}_{>0}$ such that $\bar{H}_1^{-1}(\leq c_1) := \{x \mid \bar{H}_1(x) \leq c_1\}, \bar{H}_2^{-1}(\leq c_2) := \{x \mid \bar{H}_2(x) \leq c_2\}$ are disjoint and compact as the Hessian of $\bar{H}_1, \bar{H}_2$ is positive definite in the neighborhood Υ. Since each trajectory z converges to $\mathcal{Z}_1$ as proven above, it follows that $K^{-1}\bar{x}_1, K^{-1}\bar{x}_2 \in \bar{\mathcal{Z}}_1$. Together with $\bar{x}_1 \in \Omega(x)$, this implies that there exists a finite time $t_1 > 0$ such that $x(t) \in \bar{H}_1^{-1}(\leq c_1)$ for all $t \geq t_1$ as the set $\bar{H}_1^{-1}(\leq c_1)$ is invariant by the dissipation inequality (5.18). Similarly, there exists a finite time $t_2 > 0$ such that $x(t) \in \bar{H}_2^{-1}(\leq c_2)$ for all $t \geq t_2$. This implies that the solution $x(t)$ satisfies $x(t) \in \bar{H}_1^{-1}(\leq c_1) \cap \bar{H}_2^{-1}(\leq c_2) = \emptyset$ for $t \geq \max(t_1, t_2)$ which result in a contradiction with the existence of a solution. This concludes the proof of Theorem 5.3.1. □

5.4 Variations in the controller design

In this section we propose several variations and extensions of the controller designed in the previous section. These include, among other things, the possibility to incorporate nodal power constraints, and line congestion in conjunction with transmission costs into the social welfare problem.

5.4.1 Including nodal power constraints

The results of Section 5.3 can be extended to the case where nodal constraints on the power production and consumption are included into the optimization problem (5.6). To this end, consider the social welfare problem

$$\begin{aligned} \underset{P_g,P_d,v}{\text{minimize}} \quad & -S(P_g,P_d) := C(P_g) - U(P_d) && \text{(5.19a)}\\ \text{subject to} \quad & D_c v - P_g + P_d = 0, && \text{(5.19b)}\\ & g(P_g,P_d) \leq 0 && \text{(5.19c)} \end{aligned}$$

where $g : \mathbb{R}^{2n} \to \mathbb{R}^q$ is a convex function.

Example 5.4.1 (Box constraints)**.** Note that (5.19c) captures the convex inequality constraints considered in the existing literature. For example, by choosing g as

$$g(P_g,P_d) = \begin{bmatrix} g_1(P_g,P_d) \\ g_2(P_g,P_d) \\ g_3(P_g,P_d) \\ g_4(P_g,P_d) \end{bmatrix} = \begin{bmatrix} P_g - P_g^{\max} \\ P_g^{\min} - P_g \\ P_d - P_d^{\max} \\ P_d^{\min} - P_d \end{bmatrix},$$

the resulting inequality constraints (5.19c) become $P_g^{\min} \leq P_g \leq P_g^{\max}$, $P_d^{\min} \leq P_d \leq P_d^{\max}$ which, among others, are used in [130, 132, 133].

In the sequel, we assume that (5.19) satisfies Slater's condition [12]. As a result, $(\bar{P}_g, \bar{P}_d, \bar{v})$ is an optimal solution to (5.19) if and only if there exists $\bar{\lambda} \in \mathbb{R}^n, \bar{\mu} \in \mathbb{R}^q_{\geq 0}$ satisfying the following KKT optimality conditions:

$$\begin{aligned} \nabla C(\bar{P}_g) - \bar{\lambda} + \nabla_{P_g} g(\bar{P}_g,\bar{P}_d)\bar{\mu} = 0, \\ -\nabla U(\bar{P}_d) + \bar{\lambda} + \nabla_{P_d} g(\bar{P}_g,\bar{P}_d)\bar{\mu} = 0, \\ D_c\bar{v} - \bar{P}_g + \bar{P}_d = 0, \qquad D_c^T\bar{\lambda} = 0, \\ 0 \leq g(\bar{P}_g,\bar{P}_d) \perp \bar{\mu} \geq 0. \end{aligned} \tag{5.20}$$

Here we use the convention

$$\nabla_{P_g} g(P_g,P_d) = \begin{bmatrix} \frac{\partial g_1}{\partial P_g}(P_g,P_d) & \cdots & \frac{\partial g_q}{\partial P_g}(P_g,P_d) \end{bmatrix}$$

where $\frac{\partial g_i}{\partial P_g}(P_g,P_d)$ denotes the gradient of g_i with respect to P_g for each $i \in \mathcal{I}_q$. A likewise notation is used for $\nabla_{P_d} g(P_g,P_d)$. Next, we introduce the following subsystems [52, 105]

$$\begin{aligned} \dot{x}_{\mu_i} &= (g_i(w_i))^+_{\mu_i} := \begin{cases} g_i(w_i) & \text{if } \mu_i > 0 \\ \max\{0, g_i(w)\} & \text{if } \mu_i = 0 \end{cases} \\ y_{\mu_i} &= \nabla g_i(w_i) \nabla H_{\mu_i}(x_{\mu_i}),\ H_{\mu_i}(x_{\mu_i}) = \frac{1}{2} x_{\mu_i}^T K_{\mu_i}^{-1} x_{\mu_i} \end{aligned} \tag{5.21}$$

with state $x_{\mu_i} := K_{\mu_i}\mu_i \in \mathbb{R}_{\geq 0}$, outputs $y_{\mu_i} \in \mathbb{R}^q$, inputs $w_i \in \mathbb{R}^{2n}$, and $i \in \mathcal{I}_q = \{1, \ldots, q\}$. Here $g_i(.)$ is the i'th entry of the vector-valued function $g(.) = \mathrm{col}_{i\in\mathcal{V}}\{g_i(.)\}$. Note that, for a given $i \in \mathcal{I}_q$ and for a constant input $\bar{w}_i$, the equilibrium set $\bar{\mathcal{Z}}_{\mu_i}$ of (5.21) is characterized by all $(\bar{\mu}_i, \bar{w}_i)$ satisfying

$$g_i(\bar{w}_i) \leq 0, \quad g_i(\bar{w}_i)\mu_i = 0, \quad \bar{\mu}_i \geq 0. \tag{5.22}$$

More formally, for $i \in \mathcal{I}_q$ the equilibrium set $\bar{\mathcal{Z}}_{\mu_i}$ of (5.21) is given by

$$\bar{\mathcal{Z}}_{\mu_i} := \{(\bar{\mu}_i, \bar{w}_i) \mid (\bar{\mu}_i, \bar{w}_i) \text{ satisfies (5.22)}\}.$$

Example 5.4.2 (Form of subsystems for box constraints)**.** In case the inequality constraints of Remark 5.4.1 (e.g. $P_g \leq P_g^{\max}$) are considered, the subsystems (5.21) take the decentralized form

$$\begin{aligned} \dot{x}_{\mu_i} &= (P_{gi} - P_{gi}^{\max})^+_{\mu_i} = \begin{cases} P_{gi} - P_{gi}^{\max} & \text{if } \mu_i > 0 \\ \max\{0, P_{gi} - P_{gi}^{\max}\} & \text{if } \mu_i = 0 \end{cases} \\ y_{\mu_i} &= \nabla H_{\mu_i}(x_{\mu_i}), \quad H_{\mu_i}(x_{\mu_i}) = \frac{1}{2} x_{\mu_i}^T K_{\mu_i}^{-1} x_{\mu_i}, \quad i \in \mathcal{V}, \end{aligned} \tag{5.23}$$

and similar expressions can be given for the remaining inequalities $P_g^{\min} \leq P_g$, $P_d^{\min} \leq P_d \leq P_d^{\max}$.

The subsystems (5.21) have the following passivity property, which we have proven in Chapter 3 and [105].

Proposition 5.4.3 (Shifted passivity of (5.21) [105])**.** *Let $i \in \mathcal{I}_q, (\bar{\mu}_i, \bar{w}_i) \in \bar{\mathcal{Z}}_{\mu_i}$ and define $\bar{y}_{\mu_i} := \nabla g_i(\bar{w}_i)\bar{\mu}_i$. Then* (5.21) *is passive with respect to the shifted external port-variables $\tilde{w}_i := w_i - \bar{w}_i, \tilde{y}_{\mu_i} := y_{\mu_i} - \bar{y}_{\mu_i}$. Additionally, $(\mu_i, w_i) \to \bar{\mathcal{Z}}_{\mu_i}$ as $t \to \infty$ for $(\mu_i, w_i), w_i = \bar{w}_i$ satisfying* (5.21)*.*

Consider a similar system as (5.15), given in the compact form

$$\begin{aligned} \dot{x} &= (J - R)\nabla H(x) + G(\nabla S(y) + u) \\ y &= G^T \nabla H(x) = \begin{bmatrix} P_g \\ P_d \end{bmatrix} \end{aligned} \tag{5.24}$$

where we introduced an additional input $u \in \mathbb{R}^{2n}$.

Remark 5.4.4 (Shifted passivity of (5.24))*.* Note that for any steady state $(\bar{x}, \bar{u})$ of (5.24), the latter system is passive with respect to the shifted external port-variables $\tilde{u} := u - \bar{u}$, $\tilde{y} = y - \bar{y}$, $\bar{y} := G^T \nabla H(\bar{x})$, using the local storage function

$$\bar{H}(x) := H(x) - (x - \bar{x})^T \nabla H(\bar{x}) - H(\bar{x}). \tag{5.25}$$

We interconnect the subsystems (5.21) to (5.24) in a power-preserving way by

$$w_i = w = y \quad \forall i \in \mathcal{I}_q, \qquad u = -\sum_{i\in\mathcal{I}_q} y_{\mu_i}$$

to obtain the closed-loop system

$$\dot{\eta} = D^T\omega \tag{5.26a}$$
$$M\dot{\omega} = -D\Gamma(E'_q)\,\mathbf{sin}\,\eta - A\omega + P_g - P_d \tag{5.26b}$$
$$T'_{do}\dot{E}'_q = -F(\eta)E'_q + E_f \tag{5.26c}$$
$$K_g\dot{P}_g = -\nabla C(P_g) + \lambda - \nabla_{P_g} g(P_g, P_d)\mu - \omega \tag{5.26d}$$
$$K_d\dot{P}_d = \nabla U(P_d) - \lambda - \nabla_{P_d} g(P_g, P_d)\mu + \omega \tag{5.26e}$$
$$K_v\dot{v} = -\nabla C_T(v) - D^T\lambda \tag{5.26f}$$
$$K_\lambda\dot{\lambda} = Dv - P_g + P_d \tag{5.26g}$$
$$K_{\mu_i}\dot{\mu}_i = (g_i(P_g, P_d))^+_{\mu_i}, \qquad i \in \mathcal{I}_q. \tag{5.26h}$$

Observe that the equilibrium set $\bar{\mathcal{Z}}_2$ of (5.26), expressed in the co-energy variables, is characterized by all $(\bar{z}, \bar{\mu})$ that satisfy (5.20) in addition to $\bar{\omega} = 0$, $-D\Gamma(\bar{E}'_q)\,\mathbf{sin}\,\bar{\eta} + \bar{P}_g - \bar{P}_d = 0, -F(\bar{\eta})\bar{E}'_q + E_f = 0$, and therefore corresponds to the desired operation points. Since both the subsystems (5.21) and the system (5.15) admit an *incrementally passivity* property with respect to their steady states, the closed-loop system inherits the same property provided that an equilibrium of (5.26) exists. This allows us to establish the following stability result.

Theorem 5.4.5 (Asymptotic stability of (5.26))**.** *For every $(\bar{z}, \bar{\mu}) \in \bar{\mathcal{Z}}_2$ satisfying Assumption 5.2.2 there exists a neighborhood Υ of $(\bar{z}, \bar{\mu})$ where all trajectories z satisfying* (5.26) *with initial conditions in Υ converge to the set $\bar{\mathcal{Z}}_2$ and the convergence of each such trajectory is to a point.*

Proof. Let $(\bar{z}, \bar{\mu}) \in \bar{\mathcal{Z}}_2$ and consider the shifted Hamiltonian $\bar{H}_e$ around $(\bar{x}, \bar{x}_\mu) = (K\bar{z}, K_\mu\bar{\mu})$ defined by

$$\bar{H}_e(x, x_\mu) := \bar{H}(x) + \sum_{i\in\mathcal{I}_q} \bar{H}_{\mu_i}(x_{\mu_i}) = \bar{H}(x) + \frac{1}{2}\tilde{x}_\mu^T K_{x_\mu}^{-1}\tilde{x}_\mu$$

where $\tilde{x}_\mu := x_\mu - \bar{x}_\mu$ and $\bar{H}$ is defined by (5.25). By Proposition 5.4.3 and Remark 5.4.4, the time-derivative of $\bar{H}_e$ satisfies

$$\dot{\bar{H}}_e \le \tilde{u}^T\tilde{y} + \tilde{w}^T\sum_{i\in\mathcal{I}_q}\tilde{y}_{\mu_i} = \tilde{u}^T\tilde{y} - \tilde{u}^T\tilde{y} = 0$$

where equality holds only if $P_g = \bar{P}_g, P_d = \bar{P}_d, \omega = 0, \nabla_{E'_q}H(x) = 0$. On the largest invariant set where $\dot{\bar{H}}_e = 0$ it follows by the second statement of Proposition 5.4.3 that μ is constant and therefore also $\lambda = \bar{\lambda}$ and v, η, E'_q are constant on this invariant set. We note that the right-hand side of (5.21) is discontinuous but takes the same form as in [26]. Thus we are able to apply the invariance principle for discontinuous Caratheodory systems [26, Proposition 2.1] to conclude that $(z, \mu) \to \bar{\mathcal{Z}}_2$ as $t \to \infty$ for the system (5.26). By following the same line of arguments as in the proof of Theorem 5.3.1, convergence of each trajectory to a point is proven. □

Remark 5.4.6 (Caratheodory solutions). Theorem 5.4.5 uses the Caratheodory variant of the Invariance Principle which requires that the Caratheodory solution of (5.26) is unique and that its omega-limit set is invariant [26]. These requirements are indeed satisfied by extending Lemmas 4.1-4.4 of [26] to the case where equality constraints and *nonstrict* convex/concave (utility) functions are considered in the optimization problem[3] [26, equation (3)], noting that these lemmas only require convexity/concavity instead of their strict versions. In particular, by adding a quadratic function of the Lagrange multipliers associated with the equality constraints to the Lyapunov function, it can be proven that monotonicity of the primal-dual dynamics with respect to primal-dual optimizers as stated in [26, Lemma 4.1] holds for this more general case as well, see also [25, 105].

Remark 5.4.7 (Barrier functions). Instead of using the projected dynamics (5.21) for dealing with the inequality constraints (5.19c), we can instead introduce the so called *barrier functions* $B_i = -\nu \log(-g_i(P_g, P_d))$ that are added to the objective function [12]. Simultaneously, the corresponding inequalities in the social welfare problem (5.19) are removed to obtain the modified convex optimization problem

$$\begin{aligned} \underset{P_g, P_d, v}{\text{minimize}} \quad & -S(P_g, P_d) - \nu \sum_{i \in \mathcal{I}_q} \log(-g_i(P_g, P_d)) \\ \text{subject to} \quad & D_c v - P_g + P_d = 0. \end{aligned} \tag{5.27}$$

Here $\nu > 0$ is called the *barrier parameter* and is usually chosen small. By applying the primal-dual gradient method to (5.27) it can be shown that, if the system is initialized in the interior of the feasible region, i.e. where (5.19c) holds in the strict sense, then the trajectories of the resulting gradient dynamics remain within the feasible region and the system converges to a suboptimal value of the social welfare [6, 12, 120]. However, if Slater's condition holds, this suboptimal value which depends on ν approaches the optimal value of the social welfare problem as $\nu \to 0$ [12]. The particular advantage of using barrier functions is to avoid the use of projections of the Lagrange multiplier μ and to enforce that the trajectories remain within the feasible region for all future time.

5.4.2 Including line congestion and transmission costs

The previous section shows how to include nodal power constraints into the social welfare problem. In case the network is acyclic, line congestion and power transmission costs can be incorporated into the optimization problem as well. To this end, define the (modified) social welfare by $U(P_d) - C(P_g) - C_T(v)$ where the convex function $C_T(v)$ corresponds to the power transmission cost. If security constraints on the transmission lines are included as well, the optimization problem

[3] Note that objective function of the social welfare problem (5.6) is not strictly convex in v and thus not strictly convex with respect to all optimization variables.

(5.6) modifies to

$$\begin{aligned} \underset{P_g,P_d,v}{\text{minimize}} \quad & -S(P_g,P_d,v) := C(P_g)+C_T(v)-U(P_d) && \text{(5.28a)}\\ \text{subject to} \quad & Dv-P_g+P_d=0 && \text{(5.28b)}\\ & -\kappa \le v \le \kappa, && \text{(5.28c)} \end{aligned}$$

with $\kappa \in \mathbb{R}^m_{>0}$. Note that in this case the communication graph is chosen to be identical to the topology of the physical network, i.e., $D_c = D$. As a result, the additional constraints (5.28c) bound the (virtual) power flow along the transmission lines as $|v_k| \le \kappa_k$ for each edge k. The Lagrangian of (5.28) is given by

$$\mathcal{L} = C(P_g)+C_T(v)-U(P_d)+\lambda^T(Dv-P_g+P_d)+\mu_+^T(v-\kappa)+\mu_-^T(-\kappa-v)$$

with Lagrange multipliers $\lambda \in \mathbb{R}^n,\ \mu_+,\ \mu_- \in \mathbb{R}^m_{\ge 0}$. The resulting KKT optimality conditions are given by

$$\begin{aligned} \nabla C(\bar{P}_g)-\bar{\lambda}=0, \qquad -\nabla U(\bar{P}_d)+\bar{\lambda}=0,\\ \nabla C_T(\bar{v})+D^T\bar{\lambda}+\bar{\mu}_+-\bar{\mu}_-=0,\\ -\kappa \le \bar{v} \le \kappa, \qquad D\bar{v}-\bar{P}_g+\bar{P}_d=0,\\ \bar{\mu}_+,\bar{\mu}_- \ge 0, \quad \bar{\mu}_+^T(\bar{v}-\kappa)=0, \quad \bar{\mu}_-^T(-\kappa-\bar{v})=0. \end{aligned} \tag{5.29}$$

Suppose that Slater's condition holds. Then, since the optimization problem (5.28) is convex, it follows that $(\bar{P}_g,\bar{P}_d,\bar{v})$ is an optimal solution to (5.28) if and only if there exists $\bar{\lambda} \in \mathbb{R}^n,\ \bar{\mu}=(\bar{\mu}_+,\ \bar{\mu}_-) \in \mathbb{R}^{2m}_{\ge 0}$ satisfying (5.29) [12].

By applying the gradient method to (5.28) in a similar manner as before and connecting the resulting controller with the physical model (5.2), we obtain the following closed-loop system:

$$\begin{aligned} \dot{\eta} &= D^T\omega && \text{(5.30a)}\\ M\dot{\omega} &= -D\Gamma(E'_q)\,\mathbf{sin}\,\eta - A\omega + P_g - P_d && \text{(5.30b)}\\ T'_{do}\dot{E}'_q &= -F(\eta)E'_q + E_f && \text{(5.30c)}\\ K_g\dot{P}_g &= -\nabla C(P_g)+\lambda-\omega && \text{(5.30d)}\\ K_d\dot{P}_d &= \nabla U(P_d)-\lambda+\omega && \text{(5.30e)}\\ K_v\dot{v} &= -\nabla C_T(v)-D^T\lambda-\mu_++\mu_- && \text{(5.30f)}\\ K_\lambda\dot{\lambda} &= Dv-P_g+P_d && \text{(5.30g)}\\ K_+\dot{\mu}_+ &= (v-\kappa)^+_{\mu_+} && \text{(5.30h)}\\ K_-\dot{\mu}_- &= (-\kappa-v)^+_{\mu_-}. && \text{(5.30i)} \end{aligned}$$

The latter system can partially be put into a port-Hamiltonian form, since equations (5.30a)-(5.30g) can be rewritten as

$$\begin{aligned} \dot{x} &= (J-R)\nabla H(x) + G\nabla S(y) + N\mu \\ y &= G^T \nabla H(x) \\ N &= \begin{bmatrix} 0 & 0 & 0 & 0 & -I & 0 \\ 0 & 0 & 0 & 0 & I & 0 \end{bmatrix}^T, \end{aligned} \tag{5.31}$$

where the variables x, z and the Hamiltonian H are respectively defined by (5.14) and (5.15) as before, and $\mu = (\mu_+, \mu_-)$. Since the network topology is a tree (i.e. $\ker(D) = \{0\}$), the equilibrium of (5.30) satisfies $\bar{v} = \Gamma(\bar{E}_q')\,\mathbf{sin}\,\bar{\eta}$. Hence, the controller variable v corresponds to the *physical* power flow of the network if the closed-loop system is at steady state. Consequently, the constraints and costs on v correspond to constraints and costs of the physical power flow if the system converges to an equilibrium.

Theorem 5.4.8 (Asymptotic stability of (5.30))**.** *Let the network topology be acyclic and let $(\bar{z}, \bar{\mu})$ be an (isolated) equilibrium of* (5.30) *satisfying Assumption 5.2.2. Then $(\bar{z}, \bar{\mu})$ is locally asymptotically stable.*

Proof. Let $(\bar{z}, \bar{\mu})$ be the equilibrium of (5.30). By defining the shifted Hamiltonian $\bar{H}(x)$ around $\bar{x} := K\bar{z}$ by

$$\bar{H}(x) = H(x) - (x-\bar{x})^T \nabla H(\bar{x}) - H(\bar{x})$$

one can rewrite (5.31) as

$$\begin{aligned} \dot{x} &= (J-R)\nabla \bar{H}(x) + \nabla S(y) - \nabla S(\bar{y}) + N\tilde{\mu} \\ y - \bar{y} &= G^T \nabla \bar{H}(x) \end{aligned} \tag{5.32}$$

where $\tilde{\mu} := \mu - \bar{\mu}$. Consider candidate Lyapunov function

$$V(x,\mu) = \bar{H}(x) + \frac{1}{2}\tilde{\mu}_+ K_{\mu_+}\tilde{\mu}_+ + \frac{1}{2}\tilde{\mu}_-^T K_{\mu_-}\tilde{\mu}_-$$

and observe that

$$\begin{aligned} \tilde{\mu}_+^T (v-\kappa)_{\mu_+}^+ &\le \tilde{\mu}_+^T (v-\kappa) = \tilde{\mu}_+^T(\bar{v}-\kappa+\tilde{v}) \le \tilde{\mu}_+^T \tilde{v} \\ \tilde{\mu}_-^T (-\kappa-v)_{\mu_-}^+ &\le \tilde{\mu}_-^T(-\kappa - v) \\ &= \tilde{\mu}_-^T(-\kappa-\bar{v}-\tilde{v}) \le -\tilde{\mu}_-^T\tilde{v}. \end{aligned} \tag{5.33}$$

Bearing in mind (5.32), the time-derivative of V amounts to

$$\begin{aligned} \dot{V} &= -\omega^T A\omega - (\nabla_{E_q'} H(x))^T R_q \nabla_{E_q'} H(x) + (y-\bar{y})^T(\nabla S(y) - \nabla S(\bar{y})) \\ &- \tilde{v}^T\tilde{\mu}_+ + \tilde{v}^T\tilde{\mu}_- + \tilde{\mu}_+^T(v-\kappa)_{\mu_+}^+ + \tilde{\mu}_-^T(-\kappa-v)_{\mu_-}^+ \\ &\le -\omega^T A\omega + (y-\bar{y})^T(\nabla S(y) - \nabla S(\bar{y})) - (\nabla_{E_q'} H(x))^T R_q \nabla_{E_q'} H(x) \le 0 \end{aligned}$$

where equality holds only if $\nabla_{E'_q} H(x) = 0, \omega = 0, P_g = \bar{P}_g, P_d = \bar{P}_d$. On the largest invariant set $\mathcal{S}$ where $\nabla_{E'_q} H(x) = 0, \omega = 0, P_g = \bar{P}_g, P_d = \bar{P}_d$ it follows that, since the graph contains no cycles $\lambda = \bar{\lambda}, v = \bar{v}, \mu = \bar{\mu}$ and that η, E'_q are constant, which corresponds to an equilibrium. In particular $\nabla V(x, \mu) = 0$ for all $(x, \mu) \in \mathcal{S}$ and $(\bar{x}, \bar{\mu}) \in \mathcal{S}$. Since by Assumption 5.2.2 we have $\nabla^2 V(\bar{x}, \bar{\mu}) > 0$, it follows that $(\bar{x}, \bar{\mu})$ is isolated and by (5.33) we have that $(\bar{x}, \bar{\mu})$ is Lyapunov stable. Finally, by the invariance principle for discontinuous Caratheodory systems [26] all trajectories (z, μ) of (5.30) initializing in a sufficiently small neighborhood around $(\bar{z}, \bar{\mu})$ converge to $(\bar{z}, \bar{\mu})$. □

Remark 5.4.9 (Combining nodal constraints and line congestion). It is possible to include nodal power constraints, line congestion and transmission costs simultaneously. However, as the results in this section are only valid for acyclic graphs, it should also be assumed for the more general case that the physical network is a tree.

5.4.3 Demand uncertainty

Consider again the minimization problem (5.6). As shown before, by applying the gradient method to the social welfare problem and the interconnection with the power network dynamics, the closed-loop system (5.15) is obtained. Note that in the λ-dynamics the demand P_d appears, which in practice is often uncertain. A possibility to eliminate the demand from the controller dynamics is by a state transformation [64, 92]. To this end, define the new variables

$$\hat{x} := \begin{bmatrix} \eta \\ p \\ E'_q \\ x_g \\ x_d \\ x_v \\ x_\theta \end{bmatrix} = \begin{bmatrix} I & 0 & 0 & 0 & 0 & 0 & 0 \\ 0 & I & 0 & 0 & 0 & 0 & 0 \\ 0 & 0 & I & 0 & 0 & 0 & 0 \\ 0 & 0 & 0 & I & 0 & 0 & 0 \\ 0 & 0 & 0 & 0 & I & 0 & 0 \\ 0 & 0 & 0 & 0 & 0 & I & 0 \\ 0 & I & 0 & 0 & 0 & 0 & I \end{bmatrix} x = \hat{K} \begin{bmatrix} \eta \\ p \\ E'_q \\ P_g \\ P_d \\ v \\ \theta \end{bmatrix} =: \hat{K}\hat{z},$$

i.e., $x_\theta := K_\theta \theta = p + x_\lambda$. Then the port-Hamiltonian system (5.15) transforms to

$$\begin{aligned} \dot{\hat{x}} &= \begin{bmatrix} 0 & D^T & 0 & 0 & 0 & 0 & D^T \\ -D & -A & 0 & I & -I & 0 & -A \\ 0 & 0 & -R_q & 0 & 0 & 0 & 0 \\ 0 & -I & 0 & 0 & 0 & 0 & 0 \\ 0 & I & 0 & 0 & 0 & 0 & 0 \\ 0 & 0 & 0 & 0 & 0 & 0 & -D_c^T \\ -D & -A & 0 & 0 & 0 & D_c & -A \end{bmatrix} \nabla \hat{H}(\hat{x}) + G \nabla S(y) \\ y &= G^T \nabla \hat{H}(\hat{x}) \end{aligned} \tag{5.34}$$

with G as defined in (5.16) and Hamiltonian

$$\hat{H}(\hat{x}) = H_p + \frac{1}{2}x_g^T K_g^{-1} x_g + \frac{1}{2}x_d^T K_d^{-1} x_d + \frac{1}{2}x_v^T K_v^{-1} x_v + \frac{1}{2}(x_\theta - p)K_\lambda^{-1}(x_\theta - p).$$

By writing the system of differential equations (5.34) explicitly we obtain

$$\begin{aligned}
\dot{\eta} &= D^T\omega \\
M\dot{\omega} &= -D\Gamma(E'_q)\,\mathbf{sin}\,\eta - A\omega + P_g - P_d \\
T'_{do}\dot{E}'_q &= -F(\eta)E'_q + E_f \\
K_g\dot{P}_g &= -\nabla C(P_g) + K_\lambda^{-1}(K_\theta\theta - M\omega) - \omega \\
K_d\dot{P}_d &= \nabla U(P_d) - K_\lambda^{-1}(K_\theta\theta - M\omega) + \omega \\
K_v\dot{v} &= -D_c^T K_\lambda^{-1}(K_\theta\theta - M\omega) \\
K_\theta\dot{\theta} &= D_c v - D\Gamma\,\mathbf{sin}\,\eta - A\omega.
\end{aligned} \tag{5.35}$$

Define $\bar{\mathcal{Z}}_4$ as the set of all $\hat{z}^* := (\bar{\eta}, \bar{\omega}, \bar{E}'_q, \bar{P}_g, \bar{P}_d, \bar{v}, \bar{\theta})$ that are an equilibrium of (5.35). Using the previous established tools we can prove local convergence of (5.35) to the set of optimal points $\bar{\mathcal{Z}}_4$.

Theorem 5.4.10 (Asymptotic stability of transformed system (5.35))**.** *For every $\hat{z}^* \in \bar{\mathcal{Z}}_4$ satisfying Assumption 5.2.2 there exists a neighborhood Υ around $\hat{z}^*$ where all trajectories $\hat{z}$ satisfying* (5.35) *and initializing in Υ converge to $\bar{\mathcal{Z}}_4$. In addition, the convergence of each such trajectory is to a point.*

Proof. We proceed along the same lines as in the proof of Theorem 5.3.1 where we note that the stability result of Theorem 5.3.1 is preserved after a state transformation. □

Note that the latter result holds for any gain matrices $K_g, K_d, K_v, K_\lambda, K_\theta > 0$. The controller appearing in (5.35) can be simplified by choosing $K_\lambda = K_\theta = M$. As a result, the controller dynamics is described by

$$K_g\dot{P}_g = -\nabla C(P_g) + \theta - 2\omega \tag{5.36a}$$

$$K_d\dot{P}_d = \nabla U(P_d) - \theta + 2\omega \tag{5.36b}$$

$$K_v\dot{v} = -D_c^T(\theta - \omega) \tag{5.36c}$$

$$M\dot{\theta} = D_c v - D\Gamma(E'_q)\,\mathbf{sin}\,\eta - A\omega. \tag{5.36d}$$

The main advantage of controller design (5.36) is that no information about the power supply and demand is required in the dynamic pricing algorithm (5.36c), (5.36d), where we observe that the quantity $\theta - 2\omega$ can be interpreted as the (local) electricity price for the producers and consumers. Another benefit of the proposed dynamic pricing algorithm is that, contrary to [135], no information is required about $\dot{\omega}$. On the other hand, knowledge about the physical power flows and the power system parameters M, A is required. Determining the radius of uncertainty of these parameters under which asymptotic stability is preserved

remains an open question [64]; see [69] for results in a similar setting where only the damping term A is assumed to be uncertain.

5.4.4 Relaxing the strict convexity assumption

By making a minor modification to the social welfare problem (5.6), it is possible to relax the requirement that the functions C, U are *strictly* convex and concave respectively. To this end, consider the convex optimization problem

$$\underset{P_g, P_d, v}{\text{minimize}} \quad C(P_g) - U(P_d) + \frac{1}{2}\rho||D_c v - P_g + P_d||^2 \tag{5.37a}$$

$$\text{subject to} \quad D_c v - P_g + P_d = 0, \tag{5.37b}$$

where $\rho > 0$, $C(P_g)$ is convex and $U(P_d)$ is concave. Provided that there exists a feasible solution to the minimization problem, then the set of optimal points of (5.37) is identical to the set of optimal points of (5.6) which is characterized by set of points satisfying the KKT conditions (5.8). The corresponding augmented Lagrangian of (5.37) is given by

$$\mathcal{L}_p = C(P_g) - U(P_d) - \lambda^T(D_c v + P_g - P_d) + \frac{1}{2}\rho||D_c v + P_g - P_d||^2.$$

Consequenctly, the distributed dynamics of the primal-dual gradient method applied to (5.37) amounts to

$$\begin{aligned} K_g\dot{P}_g &= -\nabla C(P_g) + \lambda - \rho(D_c v + P_g - P_d) \\ K_d\dot{P}_d &= \nabla U(P_d) - \lambda + \rho(D_c v + P_g - P_d) \\ K_v\dot{v} &= D_c^T\lambda - \rho D_c^T(D_c v + P_g - P_d) \\ K_\lambda\dot{\lambda} &= -D_c v - P_g + P_d, \end{aligned} \tag{5.38}$$

which can be written in the same port-Hamiltonian form as (5.15) where in this case

$$S(P_g, P_d, v) = U(P_d) - C(P_g) - \frac{1}{2}\rho||D_c v - P_g + P_d||^2, \tag{5.39}$$

$$G^T = \begin{bmatrix} 0 & 0 & 0 & I & 0 & 0 & 0 \\ 0 & 0 & 0 & 0 & I & 0 & 0 \\ 0 & 0 & 0 & 0 & 0 & I & 0 \end{bmatrix}, \tag{5.40}$$

$$y = G^T\nabla H(x) = \begin{bmatrix} P_g \\ P_d \\ v \end{bmatrix}. \tag{5.41}$$

We note here that the dynamics (5.38) is still distributed as still only local information (on the local power imbalance) is needed for the implementation. We are now in the position to state the following result.

Theorem 5.4.11 (Asymptotic stability of (5.15))**.** *Consider the system* (5.12) *or equivalently* (5.15) *where* S *is replaced by* (5.39) *and suppose that* C, U *are convex and concave functions respectively. Then for every* $\bar{z} \in \bar{\mathcal{Z}}_1$ *satisfying Assumption 5.2.2, where* $\bar{\mathcal{Z}}_1$ *is defined by* (5.13)*, there exists a neighborhood* Υ *around* $\bar{z}$ *wherein each trajectory* z *satisfying* (5.15) *converges to a point in* $\bar{\mathcal{Z}}_1$*.*

Proof. Let $\bar{z} \in \bar{\mathcal{Z}}_1$. By the proof of Theorem 5.3.1 it follows that

$$\dot{\bar{H}} = -\omega^T A \omega + (y - \bar{y})^T (\nabla S(y) - \nabla S(\bar{y})) - (\nabla_{E'_q} \bar{H})^T R_q \nabla_{E'_q} \bar{H},$$

where the second term can be written as

$$\begin{aligned} &(P_d - \bar{P}_d)^T (\nabla U(P_d) - \nabla U(\bar{P}_d)) - (P_g - \bar{P}_g)^T (\nabla C(P_g) - \nabla C(\bar{P}_g)) \\ &- \rho \begin{bmatrix} \tilde{P}_g \\ \tilde{P}_d \\ \tilde{v} \end{bmatrix}^T \begin{bmatrix} -I & I & -D_c \\ I & -I & D_c \\ -D_c^T & D_c^T & -D_c^T D_c \end{bmatrix} \begin{bmatrix} \tilde{P}_g \\ \tilde{P}_d \\ \tilde{v} \end{bmatrix} \leq 0 \end{aligned} \tag{5.42}$$

where $\tilde{P}_g = P_g - \bar{P}_g, \tilde{P}_d = P_d - \bar{P}_d, \tilde{v} = v - \bar{v}$. Hence, we obtain that $\dot{\bar{H}} \leq 0$ where equality holds only if $\omega = 0, \nabla_{E'_q} \bar{H}(x) = 0$ and $D_c \tilde{v} + \tilde{P}_g - \tilde{P}_d = D_c v + P_g - P_d = 0$. On the largest invariant set $\mathcal{S}$ where $\dot{\bar{H}}_c = 0$ we have $\omega = 0$ and η, E'_q are constant and (P_g, P_d, v, λ) satisfy the KKT optimality conditions (5.8). Therefore $\mathcal{S} \subset \bar{\mathcal{Z}}_1$ and by LaSalle's invariance principle there exists a neighborhood Υ around $\bar{z}$ where all trajectories z satisfying (5.15) converge to the set $\mathcal{S} \subset \bar{\mathcal{Z}}_1$. By continuing along the same lines as the proof of Theorem 5.3.1, convergence of each trajectory to a point is proven. □

Remark 5.4.12 (Damping injection)*.* Adding the quadratic term in the social welfare problem as done in (5.37a) provides an additional advantage. As this introduces more damping in the resulting gradient-method-based controller, see (5.42), it may improve the convergence properties of the closed-loop dynamics [13, 82, 96]. Moreover, the amount of damping injected into the system depends on parameter ρ, which can be chosen freely.

5.5 Conclusions and possible extensions

In this chapter a unifying and systematic energy-based approach in modeling and stability analysis of power networks has been established. Convergence of the closed-loop system to the set of optimal points using gradient-method-based controllers have been proven using passivity based arguments. This result is extended to the case where nodal power constraints are included into the problem as well. However, for line congestion and power transmission cost the power network is required to be acyclic to prove asymptotic stability to the set of optimal points.

The results established in this chapter lend themselves to many possible extensions. One possibility is to design an additional (passive) controller that

regulates the voltages to the desired values or achieves alternative objectives like (optimal) reactive power sharing. This could for example be realized by continuing along the lines of [31].

Later we observe that, see e.g. [108], the port-Hamiltonian framework also lends itself to consider higher-dimensional models for the synchronous generator compared to the third-order model used in this chapter, and thus allowing for a power-preserving with a controller. This will be the topic of Chapter 7. In addition, in the next chapter we extend some of the results of the present chapter to network-preserving models where a distinction is made between generator and load nodes.

One of the remaining open questions is how to deal with line congestion and power transmission costs in cyclic power networks with nonlinear power flows. In addition, all of the results established for the nonlinear power network only provide *local* asymptotic stability to the set of optimal points. Future research includes determining the region of attraction.

Chapter 6

Active power sharing in structure-preserving power networks

Abstract: *This chapter studies the problem of maximizing the social welfare while stabilizing both the physical power network as well as the market dynamics. For the physical power grid a third-order structure-preserving model is considered involving both frequency and voltage dynamics. By applying the primal-dual gradient method to the social welfare problem, a distributed dynamic pricing algorithm in port-Hamiltonian form is obtained. After interconnection with the physical system a closed-loop port-Hamiltonian system of differential-algebraic equations is obtained, whose properties are exploited to prove local asymptotic stability of the optimal point.*

Published as:

T.W. Stegink, C. De Persis, A.J. van der Schaft. "Stabilization of structure-preserving power networks with market dynamics." IFAC-PapersOnLine 50.1 (2017): 6737-6742.

6.1 Introduction

The future power network needs to operate reliably in the face of fluctuations resulting from distributed energy resources and the increased variability in both supply and demand. One of the feedback mechanisms that have been identified for managing this challenge is the use of real-time dynamic pricing. This feedback mechanism encourages consumers to modify their demand when it is difficult for system operator to achieve a balance between supply and demand [11]. In addition, real-time dynamic pricing allows to maximize the total *social welfare* by fairly sharing utilities and costs associated with the generation and consumption of energy among the different control areas [57].

Many of the existing dynamic pricing algorithms focus on the economic part of optimal supply-demand matching [57, 84]. However, if market mechanisms are used to determine the optimal power dispatch (with near real-time updates of the dispatch commands) dynamic coupling occurs between the market update process and the physical response of the power network dynamics [3].

Consequently, under the assumption of market-based dispatch, it is essential to consider the stability of the coupled system incorporating both market operation and electromechanical power system dynamics simultaneously.

While on this subject a vast literature is already available, we focus on a more accurate and higher order model for the physical power network than conventionally used in the literature. In particular, a structure-preserving model for the power network with a third-order order model for the synchronous generators including voltage dynamics is used. As a result, market dynamics, frequency dynamics and voltage dynamics are considered simultaneously.

Literature review

The coupling between a high-order dynamic structure-preserving power network and market dynamics has been studied before in [3]. Here a fourth-order model of the synchronous generator is used in conjunction with turbine and exciter dynamics, which is coupled to a simple model describing the market dynamics. The results established in [3] are based on an eigenvalue analysis of the linearized system.

It is shown in [113] that the third-order (*flux-decay*) model for the synchronous generator, as used in the present chapter, admits a useful passivity property that allows for a rigorous stability analysis of the interconnection with optimal power dispatch controllers, even in the presence of time-varying demand. In [115] a structure-preserving power network model is considered with turbine dynamics where a similar internal-model controller is applied, which also has applications in microgrids, see [33].

Another commonly used approach to design optimal distributed controllers in power grids is the use of the primal-dual gradient algorithm [6], which has been proven useful in network flow theory [36]. The problem formulation varies throughout the literature on power systems, with the focus being on either the generation side [64, 92], the load side [68, 69, 135] or both [130, 131].

Many of these references focus on linear power system models coupled with gradient-method-based controllers [64, 68, 69, 92, 130, 137]. In these references the property that the linear power system dynamics can be formulated as a gradient method applied to a certain optimization problem is exploited. This is commonly referred to as *reverse-engineering* of the power system dynamics [64, 92, 130]. However, this approach falls short in dealing with models involving nonlinear power flows.

Nevertheless, [131, 135] show the possibility to achieve optimal power dispatch in structure-preserving power networks with nonlinear power flows using gradient-method-based controllers. On the other hand, the controllers proposed in [131] have restrictions in assigning the controller parameters and in addition require that the topology of the physical network is a tree.

Main contributions

The contribution of this chapter is to propose a novel energy-based approach to the problem that differs substantially from the aforementioned works. We proceed along the lines of [105, 107], where a port-Hamiltonian approach to the design of gradient-method-based controllers in power networks is proposed. In those papers it is shown that both the power network as well as the controller designs admit a port-Hamiltonian representation which are then interconnected to obtain a closed-loop port-Hamiltonian system. In the present chapter we extend some of these results to structure-preserving power networks.

First it is shown that the dynamical model describing the power network as well as the market dynamics admit a port-Hamiltonian representation. Then, following [105, 107], it is proven that all the trajectories of the coupled system converge to the desired synchronous solution and to optimal power dispatch.

Since our approach is based on passivity and does not require to reverse-engineer the power system dynamics as a primal-dual gradient dynamics, it allows to deal with more complex nonlinear models of the power network. More specifically, the physical model for describing the power network in this chapter admits nonlinear power flows and time-varying voltages, and is more accurate and reliable than the classical second-order model [10, 61, 67, 89]. In addition, a distinction is made between generator nodes and loads nodes, resulting in a system of differential-algebraic equations.

The results that are established in the present chapter are valid for the case of nonlinear power flows and cyclic networks, in contrast to [64, 92, 130, 137], where the power flows are linearized and [131] where the physical network topology is a tree. Moreover, in the aforementioned references the voltages are assumed to be constant.

While the third-order model for the synchronous generators has been studied before using passivity based techniques [107, 113], the combination of gradient method based controllers with structure-preserving power network models is novel. In addition, the stability analysis does not rely on linearization and is based on energy functions which allow us to establish rigorous stability results. Moreover,

we do not impose any restrictive condition on controller design parameters for guaranteeing asymptotic stability, contrary to [131].

The remainder of this chapter is organized as follows. In Section 6.2 the preliminaries are stated. Thereafter, the power system dynamics is introduced in Section 6.3 and a port-Hamiltonian representation of the system of differential-algebraic equations is given as well in this section. Then the dynamic pricing algorithm in port-Hamiltonian form is presented in Section 6.4. The closed-loop system is analyzed in Section 6.5 and local asymptotic stability of the optimal points is proven. Finally, the conclusions and the future research directions are discussed in Section 6.6.

6.2 Preliminaries

6.2.1 Notation

Given a symmetric matrix $A \in \mathbb{R}^{n\times n}$, we write $A > 0$ ($A \geq 0$) to indicate that A is a positive (semi-)definite matrix. The set of positive real numbers is denoted by $\mathbb{R}_{>0}$ and likewise the set of nonnegative real numbers is denoted by $\mathbb{R}_{\geq 0}$. The notation $\mathbb{1}_n \in \mathbb{R}^n$ is used for the vector whose elements are equal to 1. The $n \times n$ identity matrix is denoted by I_n. Given an ordered set $\mathcal{I} = \{i_1, i_2, \ldots, i_k\}$ and a vector $v \in \mathbb{R}^n, k \leq n$, then $\mathrm{col}_{i\in\mathcal{I}}\{v_i\}, \mathrm{diag}_{i\in\mathcal{I}}\{v_i\}$ denotes the k-column vector, respectively $k\times k$ diagonal matrix whose entries are given by $v_{i_1}, v_{i_2}, \ldots, v_{i_k}$. Likewise, given vectors v_1, v_2 then $\mathrm{col}(v_1, v_2) := \left[\begin{smallmatrix} v_1 \\ v_2 \end{smallmatrix}\right]$. Let $f(x, y)$ be a differentiable function of $x \in \mathbb{R}^n, y \in \mathbb{R}^m$, then $\nabla f := \mathrm{col}(\frac{\partial f}{\partial x}, \frac{\partial f}{\partial y})$ and $\nabla_x f := \frac{\partial f}{\partial x}$ denotes the gradient of f with respect to x.

6.2.2 Differential algebraic equations

Let us consider a system of differential-algebraic equations (DAE's) of the form

$$\dot{x} = f(x, y), \tag{6.1a}$$
$$0 = g(x, y), \tag{6.1b}$$

where $x \in \mathbb{R}^n$ and $y \in \mathbb{R}^m$.

Definition 6.2.1 (Regular DAE [33])**.** Let $\mathcal{D} \subset \mathbb{R}^n \times \mathbb{R}^m$ be an open connected set. The algebraic equation $0 = g(x, y)$ is *regular* if the Jacobian of g w.r.t. y has constant full rank on $\mathcal{D}$, that is,

$$\mathrm{rank}(\nabla_y g(x, y)) = m \qquad \forall (x, y) \in \mathcal{D}.$$

If the DAE-system (6.1) is regular on $\mathcal{D}$ then by [44] the existence and uniqueness of solutions of (6.1) in $\mathcal{D}$ over an interval $\mathcal{I} \subseteq \mathbb{R}_{\geq 0}$ for any $(x(x_0, y_0, t), y(x_0, y_0, t))$ is guaranteed.

By extending the usual LaSalle's invariance principle for ordinary differential equations, we obtain an invariance principle that can be used for the stability analysis of DAE's, see [33].

Theorem 6.2.2 (Invariance principle for DAE's)**.** *Suppose the DAE* (6.1) *is regular on* $\mathcal{D}$ *and* f, g *are continuous differentiable functions. Let* $(x, y) = (\bar{x}, \bar{y})$ *be an equilibrium of* (6.1)*. Let* $V(x, y) : \mathcal{D}_V \to \mathbb{R}_{\geq 0}$ *be a smooth positive definite function on a neighborhood* $\mathcal{D}_V \subset \mathcal{D}$ *of* $(x, y) = (\bar{x}, \bar{y})$*, such that* $\dot{V}(x, y) \leq 0$*. Let* $E = \{(x, y) \in \mathcal{D}_V \mid \dot{V} = 0\}$*, and suppose that no solution can stay forever in* E*, other than the trivial solution* $(\bar{x}, \bar{y})$*. Then* $(\bar{x}, \bar{y})$ *is locally asymptotically stable.*

6.3 Power network model

Consider a power grid consisting of n buses. The network is represented by a connected and undirected graph $\mathcal{G} = (\mathcal{V}, \mathcal{E})$. Its associated node set, $\mathcal{V} = \{1, \ldots, n\} = \mathcal{V}_g \cup \mathcal{V}_d$, is partitioned in the set of generator nodes $\mathcal{V}_g$ with cardinality n_g, and the set of load nodes $\mathcal{V}_d$ with cardinality n_d. In addition, the set of edges $\mathcal{E} \subset \mathcal{V} \times \mathcal{V}$ corresponds to the set of transmission lines connecting the buses. The edges are arbitrarily labeled with a unique identifier in $\mathcal{I}_m := \{1, \ldots, m\}$ where the k-th edge connecting nodes i and j is denoted as $k \sim \{i, j\}$. Each bus represents either a synchronous generator or a frequency-dependent load [10]. It is assumed that the synchronous generators are governed by the *flux-decay model* [61] with a controllable mechanical power injection P_{gi}. By [3], the loads are assumed to have a time-varying active power demand P_{di} and a constant reactive power demand $Q_{di} = \bar{Q}_{di}$. As a result, the dynamics at each bus is given by the following equations [67, 113].

$$\dot{\delta}_i = \omega_i \qquad i \in \mathcal{V} \tag{6.2a}$$

$$M_i \dot{\omega}_i = -P_i - A_i \omega_i + P_{gi} \qquad i \in \mathcal{V}_g \tag{6.2b}$$

$$T'_{doi} \dot{E}_i = E_{fi} - E_i - (X_{di} - X'_{di}) E_i^{-1} Q_i \qquad i \in \mathcal{V}_g \tag{6.2c}$$

$$P_i = -A_i \omega_i - P_{di} \qquad i \in \mathcal{V}_d \tag{6.2d}$$

$$Q_i = \bar{Q}_{di} \qquad i \in \mathcal{V}_d \tag{6.2e}$$

Here the active and reactive power injections are given by

$$P_i = \sum_{j \in \mathcal{N}_i} B_{ij} E_i E_j \sin \delta_{ij} \qquad i \in \mathcal{V}$$

$$Q_i = B_{ii} E_i^2 - \sum_{j \in \mathcal{N}_i} B_{ij} E_i E_j \cos \delta_{ij}, \qquad i \in \mathcal{V}$$

with $B_{ii} = \sum_{j \in \mathcal{N}_i} B_{ij} + \hat{B}_{ii}$ and where $\hat{B}_{ii} \geq 0$ is the negative of the shunt susceptance at node i. See Table 6.1 for a list of symbols used in the model (6.2) and throughout the chapter.

Assumption 6.3.1 (Power network dynamics (6.2))**.** By using the model (6.2) the following assumptions are made, where most of them are standard in a broad range of literature on power network dynamics [67].

δ_i	voltage angle
ω_i	frequency deviation w.r.t. nominal frequency
E_i	transient internal voltage
E_{fi}	excitation voltage
P_{gi}, P_{di}	active power generation and demand
Q_{gi}, Q_{di}	reactive power generation and demand
M_i	moment of inertia
$\mathcal{N}_i$	set of buses connected to bus i
A_i	asynchronous damping constant
B_{ij}	negative of the susceptance of transmission line $\{i, j\}$
B_{ii}	negative of the self-susceptance
X_{di}	d-axis synchronous reactance of generator i
X'_{di}	d-axis transient reactance of generator i
T'_{doi}	open-circuit transient time constant

Table 6.1: Parameters and state variables of model (6.2).

- Lines are purely inductive, i.e., the conductance is zero. This assumption is generally valid for the case of high voltage lines connecting different control areas.
- The grid is operating around the synchronous frequency, say 50 Hz or 60 Hz.
- The voltages satisfy $E_i > 0, i \in \mathcal{V}$ for all time $t \geq 0$ and the reactive powers at the loads $Q^*_{di} \geq 0, i \in \mathcal{V}_d$ are constant.
- The excitation voltage E_{fi} is constant for all $i \in \mathcal{V}$.

Define the angular momenta $p_i = M_i\omega_i, i \in \mathcal{V}_g$. Based on the energy stored in the generators and the transmission network, the Hamiltonian is defined by

$$H_p = \frac{1}{2}\sum_{i\in\mathcal{V}_g}\left(M_i^{-1}p_i^2 + \frac{(E_i - E_{fi})^2}{X_{di} - X'_{di}}\right) + \frac{1}{2}\sum_{i\in\mathcal{V}} B_{ii}E_i^2 - \sum_{\{i,j\}\in\mathcal{E}} B_{ij}E_iE_j\cos\delta_{ij}. \tag{6.3}$$

The algebraic constraint (6.2e) corresponding to the reactive power of the load can then be written as

$$0 = -[E_d]\nabla_{E_d}H_p + \bar{Q}_d, \tag{6.4}$$

where $[E_d] := \mathrm{diag}_{i\in\mathcal{V}_d}\{E_i\}, E_d := \mathrm{col}_{i\in\mathcal{V}_d}\{E_i\}$. As the system (6.2) admits a *rotational symmetry* with respect to the voltage angles [35], it is convenient to consider a different set of coordinates. To this end, define without loss of generality the coordinates $\varphi = \hat{D}^T\delta, \delta = \mathrm{col}_{i\in\mathcal{V}}\{\delta_i\}$, where $\hat{D} \in \mathbb{R}^{n\times(n-1)}$ has full column rank and satisfies $\ker(\hat{D}^T) = \mathrm{span}\{\mathbb{1}_n\}$.

Example 6.3.2 (Possible state transformations)**.** One possibility is to define $\hat{D}$ as the incidence matrix of a tree graph with n nodes and $n-1$ edges. In that case, φ represents the angle differences $\delta_i - \delta_j$ along the edges of this tree graph.

Another possibility is to choose node n as the reference node, resulting in $\hat{D}^T = [I_{n-1} \ -\mathbb{1}_{n-1}]$, see also [33, 127].

Using this modified set of coordinates, and defining the state variable $x_p := \mathrm{col}(\varphi, p_g, E_g, E_d)$, the system (6.2) can be written in the form

$$\begin{bmatrix} \dot{\varphi} \\ \dot{p}_g \\ \dot{E}_g \\ 0 \\ 0 \end{bmatrix} = \begin{bmatrix} 0 & \hat{D}_g^T & 0 & 0 & \hat{D}_d^T \\ -\hat{D}_g & -A_g & 0 & 0 & 0 \\ 0 & 0 & -R_g & 0 & 0 \\ 0 & 0 & 0 & -[E_d] & 0 \\ -\hat{D}_d & 0 & 0 & 0 & -A_d \end{bmatrix} \nabla W_p + \begin{bmatrix} 0 \\ P_g \\ 0 \\ \bar{Q}_d \\ -P_d \end{bmatrix}, \tag{6.5}$$

$$W_p(x_p, \omega_d) = H_p(x_p) + U_p(\omega_d), \qquad U_p(\omega_d) = \frac{1}{2}\omega_d^T \omega_d.$$

Here $\hat{D}^T = \begin{bmatrix} \hat{D}_g^T & \hat{D}_d^T \end{bmatrix}, A_d = \mathrm{diag}_{i\in\mathcal{V}_d}\{A_i\} > 0, A_g = \mathrm{diag}_{i\in\mathcal{V}_g}\{A_i\} > 0, R_g = \mathrm{diag}_{i\in\mathcal{V}_g}\{\frac{X_{di}-X'_{di}}{T'_{doi}}\} > 0, \omega_d = \mathrm{col}_{i\in\mathcal{V}_d}\{\omega_i\}$ and E_g, P_g, P_d, p_g are defined likewise. The system (6.5) has external ports $(P_g, \omega_g), (P_d, \omega_d)$ which will be interconnected to the dynamic pricing algorithm introduced in the following section.

Remark 6.3.3 (Nonstandard port-Hamiltonian DAE). The system (6.5) has a slightly different form compared to conventional port-Hamiltonian DAE-systems, see [117]. In particular, H_p is the Hamiltonian of the system while U_p can be interpreted as an auxiliary energy function which is not used as part of the (shifted) storage function to prove passivity. However, by exploiting the special structure of the system (6.5), the stability analysis becomes convenient as we will show in Section 6.5.

6.4 Dynamic pricing algorithm

The social welfare is defined as $S(P_g, P_d) := U(P_d) - C(P_g)$, which consists of a utility function $U(P_d)$ of the power consumption P_d and the cost $C(P_g)$ associated to the power production P_g. We assume that $C(P_g), U(P_d)$ are strictly convex and strictly concave functions respectively. The objective is to maximize the social welfare while achieving zero frequency deviation. By analyzing the equilibria of (6.2), it follows that a necessary condition for zero frequency deviation is $\mathbb{1}_{n_g}^T P_g = \mathbb{1}_{n_d}^T P_d$. In other words, the total supply must match the total demand. It can be noted that P_g, P_d satisfy this power balance if and only if there exists a vector $v \in \mathbb{R}^{m_c}$ such that

$$-\underbrace{\begin{bmatrix} D_{cg} \\ D_{cd} \end{bmatrix}}_{D_c} v + \begin{bmatrix} P_g \\ -P_d \end{bmatrix} = 0$$

where $D_c \in \mathbb{R}^{n\times m_c}$ is the incidence matrix of some connected *communication graph* with m_c edges.

$$\begin{aligned} \max_{P_g,P_d,v}\ & U(P_d) - C(P_g) \\ \text{s.t.}\ & \begin{bmatrix} D_{cg} \\ D_{cd} \end{bmatrix} v + \begin{bmatrix} P_g \\ -P_d \end{bmatrix} = 0. \end{aligned} \tag{6.6}$$

The corresponding KKT optimality conditions amount to

$$\begin{aligned} \nabla C(\bar{P}_g) - \bar{\lambda}_g &= 0 \\ -\nabla U(\bar{P}_d) + \bar{\lambda}_d &= 0 \\ \begin{bmatrix} D_{cg}^T & D_{cd}^T \end{bmatrix} \begin{bmatrix} \bar{\lambda}_g \\ \bar{\lambda}_d \end{bmatrix} &= 0 \\ - \begin{bmatrix} D_{cg} \\ D_{cd} \end{bmatrix} \bar{v} + \begin{bmatrix} \bar{P}_g \\ -\bar{P}_d \end{bmatrix} &= 0 \end{aligned} \tag{6.7}$$

with $\lambda_g \in \mathbb{R}^{n_g}, \lambda_d \in \mathbb{R}^{n_d}$. Inspired by our previous work [105, 107] and based on the primal-dual gradient method [6, 64, 130], the following distributed dynamic pricing algorithm is proposed:

$$K_g \dot{P}_g = -\nabla C(P_g) + \lambda_g - \omega_g \tag{6.8a}$$
$$K_d \dot{P}_d = \nabla U(P_d) - \lambda_d + \omega_d \tag{6.8b}$$
$$K_v \dot{v} = -D_{cg}^T \lambda_g - D_{cd}^T \lambda_d \tag{6.8c}$$
$$K_{\lambda_g} \dot{\lambda}_g = D_{cg} v - P_g \tag{6.8d}$$
$$K_{\lambda_d} \dot{\lambda}_l = D_{cd} v + P_d \tag{6.8e}$$

where $K_g, K_d, K_v, K_{\lambda_g}, K_{\lambda_d} > 0$ are (controller design) parameters. Observe that the dynamics (6.8) has a clear economic interpretation [3, 57]: each power producer aims at maximizing their own profit which, under the assumption of perfect competition, occurs whenever their individual marginal cost equals the local price $\lambda_{gi} - \omega_{gi}$, which depends on the local frequency ω_{gi} of the physical network. At the same time, each consumer maximizes its own utility but is penalized by the local price $\lambda_{di} - \omega_{di}$.

Remark 6.4.1 (Frequency as feedback signal). The idea to use the frequency deviation in the pricing mechanism stems from our previous work [105, 107] (see also Chapters 3,4 and 5), and helps to compensate for the power supply-demand imbalance. Moreover, it allows for a power-preserving interconnection with the physical model (6.2).

The equations (6.8c), (6.8d), (6.8e) represent the distributed dynamic pricing algorithm where the quantity v represents a *virtual* power flow along the edges of the communication graph with incidence matrix D_c. We emphasize *virtual*, since v may not correspond to the real physical power flow as the communication graph (which can be designed as desired) may be different than the physical network

topology. By (6.8c) the flow v increases from areas with a lower price to areas with a relatively higher price and vice versa. Equation (6.8d) shows that the local price λ_i rises if the power outflow at node $i \in \mathcal{V}$ is greater than the local power supply plus power inflow of power at node i and vice versa. A similar statement holds for (6.8e).

An important observation is that the dynamic pricing algorithm (6.8) can be written in port-Hamiltonian form as

$$\begin{aligned}
\dot{x}_c &= \underbrace{\begin{bmatrix} 0 & 0 & 0 & I_{n_g} & 0 \\ 0 & 0 & 0 & 0 & -I_{n_d} \\ 0 & 0 & 0 & -D_{cg}^T & -D_{cd}^T \\ -I_{n_g} & 0 & D_{cg} & 0 & 0 \\ 0 & I_{n_d} & D_{cd} & 0 & 0 \end{bmatrix}}_{J_c} \nabla H_c + \underbrace{\begin{bmatrix} I_{n_g} & 0 \\ 0 & I_{n_d} \\ 0 & 0 \\ 0 & 0 \end{bmatrix}}_{g_c} \left(\begin{bmatrix} \omega_g \\ -\omega_d \end{bmatrix} + \nabla S(y_c) \right) \\
y_c &= \begin{bmatrix} I_{n_g} & 0 & 0 & 0 & 0 \\ 0 & I_{n_d} & 0 & 0 & 0 \end{bmatrix} \nabla H_c = \begin{bmatrix} P_g \\ P_d \end{bmatrix}
\end{aligned} \tag{6.9}$$

with $H_c = \frac{1}{2} x_c^T K_c^{-1} x_c$ and

$$\underbrace{\begin{bmatrix} x_g \\ x_l \\ x_v \\ x_{\lambda_g} \\ x_{\lambda_d} \end{bmatrix}}_{x_c} = \underbrace{\begin{bmatrix} K_g & 0 & 0 & 0 & 0 \\ 0 & K_d & 0 & 0 & 0 \\ 0 & 0 & K_v & 0 & 0 \\ 0 & 0 & 0 & K_{\lambda_g} & 0 \\ 0 & 0 & 0 & 0 & K_{\lambda_d} \end{bmatrix}}_{K_c} \underbrace{\begin{bmatrix} P_g \\ P_d \\ v \\ \lambda_g \\ \lambda_d \end{bmatrix}}_{z_c}.$$

Since S is a concave function it satisfies the following dissipation inequality

$$(y_c - \bar{y}_c)^T (\nabla S(y_c) - \nabla S(\bar{y}_c)) \leq 0$$

for all $y_c, \bar{y}_c \in \mathbb{R}^n$. This property implies that the system (6.9) is passive with respect to its steady states, see also [107].

6.5 Stability of the closed-loop system

It is observed that, by construction of the dynamic pricing algorithm, there is two-way coupling between the physical power network (6.2) and the market dynamics (6.8) through the ports $(P_g, \omega_g), (P_d, \omega_d)$. In fact, the interconnection between (6.2) and (6.8) is power-preserving. As a result, the closed-loop system, obtained

by combining the systems (6.5) and (6.9), takes the form

$$\begin{bmatrix} \dot{x}_c \\ \dot{\varphi} \\ \dot{p}_g \\ \dot{E}_g \\ 0 \\ 0 \end{bmatrix} = \begin{bmatrix} J_c & 0 & -G_1^T & 0 & 0 & G_2^T \\ 0 & 0 & \hat{D}_g^T & 0 & 0 & \hat{D}_d^T \\ G_1 & -\hat{D}_g & -A_g & 0 & 0 & 0 \\ 0 & 0 & 0 & -R_g & 0 & 0 \\ 0 & 0 & 0 & 0 & -[E_d] & 0 \\ -G_2 & -\hat{D}_d & 0 & 0 & 0 & -A_d \end{bmatrix} \nabla W + \begin{bmatrix} g_c \nabla S(y_c) \\ 0 \\ 0 \\ 0 \\ \bar{Q}_d^T \\ 0 \end{bmatrix} \quad (6.10)$$
$$y_c = g_c^T \nabla H_c(x_c)$$

where $W(x, \omega_d) = H_p(x_p) + U_p(\omega_d) + H_c(x_c)$, with $x = \mathrm{col}(x_c, x_p)$ and

$$G_1 = \begin{bmatrix} I_{n_g} & 0 & 0 & 0 & 0 \end{bmatrix}, \quad G_2 = \begin{bmatrix} 0 & I_{n_d} & 0 & 0 & 0 \end{bmatrix}.$$

Next, we examine the equilibria of the coupled system (6.10). From it follows from (6.8c) that $\bar{\lambda}_g = \mathbb{1}_{n_g} \bar{\lambda}_*, \lambda_d = \mathbb{1}_{n_d} \lambda_*$ for some $\lambda_* \in \mathbb{R}$. Hence, the prices $\lambda_{gi} \in \mathcal{V}_g, \lambda_{di} \in \mathcal{V}_d$ are identical at each node. From (6.8d), (6.8e) follows the power balance $\mathbb{1}_{n_g}^T \bar{P}_g = \mathbb{1}_{n_d}^T \bar{P}_d$. Finally, from (6.2b) and (6.2d) we have that $\bar{\omega}_i = 0, i \in \mathcal{V}$. This implies that at steady state the KKT optimality conditions (6.7) are satisfied. Hence, the equilibrium points of the combined system (6.2), (6.8) satisfy the optimality conditions of the social welfare problem (6.6) and, moreover, the frequency deviations are zero at steady state.

Suppose now that there exists an equilibrium $(\bar{x}_c, \bar{x}_p, \bar{\omega}_d)$ of (6.10) and define $\bar{y}_c = g_c^T \nabla H(\bar{x}_c)$. Then we define the shifted Hamiltonian [117] by

$$\bar{H}_p(x_p) = H_p(x_p) - (x_p - \bar{x}_p)^T \nabla H_p(\bar{x}_p) - H_p(\bar{x}_p),$$

and similarly $\bar{U}_p(\omega_d), \bar{H}_c(x_c)$ are defined. As a result, the algebraic equation (6.4) can be rewritten as

$$0 = -[E_d] \left(\nabla_{E_d} \bar{H}_p(x_p) + \nabla_{E_d} \bar{H}_a(x_p) \right)$$

where

$$\bar{H}_a(x_p) = E_d^T \nabla_{E_d} \bar{H}_p(\bar{x}_p) - \bar{Q}_d^T \log E_d.$$

with $\log(\cdot)$ being the element-wise natural logarithm. Observe that $\bar{H}_a$ is a convex function since, by Assumption 6.3.1, $\bar{Q}_d \geq 0$. Since the term $\bar{H}_a$ only depends on

E_d, the system (6.10) takes the equivalent form

$$\begin{bmatrix} \dot{x}_c \\ \dot{\varphi} \\ \dot{p}_g \\ \dot{E}_g \\ 0 \\ 0 \end{bmatrix} = \begin{bmatrix} J_c & 0 & -G_1 & 0 & 0 & G_2 \\ 0 & 0 & \hat{D}_g^T & 0 & 0 & \hat{D}_d^T \\ G_1^T & -\hat{D}_g & -A_g & 0 & 0 & 0 \\ 0 & 0 & 0 & -R_g & 0 & 0 \\ 0 & 0 & 0 & 0 & -[E_d] & 0 \\ -G_2^T & -\hat{D}_d & 0 & 0 & 0 & -A_d \end{bmatrix} \nabla \bar{W} + \begin{bmatrix} (g_c \nabla S(y_c) - g_c \nabla S(\bar{y}_c))^T & 0 & 0 & 0 & 0 & 0 \end{bmatrix}^T \tag{6.11}$$

where $\bar{W}(x, \omega_d) := \bar{H}(x) + \bar{U}_p(\omega_d), \bar{H}(x) := \bar{H}_p(x_p) + \bar{H}_a(x_p) + \bar{H}_c(x_c)$. After elimination of the algebraic variable ω_d, the closed-loop system (6.11) can in turn equivalently be written as

$$\begin{bmatrix} \dot{x}_c \\ \dot{\varphi} \\ \dot{p}_g \\ \dot{E}_g \\ 0 \end{bmatrix} = \begin{bmatrix} J_c - G_2 A_d^{-1} G_2^T & -G_2 A_d^{-1} \hat{D}_d & -G_1 & 0 & 0 \\ -\hat{D}_d^T A_d^{-1} G_2^T & -\hat{D}_d^T A_d^{-1} \hat{D}_d & \hat{D}_g^T & 0 & 0 \\ G_1^T & -\hat{D}_g & -A_g & 0 & 0 \\ 0 & 0 & 0 & -R_g & 0 \\ 0 & 0 & 0 & 0 & -[E_d] \end{bmatrix} \nabla \bar{H} + \begin{bmatrix} (g_c \nabla S(y_c) - g_c \nabla S(\bar{y}_c))^T & 0 & 0 & 0 & 0 \end{bmatrix}^T . \tag{6.12}$$

We are now ready to present the main convergence result.

Theorem 6.5.1 (Local asymptotic stability of (6.12))**.** *Consider system* (6.12) *and suppose that* $D_c \in \mathbb{R}^{n \times (n-1)}$ *is the incidence matrix of a tree graph. Furthermore assume that the system* (6.12) *admits an equilibrium* $\bar{x}$ *satisfying* $\nabla^2 \bar{H}(\bar{x}) > 0$*. Then* $\bar{x}$ *is locally asymptotically stable.*

Proof. The shifted Hamiltonian $\bar{H}$ satisfies

$$\begin{aligned} \dot{\bar{H}} = & -\omega_g^T A_g \omega_g - \omega_d^T A_d \omega_d - (\nabla_{E_g} \bar{H})^T R_g \nabla_{E_g} \bar{H} \\ & - (P_g - \bar{P}_g)^T (\nabla C(P_g) - \nabla C(\bar{P}_g)) \\ & + (P_d - \bar{P}_d)^T (\nabla U(P_d) - \nabla U(\bar{P}_d)) \leq 0 \end{aligned} \tag{6.13}$$

where ω_d satisfies the algebraic constraint (6.2d). Observe that $\dot{\bar{H}} = 0$ if and only if $\omega_g = 0, \omega_d = 0, \nabla_{E_g} \bar{H}(x) = 0, P_g = \bar{P}_g, P_d = \bar{P}_d$ since C, U are strictly convex/concave functions respectively. On the largest invariant set M where $\dot{\bar{H}} =$

0 we have

$$\begin{aligned} \dot{\varphi} &= 0 & \lambda_g &= \bar{\lambda}_g \\ 0 &= \hat{D}\nabla_{\varphi}\bar{H} & \lambda_d &= \bar{\lambda}_d \\ 0 &= \nabla_{E_g}\bar{H} & K_{\lambda_g}\dot{\lambda}_g &= D_{cg}(v-\bar{v}) \\ 0 &= [E_d]\nabla_{E_d}\bar{H} & K_{\lambda_d}\dot{\lambda}_d &= D_{cd}(v-\bar{v}) \\ K_v\dot{v} &= -D_{cg}^T(\lambda_g-\bar{\lambda}_g) - D_{cd}^T(\lambda_d-\bar{\lambda}_d) \end{aligned}$$

Hence, $\lambda_g = \bar{\lambda}_g, \lambda_d = \bar{\lambda}_d$ are constant and since $D_c, \hat{D}$ have full column rank it follows that $v = \bar{v}, \nabla_{\varphi}\bar{H}(x) = 0$ respectively. Hence, each element $x \in M$ satisfies $\nabla\bar{H}(x) = 0$. By (6.13) and since $\nabla\bar{H}(\bar{x}) = 0, \nabla^2\bar{H}(\bar{x}) > 0$, there exists a compact level set $\mathcal{D}$ of $\bar{H}$ around $\bar{x}$ which is forward invariant and satisfies $\mathcal{D} \cap M = \{\bar{x}\}$. Hence, by Theorem 6.2.2, $\bar{x}$ is locally asymptotically stable. □

Remark 6.5.2 (Cyclic communication graphs). While the communication graph is assumed to be a tree in Theorem 6.5.1, we expect that the convergence result can also be extended to the case of general (cyclic) connected communication graphs, requiring a slightly modified invariance principle for DAE compared to Theorem 6.2.2. However, this is beyond the scope of the chapter.

In [32] a sufficient condition is given which guarantees that the Hessian $\nabla^2\bar{H}(\bar{x})$ evaluated at the equilibrium $\bar{x}$ is positive definite, which is required in Theorem 6.5.1. Adapted for the model (6.2), the following distributed condition should be verified.

Proposition 6.5.3 (Sufficient condition for positive definite Hessian)**.** *Suppose that $\bar{x}$ (with $\bar{\varphi} = \hat{D}^T\bar{\delta}$) satisfies*

$$\begin{aligned} \frac{1}{X_{di}-X'_{di}} + B_{ii} - \sum_{j\in\mathcal{N}_i} B_{ij}\frac{\bar{E}_i + \bar{E}_j\sin^2\bar{\delta}_{ij}}{\bar{E}_i\cos\bar{\delta}_{ij}} > 0, \qquad & i \in \mathcal{V}_g \\ B_{ii} - \sum_{j\in\mathcal{N}_i} B_{ij}\frac{\bar{E}_i + \bar{E}_j\sin^2\bar{\delta}_{ij}}{\bar{E}_i\cos\bar{\delta}_{ij}} > 0, \qquad & i \in \mathcal{V}_d \end{aligned}$$

with $\bar{\delta}_{ij} \in (-\frac{\pi}{2}, \frac{\pi}{2}), \forall\{i,j\} \in \mathcal{E}$, and $\bar{E}_i > 0, \forall i \in \mathcal{V}$. Then $\nabla^2\bar{H}(\bar{x}) > 0$.

Remarkably, the above conditions are satisfied if the voltage (angle) differences and generator reactances are sufficiently small and the shunt susceptances (at the loads) are sufficiently large.

6.6 Conclusions

In this chapter an energy-based approach to the modeling and stability analysis of structure-preserving power networks with markets dynamics has been established. In particular, local convergence of the coupled system of differential-algebraic

equations to an optimal point of the social welfare problem has been proven using a suitable Lyapunov function.

A possible extension to the established results is to consider the more complex case that the loads are not frequency-dependent. This introduces additional challenges in the stability analysis as the closed-loop differential-algebraic system does not satisfy the regularity condition given in Definition 6.2.1. As a result, the extended LaSalle's invariance principle considered in the present paper cannot directly be applied to this case. Another direction for future research is to design additional controllers for the physical power network that achieve optimal reactive power sharing and/or voltage regulation. In addition, an extension could be to include generator limits and line congestion as done in Chapter 5 of this thesis. Finally, the influence of a possible delay in the communication of the dynamic pricing algorithm on the stability of the closed-loop has to be investigated.

Chapter 7

DAPI control of high-dimensional multi-machine models

Abstract: *This chapter investigates the problem of optimal frequency regulation of multi-machine power networks where each synchronous machine is described by a sixth-order model. By analyzing the physical energy stored in the network and the generators, a port-Hamiltonian representation of the multi-machine system is obtained. Moreover, it is shown that the open-loop system is passive with respect to its steady states which allows the construction of passive controllers to control the multi-machine network. As a special case, a distributed consensus based controller is designed that regulates the frequency and minimizes a global quadratic generation cost in the presence of a constant unknown demand. In addition, the proposed controller allows freedom in choosing any desired connected undirected weighted communication graph.*

Published as:

T.W. Stegink, C. De Persis, A.J. van der Schaft. "Optimal power dispatch in networks of high-dimensional models of synchronous machines." IEEE 55th Conference on Decision and Control (CDC). 2016.

7.1 Introduction

The control of power networks has become increasingly challenging over the last decades. As renewable energy sources penetrate the grid, the conventional power plants have more difficulty in keeping the frequency around the nominal value, e.g. 50 Hz, leading to an increased chance of a network failure or even a blackout.

The current developments require a better understanding of more advanced models for the power network as the grid is operating more often near its capacity constraints. Considering high-order models of, for example, synchronous machines, that better approximate the reality allows us to establish results on the control and stability of power networks that are more reliable and accurate.

At the same time, incorporating economic considerations in the power grid has become more difficult. As the scale of the grid expands, computing the optimal power production allocation in a centralized manner as conventionally is done is computationally expensive, making distributed control far more desirable compared to centralized control. In addition, often exact knowledge of the power demand is required for computing the optimal power dispatch, which is unrealistic in practical applications. As a result, there is an increased desire for distributed real-time controllers which are able to compensate for the uncertainty of the demand.

In this chapter, we propose an energy-based approach for the modeling, analysis and control of the power grid, both for the physical network as well as for the distributed controller design. Since energy is the main quantity of interest, the port-Hamiltonian framework is a natural approach to deal with the problem. Moreover, the port-Hamiltonian framework lends itself to deal with complex large-scale nonlinear systems like power networks [37, 105, 106].

The emphasis in the present chapter lies on the modeling and control of (networked) synchronous machines as they play an important role in the power network since they are the most flexible and have to compensate for the increased fluctuation of power supply and demand. However, the full-order model of the synchronous machine as derived in many power engineering books like [4, 61, 67] is difficult to analyze, see e.g. [37] for a port-Hamiltonian approach, especially when considering multi-machine networks [21, 75]. Moreover, it is not necessary to consider the full-order model when studying electromechanical dynamics [67].

On the other hand of the spectrum, many of the recent optimal controllers in power grids that deal with optimal power dispatch problems rely on the second-order (non)linear swing equations as the model for the power network [64, 92, 95, 131, 135], or the third-order model as e.g. in [113]. However, the swing equations are inaccurate and only valid on a limited time interval up to the order of a few seconds so that asymptotic stability results are often invalid for the actual system [4, 61, 67].

Hence, it is appropriate to make simplifying assumptions for the full-order model and to focus on multi-machine models with intermediate complexity which provide a more accurate description of the network compared to the second- and third-order models [4, 61, 67]. However, for the resulting intermediate-order multi-machine models the stability analysis is often carried out for the linearized system,

see [3, 61, 67]. Consequently, the stability results are only valid around a specific operating point.

Our approach is different as the nonlinear nature of the power network is preserved. More specifically, in this chapter we consider a nonlinear sixth-order reduced model of the synchronous machine that enables a quite accurate description of the power network while allowing us to perform a rigorous analysis.

In particular, we show that the port-Hamiltonian framework is very convenient when representing the dynamics of the multi-machine network and for the stability analysis. Based on the physical energy stored in the generators and the transmission lines, a port-Hamiltonian representation of the multi-machine power network can be derived. More specifically, while the system dynamics is complex, the interconnection and damping structure of the port-Hamiltonian system is sparse and, importantly, state-independent.

The latter property implies shifted passivity of the system [117] which respect to its steady states which allows the usage of passive controllers that steer the system to a desired steady state. As a specific case, we design a distributed real-time controller that regulates the frequency and minimizes the global generation cost without requiring any information about the unknown demand. In addition, the proposed controller design allows us to choose any desired undirected weighted communication graph as long as the underlying topology is connected.

The main contribution of this chapter is to combine distributed optimal frequency controllers with a high-order nonlinear model of the power network, which is much more accurate compared to the existing literature, and to prove asymptotic stability to the set of optimal points by using Lyapunov function based techniques.

Outline: The rest of the chapter is organized as follows. In Section 7.2 the preliminaries are stated and a sixth-order model of a single synchronous machine is given. Next, the multi-machine model is derived in Section 7.3. Then the energy functions of the system are derived in Section 7.4, which are used to represent the multi-machine system in port-Hamiltonian form, see Section 7.5. In Section 7.6 the design of the distributed controller is given and asymptotic stability to the set of optimal points is proven. Finally, the conclusions and the possibilities for future research are discussed in Section 7.7.

7.2 Preliminaries

Consider a power grid consisting of n buses. The network is represented by a connected and undirected $\mathcal{R}$ graph $\mathcal{G} = (\mathcal{V}, \mathcal{E})$, where the nodes, $\mathcal{V} = \mathcal{I}_n := \{1, \dots, n\}$, is the set of buses and the edges, $\mathcal{E} \subset \mathcal{V} \times \mathcal{V}$, is the set of transmission lines connecting the buses. The edges are arbitrarily labeled with a unique identifier in $\mathcal{I}_m = \{1, \dots, m\}$ where the k-th edge connecting nodes i and j is denoted as $k \sim \{i, j\}$. The ends of edge $k \sim \{i, j\}$ are arbitrary labeled with a '+' and a '-',

δ_i	rotor angle w.r.t. synchronous reference frame
ω_i	frequency deviation
P_{gi}	mechanical power injection
P_{di}	power demand
M_i	moment of inertia
X_{qi}, X_{di}	synchronous reactances
X'_{qi}, X'_{di}	transient reactances
X''_{di}, X''_{qi}	subtransient reactances
E_{fi}	exciter emf/voltage
E'_{qi}, E'_{di}	internal bus transient emfs/voltages
E''_{qi}, E''_{di}	internal bus subtransient emfs/voltages
V_{qi}, E_{di}	external bus voltages
I_{qi}, I_{di}	generator currents
T'_{qi}, T'_{di}	open-loop transient time-scales
T''_{qi}, T''_{di}	open-loop subtransient time-scales

Table 7.1: Model parameters and variables.

so that the incidence matrix D of the resulting directed graph is given by

$$D_{ik} = \begin{cases} +1 & \text{if } i \text{ is the positive end of } k \\ -1 & \text{if } i \text{ is the negative end of } k \\ 0 & \text{otherwise.} \end{cases} \tag{7.1}$$

Each bus represents a synchronous machine and is assumed to have controllable mechanical power injection and a constant *unknown* power load. The dynamics of each synchronous machine $i \in \mathcal{V}$ is assumed to be given by [67]

$$\begin{aligned} M_i\dot{\omega}_i &= P_{gi} - P_{di} - V_{di}I_{di} - V_{qi}I_{qi} \\ \dot{\delta}_i &= \omega_i \\ T'_{di}\dot{E}'_{qi} &= E_{fi} - E'_{qi} + (X_{di} - X'_{di})I_{di} \\ T'_{qi}\dot{E}'_{di} &= -E'_{di} - (X_{qi} - X'_{qi})I_{qi} \\ T''_{di}\dot{E}''_{qi} &= E'_{qi} - E''_{qi} + (X'_{di} - X''_{di})I_{di} \\ T''_{qi}\dot{E}''_{di} &= E'_{di} - E''_{di} - (X'_{qi} - X''_{qi})I_{qi}, \end{aligned} \tag{7.2}$$

see also Table 7.1.

Assumption 7.2.1 (Power system model (7.2))**.** When using model (7.2), we make the following simplifying assumptions [67]:

- The frequency of each machine is operating around the synchronous frequency.
- The stator winding resistances are zero.
- The excitation voltage E_{fi} is constant for all $i \in \mathcal{V}$.

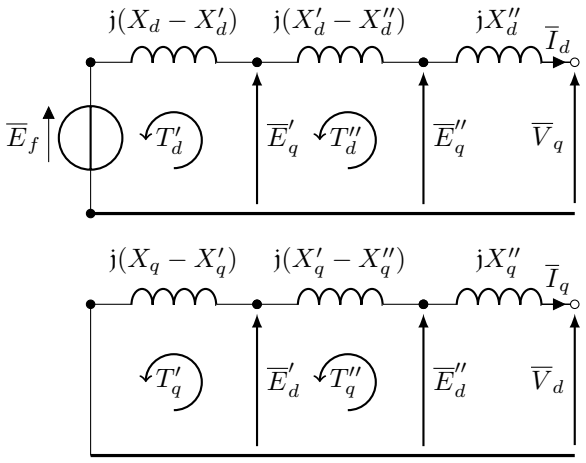

Figure 7.1: Generator equivalent circuits for both dq-axes [67]. For aesthetic reasons the subscript i is dropped.

- The *subtransient saliency* is negligible, i.e. $X''_{di} = X''_{qi}, \forall i \in \mathcal{V}$.

The latter assumption is valid for synchronous machines with damper windings in both the d- and q-axes, which is the case for most synchronous machines [67].

Remark 7.2.2 (Asynchronous damping). The effects of the damper windings is explicitly governed by the last two equations of (7.2). Consequently, there is no asynchronous damping term appearing in the frequency dynamics of the model (7.2), which is in constrast with the classical swing equations or the third-order synchronous machine model (also adopted in Chapter 5).

It is standard in the power system literature to represent the equivalent synchronous machine circuits along the dq-axes as in Figure 7.1, [61, 67]. Here we use the conventional phasor notation $\overline{E}''_i = \overline{E}''_{qi} + \overline{E}''_{di} = E''_{qi} + \mathrm{j}E''_{di}$ where $\overline{E}''_{qi} := E''_{qi}, \overline{E}''_{di} := \mathrm{j}E''_{di}, \mathrm{j} := \sqrt{-1}$, and the phasors $\overline{I}_i, \overline{V}_i$ are defined likewise [67, 90]. Remark that internal voltages E'_q, E'_d, E''_q, E''_d as depicted in Figure 7.1 are not necessarily at steady state but are governed by (7.2), where it should be noted that, by definition, the reactances of a round rotor synchronous machine satisfy $X_{di} > X'_{di} > X''_{di} > 0, X_{qi} > X'_{qi} > X''_{qi} > 0$ for all $i \in \mathcal{V}$ [61, 67].

By Assumption 7.2.1 the stator winding resistances are negligible so that synchronous machine i can be represented by a subtransient emf behind a subtransient reactance, see Figure 7.2 [61, 67]. As illustrated in this figure, the internal and external voltages are related to each other by [67]

$$\overline{E}''_i = \overline{V}_i + \mathrm{j}X''_{di}\overline{I}_i, \qquad i \in \mathcal{V}. \tag{7.3}$$

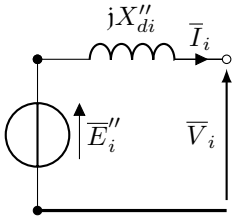

Figure 7.2: Subtransient emf behind a subtransient reactance.

7.3 Multi-machine model

Consider n synchronous machines which are interconnected by purely inductive transmission lines and assume that the network is operating at steady state. As the currents and voltages of each synchronous machine is expressed w.r.t. its local dq-reference frame, the network equations are written as [90]

$$\overline{I} = \operatorname{diag}(e^{-\mathrm{j}\delta_i})\mathcal{Y}\operatorname{diag}(e^{\mathrm{j}\delta_i})\overline{E}''. \tag{7.4}$$

Here the admittance matrix[1] $\mathcal{Y} := D(R+\mathrm{j}X)^{-1}D^T$ satisfies $\mathcal{Y}_{ij} = -G_{ij} - \mathrm{j}B_{ij}$ and $\mathcal{Y}_{ii} = G_{ii} + \mathrm{j}B_{ii} = \sum_{j\in\mathcal{N}_i} G_{ij} + \mathrm{j}\sum_{j\in\mathcal{N}_i} B_{ij}$ where G denotes the conductance and $B \in \mathbb{R}^{n\times n}_{\leq 0}$ denotes the susceptance of the network [90]. In addition, $\mathcal{N}_i$ denotes the set of neighbors of node i.

Remark 7.3.1 (Reactance X''_{di} as part of network). As the electrical circuit depicted in Figure 7.2 is in steady state (7.3), the reactance X''_{di} can also be considered as part of the network (an additional inductive line) and is therefore implicitly included into the network admittance matrix $\mathcal{Y}$, see also Figure 7.3.

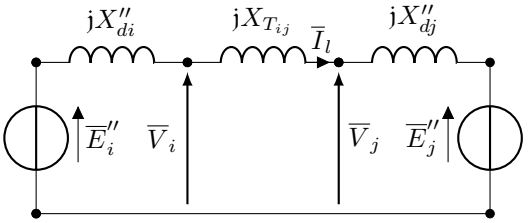

Figure 7.3: Interconnection of two synchronous machines by a purely inductive transmission line with reactance $X_{T_{ij}}$.

Since the network is purely inductive $G = 0$ which simplifies the analysis later. By equating the real and imaginary part of (7.4) we obtain the following

[1] Recall that D is the incidence matrix of the network defined by (7.1).

expressions for the dq-currents entering generator $i \in \mathcal{V}$:

$$\begin{aligned} I_{di} &= B_{ii}E''_{qi} - \sum_{j\in\mathcal{N}_i} \big[B_{ij}(E''_{dj}\sin\delta_{ij} + E''_{qj}\cos\delta_{ij})\big], \\ I_{qi} &= -B_{ii}E''_{di} - \sum_{j\in\mathcal{N}_i} \big[B_{ij}(E''_{qj}\sin\delta_{ij} - E''_{dj}\cos\delta_{ij})\big], \end{aligned} \tag{7.5}$$

where $\delta_{ij} := \delta_i - \delta_j$. By substituting (7.5) and (7.3) into (7.2) we obtain after some rewriting a sixth-order multi-machine model given by equation

$$\begin{aligned} M_i\dot{\omega}_i &= P_{gi} - P_{di} + \sum_{j\in\mathcal{N}_i} B_{ij}\big[(E''_{di}E''_{dj} + E''_{qi}E''_{qj})\sin\delta_{ij} + (E''_{di}E''_{qj} - E''_{qi}E''_{dj})\cos\delta_{ij}\big] \\ \dot{\delta}_i &= \omega_i \\ T'_{di}\dot{E}'_{qi} &= E_{fi} - E'_{qi} + (X_{di} - X'_{di})(B_{ii}E''_{qi} - \sum_{j\in\mathcal{N}_i} \big[B_{ij}(E''_{dj}\sin\delta_{ij} + E''_{qj}\cos\delta_{ij})\big]) \\ T'_{qi}\dot{E}'_{di} &= -E'_{di} + (X_{qi} - X'_{qi})(B_{ii}E''_{di} - \sum_{j\in\mathcal{N}_i} \big[B_{ij}(E''_{dj}\cos\delta_{ij} - E''_{qj}\sin\delta_{ij})\big]) \\ T''_{di}\dot{E}''_{qi} &= E'_{qi} - E''_{qi} + (X'_{di} - X''_{di})(B_{ii}E''_{qi} - \sum_{j\in\mathcal{N}_i} \big[B_{ij}(E''_{dj}\sin\delta_{ij} + E''_{qj}\cos\delta_{ij})\big]) \\ T''_{qi}\dot{E}''_{di} &= E'_{di} - E''_{di} + (X'_{qi} - X''_{qi})(B_{ii}E''_{di} - \sum_{j\in\mathcal{N}_i} \big[B_{ij}(E''_{dj}\cos\delta_{ij} - E''_{qj}\sin\delta_{ij})\big]) \end{aligned} \tag{7.6}$$

Remark 7.3.2 (Energy conservation). Since the transmission lines are purely inductive by assumption, there are no energy losses in the transmission lines implying that the following energy conservation law holds: $\sum_{i\in\mathcal{V}} P_{ei} = 0$ where $P_{ei} = \mathrm{Re}(\overline{E}_i\overline{I}_i^*) = E''_{di}I_{di} + E''_{qi}I_{qi}$ is the electrical power produced by synchronous machine i.

7.4 Energy functions

When analyzing the stability of the multi-machine system one often searches for a suitable Lyapunov function. A natural starting point is to consider the physical energy as a candidate Lyapunov function. Moreover, when we have an expression for the energy, a port-Hamiltonian representation of the associated multi-machine model (7.6) can be derived, see Section 7.5.

Remark 7.4.1 (Common scalar factor in Hamiltonian). It is notationally convenient in the definition of the Hamiltonian to multiply the energy stored in the synchronous machine and the transmission lines by the synchronous frequency ω_s since a factor ω_s^{-1} appears in each of the energy functions. As a result, the Hamiltonian has the dimension of power instead of energy. Nevertheless, we still refer to the Hamiltonian as the energy function in the sequel.

In the remainder of this section we will first identify the electrical and mechanical energy stored in each synchronous machine. Next, we identify the energy stored in the transmission lines.

7.4.1 Synchronous machine

Electrical energy

Note that, at steady state, the energy (see Remark 7.4.1) stored in the first two reactances[2] of generator i as illustrated in Figure 7.1 is given by

$$\begin{aligned} H_{edi} &= \frac{1}{2}\frac{(E'_{qi} - E_{fi})^2}{X_{di} - X'_{di}} + \frac{1}{2}\frac{(E'_{qi} - E''_{qi})^2}{X'_{di} - X''_{di}} \\ H_{eqi} &= \frac{1}{2}\frac{(E'_{di})^2}{X_{qi} - X'_{qi}} + \frac{1}{2}\frac{(E'_{di} - E''_{di})^2}{X'_{qi} - X''_{qi}}. \end{aligned} \tag{7.7}$$

Remark 7.4.2 (Energy in reactance X''_d). The energy stored in the third (subtransient) reactance will be considered as part of the energy stored in the transmission lines, see also Remark 7.3.1 and Section 7.4.2.

Mechanical energy

The kinetic energy of synchronous machine i is given by

$$H_{mi} = \frac{1}{2}M_i\omega_i^2 = \frac{1}{2}M_i^{-1}p_i^2,$$

where $p_i = M_i\omega_i$ is the angular momentum of synchronous machine i with respect to the synchronous rotating reference frame.

7.4.2 Inductive transmission lines

Consider an interconnection between two synchronous machines with a purely inductive transmission line (with reactance $X_{T_{ij}}$) at steady state, see Figure 7.3. When expressed in the local dq-reference frame of generator i, we observe from Figure 7.3 that at steady state one obtains[3]

$$\mathrm{j}X_k\overline{I}_k = \overline{E}''_i - e^{-\mathrm{j}\delta_{ik}}\overline{E}''_k, \qquad k \sim \{i,j\}, \tag{7.8}$$

where the total reactance between the internal buses of generator i and j is given by $X_k := X''_{di} + X_{T_{ij}} + X''_{dj}$. Note that at steady state the modified energy of the inductive transmission line $k \sim \{i,j\}$ between nodes i and j is given by $H_k =$

[2] In both the d- and the q-axes.

[3] The mapping from dq-reference frame k to dq-reference frame i in the phasor domain is done by multiplication of $e^{-\mathrm{j}\delta_{ik}}$ [90].

$\frac{1}{2}X_k\overline{I}_k^*\overline{I}_k$, which by (7.8) can be rewritten as

$$\begin{aligned} H_k = &- B_{ij}\Big[\big(E''_{di}E''_{qj} - E''_{dj}E''_{qi}\big)\sin\delta_{ij} - \big(E''_{di}E''_{dj} + E''_{qi}E''_{qj}\big)\cos\delta_{ij} \\ &+ \tfrac{1}{2}E''^2_{di} + \tfrac{1}{2}E''^2_{dj} + \tfrac{1}{2}E''^2_{qi} + \tfrac{1}{2}E''^2_{qj}\Big], \end{aligned} \tag{7.9}$$

where the line susceptance satisfies $B_{ij} = -\frac{1}{X_k} < 0$, $k \sim \{i,j\}$ [90].

7.4.3 Total energy

The total physical energy of the multi-machine system is equal to the sum of the individual energy functions:

$$H = \sum_{i\in\mathcal{V}} \big(H_{edi} + H_{eqi} + H_{mi}\big) + \sum_{k\in\mathcal{E}} H_k. \tag{7.10}$$

7.5 Port-Hamiltonian representation

Using the energy functions from the previous section, the multi-machine model (7.6) can be put into a port-Hamiltonian form. To this end, we derive expressions for the gradient of each energy function.

7.5.1 Transmission line energy

Recall that the energy stored in transmission line $k \sim \{i,j\}$ between internal buses i and j is given by (7.9). It can be verified that the gradient of the *total* energy stored in the transmission lines $H_L := \sum_{k\in\mathcal{E}} H_k$ takes the form

$$\begin{bmatrix} \frac{\partial H_L}{\partial \delta_i} \\ \frac{\partial H_L}{\partial E''_{qi}} \\ \frac{\partial H_L}{\partial E''_{di}} \end{bmatrix} = \begin{bmatrix} E''_{di}I_{di} + E''_{qi}I_{qi} \\ -I_{di} \\ I_{qi} \end{bmatrix} = \begin{bmatrix} P_{ei} \\ -I_{di} \\ I_{qi} \end{bmatrix},$$

where I_{di}, I_{qi} are given by (7.5). Here it is used that the self-susceptances satisfy $B_{ii} = \sum_{j\in\mathcal{N}_i} B_{ij}$ for all $i \in \mathcal{V}$.

State transformation

In the sequel, it is more convenient to consider a different set of variable describing the voltage angle differences. Define for each edge $k \sim \{i,j\} \in \mathcal{E}$, $\eta_k := \delta_{ij} = \delta_i - \delta_j$ where i,j are respectively the positive and negative ends of k. In vector form we obtain $\eta = D^T\delta \in \mathbb{R}^m$, and observe that this implies $D\frac{\partial H}{\partial \eta} = D\frac{\partial H_L}{\partial \eta} = P_e$.

7.5.2 Electrical energy of the synchronous generator

Further, notice that the electrical energy stored in the equivalent circuits along the d- and q-axis of generator i is given by (7.7) and satisfies

$$\begin{bmatrix} X_{di}-X'_{di} & X_{di}-X'_{di} \\ 0 & X'_{di}-X''_{di} \end{bmatrix} \begin{bmatrix} \frac{\partial H_{edi}}{\partial E'_{qi}} \\ \frac{\partial H_{edi}}{\partial E''_{qi}} \end{bmatrix} = \begin{bmatrix} E'_{qi}-E_{fi} \\ E''_{qi}-E'_{qi} \end{bmatrix}$$
$$\begin{bmatrix} X_{qi}-X'_{qi} & X_{qi}-X'_{qi} \\ 0 & X'_{qi}-X''_{qi} \end{bmatrix} \begin{bmatrix} \frac{\partial H_{eqi}}{\partial E'_{di}} \\ \frac{\partial H_{eqi}}{\partial E''_{di}} \end{bmatrix} = \begin{bmatrix} E'_{di} \\ E''_{di}-E'_{di} \end{bmatrix}.$$

By the previous observations, and by aggregating the states, the dynamics of the multi-machine system can now be written in the form

$$\begin{aligned} \dot{x} = &\begin{bmatrix} 0 & -D & 0 & 0 & 0 & 0 \\ D^T & 0 & 0 & 0 & 0 & 0 \\ 0 & 0 & -(T'_d)^{-1}\hat{X}_d & 0 & -(T'_d)^{-1}\hat{X}_d & 0 \\ 0 & 0 & 0 & -(T'_q)^{-1}\hat{X}_q & 0 & -(T'_q)^{-1}\hat{X}_q \\ 0 & 0 & 0 & 0 & -(T''_d)^{-1}\hat{X}'_d & 0 \\ 0 & 0 & 0 & 0 & 0 & -(T''_q)^{-1}\hat{X}'_q \end{bmatrix} \nabla H(x) \\ &+ g(P_g - P_d), \\ y = g^T \nabla H(x) = M^{-1}p = \omega, \qquad & g = \begin{bmatrix} I & 0 & 0 & 0 & 0 & 0 \end{bmatrix}^T. \end{aligned} \tag{7.11}$$

Here the Hamiltonian is given by (7.10) and $\hat{X}_{di} := X_{di} - X'_{di}, \hat{X}'_{di} := X'_{di} - X''_{di}, \hat{X}_d = \mathrm{diag}_{i\in\mathcal{V}}\{\hat{X}_{di}\}$ and $\hat{X}'_d, \hat{X}_q, \hat{X}'_q$ are defined likewise. In addition, $T'_d = \mathrm{diag}_{i\in\mathcal{V}}\{T'_{di}\}$ and T'_d, T_q, T'_q are defined similarly. Observe that the multi-machine system (7.11) is of the form

$$\begin{aligned} \dot{x} &= (J-R)\nabla H(x) + gu \\ y &= g^T \nabla H(x) \end{aligned} \tag{7.12}$$

where $J = -J^T$, $R = R^T$ are respectively the anti-symmetric and symmetric part of the matrix depicted in (7.11). Notice that the dissipation matrix of the *electrical part* is positive definite (which implies $R \geq 0$) if

$$\begin{bmatrix} 2\frac{X_{di}-X'_{di}}{T'_{di}} & \frac{X_{di}-X'_{di}}{T'_{di}} \\ \frac{X_{di}-X'_{di}}{T'_{di}} & 2\frac{X'_{di}-X''_{di}}{T''_{di}} \end{bmatrix} > 0, \qquad \begin{bmatrix} 2\frac{X_{qi}-X'_{qi}}{T'_{qi}} & \frac{X_{qi}-X'_{qi}}{T'_{qi}} \\ \frac{X_{qi}-X'_{qi}}{T'_{qi}} & 2\frac{X'_{qi}-X''_{qi}}{T''_{qi}} \end{bmatrix} > 0, \qquad \forall i \in \mathcal{V},$$

which, by invoking the Schur complement, holds if and only if

$$\begin{matrix} 4(X'_{di}-X''_{di})T'_{di} - (X_{di}-X'_{di})T''_{di} > 0 \\ 4(X'_{qi}-X''_{qi})T'_{qi} - (X_{qi}-X'_{qi})T''_{qi} > 0 \end{matrix}, \qquad \forall i \in \mathcal{V}. \tag{7.13}$$

Proposition 7.5.1 (Positive semi-definite dissipation matrix)**.** *Suppose that for all $i \in \mathcal{V}$ the following holds:*

$$\begin{aligned} 4(X'_{di} - X''_{di})T'_{di} - (X_{di} - X'_{di})T''_{di} > 0 \\ 4(X'_{qi} - X''_{qi})T'_{qi} - (X_{qi} - X'_{qi})T''_{qi} > 0. \end{aligned} \tag{7.14}$$

Then (7.11) *is a port-Hamiltonian representation of the multi-machine network* (7.6)*.*

It should be stressed that (7.14) is not a restrictive assumption since $T''_{di} \ll T'_{di}, T''_{qi} \ll T'_{qi}$ for a realistic generator, see also Table 4.2 of [61], Table 4.3 of [67] and particularly Proposition 2.7.2 in Chapter 2 of this thesis. Because the interconnection and damping structure $J - R$ of (7.11) is state-independent, the shifted Hamiltonian

$$\bar{H}(x) = H(x) - (x - \bar{x})^T \nabla H(\bar{x}) - H(\bar{x}) \tag{7.15}$$

acts as a local storage function for proving passivity in a neighborhood of a steady state $\bar{x}$ of (7.12), provided that the Hessian of H evaluated at $\bar{x}$ (denoted as $\nabla^2 H(\bar{x})$) is positive definite[4].

Proposition 7.5.2 (Shifted passivity)**.** *Let $(\bar{x}, \bar{u}, \bar{y})$ correspond to a steady state of* (7.12) *and satisfy $\nabla^2 H(\bar{x}) > 0$, $\bar{y} = g^T \nabla H(\bar{x})$. Then the system* (7.12) *is passive in a neighborhood of $\bar{x}$ with respect to the shifted external port-variables $(u - \bar{u}, y - \bar{y})$.*

Proof. Define the shifted Hamiltonian by (7.15), then we obtain

$$\begin{aligned} \dot{x} &= (J - R)\nabla H(x) + gu \\ &= (J - R)(\nabla \bar{H}(x) + \nabla H(\bar{x})) + gu \\ &= (J - R)\nabla \bar{H}(x) + g(u - \bar{u}) \\ y - \bar{y} &= g^T(\nabla H(x) - \nabla H(\bar{x})) = g^T \nabla \bar{H}(x). \end{aligned} \tag{7.16}$$

As $\nabla^2 H(\bar{x}) > 0$ we have that $\bar{H}(\bar{x}) = 0$ and $\bar{H}(x) > 0$ for all $x \neq \bar{x}$ in a sufficiently small neighborhood around $\bar{x}$. Hence, by (7.16) the passivity property automatically follows where $\bar{H}$ acts as a local storage function of the multi-machine system. □

7.6 Minimizing generation costs

The objective is to minimize the total quadratic generation cost while achieving zero frequency deviation. By analyzing the steady states of (7.6), it follows that a necessary condition for zero frequency deviation is $\mathbb{1}^T P_g = \mathbb{1}^T P_d$, i.e., the total supply must match the total demand. Therefore, consider the following convex

[4] Observe that $\nabla^2 H(x) = \nabla^2 \bar{H}(x)$ for all x.

minimization problem:

$$\begin{aligned} \underset{P_g}{\text{minimize}} \quad & \frac{1}{2} P_g^T Q P_g \\ \text{subject to} \quad & \mathbb{1}^T P_g = \mathbb{1}^T P_d, \end{aligned} \tag{7.17}$$

where $Q = Q^T > 0$ and P_d is a constant *unknown* power load.

Remark 7.6.1 (More general quadratic cost functions). Note that that minimization problem (7.17) is easily extended to quadratic cost functions of the form $\frac{1}{2} P_g^T Q P_g + b^T P_g$ for some $b \in \mathbb{R}^n$. However, for simplicity of notation this extension is omitted in this chapter.

As the minimization problem (7.17) is convex, it follows that P_g is an optimal solution if and only if the Karush-Kuhn-Tucker conditions are satisfied [12]. Hence, the optimal point of (7.17) is given by

$$P_g^* = Q^{-1} \mathbb{1} \lambda^*, \qquad \lambda^* = \frac{\mathbb{1}^T P_d}{\mathbb{1}^T Q^{-1} \mathbb{1}} \tag{7.18}$$

Next, based on the design of [113] and the *distributed averaging proportional integral (DAPI)* control proposed in [95], we consider a distributed controller of the form

$$\begin{aligned} T \dot{\theta} &= -L_c \theta - Q^{-1} \omega \\ P_g &= Q^{-1} \theta - K \omega \end{aligned} \tag{7.19}$$

where $T = \operatorname{diag}_{i \in \mathcal{V}}\{T_i\} > 0, K = \operatorname{diag}_{i \in \mathcal{V}}\{k_i\} > 0$ are controller parameters and $\theta \in \mathbb{R}^n$ is the controller variable. In addition, L_c is the Laplacian matrix of some connected undirected weighted communication graph. The controller (7.19) consists of three parts. Firstly, the term $-K\omega$ corresponds to a primary (proportional) controller and adds damping into the system. The term $-Q^{-1}\omega$ corresponds to secondary (integral) control for guaranteeing zero frequency deviation on longer time-scales. Finally, the term $-L_c\theta$ corresponds to tertiary (distributed averaging) control for achieving optimal production allocation over the network. We note that (7.19) admits the port-Hamiltonian representation

$$\begin{aligned} \dot{\vartheta} &= -L_c \nabla H_c(\vartheta) - Q^{-1} \omega \\ P_g &= Q^{-1} \nabla H_c(\vartheta) - K\omega, \qquad H_c(\vartheta) = \frac{1}{2} \vartheta^T T^{-1} \vartheta, \end{aligned} \tag{7.20}$$

where $\vartheta := T\theta$. By interconnecting the controller (7.20) with (7.11), the closed-loop system amounts to

$$\begin{aligned} \begin{bmatrix} \dot{x} \\ \dot{\vartheta} \end{bmatrix} &= \begin{bmatrix} J - R - R_K & G^T \\ -G & -L_c \end{bmatrix} \nabla H_{\mathtt{e}}(x, \vartheta) - \begin{bmatrix} g \\ 0 \end{bmatrix} P_d \\ G &= \begin{bmatrix} Q^{-1} & 0 & 0 & 0 & 0 & 0 \end{bmatrix} \end{aligned} \tag{7.21}$$

where the matrix $J - R$ is given as in (7.11), $H_{\mathtt{e}} := H + H_c$, and $R_K = \operatorname{blockdiag}(0, K, 0, 0, 0, 0)$. Define the set of steady states of (7.21) by Ω and observe that any $x_{\mathtt{e}} := (x, \vartheta) \in \Omega$ satisfies the optimality conditions (7.18) and $\omega = 0$.

To show asymptotic stability of the closed-loop system we need the following assumption.

Assumption 7.6.2 (Hessian condition)**.** We have $\Omega \neq \emptyset$ and there exists $\bar{x}_{\mathsf{e}} \in \Omega$ such that $\nabla^2 H_{\mathsf{e}}(\bar{x}_{\mathsf{e}}) > 0$.

Remark 7.6.3 (Sufficient conditions for positive definite Hessian). While the Hessian condition of Assumption 7.6.2 is required for proving local asymptotic stability of (7.21), guaranteeing that this condition holds can be bothersome. However, while we omit the details, it can be shown that $\nabla^2 H_{\mathsf{e}}(\bar{x}_{\mathsf{e}}) > 0$ if

- the generator reactances are small compared to the transmission line reactances.
- the subtransient voltage differences are small.
- the rotor angle differences are small.

which hold for typical operating conditions.

Theorem 7.6.4 (Local asymptotic stability)**.** *Let P_d be constant and $\bar{x}_{\mathsf{e}} \in \Omega$ such that Assumption 7.6.2 is satisfied. Then all trajectories of the closed-loop system* (7.21) *initialized in a sufficiently small neighborhood around $\bar{x}_{\mathsf{e}}$ converge to the set of optimal points Ω.*

Proof. Let $\bar{x}_{\mathsf{e}} \in \Omega$ be an equilibrium satisfying Assumption 7.6.2 and define the shifted Hamiltonian $\bar{H}_{\mathsf{e}}$ as in (7.15). Observe by (7.16) that the shifted Hamiltonian defined by (7.15) satisfies

$$\dot{\bar{H}}_{\mathsf{e}} = -(\nabla \bar{H}_{\mathsf{e}})^T \operatorname{blockdiag}(R + R_K, L_c) \nabla \bar{H}_{\mathsf{e}} \leq 0$$

where equality holds if and only if $\omega = 0$, $T^{-1}\vartheta = \theta = \mathbb{1}\theta^* $ for some $\theta^* \in \mathbb{R}$, and $\nabla_E \bar{H}_{\mathsf{e}}(x_{\mathsf{e}}) = \nabla_E H_{\mathsf{e}}(x_{\mathsf{e}}) = 0$. Here $\nabla_E H_{\mathsf{e}}(x_{\mathsf{e}})$ is the gradient of H_{e} with respect to the internal voltages E'_q, E'_d, E''_q, E''_d. By Assumption 7.6.2 there exists a compact neighborhood Υ around $\bar{x}_{\mathsf{e}}$ which is forward invariant. By invoking LaSalle's invariance principle, trajectories initialized in Υ converge to the largest invariant set where $\dot{\bar{H}}_{\mathsf{e}} = 0$. On this set $\omega, \eta, \theta, E'_q, E'_d, E''_q, E''_d$ are constant and, more specifically, $\omega = 0$, $\theta = \mathbb{1}\lambda^* = \mathbb{1}\frac{\mathbb{1}^T P_d}{\mathbb{1}^T Q^{-1}\mathbb{1}}$ corresponds to an optimal point of (7.17) as $P_g = Q^{-1}\mathbb{1}\lambda^*$ where λ^* is defined in (7.18). We conclude that the trajectories of the closed-loop system (7.21) initialized in a sufficiently small neighborhood around $\bar{x}_{\mathsf{e}}$ converge to the set of optimal points Ω. □

7.7 Conclusions

We have shown that a much more advanced multi-machine model than conventionally used can be analyzed using the port-Hamiltonian framework. Based on the energy functions of the system, a port-Hamiltonian representation of the model is obtained. Moreover, the system is proven to be incrementally passive which allows

the use of a passive controller that regulates the frequency in an optimal manner, even in the presence of an unknown constant demand.

While the focus in this chapter is about (optimal) frequency regulation, further effort is required to investigate the possibilities of (optimal) voltage control using passive controllers. Another extension is to consider the case where inverters and frequency dependent loads are included into the network as well. Finally, one could look at the possibility to include transmission line resistances in the network.

Chapter 8

Primal-dual dynamics with hard inequality constraints

Abstract: *In this chapter we study the convergence of projected primal-dual dynamics under mild conditions on the (general) optimization problem. In particular, we do not require strict convexity of the objective function nor uniqueness of the optimizer. By regarding the inequality constraints as hard constraints, we construct a suitable primal-dual dynamics in the complementarity formalism. We establish pointwise asymptotic stability of the set primal-dual optimizers by a suitable invariance principle involving two different Lyapunov functions. In addition, we show how these results can be applied for online optimization in data centers.*

Published as:

T.W. Stegink, T. Van Damme, C. De Persis, "Convergence of projected primal-dual dynamics with applications in data centers." 7th IFAC Workshop on Distributed Estimation and Control in Networked Systems (NecSys), 2018.

8.1 Introduction

The (constrained) primal-dual dynamics is a well-known continuous-time algorithm for determining the primal-dual optimizers of a constrained convex optimization problem. Research on such dynamics has a rich history starting from the classical work of [6] and has regained interest in the last decade, see for example [52], [26], [40], and [36]. In particular, the passivity property the primal-dual dynamics naturally admits (see [105]) has been exploited in numerous applications including network flow control [126], power networks [107], data centers [116] and energy efficient buildings [43].

However, throughout the literature several assumptions on the underlying optimization problem are typically made. Firstly, most works consider *soft* constraints meaning that the constraints may be violated throughout execution of the algorithm. However, this may not be feasible when considering for example (input) saturation or nonnegativity constraints. In addition, in the previous mentioned references strict convexity of the objective function is required for the stability analysis. An exception is the work of [81], but here (i) linear programs are considered which (ii) are in standard form.

In this chapter we relax some of the commonly made assumptions in the literature while retaining the asymptotic stability properties of the primal-dual dynamics. More specifically, our contributions are summarized as follows.

1. We consider *hard* inequality constraints, that is, constraints that may not be violated throughout execution of the algorithm.

2. A general form of the (in)equality constraints is considered, not only (decoupled) box constraints.

3. Only convexity is required for the objective function, capturing also the special case of linear programs.

4. We do not assume uniqueness of the optimal point. Instead, we establish convergence

   (a) to the set of primal-dual optimizers.

   (b) to a point within this set.

5. As an application, we show the results can be used for online thermal-aware job scheduling in data centers.

In our problem setup, we consider a general constrained convex optimization problem and write the associated primal-dual dynamics as a complementarity system. By implicitly using the equivalence with evolutionary variational inequalities and projected dynamical systems as shown in [15], we can show that there exists a unique (slow) solution of the primal-dual dynamics, which in addition is continuous with respect to the initial condition. These properties of the dynamics are exploited to establish pointwise asymptotic stability of the set of primal-dual optimizers.

In the last part of this chapter, we apply the suggested primal-dual algorithm to find setpoints for earlier established controllers, see [116], which minimizes the energy consumption of the cooling equipment in data centers. Due to the highly dynamic environment inside data centers where the optimal solution of the energy minimization problem changes very frequently, it is natural to look into ways of solving the optimization problem in a dynamic way. This is more so the case when the changes in the optimal solution are comparatively small over time as well. As such we will study the convergence behavior of our algorithm.

Notation:

For $A \in \mathbb{R}^{m\times n}$, we let $\|A\|$ denote the induced 2-norm. Given $v \in \mathbb{R}^n$ and positive definite matrix $A \in \mathbb{R}^{n\times n}$, we write $\|v\|_A := \sqrt{v^T A v}$. For vectors $u, v \in \mathbb{R}^n$ we write $u \perp v$ if $u^T v = 0$. We use the compact notational form $0 \geq u \perp v \geq 0$ to denote the complementarity conditions $u \leq 0, v \geq 0, u \perp v$.

8.2 Primal-dual dynamics (hard constraints)

We consider a convex optimization problem of the form

$$\underset{x\in\mathbb{R}^n}{\text{minimize}}\ f(x) \tag{8.1a}$$

$$\text{subject to}\ \ Ax = b \tag{8.1b}$$

$$g(x) \leq 0, \tag{8.1c}$$

with $g(.) = \text{col}(g_1(.), \ldots, g_q(.)), A \in \mathbb{R}^{m\times n}, b \in \mathbb{R}^m$. The inequality (8.1c) holds element-wise. For problem (8.1) we assume the following.

Assumption 8.2.1 (Convexity and Slater's condition)**.**
$f, g_1, \ldots, g_q : \mathbb{R}^n \to \mathbb{R}$ are continuously differentiable convex functions and there exists an $x \in \mathbb{R}^n$ such that $g_i(x) < 0, \forall i = 1, \ldots, q$.

In particular, Assumption 8.2.1 ensures that strong duality of problem (8.1) holds, see [12]. As a result $\bar{x} \in \mathbb{R}^n$ is an optimizer of (8.1) if and only if there exists $\bar{\lambda} \in \mathbb{R}^m, \bar{\mu} \in \mathbb{R}^q$ such that the Karush–Kuhn–Tucker (KKT) optimality conditions of (8.1), which are given by

$$\begin{aligned} 0 &= \nabla f(\bar{x}) + A^T\bar{\lambda} + \nabla g(\bar{x})\bar{\mu}, \\ 0 &= A\bar{x} - b, \\ 0 &\geq g(\bar{x}) \perp \bar{\mu} \geq 0, \end{aligned} \tag{8.2}$$

are satisfied. Here we use the convention $\nabla g(.) = \begin{bmatrix}\nabla g_1(.) & \ldots & \nabla g_q(.)\end{bmatrix}$. It will be convenient later to define the set of optimal points by

$$\bar{\mathcal{X}} = \{(\bar{x}, \bar{\lambda}) \mid \exists \bar{\mu} \in \mathbb{R}^q \text{ such that (8.2) holds}\} \subset \mathbb{R}^{n+m}.$$

In the sequel, we assume that there exists at least one primal-dual triple $(\bar{x}, \bar{\lambda}, \bar{\mu})$ satisfying (8.2), i.e., $\bar{\mathcal{X}} \neq \emptyset$. Based on the KKT conditions (8.2), we propose the following projected primal-dual dynamics to deal with the hard constraints (8.1c).

$$\dot{x} \overset{\text{a.e.}}{=} -\nabla f(x) - A^T\lambda - \nabla g(x)\mu - A^T\Xi(Ax - b), \tag{8.3a}$$

$$\dot{\lambda} \overset{\text{a.e.}}{=} Ax - b, \tag{8.3b}$$

$$0 \overset{\text{a.e.}}{\geq} g(x) \perp \mu \overset{\text{a.e.}}{\geq} 0. \tag{8.3c}$$

Here 'a.e.' stands for almost everywhere, and $\Xi \in \mathbb{R}^{m\times m}$ is a positive definite matrix. Note that the last term of (8.3a) does not alter the equilibria of (8.3). Moreover, this *augmented* term improves the convergence rate of the dynamics (see e.g. [96]) and allows for weaker assumptions on the objective function for the convergence as we will show later. The state variables x, λ are denoted compactly as $\mathtt{x} := (x, \lambda) \in \mathbb{R}^{\mathtt{n}}$, with $\mathtt{n} = m + n$. As observed from (8.3), the (x, λ)-dynamics are projected on the closed convex set $K = \{\mathtt{x} \in \mathbb{R}^{\mathtt{n}} \mid g(x) \leq 0\}$. Furthermore note that the set of equilibria of (8.3) is identical to $\bar{\mathcal{X}} \subset K$.

The following result guarantees the existence and uniqueness of a solution $\mathtt{x}(t, t_0, \mathtt{x}_0)$ of (8.3) for $t \geq t_0$ and $\mathtt{x}_0 \in K$. Moreover, the unique solution can be proven to be *slow*, that is, $\dot{\mathtt{x}}(t)$ is of minimal norm in the set it belongs to:[1]

$$\begin{aligned} \dot{x} &= -\nabla f(x) - A^T\lambda - A^T\Xi(Ax - b) - \nabla g(x)\mu, \\ \dot{\lambda} &= Ax - b, \end{aligned} \tag{8.4}$$

$$\mu \in \underset{\substack{\hat{\mu}_i \geq 0, i \in I(x) \\ \hat{\mu}_i = 0, i \notin I(x)}}{\arg\min} \|\nabla f(x) + A^T\lambda + A^T\Xi(Ax - b) + \nabla g(x)\hat{\mu}\| \tag{8.5}$$

with $I(x) := \{i \mid g_i(x) = 0\}$ and $\dot{\mathtt{x}} \equiv \dot{\mathtt{x}}(t; t_0, \mathtt{x}_0), \mu \equiv \mu(t)$.

Proposition 8.2.2 (Existence and uniqueness of solutions)**.**
Let Assumption 8.2.1 hold. Then for each $\mathtt{x}_0 \in K$, there exists a unique solution $\mathtt{x}(t; t_0, \mathtt{x}_0) \in C^0([t_0, \infty); \mathbb{R}^{\mathtt{n}})$ of (8.3), which is slow and right-differentiable on $[t_0, \infty)$.

Proof. Let the function F be defined by

$$F(\mathtt{x}) = F(x, \lambda) = \begin{bmatrix} \nabla f(x) + A^T\lambda + A^T\Xi(Ax - b) \\ -(Ax - b) \end{bmatrix}.$$

We observe that F is *hypomonotone*, see [16, Remark 3]. Then the existence and uniqueness of solutions of the system (8.3) is guaranteed by [15, Theorem 1] as K is closed and convex, F is a hypomonotone operator and the fact that the constraint qualifications are guaranteed by Slater's condition (Assumption 8.2.1). □

[1] Note that by exploiting closedness and convexity of (8.5), at each time t there is a unique $\dot{x}(t)$ (and $\dot{\lambda}(t)$) of minimal norm.

In addition, the solutions of (8.3) are continuous with respect to the initial condition, which is crucial for showing that the *limit set* $\Omega(\mathtt{x}_0)$ defined by (8.6) is invariant

$$\Omega(\mathtt{x}_0) := \{z \mid \exists\{\tau_i\} \subset [t_0, \infty); \tau_i \to \infty, \mathtt{x}(\tau_i; t_0, \mathtt{x}_0) \to z\}. \tag{8.6}$$

Proposition 8.2.3 (Continuity w.r.t. the initial condition)**.**
Consider the system (8.2) *and suppose Assumption 8.2.1 holds. Let $t \geq t_0$ be fixed. Then the function* (8.7) *is continuous.*

$$\mathtt{x}(t; t_0, .) : K \to \mathbb{R}^n, \qquad \mathtt{x}_0 \mapsto \mathtt{x}(t; t_0, \mathtt{x}_0) \tag{8.7}$$

Proof. The claim follows from the fact that F is monotone, the equivalence between complementarity systems and evolutionary variational inequalities, and [16, Theorem 2]. □

Now we come to the main result, which establishes pointwise asymptotic stability of (8.3).

Theorem 8.2.4 (Convergence of primal-dual dynamics (8.3))**.**
Consider system (8.3) *and let Assumption 8.2.1 hold. The set of optimizers $\bar{\mathcal{X}}$ is asymptotically stable. Moreover, the convergence of each trajectory $\mathtt{x}(t, t_0, \mathtt{x}_0)$ of* (8.3) *with $\mathtt{x}_0 \in K$ is to a point in $\bar{\mathcal{X}}$.*

Remark 8.2.5 (Structure of the proof). The proof of Theorem 8.2.4 consists of two parts. Firstly, we invoke the usual arguments of the invariance principle along the lines of [16] to show convergence to the nonempty limit set. Here we exploit the properties of the complementarity system which allows for a more convenient and shorter proof. For completeness, we include the full proof of this result. In the second part of the proof we use ideas from [7] to further characterize the limit set and to show that it is contained in the set of equilibria. We finalize the proof by showing that the convergence is to a point.

Proof. Let $\bar{\mathtt{x}} := (\bar{x}, \bar{\lambda}) \in \bar{\mathcal{X}}$ and let $\mathtt{x}_0 := (x_0, \lambda_0) \in K$ be given. We show first that limit set $\Omega(\mathtt{x}_0)$ is invariant.

Invariance of $\Omega(\mathtt{x}_0)$: Let $z \in \Omega(\mathtt{x}_0)$ be given. Then there exists a time sequence $\tau_i, i = 1, 2, \ldots$ with $\tau_i \to \infty$ as $i \to \infty$ such that $\lim_{i\to\infty} \mathtt{x}(\tau_i; t_0, \mathtt{x}_0) = z$. Let $\tau \geq t_0$ be given. By continuity with respect to the initial conditions (Proposition 8.2.3) we have $\lim_{i\to\infty} \mathtt{x}(t; t_0, z_i) = \mathtt{x}(t; t_0, z)$. Then by the uniqueness of solutions (Proposition 8.2.2) we have $\mathtt{x}(\tau; t_0, \mathtt{x}(\tau_i; t_0, \mathtt{x}_0)) = \mathtt{x}(\tau - t_0 + \tau_i; t_0, \mathtt{x}_0)$ and therefore $\lim_{i\to\infty} \mathtt{x}(\tau - t_0 + \tau_i; t_0, \mathtt{x}_0) = \mathtt{x}(\tau, t_0, z)$. Setting $w_i = \tau - t_0 + \tau_i$ we see that $w_i \geq t_0, w_i \to \infty$ and $\mathtt{x}(w_i; t_0, \mathtt{x}_0) \to \mathtt{x}(\tau; t_0, z)$. Thus $\mathtt{x}(\tau; t_0, z) \in \Omega(\mathtt{x}_0)$.

Limit points correspond to sublevel set of V: Consider the function $V(\mathtt{x}) = V(x, \lambda) = \frac{1}{2}\|x - \bar{x}\|^2 + \frac{1}{2}\|\lambda - \bar{\lambda}\|^2$, then there exists a compact sublevel set Ψ of V such that $\mathtt{x}_0 \in \Psi$ since V is radially unbounded. We claim that

$$V(y) = k, \quad \forall y \in \Omega(\mathtt{x}_0). \tag{8.8}$$

Let $T > 0$ be given. Let us define the mapping $V^* : [t_0, \infty) \to \mathbb{R}$ by $V^*(t) = V(\mathtt{x}(t; t_0, \mathtt{x}_0))$. The function $\mathtt{x}(.) \equiv \mathtt{x}(.; t_0, \mathtt{x}_0)$ is absolutely continuous on $[t_0, t_0 + T]$ and thus V^* is a.e. strongly differentiable on $[t_0, t_0+T]$. Specifically, by writing $x = x(t), \lambda = \lambda(t)$, we have

$$\begin{aligned}
\frac{dV^*}{dt}(t) &= \langle \nabla V(\mathtt{x}(t)), \frac{d\mathtt{x}}{dt}(t) \rangle = -(x - \bar{x})^T (\nabla f(x) + A^T \lambda) \\
&-(x - \bar{x})^T (A^T \Xi (Ax - b) + \nabla g(x)\mu) + (\lambda - \bar{\lambda})^T (Ax - b) \\
&\overset{(8.2)}{=} -(x - \bar{x})^T (\nabla f(x) - \nabla f(\bar{x}) + \nabla g(x)\mu - \nabla g(\bar{x})\bar{\mu}) \\
&- \|Ax - b\|^2_\Xi + (x - \bar{x})^T (A^T(\lambda - \bar{\lambda}) - A^T(\lambda - \bar{\lambda})) \\
&\leq -(x - \bar{x})^T (\nabla f(x) - \nabla f(\bar{x})) + (g(x))^T \bar{\mu} + (g(\bar{x}))^T \mu \\
&- \|Ax - b\|^2_\Xi \leq 0, \qquad \text{a.e. } t \in [t_0, t_0 + T].
\end{aligned} \tag{8.9}$$

We have $\mathtt{x} \in C^0([t_0, t_0 + T]; \mathbb{R}^{\mathtt{n}})$, $\frac{d\mathtt{x}}{dt} \in L^\infty(t_0, t_0 + T; \mathbb{R}^{\mathtt{n}})$ and $V \in C^1(\mathbb{R}^{\mathtt{n}}; \mathbb{R})$. It follows that $V^* \in W^{1,1}(t_0, t_0 + T; \mathbb{R}^{\mathtt{n}})$ and thus V^* is non-increasing on $[t_0, t_0 + T]$. Since T has been chosen arbitrary, V^* is non-increasing on $[t_0, \infty)$. By continuity of $\mathtt{x}(t)$ it then follows that the *orbit* $\gamma(\mathtt{x}_0) := \{\mathtt{x}(\tau; t_0, \mathtt{x}_0); t \geq t_0\}$ satisfies $\gamma(\mathtt{x}_0) \subset \Psi \cap K$ as Ψ is a compact sublevel set of V. It results that

$$\lim_{\tau \to \infty} V(\mathtt{x}(\tau; t_0, \mathtt{x}_0)) = k,$$

for some $k \in \mathbb{R}$. Let $y \in \Omega(\mathtt{x}_0)$. There exists $\{\tau_i\} \subset [t_0, \infty)$ such that $\tau_i \to \infty$ and $\mathtt{x}(\tau_i, t_0, \mathtt{x}_0) \to y$. By continuity,

$$\lim_{i \to \infty} V(\mathtt{x}(\tau_i; t_0, \mathtt{x}_0)) = V(y). \tag{8.10}$$

Therefore, $V(y) = k$. Here, y has been chosen arbitrary in $\Omega(\mathtt{x}_0)$ and thus (8.8) holds. In addition, the set $\gamma(\mathtt{x}_0)$ is bounded and thus $\Omega(\mathtt{x}_0)$ is non-empty and

$$\lim_{\tau \to \infty} d(\mathtt{x}(\tau, t_0, \mathtt{x}_0), \Omega(\mathtt{x}_0)) = 0. \tag{8.11}$$

Dynamics on sublevel sets of V: Let $z \in \Omega(\mathtt{x}_0)$ be given. By the invariance of $\Omega(\mathtt{x}_0)$ we see that $\mathtt{x}(t; t_0, z) \in \Omega(\mathtt{x}_0), \forall t \geq t_0$ and thus $V(\mathtt{x}(t; t_0, z)) = k, \ \forall t \geq t_0$. It results that

$$\frac{d}{dt} V(\mathtt{x}(t; t_0, z)) = 0, \quad \text{a.e. } t \geq t_0. \tag{8.12}$$

Consequently, by (8.9) we have

$$\begin{aligned}
Ax(t) &= b, \qquad & \nabla f(x(t)) &= \nabla f(\bar{x}), \\
(g(x(t)))^T \bar{\mu} &= 0, \qquad & (g(\bar{x}))^T \mu(t) &= 0,
\end{aligned}$$

a.e. $t \geq t_0$ where $\mathtt{x}(t) \equiv \mathtt{x}(t; t_0, z)$. In particular, by (8.3)

$$\begin{aligned} \dot{x}(t) &= c - \nabla g(x(t))\mu(t), \\ \dot{\lambda}(t) &= 0, \\ 0 \geq g(x(t)) &\perp \mu(t) \geq 0, \end{aligned} \tag{8.13}$$

a.e. $t \geq t_0$ where $c = -\nabla f(\bar{x}) - A^T\lambda(t_0)$ is constant. Since the unique solution of (8.13) is slow, at any time $t \geq t_0$, $\mu(t)$ minimizes the norm of $\dot{x}(t)$ (and $\dot{\lambda}(t)$):

$$\mu(t) \in U(x(t)) := \underset{\substack{\hat{\mu}_i \geq 0, i \in I(x(t)) \\ \hat{\mu}_i = 0, i \notin I(x(t))}}{\arg\min} \{\|c - \nabla g(x(t))\hat{\mu}\|\}, \tag{8.14}$$

where $I(x) := \{i \mid g_i(x) = 0\}$, see also [87] and [15]. For notational convenience we do not explicitly write time-dependency of the variables in the following part of the proof. Instead of considering (8.14), at each time $t \geq t_0$ we can set $\mu_i = 0$ for $i \neq I(x)$ and for $i \in I(x)$ solve the the equivalent minimization problem

$$\begin{aligned} &\underset{\mu_{I(x)}}{\text{minimize}} \ \frac{1}{2}\|c - \nabla g_{I(x)}(x)\mu_{I(x)}\|^2 \\ &\text{subject to } \mu_{I(x)} \geq 0, \end{aligned} \tag{8.15}$$

where $g_{I(x)}(.)$ is formed similarly as $g(.)$ but by taking only the g_i's with $i \in I(x)$ and likewise $\mu_{I(x)} = \mathrm{col}_{i \in I(x)}(\mu_i)$ is defined. The Lagrangian of (8.15) takes the form

$$L = \frac{1}{2}\|c - \nabla g_{I(x)}(x)\mu_{I(x)}\|^2 - \nu_{I(x)}^T \mu_{I(x)},$$

which results in the following KKT optimality conditions.

$$\nabla g_{I(x)}(x)^T(c - \nabla g_{I(x)}(x)\mu_{I(x)}) + \nu_{I(x)} = 0, \tag{8.16}$$

$$0 \leq \nu_{I(x)} \perp \mu_{I(x)} \geq 0. \tag{8.17}$$

In particular, by premultiplying (8.16) with $\mu_{I(x)}^T$ we have

$$\|\nabla g_{I(x)}(x)\mu_{I(x)}\|^2 = c^T \nabla g_{I(x)}(x)\mu_{I(x)} \ \text{ a.e. } t \geq t_0. \tag{8.18}$$

Nonincreasing function W: Define the map $W : \mathbb{R}^{\mathtt{n}} \to \mathbb{R}$ as $W(\mathtt{x}) = -c^T x$, then

$$\begin{aligned} &\frac{d}{dt}W(\mathtt{x}(t; t_0, z)) = \langle \nabla W(\mathtt{x}), \dot{\mathtt{x}} \rangle = \langle \tfrac{\partial W}{\partial x}(x, \lambda), c - \nabla g(x)\mu \rangle \\ &= -c^T c + c^T \nabla g(x)\mu = -c^T c + c^T \nabla g_{I(x)}(x)\mu_{I(x)} \\ &\overset{(8.18)}{=} -c^T c + 2c^T \nabla g_{I(x)}(x)\mu_{I(x)} - \|\nabla g_{I(x)}(x)\mu_{I(x)}\|^2 \\ &= -\|c - \nabla g_{I(x)}(x)\mu_{I(x)}\|^2 \leq 0, \quad \text{a.e. } t \geq t_0. \end{aligned} \tag{8.19}$$

By using the same arguments as before, $W^*(t) := W(\mathtt{x}(t;t_0,z))$ is non-increasing on $[t_0,\infty)$. Moreover, we have $\gamma(z) \in K \cap \Psi$ and thus W^* is bounded from below on $[t_0,\infty)$. It results that

$$\lim_{\tau\to\infty} W(\mathtt{x}(\tau;t_0,z)) = \alpha, \tag{8.20}$$

for some $\alpha \in \mathbb{R}$.

Limit points correspond to sublevel sets of W: Since $z \in \Omega(\mathtt{x}_0)$, there exists a sequence $\{\tau_i\} \subset [t_0,\infty)$ such that $\tau_i \to \infty$ and $\lim_{i\to\infty} \mathtt{x}(\tau_i,t_0,\mathtt{x}_0) = z$. By the uniqueness of solutions we have that $\mathtt{x}(\tau;t_0,\mathtt{x}(\tau_i;t_0,\mathtt{x}_0)) = \mathtt{x}(\tau - t_0 + \tau_i;t_0,\mathtt{x}_0)$. By taking the limit $i\to\infty$ and the continuity with respect to the initial condition we therefore have that

$$\lim_{i\to\infty} \mathtt{x}(\tau;t_0,\mathtt{x}(\tau_i;t_0,\mathtt{x}_0)) = \mathtt{x}(\tau,t_0,z) = \lim_{i\to\infty} \mathtt{x}(\tau - t_0 + \tau_i;t_0,\mathtt{x}_0).$$

As a result, by (8.20)

$$\lim_{\tau\to\infty} W(\lim_{i\to\infty} \mathtt{x}(\tau - t_0 + \tau_i;t_0,\mathtt{x}_0)) = \lim_{t\to\infty} W(\mathtt{x}(t;t_0,\mathtt{x}_0)) = \alpha.$$

By repeating the same arguments as for (8.10), we have

$$W(y) = \alpha \qquad \forall y \in \Omega(\mathtt{x}_0).$$

Limit points are equilibria: In particular, $W(z) = \alpha$ and

$$W(\mathtt{x}(t;t_0,z)) = \alpha \qquad \forall t \geq t_0,$$

as $\mathtt{x}(t;t_0,z) \in \Omega(\mathtt{x}_0), \forall t \geq t_0$. It results that

$$\frac{d}{dt} W(\mathtt{x}(t;t_0,z) = 0 \qquad \text{a.e. } t \geq t_0,$$

and thus $c = \nabla g_{I(x)}(x)\mu_{I(x)} = \nabla g(x)\mu$ by (8.19), stating that $\dot{\mathtt{x}}(t;t_0,z) = 0, \forall t \geq t_0$. Hence, $z \in \bar{\mathcal{X}}$. Since z was chosen arbitrary, it follows that $\Omega(\mathtt{x}_0) \subset \bar{\mathcal{X}}$.

Asymptotic stability of $\bar{\mathcal{X}}$: Since $\mathtt{x}_0 \in K, \bar{\mathtt{x}} \in \bar{\mathcal{X}}$ were chosen arbitrary, each point in $\bar{\mathcal{X}}$ is Lyapunov stable. In addition, by (8.11) and $\Omega(\mathtt{x}_0) \subset \bar{\mathcal{X}}$ we obtain for each $\mathtt{x}_0$,

$$\lim_{\tau\to\infty} d(\mathtt{x}(\tau,t_0,\mathtt{x}_0),\bar{\mathcal{X}}) = 0. \tag{8.21}$$

Hence, the set $\bar{\mathcal{X}}$ is asymptotically stable. Finally, we show that the convergence is to a point.

Convergence to a point: Let $\mathtt{x}_0 \in K$ and consider the function $\tilde{V}(\mathtt{x}) = \frac{1}{2}\|\mathtt{x} - z\|^2$ where $z \in \Omega(\mathtt{x}_0) \subset \bar{\mathcal{X}}$. Then there exists a sequence $\{\tau_i\} \subset [t_0,\infty)$ such that $\mathtt{x}(\tau_i;t_0,\mathtt{x}_0) \to z$. Given $\epsilon > 0$, let $k \in \mathbb{Z}$ be such that $\frac{1}{2}\|\mathtt{x}(\tau_k;t_0,\mathtt{x}_0) - z\|^2 \leq \epsilon$. Then we know that $\frac{1}{2}\|\mathtt{x}(t;t_0,\mathtt{x}_0) - z\|^2 \leq \epsilon$ for all $t \geq \tau_k$ as the sublevel set $\{\mathtt{x} \mid \tilde{V}(\mathtt{x}) \leq \epsilon\} = \{\mathtt{x} \mid \frac{1}{2}\|\mathtt{x} - z\|^2 \leq \epsilon\}$ of $\tilde{V}$ is forward invariant by (8.9), taking

$V^*(t) = \tilde{V}(\mathtt{x}(t; t_0, \mathtt{x}_0))$. As $\epsilon > 0$ can be taken arbitrary small, we conclude that the convergence is to a point. □

Remark 8.2.6 (Comparison with [40]). The dynamics (8.3) can be interpreted as special case of the projected saddle point dynamics of [40]. To see this, define

$$H(x,\lambda) = \begin{cases} h(x,\lambda) & \text{if } g(x) \leq 0 \\ \infty & \text{if } g(x) \not\leq 0 \end{cases},$$
$$h(x,\lambda) = f(x) + \lambda^T(Ax-b) + \|Ax-b\|_\Xi^2,$$

and note that $\dot{x} = P_{T_{K_x}(x)}(-\nabla_x h(x,\lambda)), \dot{\lambda} = \nabla_\lambda h(x,\lambda)$ with $K_x = \{x \in \mathbb{R}^n \mid g(x) \leq 0\}$ and $T_{K_x}(x)$ denoting the tangent cone at x with respect to K_x. However, it remains an open question whether [40, Assumption 3.2] holds for this case, which in that work is required for establishing pointwise asymptotic stability.

8.2.1 Primal-dual dynamics with gains

Now we discuss briefly how we can extend the previous results to the modified projected primal-dual dynamics

$$\begin{aligned} L_x L_x^T \dot{x} &\overset{\text{a.e.}}{=} -\nabla f(x) - A^T\lambda - A^T\Xi(Ax-b) - \nabla g(x)\mu, \\ L_\lambda L_\lambda^T \dot{\lambda} &\overset{\text{a.e.}}{=} Ax - b, \\ 0 &\overset{\text{a.e.}}{\geq} g(x) \perp \mu \overset{\text{a.e.}}{\geq} 0. \end{aligned} \tag{8.22}$$

with symmetric gain matrices of the form $L_x L_x^T > 0, L_\lambda L_\lambda^T > 0, L_x \in \mathbb{R}^{n\times n}, L_\lambda \in \mathbb{R}^{m\times m}$. Define $\tilde{x} = L_x^T x, \tilde{\lambda} = L_\lambda^T \lambda$ and define $\tilde{f} : \mathbb{R}^n \to \mathbb{R}$ as $\tilde{x} \mapsto f(L_x^{-T}\tilde{x})$, and $\tilde{g} : \mathbb{R}^n \to \mathbb{R}^{1\times q}$ as $\tilde{x} \mapsto g(L_x^{-T}\tilde{x})$. In addition, let $\tilde{A} = L_\lambda^{-1} A L_x^{-T}, \tilde{b} = L_\lambda^{-1} b, \tilde{\Xi} = L_\lambda \Xi L_\lambda^T, \tilde{\mu} = \mu$. We observe that the system (8.22) can then be rewritten as

$$\begin{aligned} \dot{\tilde{x}} &\overset{\text{a.e.}}{=} -\nabla \tilde{f}(\tilde{x}) - \tilde{A}^T\tilde{\lambda} - \tilde{A}^T\tilde{\Xi}(\tilde{A}\tilde{x} - \tilde{b}) - \nabla\tilde{g}(\tilde{x})\tilde{\mu}, \\ \dot{\tilde{\lambda}} &\overset{\text{a.e.}}{=} \tilde{A}\tilde{x} - \tilde{b}, \\ 0 &\overset{\text{a.e.}}{\geq} \tilde{g}(\tilde{x}) \perp \tilde{\mu} \overset{\text{a.e.}}{\geq} 0. \end{aligned} \tag{8.23}$$

It is easily seen that $\tilde{f}, \tilde{g}_i, i = 1, \ldots, q$ are convex functions. Hence, by applying Theorem 8.2.4 to (8.23), we establish convergence to an (optimal) equilibrium for both the transformed system (8.23) as well as the original system (8.22) with positive definite gain matrices.

8.2.2 Strict convexity case

The convergence result of Theorem 8.2.4 relies on the fact that Ξ which appears in (8.3) is a positive definite matrix. Indeed, if this assumption is not satisfied, then oscillations may occur or the trajectories are divergent.

Example 8.2.7 (No convergence if $\Xi \not\succ 0$)**.** Consider the simple optimization problem

$$\begin{aligned} \underset{x\in\mathbb{R}}{\text{minimize}} \quad & x \\ \text{subject to} \quad & x = 1 \end{aligned}$$

which by (8.3) results in the following primal-dual dynamics

$$\begin{aligned} \dot{x} &= -1 - \lambda - \Xi(x-1) \\ \dot{\lambda} &= x - 1 \end{aligned} \tag{8.24}$$

with $\Xi \in \mathbb{R}$. The convergence of (8.24) is guaranteed for $\Xi > 0$ by Theorem 8.2.4. However, the trajectories are oscillatory for $\Xi = 0$ and divergent for $\Xi < 0$.

On the other hand, under the assumption that the objective function f is strictly convex, the convergence result is unaffected for any positive semi-definite Ξ.

Proposition 8.2.8 (Asymptotic stability of (8.3) for $\Xi \geq 0$)**.** *Consider system* (8.3) *and let Assumption 8.2.1 hold. Assume furthermore that f is strictly convex and Ξ is a positive semi-definite matrix. The set of optimizers $\bar{\mathcal{X}}$ is asymptotically stable. Moreover, the convergence of each trajectory $\mathtt{x}(t, t_0, \mathtt{x}_0)$ of* (8.3) *with $\mathtt{x}_0 \in K$ is to a point in $\bar{\mathcal{X}}$.*

Proof. The proof of Proposition 8.2.8 is analogous to the proof of Theorem 8.2.4 with the following changes. Let $(z_x, z_\lambda) \in \Omega(\mathtt{x}_0)$. Since f is strictly convex it follows by (8.9) and (8.12) that $x(t; t_0, z_x) = \bar{x}$ and $\lambda(t; t_0, z_\lambda) = z_\lambda$ for all $t \geq t_0$. As a result, $\Omega(\mathtt{x}_0) \subset \bar{\mathcal{X}}$. □

8.3 Application in data centers

A practical application of above theory can be found when considering energy savings in data centers, see [116]. Data centers are large consumers of electricity which comes with proportionally high operating costs. In order to drive down these costs, researchers and data center operators have looked into ways of reducing these energy costs. One way to reduce energy consumption is by increasing the efficiency of the cooling process in the data center.

A data center consists of a multitude of computing racks, each generating heat proportional to the workload assigned to that computing rack. The generated heat is cooled via cold air which is sucked through the racks. A Computer Room Air Conditioner (CRAC) unit blows the cold air into the data center, extracts the hot air which exits the racks, and cools the air again to a target setpoint temperature. Modeling the thermodynamics of the system, the change of the rack temperature is given by

$$\frac{d}{dt}T_{\text{out}}(t) = G(T_{\text{out}}(t) - \mathbb{1}T_{\text{sup}}(t)) + M^{-1}P(t). \tag{8.25}$$

Here

$$T_{\text{out}}(t) := \begin{bmatrix} T_{\text{out}}^1(t) & T_{\text{out}}^2(t) & \cdots & T_{\text{out}}^n(t) \end{bmatrix}^T$$

is the vector collecting the temperature [°C] of the exhaust air at the racks, and

$$\begin{aligned} G &:= \rho c_p M^{-1}(\Gamma^T - I_n)F, \\ F &:= \operatorname{diag}(f_1, \quad f_2, \quad \cdots, \quad f_n), \\ M &:= \operatorname{diag}(c_p m_1, \quad c_p m_2, \quad \cdots, \quad c_p m_n), \\ \Gamma &:= [\gamma_{ij}]_{n\times n}, \end{aligned}$$

where ρ [kg m^{-3}] is the density of the air in the racks, c_p [J °C^{-1} kg^{-1}] is the specific heat capacity of air, f_i [m^3 s^{-1}] is the air flow rate through rack i, m_i [kg] is the mass of the air inside rack i, and γ_{ij} is the percentage of the air flow which recirculates from rack i to rack j. Furthermore T_{sup} [°C] is the temperature setpoint of the cold air exiting the CRAC unit, and P is the vector collection the power consumption of each rack. The power consumption P is modeled as the linear function

$$P(t) = V + WD(t), \tag{8.26}$$

where

$$\begin{aligned} P(t) &:= \begin{bmatrix} P_1(t) & P_2(t) & \cdots & P_n(t) \end{bmatrix}^T, \\ V &:= \begin{bmatrix} v_1 & v_2 & \cdots & v_n \end{bmatrix}^T, \\ W &:= \operatorname{diag}(w_1, \quad w_2, \quad \cdots, \quad w_n), \\ D(t) &:= \begin{bmatrix} D_1(t) & D_2(t) & \cdots & D_n(t) \end{bmatrix}^T. \end{aligned}$$

Here v_i [Watts] is the power consumption for the racks being powered on, w_i [Watts CPU^{-1}] is the power consumption per CPU in use, and $D_i(t)$ the number of CPU's the scheduler assigns to rack i at time t.

The key part here is that it is impossible to completely extract the hot air from the data center. Some leakages occur and these cause inefficiencies in the cooling system of the data center. These leakages are captured in the recirculation parameters, γ_{ij}, and cause an uneven temperature profile among the racks. Since the CRAC unit cannot cool a single rack and any change to the temperature setpoint T_{sup} affects all the racks, an uneven temperature profile results in much wasted cooling efforts.

To find the optimal temperature profile at a given workload level, which results in the lowest possible energy consumption of the cooling equipment, we set up an optimization problem. From [116, Theorem 1] we obtain the optimization problem

$$\begin{aligned} \underset{T_{\text{out}}}{\text{minimize}} \quad & c^T T_{\text{out}} && \text{(8.27a)} \\ \text{subject to} \quad & 0 \le AT_{\text{out}} + b(D^*) \le D_{\max} && \text{(8.27b)} \\ & T_{\text{out}} \le T_{\text{safe}}, && \text{(8.27c)} \end{aligned}$$

where D^* is the total workload which has to processed by the data center at a given time, T_{safe} is the maximally allowed temperature of the racks, $D_{\max}$ is the computational capacity of the racks, and $AT_{\text{out}} + b(D^*) = D$ is the relation between the chosen temperature profile and the necessary workload allocation to achieve that temperature profile. The solution to (8.27), $\bar{T}_{\text{out}}$, is the desired temperature distribution which guarantees the minimal energy consumption of the cooling equipment in the data center. With this solution, and (8.27b) and a similar relation for T_{sup}, it is then possible to calculate the optimal inputs for the cooling equipment and the workload distribution, D.

In [116] controllers were designed to dynamically adjust T_{sup} and D in response to changing workload levels, D^*, based on temperature measurements at the racks,

$$\begin{aligned} \dot{T}_{\text{sup}} &= K_1(T_{\text{out}} - \bar{T}_{\text{out}}), \\ \dot{D} &= K_2(T_{\text{out}} - \bar{T}_{\text{out}}), \end{aligned}$$

where K_1 and K_2 are gains depending on the data center parameters.

Ideally $\bar{T}_{\text{out}}$ is equal to T_{safe}, however at very high or very low workload levels the computational bounds will cause the optimal solution to deviate from T_{safe}. To allow for these edge cases we apply the proposed primal-dual algorithm from this chapter to find the optimal temperature profile. Adapted to the example of data centers, and augmented with an arbitrary gain $L_{\bar{T}_{\text{out}}} \in \mathbb{R}^{n \times n}$, this algorithm is given by

$$\begin{aligned} L_{\bar{T}_{\text{out}}} \dot{\bar{T}}_{\text{out}} &= -c - \begin{bmatrix} -A & A & I \end{bmatrix} \mu \\ 0 &\geq \begin{bmatrix} -A \\ A \\ I \end{bmatrix} \bar{T}_{\text{out}} + \begin{bmatrix} -b \\ b - D_{\max} \\ -T_{\text{safe}} \end{bmatrix} \perp \mu \geq 0. \end{aligned} \tag{8.28}$$

8.3.1 Simulation results

To test the performance of the algorithm we simulate a realistic data center setting where a high level of workload is applied to the data center, i.e. 91.7% of the total computing capacity of the data center. The simulations results are given in Figure 8.1 to 8.3. The same simulation setup is used as in [116], where the data center consists of 30 racks, each with a maximum allowed temperature of $T_{\text{safe}} = 30$ °C, and a computational capacity of $D_{\max} = 20$ tasks. To have the convergence time within acceptable limits we set the gain $L_{\bar{T}_{\text{out}}} = \frac{1}{20} I_n$. The simulation is initialized relatively far away from the optimal solution and we see in Figure 8.1 that using our primal-dual algorithm, the estimated optimal solution $\bar{T}_{\text{out}}^{est}$ converges to the real optimal solution of (8.27), $\bar{T}_{\text{out}}^{sol}$, in 4 seconds. To check that the constraints are indeed not violated during the transient, the temperature evolution is plotted in Figure 8.2, and the workload assignment is plotted in 8.3. Here we see that the temperature never exceeds the safe threshold of $30°C$ and that the assigned workload never exceeds the computational bound of 20 tasks.

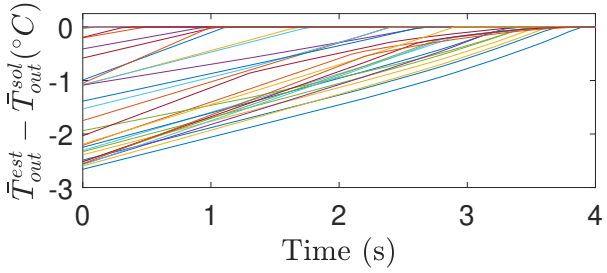

Figure 8.1: Convergence of $\bar{T}_{\text{out}}^{est}$ to the solution of optimization problem (8.27), $\bar{T}_{\text{out}}^{sol}$. Within 4 seconds our primal-dual algorithm converges to the real optimal solution.

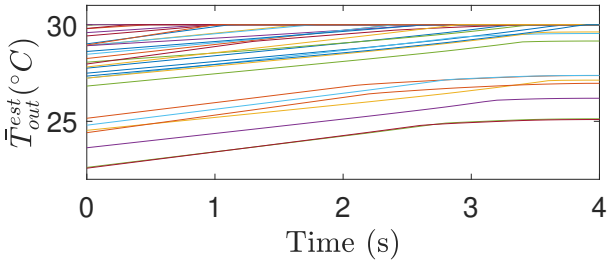

Figure 8.2: Evolution of the estimated optimal temperature of each rack. The safe temperature threshold of 30 °C is not violated during the transient.

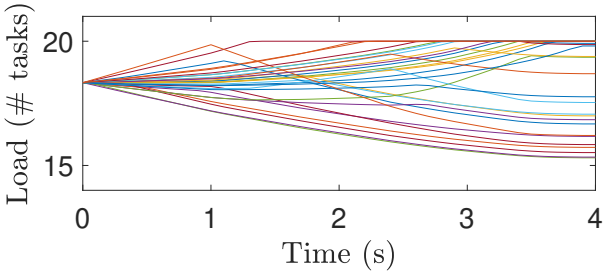

Figure 8.3: Evolution of the estimated optimal workload assignment to each rack. The computational capacity of each rack, between 0 and 20 tasks is never violated during transient.

8.4 Conclusions

We considered the stability of constrained primal-dual dynamics represented by a complementarity system. For each unique (slow) solution initialized in the feasible set, we established the convergence to a primal-dual optimizer of the underlying constrained optimization problem. The stability proof involves the use of a generalized invariance principle using two different storage functions and the result relies only on mild assumptions including the convexity of the objective function and the existence of at least one primal-dual optimizer. Simulations on online optimization in data centers illustrated the applicability of our results.

Future research includes studying the robustness of the proposed dynamics, possibly in the lines of [27] and [81]. Another research direction is to study initialization-free algorithms as for example in [128] which allows for a plug-and-play implementation of the constrained primal-dual dynamics. Lastly, a future research direction is to study the interconnection of the proposed dynamics with other physical systems (including power networks) to analyze real-time applications of the algorithm in dynamic environments.

Part III

Competitive real-time electricity markets

Introduction

In the last decades, there has been a massive expansion of renewable energy resources (RES) in many countries of the world. More and more small distributed generation units such as small hydro, biomass, biogas, solar and wind power plants are connected to the grid, typically at the lower voltage levels. As a result, the structure of the energy system in terms of energy production is changing to decentralized generation units located in distribution grids. This has resulted in several trends including (i) the non-continuous power generation of RES requires balancing their production to follow the load (ii) distributed energy resources (DERs) must provide system services such as frequency regulation (iii) it is becoming more challenging to economically dispatch generation from centralized locations [124].

In the current operation, ancillary services like frequency regulation are typically provided by conventional big generation units. They are activated either automatically or upon request of the transmission system operators[2] (TSO's). Once renewable energy resources in distribution grids displace such units either completely or temporarily, the ancillary services must be provided by DERs via the distribution system operators (DSO). The observability and controllability of the distributed energy resources units connected to the distribution grids are inevitable requirements to provide such services. Consequently, the management of DERs becomes more and more important and there is a growing need to coordinate also with control centers at the distribution level. Among these things, they coordinate power dispatch and ensure continuous operation to avoid grid instability. In support of these activities, control centers at the transmission level include a range of monitoring functions such as continuous observation of frequency deviation, real and reactive tie-line flows, and generation output with the aim to act against active power imbalances. In addition, by merging the dispatch potential of several (DER) units to a single potential, the TSO can make use of such aggregated dispatch potentials to achieve economic dispatch at the transmission level.

Market design

As mentioned above, DERs can potentially provide services in a cost-effective manner, including frequency control for the TSO. To tap the potential of DERs and ensure cost-effective solutions, regulators must create and define new market mechanisms to enable those services. Such local market mechanisms will have to be integrated into the (frequency) regulation framework to allow to take advantage

[2]The United States has a similar organizational entity called the independent system operator (ISO).

of flexibility services from DERs [41]. This calls for a new comprehensive system of prices, which would serve to coordinate resources installed and operated at separate locations, and in this way, unlock the provision of flexibility and value the different services provided. A few of the characteristics of such a price system are described below, see also [124] and references therein.

Firstly, an increase time-differentiation in prices in envisioned as the marginal system costs may vary significantly at various times, reflecting the marginal costs of different technologies. This would improve not only the efficient system operation but potentially, in the long run, also the DER investment made by network users. In addition, increasing locational price differentiation for energy will deliver efficiency gains and provide economic incentives for optimal location and dispatch of DERs. Also the power system characteristics and the regulatory context need to be considered. Since the electricity services value varies in time and location, the prices should therefore reflect those variations. Furthermore, the improvements in the design of the system of prices could significantly change the profits and potentially increase the volatility of prices [85]. Therefore, also price stability and the competitive aspect of the market has to be taken into account.

Contributions

In part III of this thesis, we deal with several aspects of these challenges outlined above. The background of this part of the research is that we consider an (US) electricity market consisting of an independent system operator (ISO) and a group of (virtual) large scale generators. The goal of the ISO is solve the economic dispatch problem while regulating the grid frequency to its nominal value while. Each strategic generator seeks to maximize its individual profit and is not willing to share its cost function with anyone. The ISO operates the market, where generators bid prices at which there are willing to provide power, and makes power generation assignments based on them. Our first contribution is that we analyze the underlying price-competition game among the generators, where the generators act as price-setters instead of price-takers as what is typically assumed in the literature. In particular, we characterize the Nash equilibria that correspond to optimal power dispatch which we call *efficient Nash equilibria* and we establish the existence of such an equilibrium and provide a sufficient condition for its uniqueness. We also propose continuous-time and discrete-time Nash equilibrium seeking schemes that capture the negotiation process between the generators and the ISO. In these schemes, each generator adjust its bid in a myopically selfish fashion based on its current bid and the production level that the ISO requests from them. At the same time, the ISO adjusts the generation setpoints to minimize the total payment to the generators according to both the generator bids and the local frequency deviation. The use of the local frequency error as a feedback signal in the bidding process couples the ISO-generator coordination scheme with the continuous-time swing dynamics of the power network. We show that each equilibrium of the interconnected system corresponds to an efficient Nash equilibrium, optimal generation levels and zero frequency regulation. By a rigorous

stability analysis, we furthermore establish local (exponential) convergence to such an equilibrium by utilizing suitable Lyapunov functions for the closed-loop system. In particular, we show that the coupled dynamics is robust against additive disturbances by establishing its local input-to-state stability (LISS) property using a suitable LISS Lyapunov function.

Outline

Chapter 9: In this chapter, we study a frequency-aware continuous-time bidding mechanism for real-time electricity markets. We start with the description of the physical power network defined by the swing equations and then state the economic dispatch problem with nonnegativity constraints. Here we also define the inelastic market game of the generators and give the definition of an efficient Nash equilibrium. For such an equilibrium, we establish its existence and give a sufficient condition for its uniqueness. Then we introduce a dynamic bidding scheme between the ISO and the generators which also takes into account the physical frequency deviation of the network. We analyze its interconnection with the swing dynamics and show that its dynamics can be described by a complementarity system. For the closed-loop system we establish convergence to an efficient Nash equilibrium, economic dispatch and zero frequency deviation by providing a suitable Lyapunov function and by invoking a suitable invariance principle.

Chapter 10: Compared to Chapter 9, here we consider an iterative bidding mechanism coupled with the continuous-time frequency swing dynamics, resulting in an hybrid system considering both discrete and continuous updates. After stating the existence and uniqueness of an efficient Nash equilibrium, we establish local input-to-state stability (LISS) of the continuous-time variant of the interconnected system by constructing a LISS Lyapunov function. In particular, this guarantees local exponential convergence to an equilibrium corresponding to an efficient Nash equilibrium, cost efficiency and frequency regulation. The LISS property is then used to show that its hybrid implementation, composed of the discrete bidding scheme and the continuous evolution of the frequency dynamics, is asymptotically stable. Specifically, based on the mismatch between the continuous-time and hybrid implementations, we establish bounds on the discrete step sizes for the bidding iterates and market clearing instances that guarantee the convergence of the coupled system.

Chapter 9

Frequency-aware Bertrand market mechanism

Abstract: *This chapter studies real-time bidding mechanisms for economic dispatch and frequency regulation in electrical power networks. We consider a market administered by an independent system operator (ISO) where a group of strategic generators participate in a Bertrand game of competition. Generators bid prices at which they are willing to produce electricity. Each generator aims to maximize their profit, while the ISO seeks to minimize the total generation cost and to regulate the frequency of the system. We consider a continuous-time bidding process coupled with the swing dynamics of the network through the use of frequency as a feedback signal for the negotiation process. We analyze the stability of the resulting interconnected system, establishing frequency regulation and the convergence to a Nash equilibrium and optimal generation levels. The results are verified in the IEEE 14-bus benchmark case.*

Published as:

T.W. Stegink, A. Cherukuri, C. De Persis, A.J. van der Schaft, J. Cortés. "Stable interconnection of continuous-time price-bidding mechanisms with power network dynamics." Proceedings of the 20th Power Systems Computation Conference (PSCC), 2018.

9.1 Introduction

Power generation dispatch is typically done in a hierarchical fashion, where the different layers are separated according to their time scales. Broadly, at the top layer economic efficiency is ensured via market clearing and at the bottom layer frequency control and regulation is achieved via primary and secondary controllers. However, the intermittent and uncertain nature of distributed energy resources (DERs) and their integration into the power grid represents a major challenge to the current design. Of particular concern is the need to maintain both frequency regulation and cost efficiency of regulation reserves in the face of increasing fluctuations in renewables. To this end, we propose an integrated dynamic market mechanism which combines the real-time market and frequency regulation, allowing competitive market players, including renewable generation, to negotiate electricity prices while using the most recent information on the grid frequency.

Literature review

The combination of economic dispatch and frequency regulation has received increasing attention in recent years. Various works have sought to move beyond the traditional and compartmentalized hierarchical control layers to instead simultaneously achieve frequency stabilization and economic dispatch in power networks [65, 113, 131] and microgrids [20, 35]. Along this line of research, the various agents involved work cooperatively towards the satisfaction of a common goal. An alternative body of research has investigated the use of price-based incentives for economic generation- and demand-side management and frequency regulation [3, 93, 107]. To achieve these goals, these works consider dynamic pricing mechanisms in conjunction with system dynamics of the power network. We also adopt this approach, with the important distinction that here we allow generators to bid in the market (hence, they are price-setters rather than price-takers). This viewpoint results in a Bertrand game of competition among the generators. Our previous work [23, 24] studied this type of games established that iterative bidding can achieve convergence to an optimal allocation of power generation, without considering the effects on the dynamics of the power network. The underlying assumption was that generation setpoints could be commanded after convergence, which in practice poses a limitation, considering the fast time-scales at which DERs operate. Instead, this chapter proposes an online bidding scheme where the setpoints are updated continuously throughout time to better cope with fast changes in the network. In this way, we tackle simultaneously both frequency regulation, optimal power dispatch and the competitive aspect among the generators.

Statement of contributions

We consider an electrical power network consisting of an independent system operator (ISO) and a group of competitive generators. Each generator seeks to maximize its individual profit, while the ISO aims to solve the economic

dispatch problem and regulate the frequency. Since the generators are not willing to share their cost functions, the ISO is unable to solve the economic dispatch problem. Instead, it has the generators compete in a bidding market where they submit bids to the ISO in the form of a price at which they are willing to produce electricity. In return, the ISO determines the power generations levels the generators have to meet. We analyze the underlying Bertrand game among the generators and characterize the Nash equilibria that correspond to optimal power dispatch termed *efficient Nash equilibria*. In particular, we establish the existence of such efficient Nash equilibria and provide a sufficient condition for its uniqueness. We also propose a Nash equilibrium seeking scheme in the form of a continuous-time bidding process that captures the interaction between the generators and the ISO. In this scheme, the generators adjust their bid based on their current bid and the production level that the ISO requests from them with the aim to maximize their profit. At the same time, the ISO adjusts the generation setpoints to minimize the total payment to the generators while taking the power balance and frequency deviation into account. Moreover, along the execution of the algorithm the nonnegativity constraints on the bids and power generation quantities are satisfied. The use of the local frequency error as a feedback signal in the negotiation process couples the ISO-generator coordination scheme with the swing dynamics of the power network. We show that each equilibrium of the interconnected system corresponds to an efficient Nash equilibrium, optimal generation levels and zero frequency regulation. We furthermore establish local convergence to such an equilibrium by invoking a suitable invariance principle for the closed-loop projected dynamical system. Finally, the numerical results on the IEEE 14-bus benchmark show fast convergence of the closed-loop system to an optimal equilibrium, even under sudden changes of the load and the cost functions.

Notation

Let $\mathbb{R}, \mathbb{R}_{\geq 0}, \mathbb{R}_{>0}$ be the set of real, nonnegative real, and positive real numbers, respectively. We write the set $\{1, \dots, n\}$ compactly as $\mathcal{I}_n$. We denote by $\mathbb{1} \in \mathbb{R}^n$ the vector whose elements are equal to 1. Given a twice differentiable function $f : \mathbb{R}^n \to \mathbb{R}$, its gradient and its Hessian evaluated at x is written as $\nabla f(x)$ and $\nabla^2 f(x)$, respectively. A twice continuously differentiable function $f : \mathbb{R}^n \to \mathbb{R}$ is *strongly convex* on $S \subset \mathbb{R}^n$ if it is convex and, for some $\mu > 0$, its Hessian satisfies $\nabla^2 f(x) > \mu I$ for all $x \in S$. For scalars $a, b \in \mathbb{R}$ we denote by $[a]_b^+$ the operator

$$[a]_b^+ = \begin{cases} a & \text{if } b > 0 \\ \max(a, 0) & \text{if } b = 0. \end{cases} \tag{9.1}$$

For vectors $a, b \in \mathbb{R}^n$, $[a]_b^+$ denotes the vector whose i-th element is given by $[a_i]_{b_i}^+$ for $i \in \mathcal{I}_n$. For $A \in \mathbb{R}^{m \times n}$, the induced 2-norm is denoted by $\|A\|$. Given $v \in \mathbb{R}^n, K \in \mathbb{R}^{n \times n}$, we write $\|v\|_K := \sqrt{v^T K v}$. Given a set of numbers $v_1, v_2, \dots, v_n \in \mathbb{R}$, $\mathrm{col}(v_1, \dots, v_n)$ denotes the column vector $\big[v_1, \dots, v_n\big]^T$ and likewise $\mathrm{diag}(v_1, \dots, v_n)$ denotes the $n \times n$ diagonal matrix with entries $v_1, \dots, v_n$ on the diagonal. For $u, v \in \mathbb{R}^n$ we write $u \perp v$ if $u^T v = 0$. We use the

compact notational form $0 \leq u \perp v \geq 0$ to denote the complementarity conditions $u \geq 0, v \geq 0, u \perp v$. The notations $\mathbf{sin}(.)$ and $\mathbf{cos}(.)$ are used to represent the element-wise sine and cosine functions respectively.

9.2 Power network model and dynamics

We consider an electrical power network consisting of n buses and m transmission lines. The network is represented by a connected and undirected graph $\mathcal{G} = (\mathcal{V}, \mathcal{E})$, where nodes $\mathcal{V} = \mathcal{I}_n$ represent buses and edges $\mathcal{E} \subset \mathcal{V} \times \mathcal{V}$ are the transmission lines connecting the buses. The edges are arbitrarily labeled with a unique identifier in $\mathcal{I}_m$ and the ends of each edge are arbitrary labeled with '+' and '-'. The incidence matrix $D \in \mathbb{R}^{n \times m}$ of the resulting directed graph is

$$D_{ik} = \begin{cases} +1 & \text{if } i \text{ is the positive end of edge } k, \\ -1 & \text{if } i \text{ is the negative end of edge } k, \\ 0 & \text{otherwise.} \end{cases}$$

Each bus i represents a control area and is assumed to have one generator and a load P_{di}. The dynamics at the buses is assumed to be governed by the *swing equations* [67], given by

$$\begin{aligned} \dot{\delta} &= \omega \\ M\dot{\omega} &= -D\Gamma\, \mathbf{sin}(D^T\delta) - A\omega + P_g - P_d \end{aligned} \tag{9.2}$$

with $P_d = \mathrm{col}(P_{d1}, \ldots, P_{dn})$. Here $\Gamma = \mathrm{diag}(\gamma_1, \ldots, \gamma_m)$, where $\gamma_k = B_{ij}V_iV_j = B_{ji}V_iV_j$ and $k \in \mathcal{I}_m$ corresponds to the edge between nodes i and j. Table 9.1 presents a list of symbols employed in the model (9.2).

$\delta \in \mathbb{R}^n$	voltage phase angle
$\omega \in \mathbb{R}^n$	frequency deviation w.r.t. the nominal frequency
$P_g \in \mathbb{R}^n_{\geq 0}$	power generation
$P_d \in \mathbb{R}^n_{\geq 0}$	power load
$M \in \mathbb{R}^{n \times n}_{\geq 0}$	diagonal matrix of moments of inertia
$A \in \mathbb{R}^{n \times n}_{\geq 0}$	diagonal matrix of asynchronous damping constants
$V_i \in \mathbb{R}_{>0}$	voltage magnitude at bus i
$B_{ij} \in \mathbb{R}_{>0}$	negative of the susceptance of transmission line (i, j)

Table 9.1: State variables and parameters of swing equations (9.2).

For the stability analysis carried out later, it is convenient to work with the voltage phase angle differences $\varphi = D_t^T\delta \in \mathbb{R}^{n-1}$. Here $D_t \in \mathbb{R}^{n \times (n-1)}$ is the incidence matrix of an arbitrary tree graph on the set of buses $\mathcal{I}_n$ (e.g., a spanning

tree of the physical network). Furthermore, let $U(\varphi) = -\mathbb{1}^T \Gamma \cos(D^T D_t^{\dagger T} \varphi)$, where $D_t^\dagger = (D_t^T D_t)^{-1} D_t^T$ denotes the Moore-Penrose pseudo-inverse of D_t. Then the physical system (9.2) in the (φ, ω)-coordinates takes the form

$$\begin{aligned} \dot{\varphi} &= D_t^T \omega \\ M\dot{\omega} &= -D_t \nabla U(\varphi) - A\omega + P_g - P_d, \end{aligned} \tag{9.3}$$

where we observe that $D_t D_t^\dagger D = (I - \frac{1}{n}\mathbb{1}\mathbb{1}^T)D = D$.

9.3 Problem description

In this section we formulate the problem statement, introduce the necessary game-theoretic tools and discuss the goals of the chapter.

9.3.1 ISO-generator coordination

Taking as starting point the electrical power network model described in Section 9.2, here we outline the elements of the ISO-generator coordination problem following the exposition of [23, 24]. Let $C_i : \mathbb{R}_{\geq 0} \to \mathbb{R}_{\geq 0}$ be the cost incurred by generator $i \in \mathcal{I}_n$ in producing P_{gi} units of power. We assume C_i is strongly convex on the domain $\mathbb{R}_{\geq 0}$ and satisfies $\nabla C_i(0) \geq 0$. Given the total network cost

$$C(P_g) := \sum_{i \in \mathcal{I}_n} C_i(P_{gi}) \tag{9.4}$$

and a power load P_d, the ISO seeks to solve the *economic dispatch (ED)* problem

$$\begin{aligned} \underset{P_g}{\text{minimize}} \quad & C(P_g), && \text{(9.5a)} \\ \text{subject to} \quad & \mathbb{1}^T P_g = \mathbb{1}^T P_d, && \text{(9.5b)} \\ & P_g \geq 0, && \text{(9.5c)} \end{aligned}$$

and, at the same time, to regulate the frequency of the physical power network. We assume the total load to be positive, i.e., $\mathbb{1}^T P_d > 0$ such that (9.5) is feasible. Since the constraints (9.5b) (9.5c) are affine, Slater's condition holds implying that (9.5) has zero duality gap. We can also show that its primal-dual optimizer $(P_g^*, \lambda^*, \mu^*)$ (where λ^* corresponds to (9.5b) and μ^* corresponds to (9.5c)) is unique by exploiting strong convexity of C. We assume that for the power injection $P_g = P_g^*$, there exists an equilibrium $(\bar{\varphi}, \bar{\omega})$ of (9.3) that satisfies $D^T D_t^{\dagger T} \bar{\varphi} \in (-\pi/2, \pi/2)^m$. The latter assumption is standard and is referred to as the *security constraint* in the power systems literature [67].

We note that the ISO cannot determine the optimizer of the ED problem (9.5) because generators are strategic and they do not reveal their cost functions to anyone. Instead, the ISO operates a market where each generator $i \in \mathcal{I}_n$ submit a bid $b_i \in \mathbb{R}_{\geq 0}$ in the form of a price at which it is willing to provide power. Based on these bids, the ISO aims to find the power allocation that meets the

load and minimizes the total payment to the generators. Thus instead of solving the ED problem (9.5) directly, the ISO considers, given a bid $b \in \mathbb{R}^n_{\geq 0}$, the convex optimization problem

$$\begin{aligned} \underset{P_g}{\text{minimize}} \quad & b^T P_g, && \text{(9.6a)} \\ \text{subject to} \quad & \mathbb{1}^T P_g = \mathbb{1}^T P_d, && \text{(9.6b)} \\ & P_g \geq 0. && \text{(9.6c)} \end{aligned}$$

A fundamental difference between (9.5) and (9.6) is that the latter optimization is linear and may in general have multiple solutions. Let $P_g^{\text{opt}}(b)$ be the optimizer of (9.6) the ISO selects given bids b and note that this might not be unique. Knowing the ISO's strategy, each generator i bids a quantity $b_i \geq 0$ to maximize its payoff

$$\Pi_i(b_i, P_{gi}^{\text{opt}}(b)) := P_{gi}^{\text{opt}}(b) b_i - C_i(P_{gi}^{\text{opt}}(b)), \tag{9.7}$$

where $P_{gi}^{\text{opt}}(b)$ is the i-th component of the optimizer $P_g^{\text{opt}}(b)$. Note that this function is not continuous in the bid b. Since each generator is strategic, we analyze the market clearing, and hence the dispatch process explained above using tools from game theory [8, 39].

9.3.2 Inelastic electricity market game

We define the *inelastic electricity market game* as

- Players: the set of generators $\mathcal{I}_n$.
- Action: for each player i, the bid $b_i \in \mathbb{R}_{\geq 0}$.
- Payoff: for each player i, the payoff Π_i defined in (9.7).

In the sequel we interchangeably use the notation $b \in \mathbb{R}^n_{\geq 0}$ and $(b_i, b_{-i}) \in \mathbb{R}^n_{\geq 0}$ for the bid vector, where $b_{-i} \in \mathbb{R}^{n-1}_{\geq 0}$ represents the bids of all players except i. We note that the payoff of generator i not only depends on the bids of the other players but also on the optimizer $P_g^{\text{opt}}(b)$ the ISO selects. Therefore, the concept of a Nash equilibrium is defined slightly differently compared to the usual one.

Definition 9.3.1 (Nash equilibrium [23])**.** A bid profile $b^* \in \mathbb{R}^n_{\geq 0}$ is a *Nash equilibrium* of the inelastic electricity market game if there exists an optimizer $P_g^{\text{opt}}(b^*)$ of (9.6) such that for each $i \in \mathcal{I}_n$,

$$\Pi_i(b_i, P_{gi}^{\text{opt}}(b_i, b^*_{-i})) \leq \Pi_i(b^*_i, P_{gi}^{\text{opt}}(b^*))$$

for all $b_i \in \mathbb{R}_{\geq 0}$ with $b_i \neq b^*_i$ and all optimizers $P_{gi}^{\text{opt}}(b_i, b^*_{-i})$ of (9.6) given bids (b_i, b^*_{-i}).

We are particularly interested in bid profiles for which the optimizer of (9.5) is also a solution to (9.6). This is captured in the following definition.

Definition 9.3.2 (Efficient bid and efficient Nash equilibrium)**.** An *efficient bid* of the inelastic electricity market is a bid $b^* \in \mathbb{R}^n_{\geq 0}$ for which the optimizer P_g^* of (9.5) is also an optimizer of (9.6) given bids $b = b^*$ and

$$P_{gi}^* = \arg\max_{P_{gi} \geq 0} \{P_{gi} b_i^* - C_i(P_{gi})\} \quad \text{for each } i \in \mathcal{I}_n. \tag{9.8}$$

A bid $b^* \in \mathbb{R}^n_{\geq 0}$ is an *efficient Nash equilibrium* of the inelastic electricity market game if it is an efficient bid and a Nash equilibrium.

At the efficient Nash equilibrium, the optimizer of the ED problem coincides with the production levels that maximize the individual profits (9.7) of the generators. This justifies studying the efficient Nash equilibria.

9.3.3 Chapter objectives

Given the problem setup described above, neither the ISO nor the individual strategic generators are able to determine the efficient Nash equilibrium a priori. As a first objective, we are interested in designing a Nash equilibrium seeking mechanism in the form of a bidding process where the generators coordinate with the ISO to dynamically update their bids and production levels, while respecting the nonnegativity constraints throughout its execution. Our second objective is the characterization of the stability properties of the interconnection of the bidding process with the physical dynamics of the power network.

9.4 Existence and uniqueness of Nash equilibria

In this section we establish existence of an efficient Nash equilibrium and also provide a condition for its uniqueness. While [23] has established the existence of one specific efficient Nash equilibrium, we provide in the following result a characterization of all efficient Nash equilibria.

Proposition 9.4.1. *(Characterization of efficient Nash equilibria): Let $(P_g^*, \lambda^*, \mu^*)$ be the unique primal-dual optimizer of (9.5), that is, $P_g^* \in \mathbb{R}^n, \lambda^* \in \mathbb{R}, \mu^* \in \mathbb{R}^n$ satisfy the Karush-Kuhn-Tucker (KKT) conditions*

$$\begin{aligned} \nabla C(P_g^*) = \mathbb{1}\lambda^* + \mu^*, \qquad \mathbb{1}^T P_g^* = \mathbb{1}^T P_d, \\ 0 \leq P_g^* \perp \mu^* \geq 0. \end{aligned} \tag{9.9}$$

Suppose $P_{gi}^* > 0$ for at least two distinct generators. Then, any $b^* \in \mathbb{R}^n_{\geq 0}$ satisfying $\mathbb{1}\lambda^* \leq b^* \leq \nabla C(P_g^*)$ is an efficient Nash equilibrium of the inelastic electricity market game.

Proof. Let $(P_g^*, \lambda^*, \mu^*)$ satisfy (9.9), then in particular $\mathbb{1}\lambda^* \leq \nabla C(P_g^*)$. Fix any bid $b^* \in \mathbb{R}^n_{\geq 0}$ satisfying $\mathbb{1}\lambda^* \leq b^* \leq \nabla C(P_g^*)$. We will now prove that b^* is efficient.

Define $\nu^* := b^* - \mathbb{1}\lambda^*$ and note that $(P_g^*, \lambda^*, \nu^*)$ satisfies

$$\begin{aligned} b^* &= \mathbb{1}\lambda^* + \nu^*, \qquad \mathbb{1}^T P_g^* = \mathbb{1}^T P_d \\ 0 &\leq P_g^* \perp \nu^* \geq 0. \end{aligned} \tag{9.10}$$

We note that Slater's condition holds for (9.6) and its KKT conditions are given by (9.10). Consequently, P_g^* is a primal optimizer of (9.6). In addition, the bid b^* satisfies

$$P_{gi}^* = \underset{P_{gi} \geq 0}{\arg\max} \{P_{gi} b_i^* - C_i(P_{gi})\} \quad \text{for each } i \in \mathcal{I}_n. \tag{9.11}$$

This is true as for each $i \in \mathcal{I}_n$, the following optimality conditions

$$\nabla C_i(P_{gi}^*) = b_i^* + \eta_i^*, \qquad 0 \leq P_{gi}^* \perp \eta_i^* \geq 0,$$

are satisfied for $\eta_i^* = \nabla C_i(P_{gi}^*) - b_i^*$. Note that in the above set of conditions, $P_{gi}^* \eta_i^* = 0$ because if $P_{gi}^* > 0$, then $\nabla C_i(P_{gi}^*) = \lambda^* = b_i^*$. Thus, we have established that b^* is efficient. In the remainder of the proof we show that b^* is a Nash equilibrium. Suppose generator i deviates from the bid b_i^*. We distinguish between two cases. Suppose first that $b_i > b_i^*$, then by replacing b^* by (b_i, b_{-i}^*) in (9.6) and checking the optimality conditions, we obtain $P_{gi}^{\text{opt}}(b_i, b_{-i}^*) = 0$ as, by assumption, there is at least one other generator j such that $b_j^* = \lambda^* < b_i$. Without loss of generality assume that $P_{gi}^* > 0$ since otherwise $\Pi_i(b_i^*, P_{gi}^*) = \Pi_i(b_i, P_{gi}^{\text{opt}}(b_i, b_{-i}^*))$. For $P_{gi}^* > 0$, we have $b_i^* = \nabla C_i(P_{gi}^*)$ and therefore $\nabla C_i(P_{gi}) \leq b_i^*$ for all $P_{gi} \in [0, P_{gi}^*]$. As a result

$$\Pi_i(b_i, P_{gi}^{\text{opt}}(b_i, b_{-i}^*)) = C(0) \leq \Pi_i(b_i^*, P_{gi}^*)$$

This shows that a bid $b_i > b_i^*$ does not increase its payoff. Suppose now that $b_i < b_i^*$, then

$$\begin{aligned} &\Pi_i(b_i, P_{gi}^{\text{opt}}(b_i, b_{-i}^*)) = b_i P_{gi}^{\text{opt}}(b_i, b_{-i}^*)) - C_i(P_{gi}^{\text{opt}}(b_i, b_{-i}^*)) \\ &\leq b_i^* P_{gi}^{\text{opt}}(b_i, b_{-i}^*)) - C_i(P_{gi}^{\text{opt}}(b_i, b_{-i}^*)) \\ &\leq b_i^* P_{gi}^* - C_i(P_{gi}^*) = \Pi_i(b_i^*, P_{gi}^*) \end{aligned}$$

where the second inequality follows from (9.11) as b^* is efficient. Hence, each generator i has no incentive to deviate from bid b_i^* given b_{-i}^*. We conclude that b^* is an efficient Nash equilibrium of the inelastic electricity market game. □

The proof of Proposition 9.4.1 shows that if $P_{gi}^* > 0$, then generator i's efficient Nash equilibrium bid b_i^* is equal to the (unique) Lagrange multiplier λ^* associated to the power balance (9.5b). In the other case that $P_{gi}^* = 0$, generator i's Nash equilibrium bid is larger than or equal to λ^*. This represents the case that generator i's marginal costs at zero power production is larger than or equal to the market clearing price, and hence generator i is not willing to produce any electricity in that case. The underlying assumption in Proposition 9.4.1 is that at

least two generators have a positive production at the optimal generation levels. We assume this condition holds for the remainder of the chapter unless stated otherwise.

The previous observations lead to the identification of the same sufficient condition as in [23] to guarantee the uniqueness of the efficient Nash equilibrium, which we state here for completeness.

Corollary 9.4.2 (Uniqueness of the efficient Nash equilibrium [23])**.** *Let* $(P_g^*, \lambda^*, \mu^*)$ *be the primal-dual optimizer of* (9.5) *and suppose that* $P_g^* > 0$*, then* $b^* = \nabla C(P_g^*) = \mathbb{1}\lambda^*$ *is the unique efficient Nash equilibrium of the inelastic electricity market game.*

Remark 9.4.3 (Any efficient Nash equilibrium is positive). We observe from the optimality conditions (9.9) that, since $\mathbb{1}^T P_d > 0$, and $P_g^* \geq 0$, we must have that $P_{gi}^* > 0$ and $\mu_i^* = 0$ for some $i \in \mathcal{I}_n$. As $\nabla C_i(P_{gi}^*) > 0$ by the strict convexity of C_i and the assumption $\nabla C_i(0) \geq 0$, this implies that $\lambda^* > 0$ and therefore also $b^* > 0$. •

9.5 Interconnection of bid update scheme with power network dynamics

In this section we introduce a Nash equilibrium seeking mechanism between the generators and the ISO. Each generator dynamically updates its bid based on the power generation setpoint received from the ISO, while the ISO changes the power generation setpoints depending on the generator bids and the frequency of the network. This update mechanism of the bids and the setpoints is written as a continuous-time dynamical system. We assume that each generator can only communicate with the ISO and is not aware of the number of other generators participating, their respective cost functions, or the load at its own bus. We study the interconnection of the online bidding process with the power system dynamics and establish local convergence to an efficient Nash equilibrium, optimal power dispatch, and zero frequency deviation.

9.5.1 Price-bidding mechanism

In our design, each generator $i \in \mathcal{I}_n$ changes its bid $b_i \geq 0$ according to the projected dynamical system

$$K_{bi}\dot{b}_i = [P_{gi} - \nabla C_i^*(b_i)]_{b_i}^+, \tag{9.12a}$$

with gain $K_{bi} > 0$. The projection operator in the above dynamics ensures that trajectories starting in the nonnegative orthant remain there. The map $C_i^* : \mathbb{R}_{\geq 0} \to \mathbb{R}_{\geq 0}$ denotes the *convex conjugate* of the cost function C_i and is defined as

$$C_i^*(b_i) := \max_{P_{gi} \geq 0} \{b_i P_{gi} - C_i(P_{gi})\}.$$

Using tools from convex analysis [46, Section I.6], one can deduce that C_i^* is convex and continuously differentiable on the domain $\mathbb{R}_{\geq 0}$ and strictly convex on the domain $[\nabla C_i(0), \infty)$. Moreover, its gradient satisfies $\nabla C_i^*(b_i) = \arg\max_{P_{gi}\geq 0}\{b_i P_{gi} - C_i(P_{gi})\}$ for all $b_i \geq 0$.

The motivation behind the update law (9.12a) is as follows. Given the bid $b_i > 0$, generator i seeks to produce power that maximizes its profit, which is given by

$$P_{gi}^{\mathrm{des}} = \nabla C_i^*(b_i) = \arg\max_{P_{gi}\geq 0}\{b_i P_{gi} - C_i(P_{gi})\}.$$

However, if the ISO requests more power from the generator compared to its desired quantity, i.e., $P_{gi} > P_{gi}^{\mathrm{des}}$, then i will increase its bid to increase its profit. On the other hand if $P_{gi} < P_{gi}^{\mathrm{des}}$, then i will decrease its bid.

For the ISO we also provide an update law which depends on the generator bids and the network frequency. This involves seeking a primal-dual optimizer of (9.6) or, equivalently, finding a saddle-point of the augmented Lagrangian

$$\mathcal{L}(P_g, \lambda) = b^T P_g + \lambda \mathbb{1}^T(P_d - P_g) + \rho\|\mathbb{1}^T(P_d - P_g)\|^2,$$

with parameter $\rho > 0$. By writing the associated projected saddle-point dynamics (see e.g., [25, 40]), the ISO dynamics takes the form

$$\begin{aligned} K_g\dot{P}_g &= [\mathbb{1}\lambda - b + \rho\mathbb{1}\mathbb{1}^T(P_d - P_g) - \sigma^2\omega]^+_{P_g}, \\ k_\lambda\dot{\lambda} &= \mathbb{1}^T(P_d - P_g), \end{aligned} \tag{9.12b}$$

with design parameters $\sigma, k_\lambda \in \mathbb{R}_{>0}$ and diagonal positive definite matrix $K_g \in \mathbb{R}^{n\times n}$. Bearing in mind the ISO's second objective of driving the frequency deviation to zero, we add the feedback signal $-\sigma^2\omega$ to adjust the generation based on the frequency deviation in the grid.

The dynamics (9.12b) can be interpreted as follows. If generator i bids higher than the Lagrange multiplier λ (which can be interpreted as a price) associated with the power balance constraint (9.6b), then the power generation setpoint at node i is decreased, and vice versa. The terms $\rho\mathbb{1}\mathbb{1}^T(P_g - P_d)$ and $-\sigma^2\omega$ in (9.12b) help to compensate for the supply-demand mismatch in the network.

In the following, we analyze the equilibria and the stability of the interconnection of the physical power network dynamics (9.3) with the bidding process (9.12). We assume that the bids and power generations are initialized within the feasible domain, i.e., $b(0) \geq 0, P_g(0) \geq 0$.

9.5.2 Equilibrium analysis of the interconnected system

The closed-loop system composed of the ISO-generator bidding scheme (9.12) and the power network dynamics (9.3) is described by

$$\dot{\varphi} = D_t^T \omega \tag{9.13a}$$
$$M\dot{\omega} = -D_t \nabla U(\varphi) - A\omega + P_g - P_d \tag{9.13b}$$
$$K_b \dot{b} = [P_g - \nabla C^*(b)]_b^+ \tag{9.13c}$$
$$K_g \dot{P}_g = [\mathbb{1}\lambda - b + \rho \mathbb{1}\mathbb{1}^T (P_d - P_g) - \sigma^2 \omega]_{P_g}^+ \tag{9.13d}$$
$$k_\lambda \dot{\lambda} = \mathbb{1}^T (P_d - P_g) \tag{9.13e}$$

where $C^*(b) := \sum_{i \in \mathcal{I}_n} C_i^*(b_i)$, $K_b = \mathrm{diag}(K_{b1}, \dots, K_{bn}) \in \mathbb{R}^{n \times n}$. We investigate the equilibria of (9.13). In particular, we are interested in equilibria that correspond simultaneously to an efficient Nash equilibrium, economic dispatch and frequency regulation, as specified next.

Definition 9.5.1 (Efficient equilibrium)**.** An equilibrium $\bar{x} = \mathrm{col}(\bar{\varphi}, \bar{\omega}, \bar{b}, \bar{P}_g, \bar{\lambda})$ of (9.13) is *efficient* if $\bar{\omega} = 0$, $\bar{b}$ is an efficient Nash equilibrium, and $\bar{P}_g$ is a primal optimizer of (9.5).

The next result shows that all equilibria of (9.13) are efficient.

Proposition 9.5.2. *(Equilibria are efficient): Any equilibrium $\bar{x} = \mathrm{col}(\bar{\varphi}, \bar{\omega}, \bar{b}, \bar{P}_g, \bar{\lambda})$ of (9.13) is efficient.*

Proof. Let $\bar{x}$ be an equilibrium of (9.13), then there exist $\bar{\mu}_b, \bar{\mu}_g \in \mathbb{R}^n$ such that

$$0 = D_t^T \bar{\omega} \tag{9.14a}$$
$$0 = -D_t \nabla U(\bar{\varphi}) - A\bar{\omega} + \bar{P}_g - P_d \tag{9.14b}$$
$$0 = \bar{P}_g - \nabla C^*(\bar{b}) + \bar{\mu}_b \tag{9.14c}$$
$$0 = \mathbb{1}\bar{\lambda} - \bar{b} + \bar{\mu}_g \tag{9.14d}$$
$$0 = \mathbb{1}^T (P_d - \bar{P}_g) \tag{9.14e}$$
$$0 \le \bar{b} \perp \bar{\mu}_b \ge 0 \tag{9.14f}$$
$$0 \le \bar{P}_g \perp \bar{\mu}_g \ge 0 \tag{9.14g}$$

We first show that $\bar{\omega} = 0$. From (9.14a) it follows that $\bar{\omega} = \mathbb{1}\omega_s$ for some $\omega_s \in \mathbb{R}$. Then by pre-multiplying (9.14b) by $\mathbb{1}^T$ and using (9.14e) we obtain $\mathbb{1}^T A \mathbb{1} \omega_s = 0$, which implies that $\bar{\omega} = \mathbb{1}\omega_s = 0$. We prove next that $\bar{P}_g$ is a primal optimizer of (9.5). We claim that $\bar{\mu}_b = 0$ since, by contraction, if $\bar{\mu}_{bi} > 0$ for some $i \in \mathcal{I}_n$, then $\bar{b}_i = 0$ and therefore $0 = \bar{P}_{gi} - \nabla C_i^*(\bar{b}_i) + \bar{\mu}_{bi} = \bar{P}_{gi} + \bar{\mu}_{bi} > 0$, see also Remark 9.4.3. Therefore, (9.14c) implies that $\bar{P}_g = \nabla C^*(\bar{b}) = \arg\max_{P_g \ge 0} \{P_g^T \bar{b} - C(P_g)\}$ and thus satisfies the optimality conditions

$$\nabla C(\bar{P}_g) = \bar{b} + \bar{\eta}, \quad 0 \le \bar{P}_g \perp \bar{\eta} \ge 0, \tag{9.15}$$

for some $\bar{\eta}$. Let us define $\bar{\mu} = \bar{b} + \bar{\eta} - \mathbb{1}\bar{\lambda} \ge 0$ where the inequality holds by (9.14d). By (9.14g) and (9.15) we have $\bar{P}_g^T \bar{\mu} = \bar{P}_g^T (\bar{b} - \mathbb{1}\bar{\lambda}) = P_g^T \bar{\mu}_g = 0$. Hence, $(\bar{P}_g, \bar{\lambda}, \bar{\mu})$

satisfies

$$\begin{aligned} \nabla C(\bar{P}_g) = \mathbb{1}\bar{\lambda} + \bar{\mu}, \qquad \mathbb{1}^T \bar{P}_g = \mathbb{1}^T P_d, \\ 0 \leq \bar{P}_g \perp \bar{\mu} \geq 0, \end{aligned} \tag{9.16}$$

implying that $(\bar{P}_g, \bar{\lambda}, \bar{\mu})$ is a primal-dual optimizer of (9.5). Furthermore, (9.15) implies $\bar{b} \leq \nabla C(\bar{P}_g)$ and thus, by Proposition 9.4.1, $\bar{b}$ is an efficient Nash equilibrium. Hence, $\bar{x}$ is an efficient equilibrium of (9.13). □

9.5.3 Convergence analysis

In this section we establish the local asymptotic convergence of (9.13) to an efficient equilibrium.

Theorem 9.5.3. *Consider the subset of (efficient) equilibria,*

$$\begin{aligned} \mathcal{X} := \{\bar{x} = \operatorname{col}(\bar{\varphi}, \bar{\omega}, \bar{b}, \bar{P}_g, \bar{\lambda}) : \bar{x} \text{ is an equilibrium of } (9.13) \\ \text{and } D^T D_t^{\dagger T} \bar{\varphi} \in (-\pi/2, \pi/2)^m\}. \end{aligned}$$

Then $\mathcal{X}$ is locally asymptotically stable under (9.13)*. Moreover, the convergence is to a point.*

Proof of Theorem 9.5.3. Our proof strategy to show local convergence to $\mathcal{X}$ is based on applying Theorem 9.5.4, which is a special case of the invariance principle stated in [16] adapted for complementarity systems. We restate that theorem below.

Theorem 9.5.4 (Invariance principle for complementarity systems [16])**.** *Consider the system*

$$\dot{x} = F(x) + C^T \Lambda \tag{9.17a}$$

$$0 \leq Cx + d \perp \Lambda \geq 0 \tag{9.17b}$$

with Lipschitz continuous F and let K be the polyhedron

$$K = \{x : Cx + d \geq 0\}. \tag{9.18}$$

Let $\Psi \subset \mathbb{R}^n$ be a compact set and $V : \mathbb{R}^n \to \mathbb{R}$ be a continuous differentiable function such that

$$\begin{aligned} &\textbf{(I)} \quad x - \nabla V(x) \in K, \qquad \text{for all } x \in \partial K \cap \Psi, \\ &\textbf{(II)} \quad \langle \nabla V(x), F(x) \rangle \leq 0, \quad \text{for all } x \in K \cap \Psi. \end{aligned}$$

Let $E \subset \mathbb{R}^n$ be given by

$$E := \{x \in K \cap \Psi : \langle F(x), \nabla V(x) \rangle = 0\}$$

and denote the largest invariant subset of E by $\mathcal{M}$. Then, for each $x_0 \in K$ such that its orbit satisfies $\gamma(x_0) \subset \Psi$, we have

$$\lim_{t\to\infty} d(x(t;t_0,x_0),\mathcal{M}) = 0.$$

Proof of Theorem 9.5.3 (continued). To be able to apply Theorem 9.5.4, we rewrite the projected dynamical system (9.13) as the equivalent complementarity system[1]

$$\dot{\varphi} = D_t^T \omega \tag{9.19a}$$
$$M\dot{\omega} = -D_t \nabla U(\varphi) - A\omega + P_g - P_d \tag{9.19b}$$
$$K_b \dot{b} = P_g - \nabla C^*(b) + \mu_b \tag{9.19c}$$
$$K_g \dot{P}_g = \mathbb{1}\lambda - b + \rho \mathbb{1}\mathbb{1}^T(P_d - P_g) - \sigma^2\omega + \mu_g \tag{9.19d}$$
$$k_\lambda \dot{\lambda} = \mathbb{1}^T(P_d - P_g) \tag{9.19e}$$
$$0 \le b \perp \mu_b \ge 0 \tag{9.19f}$$
$$0 \le P_g \perp \mu_g \ge 0, \tag{9.19g}$$

where $\mu_b, \mu_g \in \mathbb{R}^n$. We write (9.19) in the compact form

$$\dot{x} = F(x) + C^T \Lambda \tag{9.20a}$$
$$0 \le Cx + d \perp \Lambda \ge 0 \tag{9.20b}$$

with $x = \mathrm{col}(\varphi, \omega, b, P_g, \lambda), \Lambda = \mathrm{col}(\mu_b, \mu_g)$, and

$$F(x) = \begin{bmatrix} D_t^T \omega \\ M^{-1}(-D_t \nabla U(\varphi) - A\omega + P_g - P_d) \\ K_b^{-1}(P_g - \nabla C^*(b)) \\ K_g^{-1}(\mathbb{1}\lambda - b + \rho\mathbb{1}\mathbb{1}^T(P_d - P_g) - \sigma^2\omega) \\ k_\lambda^{-1}\mathbb{1}^T(P_d - P_g) \end{bmatrix} \tag{9.21a}$$

$$C = \begin{bmatrix} 0 & 0 & K_b^{-1} & 0 & 0 & 0 \\ 0 & 0 & 0 & K_g^{-1} & 0 & 0 \end{bmatrix}, \quad d = 0 \in \mathbb{R}^{2n}. \tag{9.21b}$$

Note that F is Lipschitz continuous[2]. For the equivalence of the projected dynamical system (9.13) and the complementarity system (9.19) to hold, we consider absolutely continuous solutions $t \mapsto x(t)$ that satisfy (9.19) almost everywhere (in time) in the sense of Lebesgue measure. In addition, we consider (unique) solutions of (9.20) that are *slow*. That is, at each time t, Λ satisfies (9.20b) and is such that $\dot{x}(t)$ is of minimal norm, see also [15].

Let $\bar{x} \in \mathcal{X}$ be arbitrary and fixed for the remainder of the proof. For aesthetic reasons we first consider the case where $\sigma = 1$ in (9.13d) or (9.19d) and later we explain how to generalize the convergence result. Consider the function V defined

[1] See also [15, Theorem 1] for more details.

[2] Here we observe that, since C is continuously differentiable and μ-strongly convex on $\mathbb{R}_{\ge 0}$, C^* is $\frac{1}{\mu}$-Lipschitz continuous on $\mathbb{R}_{\ge 0}$.

by

$$V(x) = U(\varphi) - (\varphi - \bar{\varphi})^T \nabla U(\bar{\varphi}) - U(\bar{\varphi}) + \frac{1}{2}||x - \bar{x}||_K^2 \tag{9.22}$$

with $K = \text{blockdiag}(0, M, K_b, K_g, k_\lambda)$. Note that $V(\bar{x}) = 0, \nabla V(\bar{x}) = 0$ and, since $D^T D_t^{\dagger T} \bar{\varphi} \in (-\pi/2, \pi/2)^m$, $\nabla^2 V(\bar{x}) > 0$. Consequently, there exists a compact level set Ψ of V around $\bar{x}$. We show now that the two conditions of Theorem 9.5.4 are satisfied.

Condition (I): For C given in (9.21b) and $d = 0$ the polyhedron (9.18) takes the form

$$K = \{x = \text{col}(\varphi, \omega, b, P_g, \lambda) : b \geq 0, P_g \geq 0\}.$$

Consequently, for all $x \in \partial K \cap \Psi$ we have

$$x - \nabla V(x) = \begin{bmatrix} \varphi - \nabla U(\varphi) + \nabla U(\bar{\varphi}) \\ \omega - M\omega \\ b - K_b(b - \bar{b}) \\ P_g - K_g(P_g - \bar{P}_g) \\ \lambda - k_\lambda(\lambda - \bar{\lambda}) \end{bmatrix} = \begin{bmatrix} * \\ * \\ K_b \bar{b} \\ K_g \bar{P}_g \\ * \end{bmatrix} \in K.$$

Condition (II): Since $\bar{x} \in \mathcal{X}$ there exists $\bar{\Lambda}$ such that $F(\bar{x}) + C^T \bar{\Lambda} = 0$. As a result, for each $x \in K$ we have

$$\begin{aligned} \langle \nabla V(x), F(x) \rangle &= \langle \nabla V(x), F(x) - F(\bar{x}) - C^T \bar{\Lambda} \rangle \\ &= (\nabla U(\varphi) - \nabla U(\bar{\varphi})) D^T \omega \\ &+ \omega^T (-D(\nabla U(\varphi) - \nabla U(\bar{\varphi})) - A\omega + P_g - \bar{P}_g) \\ &+ (b - \bar{b})^T (P_g - \nabla C^*(b) - \bar{P}_g + \nabla C^*(\bar{b}) - \bar{\mu}_b) \\ &+ (P_g - \bar{P}_g)^T (\mathbb{1}(\lambda - \bar{\lambda}) - b + \bar{b} + \rho \mathbb{1}\mathbb{1}^T (\bar{P}_g - P_g) \\ &- \sigma^2 \omega - \bar{\mu}_g) + (\lambda - \bar{\lambda}) \mathbb{1}^T (\bar{P}_g - P_g) \\ &= -\omega^T A \omega - (b - \bar{b})^T (\nabla C^*(b) - \nabla C^*(\bar{b})) \\ &- \rho \|\mathbb{1}^T (\bar{P}_g - P_g)\|^2 - (b - \bar{b})^T \bar{\mu}_b - (P_g - \bar{P}_g)^T \bar{\mu}_g \leq 0 \end{aligned} \tag{9.23}$$

where the inequality holds because C^* is convex, $\bar{b}^T \bar{\mu}_b = 0, \bar{P}_g^T \bar{\mu}_g = 0$ and $\bar{\mu}_b, \bar{\mu}_g, b, P_g \geq 0$. Hence, the second condition of Theorem 9.5.4 is satisfied.

Invariance of Ψ: We note that (9.23) does not necessarily imply that Ψ is forward invariant. We show this next. Observe that for each x, Λ satisfying $0 \leq Cx \perp \Lambda \geq 0$ we have

$$\begin{aligned} \langle \nabla V(x), F(x) + C^T \Lambda \rangle &= \langle \nabla V(x), F(x) \rangle + \langle \nabla V(x), C^T \Lambda \rangle \leq \langle \nabla V(x), C^T \Lambda \rangle \\ &= (b - \bar{b})^T \mu_b + (P_g - \bar{P}_g)^T \mu_g = -\bar{b}^T \mu_b - \bar{P}_g^T \mu_g \leq 0. \end{aligned} \tag{9.24}$$

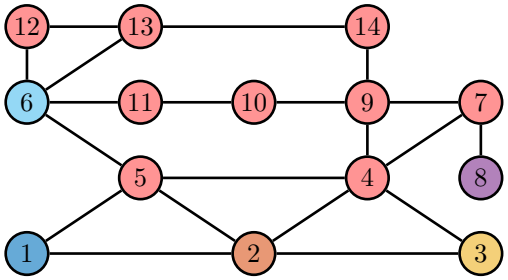

Figure 9.1: Schematic of the modified IEEE 14-bus benchmark. Each edge in the graph represents a transmission line. Red nodes represent loads. All the other nodes represent synchronous generators, with different colors that match the ones used in Figure 9.2. The physical dynamics are modeled by (9.2).

Hence, the V is non-increasing along trajectories initialized in $K \cap \Psi$. Since Ψ is a level set of V, this implies that Ψ is forward invariant.

Largest invariant set: Define

$$E = \{x \in K \cap \Psi \ : \ \langle F(x), \nabla V(x) \rangle = 0\}$$

and denote the largest invariant subset of E by $\mathcal{M}$. By (9.23) we note that each $x \in \mathcal{M}$ satisfies $\omega = 0, \mathbb{1}^T(P_d - P_g) = 0$ and, $b_i = \bar{b}_i > 0$ (otherwise, if $\bar{b}_i = 0$, then $0 = \bar{P}_{gi} - \nabla C_i^*(\bar{b}_i) + \bar{\mu}_{bi} = \bar{P}_{gi} + \bar{\mu}_{bi} > 0$, which results in a contradiction) for each $i \in \mathcal{I}_n$ with $\bar{P}_{gi} > 0$ as C_i^* is strictly convex around such $\bar{b}_i$. For these i, $P_{gi} = \bar{P}_{gi} > 0$ by (9.13c) and $b_i = \lambda = \bar{\lambda}$ by (9.13d). For each $x \in \mathcal{M}$ and $i \in \mathcal{I}_n$ with $\bar{P}_{gi} = 0$, we have $\nabla C_i^*(b_i) = \nabla C_i^*(\bar{b}_i) = 0$ by the convexity of C_i and thus $P_{gi} = \bar{P}_{gi} = \mu_{b_i} = 0$ and thus $b_i = \lambda + \mu_{gi}$. Hence, $\mathcal{M} \subset \mathcal{X}$ and therefore each trajectory initialized in Ψ converges to $\mathcal{X}$. Moreover, from (9.24), we deduce that $\bar{x}$ is stable. Since this equilibrium has been chosen arbitrarily, we conclude that every point in $\mathcal{X}$ is Lyapunov stable, implying that convergence of the trajectories is to a point.

The proof for the case $\sigma > 0, \sigma \neq 1$ proceeds in the same way as before except that we appropriately scale the Lyapunov function. Specifically, we define the Lyapunov function V as in (9.22) but with $K = \text{blockdiag}(0, M, \sigma K_b, \sigma K_g, \sigma k_\lambda) > 0$. □

9.6 Simulations

We simulate the closed-loop dynamics (9.13) for the modified IEEE 14-bus benchmark model illustrated in Figure 9.1. We assume quadratic costs at each node $i \in \mathcal{I}_{14}$ of the form

$$C_i(P_{gi}) = \frac{1}{2} q_i P_{gi}^2 + c_i P_{gi}$$

with $q_i > 0$ and $c_i \geq 0$. In the original 14-bus model, nodes $1, 2, 3, 6, 8$ have synchronous generators while the other nodes are load nodes and have no power generation. We replicate this by increasing the cost (by setting $q_i, c_i \gg 0$) at the load nodes to ensure positive power generation is not profitable at them. In addition, we choose $M_i \in [4, 5.5]$ for generator nodes $i \in \{1, 2, 3, 6, 8\}$ and $M_i \ll 1$ for the load nodes. We set $A_i \in [2, 3], V_i \in [1, 1.06]$ for all $i \in \mathcal{I}_n$ and $\rho = 300$. At $t = 0\,\text{s}$, the load (in MW's) is given by

$$P_d = (0, 22, 80, 48, 7.6, 11, 0, 0, 30, 9.0, 3.5, 6.1, 14, 15).$$

Initially, we set $(q_1, q_2, q_3, q_6, q_8) = (26, 70, 150, 150, 300)$ and $(c_1, c_2, c_3, c_6, c_8) = (7.5, 30, 90, 82.5, 75)$. The system (9.13) is initialized at steady state at the optimal generation level

$$(P_{g1}, P_{g2}) = (201, 44)$$

and with $P_{gi} = 0$ for all other nodes. Figure 9.2 shows the evolution of the system in the case when $\sigma = 300$ and Figure 9.3 in the case when $\sigma = 0$. Note that in the latter case, there is no frequency signal fed back into the bidding process, so the dynamics (9.13) effectively becomes a cascaded system (where the bidding process drives the physical dynamics of the power network). At $t = 1\,\text{s}$ the load at node 3 is increased from 80 MW to 94.2 MW and the trajectories converge to a new efficient equilibrium with optimal power generation level $(P_{g1}, P_{g2}) = (211, 48)$ and $P_{gi} = 0$ for all other nodes. Furthermore, at steady state generators $1, 2$ bid equal to the Lagrange multiplier while generators $3, 6, 8$ bid their marginal cost at zero production ($b_i = c_i$, for $i = 3, 6, 8$) and thus, by Proposition 9.4.1, we know that this corresponds to an efficient Nash equilibrium.

At $t = 15\,\text{s}$ the cost of producing electricity is decreased in areas $3, 6, 8$ by setting $(q_3, q_6, q_8) = (60, 75, 68)$ and $(c_3, c_6, c_8) = (38, 45, 23)$. This allows these generators to make profit by participating in the bidding process and results in a reduction of the total cost of the generation from 9711 \$/h to 8540 \$/h. As illustrated in both Figures 9.2 and 9.3, the power generations converge to the new optimal steady state given by

$$(P_{g1}, P_{g2}, P_{g3}, P_{g6}, P_{g8}) = (161, 29, 21, 7, 41).$$

In addition, we observe that after each change of either the load or the cost function, the frequency is stabilized and the bids converge to a new efficient Nash equilibrium. The fact that the frequency transients are better in Figure 9.2 than in Figure 9.3 is consistent, since in the latter case there is no frequency feedback in the bidding process.

9.7 Conclusions

We have studied a market-based power dispatch scheme and its interconnection with the swing dynamic of the physical network. From the market perspective, we

have considered a continuous-time bidding scheme that describes the negotiation process between the independent system operator and a group of competitive generators. Using the frequency as a feedback signal in the bidding dynamics, we have shown that the interconnected projected dynamical system provably converges to an efficient Nash equilibrium (where generation levels minimize the total cost) and to zero frequency deviation. In this way, competitive generators are enabled to participate in the real-time electricity market without compromising efficiency and stability of the power system. Future work consists of investigating finite-horizon scenarios and incorporating generator bounds and power flow constraints in the economic dispatch formulation.

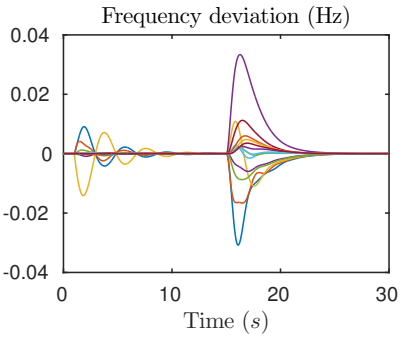

(a) Evolution of the frequency deviation. After each change of the load or the cost functions, the frequency is restored to its nominal value.

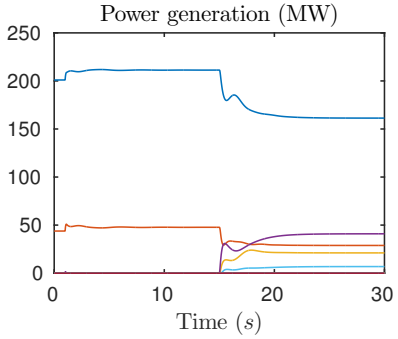

(b) Evolution of the power generation at each node. After the change of the cost functions in nodes $3, 6, 8$, there is more competition among the generators, resulting in lower power productions at node 1 and 2.

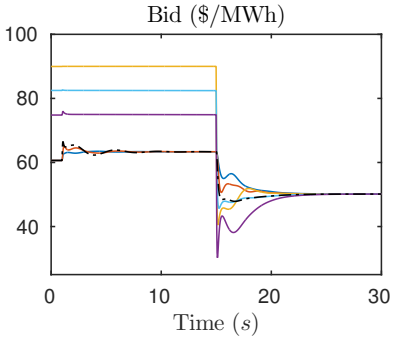

(c) Evolution of the bids and the Lagrange multiplier (represented by the dashed black colored line). Initially, the marginal costs (and the bids) at zero power production are higher than the market equilibrium price for nodes $3, 6, 8$.

Figure 9.2: Simulations of the interconnection (9.13) between the ISO-generation bidding mechanism and the power network dynamics with $\sigma = 300$. At $t = 1\,\mathrm{s}$ the load at node 3 is increased from $80\,\mathrm{MW}$ to $94.2\,\mathrm{MW}$. At $t = 15\,\mathrm{s}$ the marginal cost decreases at nodes $3, 6, 8$ which allows these generators to make profit by lowering their bids to have a positive power production as illustrated in plots (b) and (c).

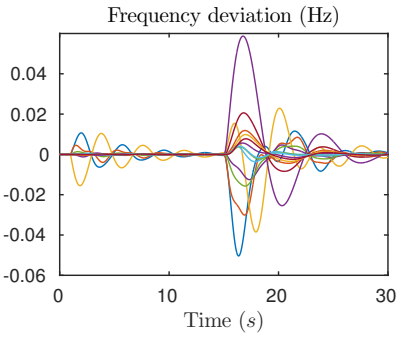

(a) Evolution of the frequency deviations with $\sigma = 0$. Compared to Figure 9.2(a), there are more oscillations and a larger overshoot of the frequency deviations.

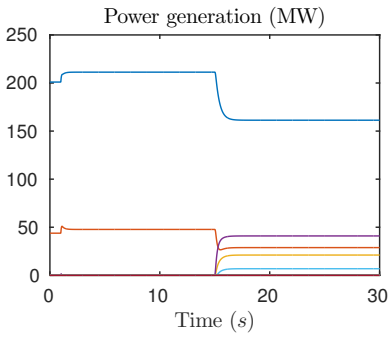

(b) Evolution of the power generations at each node. As $\sigma = 0$, the generations are updated only according to the bidding process without using any frequency measurements.

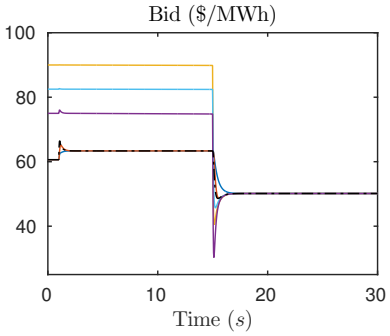

(c) Evolution of the bids and the Lagrange multiplier. Compared to Figure 9.2(c), the convergence is faster in this scenario because the bidding process does not take into account its impact on the dynamics of the power network.

Figure 9.3: Simulations of the interconnection (9.13) between the ISO-generation bidding mechanism and the power network dynamics for the case of $\sigma = 0$, i.e., when there is no frequency feedback signal in the bidding process. The scenario is the same as in Figure 9.2. As illustrated, the closed-loop system also converges in this case to an efficient equilibrium.

Chapter 10

Integrating iterative bidding and frequency regulation

Abstract *This chapter considers a real-time electricity market involving an independent system operator (ISO) and a group of strategic generators. The ISO operates a market where generators bid prices at which there are willing to provide power. The ISO makes power generation assignments with the goal of solving the economic dispatch problem and regulating the network frequency. We propose a multi-rate hybrid algorithm for bidding and market clearing that combines the discrete nature of iterative bidding with the continuous nature of the frequency evolution in the power network. We establish sufficient upper bounds on the inter-event times that guarantee that the proposed algorithm asymptotically converges to an equilibrium corresponding to an efficient Nash equilibrium and zero frequency deviation. Our technical analysis builds on the characterization of the robustness properties of the continuous-time version of the bidding update process interconnected with the power network dynamics via the identification of a novel LISS-Lyapunov function. Simulations on the IEEE 14-bus system illustrate our results.*

Published as:

T.W. Stegink, A. Cherukuri, C. De Persis, A.J. van der Schaft, J. Cortés. "Hybrid interconnection of iterative bidding and power network dynamics for frequency regulation and optimal dispatch." IEEE Transactions on Control of Network Systems, pp. 1-1. DOI: 10.1109/TCNS.2018.2856404.

T.W. Stegink, A. Cherukuri, C. De Persis, A.J. van der Schaft, J. Cortés. "Integrating iterative bidding in electricity markets and frequency regulation." American Control Conference (ACC), 2018, pp. 6182-6187.

10.1 Introduction

The dispatch of power generation in the grid has been traditionally done in a hierarchical fashion. Broadly speaking, cost efficiency is ensured via market clearing at the upper layers and frequency regulation is achieved via primary and secondary controllers at the bottom layers. Research on improving the performance of these layers has mostly developed independently from each other, motivated by their separation in time-scales. The increasing penetration of renewables poses significant challenges to this model of operation because of its intermittent and uncertain nature, see e.g., [47, 48]. At the same time, the penetration of renewables also presents an opportunity to rethink the architecture and its hierarchical separation towards the goal of improving efficiency and adaptiveness. A key aspect to achieve the integration of different layers is the characterization of the robustness properties of the mechanisms used at each layer, since variables at the upper layers cannot be assumed in steady state any more at the lower ones. These considerations motivate our work on iterative bidding schemes combined with continuous physical network dynamics and the correctness analysis of the resulting multi-rate hybrid interconnected system.

Literature review

The integration of economic dispatch and frequency regulation in power networks has attracted increasing attention in the last decades. Many recent works [35, 65, 80, 113, 121, 131, 134, 136] envision merging the design of primary, secondary, and tertiary control layers for several models of the power network/micro-grid dynamics with the aim of bridging the gap between long-term optimization and real-time frequency control. In scenarios where generators are price-takers, the literature has also explored the use of market mechanisms to determine the optimal allocation of power generation and to stabilize the frequency with real-time (locational marginal) pricing, see [3, 93, 94, 107]. Our present work shares with [97, 98] the use of dynamic iterative bidding schemes by the ISO, although in these works the setting is stochastic, the agents react in a price-taking manner, and their dynamics is assumed to be decoupled from one another. Instead, [24] proposes iterative bidding schemes where the generators are strategic, leading to efficient Nash equilibria where power generation levels minimize the total cost as intended by the ISO. Inspired by [24] and [107], our work [102] has shown that the integration with the frequency dynamics of the network can also be achieved in scenarios where generators are price-setters. However, the integration in [102] relies on a continuous-time model for the bidding process, where the frequency coming from the power network dynamics enters as a feedback signal in the negotiation process. Instead, we account here for the necessarily discrete nature of the bidding process and explore the design of provably correct multi-rate hybrid implementations that realize this integration. This involves the identification of a strictly decreasing Lyapunov function (compared to the weak Lyapunov function employed in [102]) that allows us to go beyond the characterization of asymptotic stability of the continuous-time dynamics and establish strong

robustness guarantees. These guarantees set the basis for our design here of a provably correct, multi-rate hybrid algorithm implementation.

Statement of contributions

We consider an electrical power network consisting of an ISO and a group of strategic generators. The ISO seeks to ensure that the generation meets the load with the minimum operation cost and the grid frequency is regulated to its nominal value. Each generator seeks to maximize its individual profit and does not share its cost function with anyone. The ISO operates the market, where generators bid prices at which there are willing to provide power, and makes power generation assignments based on the bids and the local frequency measurements. Our goal is to design mechanisms that ensure the stability of the interconnection between the ISO-generator bidding process and the physical network dynamics while accounting for the different nature (iterative in the first case, evolving in continuous time in the second) of each process. Our starting point is a continuous-time bid update scheme coupled with the physical dynamics of the power network whose equilibrium corresponds to an efficient Nash equilibrium and zero frequency deviation. Our first contribution is the characterization of the robustness properties of these dynamics against additive disturbances. To achieve this, we identify a novel local Lyapunov function that includes the energy function of the closed-loop system. The availability of this function not only leads us to establish local exponential convergence to the desired equilibrium, but also allows us rigorously establish its local input-to-state stability properties. Building on these results, our second contribution develops a time-triggered hybrid implementation that combines the discrete nature of iterative bidding with the continuous nature of the frequency evolution in the power network. In our design, we introduce two iteration loops, one (faster) inner-loop for the bidding process that incorporates at each step the frequency measurements, and one (slower) outer-loop for the market clearing and the updates in the power generation levels, that are sent to the continuous-time power network dynamics. We refer to this multi-rate hybrid implementation as time-triggered because we do not necessarily prescribe the time schedules to be periodic. To analyze its convergence properties, we regard the time-triggered implementation as an approximation of the continuous-time dynamics and invoke the robustness properties of the latter, interpreting as a disturbance their mismatch. This allows us to derive explicit upper bounds on the length between consecutive triggering times that guarantee that the time-triggered implementation remains asymptotically convergent. The computation of these upper bounds does not require knowledge of the efficient Nash equilibrium. Simulations on the IEEE 14-bus power network illustrate our results.

Notation

Let $\mathbb{R}, \mathbb{R}_{\geq 0}, \mathbb{R}_{>0}, \mathbb{Z}_{\geq 0}, \mathbb{Z}_{\geq 1}$ be the set of real, nonnegative real, positive real, nonnegative integer, and positive integer numbers, respectively. For $m \in \mathbb{Z}_{\geq 1}$, we use the shorthand notation $\mathcal{I}_m = \{1, \ldots, m\}$. For $A \in \mathbb{R}^{m \times n}$, we let $\|A\|$ denote

the induced 2-norm. Given $v \in \mathbb{R}^n, A = A^T \in \mathbb{R}^{n\times n}$, we denote $\|v\|_A^2 := v^T A v$. The notation $\mathbb{1} \in \mathbb{R}^n$ is used for the vector whose elements are equal to 1. The Hessian of a twice-differentiable function $f : \mathbb{R}^n \to \mathbb{R}$ is denoted by $\nabla^2 f$.

10.2 Power network frequency dynamics

Here we present the model of the physical power network that describes the evolution of the grid frequency. The network is represented by a connected, undirected graph $\mathcal{G} = (\mathcal{V}, \mathcal{E})$, where nodes $\mathcal{V} = \mathcal{I}_n$ represent buses and edges $\mathcal{E} \subset \mathcal{V} \times \mathcal{V}$ are the transmission lines connecting the buses. Let m denote the number of edges, arbitrarily labeled with a unique identifier in $\mathcal{I}_m$. The ends of each edge are also arbitrary labeled with '+' and '-', so that we can associate to the graph the incidence matrix $D \in \mathbb{R}^{n\times m}$ given by

$$D_{ik} = \begin{cases} +1 & \text{if } i \text{ is the positive end of edge } k, \\ -1 & \text{if } i \text{ is the negative end of edge } k, \\ 0 & \text{otherwise.} \end{cases} \tag{10.1}$$

A spanning tree $\mathcal{T}$ is as a connected acyclic subgraph of $\mathcal{G}$ that contains all vertices of $\mathcal{G}$. The incidence matrix $D_{\mathcal{T}}$ associated to $\mathcal{T}$ is constructed as in (10.1). Each bus represents a control area and is assumed to have one generator and one load. Following [67], the dynamics at the buses is described by the *swing equations* (10.2).

$$\begin{aligned} \dot{\delta} &= \omega \\ M\dot{\omega} &= -D\Gamma \sin(D^T\delta) - A\omega + P_g - P_d \end{aligned} \tag{10.2}$$

Here $\Gamma = \operatorname{diag}\{\gamma_1, \ldots, \gamma_m\} \in \mathbb{R}^{m\times m}, \gamma_k = B_{ij}V_iV_j$, where $k \in \mathcal{I}_m$ corresponds to the edge between nodes i and j. For the asymptotic stability analysis carried out in Sections 10.4 and 10.5, we assume that the load P_d is constant. Table 10.1 specifies the meaning of the symbols used in the model (10.2). The validity of this

$\delta \in \mathbb{R}^n$	(vector of) voltage phase angles
$\omega \in \mathbb{R}^n$	frequency deviation w.r.t. the nominal frequency
$V_i \in \mathbb{R}_{>0}$	voltage magnitude at bus i
$P_d \in \mathbb{R}^n$	power load
$P_g \in \mathbb{R}^n$	power generation
$M \in \mathbb{R}^{n\times n}_{\geq 0}$	diagonal matrix of moments of inertia
$A \in \mathbb{R}^{n\times n}_{\geq 0}$	diagonal matrix of asynchronous damping constants
$B_{ij} \in \mathbb{R}_{\geq 0}$	negative of the susceptance of transmission line (i, j)

Table 10.1: Parameters and state variables of model (10.2).

model relies on the following assumptions, which are standard in the literature on power network dynamics [61, 67], and we state here for completeness.

Assumption 10.2.1. *(Swing equation model):* For the power network dynamics described by (10.2), the following hold:

- Lines are lossless, i.e., the conductance of all lines is zero. This is generally valid for transmission lines;
- Nodal voltages V_i are constant;
- Reactive power flows are ignored;
- Network is balanced such that the three-phase network can be analyzed by a single phase.

To avoid issues in the stability analysis of (10.2) due to the rotational invariance of δ, see e.g., [34], we introduce a new set of variables. To this end, consider an arbitrary spanning tree $\mathcal{T}$ of $\mathcal{G}$ and let $D_{\mathcal{T}}$ be its associated incidence matrix. Consider $\varphi = D_{\mathcal{T}}^T \delta \in \mathbb{R}^{n-1}$ representing the voltage phase angle differences along the edges of this spanning tree. The physical energy stored in the transmission lines is given by

$$U(\varphi) = -\mathbb{1}^T \Gamma \cos(D^T D_t^{\dagger T} \varphi). \tag{10.3}$$

By noting that $D_t D_t^\dagger D = (I - \frac{1}{n}\mathbb{1}\mathbb{1}^T)D = D$, the physical system (10.2) in the (φ, ω)-coordinates takes the form

$$\begin{aligned} \dot{\varphi} &= D_t^T \omega \\ M\dot{\omega} &= -D_t \nabla U(\varphi) - A\omega + P_g - P_d \end{aligned} \tag{10.4}$$

In the sequel we assume that, for the power generation $P_g = \bar{P}_g$, there exists an equilibrium $\mathrm{col}(\bar{\varphi}, \bar{\omega})$ of (10.4) that satisfies $D^T D_t^{\dagger T} \bar{\varphi} \in (-\frac{\pi}{2}, \frac{\pi}{2})^m$. The latter assumption is standard and often referred to as the *security constraint* [67].

10.3 Problem statement

In this section we formulate the problem statement and then discuss the chapter objectives. We start from the power network model introduced in Section 10.2 and then explain the game-theoretic model describing the interaction between the ISO and the generators following the exposition of [23, 24].

The cost incurred by generator $i \in \mathcal{I}_n$ in producing P_{gi} units of power is given by

$$C_i(P_{gi}) := \frac{1}{2} q_i P_{gi}^2 + c_i P_{gi}, \tag{10.5}$$

where $q_i > 0$ and $c_i \geq 0$. The total network cost is then

$$C(P_g) := \sum_{i \in \mathcal{I}_n} C_i(P_{gi}) = \frac{1}{2} P_g^T Q P_g + c^T P_g, \tag{10.6}$$

with $Q = \mathrm{diag}\{q_1, \ldots, q_n\}$ and $c = \mathrm{col}(c_1, \ldots, c_n)$. Given the cost (10.6) and the constant power loads P_d, the ISO seeks to solve the *economic dispatch problem*

$$\underset{P_g}{\text{minimize}} \quad C(P_g), \tag{10.7a}$$

$$\text{subject to} \quad \mathbb{1}^T P_g = \mathbb{1}^T P_d, \tag{10.7b}$$

and, at the same time, regulate the network frequency to its nominal value. Since the function C is strongly convex, there exists a unique optimizer P_g^* of (10.7). However, we assume that the generators are strategic and they do not reveal their cost functions to anyone, including the ISO. Consequently, the ISO is unable to determine the optimizer of (10.7). Instead, it determines the power dispatch according to a market clearing procedure in which each generator submits bids to the ISO.

We consider price-based bidding: each generator $i \in \mathcal{I}_n$ submits the price per unit electricity $b_i \in \mathbb{R}$ at which it is willing to provide power. Based on these bids, the ISO finds the power generation allocation that minimizes the total generator payment while meeting the load. More precisely, given the bid $b = \mathrm{col}(b_1, \ldots, b_n)$, the ISO solves

$$\underset{P_g \in \mathbb{R}^n}{\text{minimize}} \quad b^T P_g, \tag{10.8a}$$

$$\text{subject to} \quad \mathbb{1}^T P_g = \mathbb{1}^T P_d. \tag{10.8b}$$

The optimization problem (10.8) is linear and may in general have multiple (unbounded) solutions. Among these solutions, let $P_g^{\mathrm{opt}}(b) = \mathrm{col}(P_{g1}^{\mathrm{opt}}(b), \ldots, P_{gn}^{\mathrm{opt}}(b))$ be the optimizer of (10.8) the ISO selects given bids b. Knowing this process, each generator i aims to bid a quantity b_i to maximize its payoff

$$\Pi_i(b_i, P_{gi}^{\mathrm{opt}}(b)) := P_{gi}^{\mathrm{opt}}(b) b_i - C_i(P_{gi}^{\mathrm{opt}}(b)). \tag{10.9}$$

For an unbounded optimizer we have $\Pi_i(b_i, \pm\infty) = -\infty$. To analyze the clearing of the market, we resort to tools from game theory [39]. To this end, we define the *inelastic electricity market game*:

- Players: the set of generators $\mathcal{I}_n$.
- Action: for each player $i \in \mathcal{I}_n$, the bid $b_i \in \mathbb{R}$.
- Payoff: for each player $i \in \mathcal{I}_n$, the payoff Π_i in (10.9).

We refer to the game as *inelastic*, as the load is not affected by the bids b_i. For the bid vector we interchangeably use the notation $b \in \mathbb{R}^n$ and $(b_i, b_{-i}) \in \mathbb{R}^n$, where b_{-i} represents the bids of all players except i. A bid profile $b^* \in \mathbb{R}^n$ is a *Nash*

equilibrium if there exists an optimizer $P_g^{\mathrm{opt}}(b^*)$ of (10.8) such that $\forall i \in \mathcal{I}_n$,

$$\Pi_i(b_i, P_{gi}^{\mathrm{opt}}(b_i, b_{-i}^*)) \leq \Pi_i(b_i^*, P_{gi}^{\mathrm{opt}}(b^*))$$

for all $b_i \neq b_i^*$ and all optimizers $P_{gi}^{\mathrm{opt}}(b_i, b_{-i}^*)$ of (10.8). In particular, we are interested in bid profiles that can be associated to economic dispatch. More specifically, a bid $b^* \in \mathbb{R}^n$ is *efficient* is a bid if there exists an optimizer P_g^* of (10.7) which is also an optimizer of (10.8) given bids $b = b^*$ and

$$P_{gi}^* = \arg\max_{P_{gi}} \{P_{gi} b_i^* - C_i(P_{gi})\} \text{ for all } i \in \mathcal{I}_n. \tag{10.10}$$

A bid b^* is an *efficient Nash equilibrium* if it is both efficient and a Nash equilibrium. At the efficient Nash equilibrium, the optimal generation allocation determined by (10.7) coincides with the production that the generators are willing to provide, maximizing their profit (10.9). Following the same arguments as in the proof of [23, Lemma 3.2] and Chapter 9, one can establish the existence and uniqueness of the efficient Nash equilibrium.

Proposition 10.3.1. *(Existence and uniqueness of efficient Nash equilibrium): Let (P_g^*, λ^*) be a primal-dual optimizer of* (10.7)*, then $b^* = \nabla C(P_g^*) = \mathbb{1}\lambda^*$ is the unique efficient Nash equilibrium of the inelastic electricity market game.*

In the scenario described above, neither the ISO nor the individual strategic generators are able to determine the efficient Nash equilibrium beforehand. Our goal is then to design an online bidding algorithm where ISO and generators iteratively exchange information about the bids and the generation quantities before the market is cleared and dispatch commands are sent. The algorithm should be truly implementable, meaning that it should account for the discrete nature of the bidding process, and at the same time ensure that network frequency, governed by the continuous-time power system dynamics, is regulated to its nominal value. The combination of these two aspects leads us to adopt a hybrid implementation strategy to tackle the problem.

10.4 Robustness of the continuous-time bid and power-setpoint update scheme

In this section, we introduce a continuous-time dynamics that prescribes a policy for bid updates paired with the frequency dynamics of the power network whose equilibrium corresponds to an efficient Nash equilibrium and zero frequency deviation. In this scheme, generators update their bids in a decentralized fashion based on the power generation quantities received by the ISO, while the ISO changes the generation quantities depending on both the generator bids and the network frequency. This design is a simplified version of the one proposed in our previous work [102]. The main contribution of our treatment here is the identification of a novel Lyapunov function that, beyond helping establish local exponential convergence, allows us to characterize the input-to-state stability properties of the

dynamics. We build on this characterization later to develop our time-triggered hybrid implementation that solves the problem outlined in Section 10.3.

10.4.1 Bidding process coupled with physical network dynamics

Recall from Section 10.3 that given bid b_i, generator $i \in \mathcal{I}_n$ wants to produce the amount of power that maximizes its individual profit, given by

$$P_{gi}^{\text{des}} := \arg\max_{P_{gi}} \{b_i P_{gi} - C_i(P_{gi})\} = q_i^{-1}(b_i - c_i) \tag{10.11}$$

Hence, if the ISO wants generator i to produce more power than its desired quantity, that is $P_{gi} > P_{gi}^{\text{des}}$, generator i will increase its bid, and vice versa. Bearing this rationale in mind, the generators update their bids according to

$$K_b \dot{b} = P_g - Q^{-1} b + Q^{-1} c. \tag{10.12a}$$

Here $K_b \in \mathbb{R}^{n \times n}$ is a diagonal positive definite matrix. Next, we provide an update law for the ISO depending on the bid $b \in \mathbb{R}^n$ and the local frequency of the power network. The ISO updates its actions according to

$$\begin{aligned} K_g \dot{P}_g &= \mathbb{1}\lambda - b + \rho \mathbb{1}\mathbb{1}^T (P_d - P_g) - \sigma^2 \omega \\ k_\lambda \dot{\lambda} &= \mathbb{1}^T (P_d - P_g) \end{aligned} \tag{10.12b}$$

with parameters $\rho, \sigma, k_\lambda \in \mathbb{R}_{>0}$ and where $K_g \in \mathbb{R}^{n \times n}$ is a diagonal positive definite gain matrix.

The intuition behind the dynamics (10.12b) is explained as follows. If generator i bids higher than the Lagrange multiplier λ (sometimes referred to as the *shadow price* [110]) associated to (10.8b), then the power generation (setpoint) of node i is decreased, and vice versa. By adding the term with $\rho > 0$, one can enhance the convergence rate of (10.12b), see e.g., [13]. We add the feedback signal $-\sigma^2\omega$ to compensate for the frequency deviations in the physical system. Interestingly, albeit we do not pursue this here, the dynamics (10.12) could also be implemented in a distributed way without the involvement of a central regulating authority like the ISO.

For the remainder of the chapter, we assume that there exists an equilibrium $\bar{x} = \text{col}(\bar{\varphi}, \bar{\omega}, \bar{b}, \bar{P}_g, \bar{\lambda})$ of (10.4)-(10.12) such that $D^T D_t^{\dagger T} \bar{\varphi} \in (-\pi/2, \pi/2)^m$ (cf. Section 10.2). Note that this equilibrium satisfies

$$\begin{aligned} \bar{\lambda} &= \frac{\mathbb{1}^T (P_d + Q^{-1} c)}{\mathbb{1}^T Q^{-1} \mathbb{1}} > 0, \qquad \bar{\omega} = 0, \quad \bar{b} = \mathbb{1}\bar{\lambda}, \\ \bar{P}_g &= Q^{-1}\mathbb{1}\bar{\lambda} - Q^{-1} c, \qquad \mathbb{1}^T \bar{P}_g = \mathbb{1}^T P_d. \end{aligned} \tag{10.13}$$

In particular, at the steady state, the frequency deviation is zero, the power balance $\mathbb{1}^T \bar{P}_g = \mathbb{1}^T P_d$ is satisfied, and $\mathbb{1}\bar{\lambda} = \bar{b} = \nabla C(\bar{P}_g)$, implying that $\bar{P}_g$ is a primal optimizer of (10.7) and $\bar{b}$ is an efficient Nash equilibrium by Proposition 10.3.1.

Hence, at steady state the generators do not have any incentive to deviate from the equilibrium bid.

10.4.2 Local input-to-state (LISS) stability

While the ISO dynamics (10.12b) is a saddle-point dynamics of the linear optimization problem (10.8) (and hence, potentially unstable), we show next that the interconnection of the physical power network dynamics (10.4) with the bidding process (10.12) is locally exponentially stable and, furthermore, robust to additive disturbances. For $x = \mathrm{col}(\varphi, \omega, b, P_g, \lambda)$, define the function

$$\begin{aligned} V(x) = U(\varphi) - (\varphi - \bar{\varphi})^T \nabla U(\bar{\varphi}) - U(\bar{\varphi}) + \tfrac{1}{2}\omega^T M \omega \\ + \tfrac{1}{2\sigma^2}(\|b - \bar{b}\|^2_{K_b} + \|P_g - \bar{P}_g\|^2_{K_g} + \|\lambda - \bar{\lambda}\|^2_{k_\lambda}). \end{aligned} \tag{10.14}$$

Then the closed-loop system obtained by combining (10.4) and (10.12) is compactly written as

$$\dot{x} = F(x) = \mathcal{Q}^{-1}\mathcal{A}\mathcal{Q}^{-1}\nabla V(x) \tag{10.15}$$

with $\mathcal{Q} = \mathcal{Q}^T = \mathrm{blockdiag}(I, M, \frac{K_b}{\sigma}, \frac{K_g}{\sigma}, \frac{k_\lambda}{\sigma}) > 0$ and

$$\mathcal{A} = \begin{bmatrix} 0 & D_t^T & 0 & 0 & 0 \\ -D_t & -A & 0 & \sigma I & 0 \\ 0 & 0 & -Q^{-1} & I & 0 \\ 0 & -\sigma I & -I & -\rho \mathbb{1}\mathbb{1}^T & \mathbb{1} \\ 0 & 0 & 0 & -\mathbb{1}^T & 0 \end{bmatrix}.$$

By exploiting the structure of the system, we obtain the dissipation inequality

$$\dot{V} = \frac{1}{2}(\nabla V(x))^T \mathcal{Q}^{-1}(\mathcal{A} + \mathcal{A}^T)\mathcal{Q}^{-1}\nabla V(x) \leq 0 \tag{10.16}$$

However, since $\mathcal{R} := -\frac{1}{2}(\mathcal{A} + \mathcal{A}^T)$ is only positive semi-definite, V is not strictly decreasing along the trajectories of (10.15). Nevertheless, one can employ this function, cf. [102], and invoke the LaSalle Invariance Principle to characterize the local asymptotic convergence properties of the dynamics. Here, we show that, in fact, the dynamics is locally input-to-state (LISS) stable, as defined in [99], and therefore robust to additive disturbances [24]. Our key tool to establish this is the identification of a LISS-Lyapunov function, which in general is far from trivial for dynamics that involve saddle-point dynamics. To this end, consider the system

$$\dot{x} = F(x) + Bd \tag{10.17}$$

with $B \in \mathbb{R}^{4n \times q}$ and a disturbance signal $d \in \mathbb{R}^q$. While the function V defined in (10.14) does not qualify for being a LISS Lyapunov function, the next result shows that adding suitable cross-terms to it yields an LISS-Lyapunov function for the system (10.17).

Theorem 10.4.1. *(LISS-Lyapunov function for the interconnected dynamics): Consider the interconnected dynamics* (10.17) *and define the function*

$$W_\epsilon(x) = V(x) + \epsilon_0\epsilon_1(\varphi-\bar{\varphi})^T D_t^\dagger M\omega \\ - \tfrac{\epsilon_0\epsilon_2}{\sigma^2}(b-\bar{b})^T K_g(P_g-\bar{P}_g) - \tfrac{\epsilon_0\epsilon_3}{\sigma^2}(\lambda-\bar{\lambda})\mathbb{1}^T K_g(P_g-\bar{P}_g), \tag{10.18}$$

with parameters $\epsilon = \mathrm{col}(\epsilon_0,\epsilon_1,\epsilon_2,\epsilon_3) \in \mathbb{R}^4_{>0}$ *and* V *given by* (10.14)*. Given the equilibrium* $\bar{x} = \mathrm{col}(\bar{\varphi},\bar{\omega},\bar{b},\bar{P}_g,\bar{\lambda})$ *of* (10.15)*, let* $\bar{\eta} = D^T D_t^{\dagger T}\bar{\varphi}$*. For* γ *such that* $\|\bar{\eta}\|_\infty < \gamma < \frac{\pi}{2}$*, define the closed convex set*

$$\Omega = \{x = \mathrm{col}(\varphi,\omega,b,P_g,\lambda) \mid D^T D_t^{\dagger T}\varphi \in [-\gamma,\gamma]^m\}. \tag{10.19}$$

Then there exist sufficiently small ϵ *such that* W_ϵ *is an LISS-Lyapunov function of* (10.17) *on* Ω*. In particular, there exist constants* $\alpha,\chi,c_1,c_2>0$ *such that for all* $x\in\Omega$ *and all* d *satisfying* $\|d\| \le \chi\|x-\bar{x}\|$*,*

$$\tfrac{1}{2}c_1\|x-\bar{x}\|^2 \le W_\epsilon(x) \le \tfrac{1}{2}c_2\|x-\bar{x}\|^2, \tag{10.20a}$$

$$(\nabla W_\epsilon(x))^T(F(x)+Bd) \le -\alpha\|x-\bar{x}\|^2. \tag{10.20b}$$

We observe that, using the characterization (10.20) and [56, Theorem 4.10], each trajectory of (10.15) initialized in a compact level set contained in Ω exponentially converges to the equilibrium $\bar{x}$ corresponding to economic dispatch and the efficient Nash equilibrium. Moreover, we exploit the local ISS property of (10.17) guaranteed by Theorem 10.4.1 in Section 10.5 to develop a time-triggered hybrid implementation. The rest of this section is devoted to the proof of Theorem 10.4.1.

Proof of Theorem 10.4.1. We structure the proof of Theorem 10.4.1 in two separate parts, corresponding to the inequalities (10.20a) and (10.20b), respectively.

Positive definiteness of Lyapunov function W_ϵ

Let $\bar{x}$ be the equilibrium of (10.15) satisfying the hypothesis. We now prove the existence of constants $c_1,c_2,\epsilon_0>0$ such that (10.20a) holds, given the constants $\epsilon_1,\epsilon_2,\epsilon_3>0$. The Hessian of W_ϵ (eq. (10.18)) is given by a block-diagonal matrix $\nabla^2 W_\epsilon(x) = \mathrm{blockdiag}(H_1(\varphi), H_2)$ with the upper left block given by

$$H_1(\varphi) = \begin{bmatrix} \nabla^2 U(\varphi) & \epsilon_0\epsilon_1 D_t^\dagger M \\ \epsilon_0\epsilon_1 M D_t^{\dagger T} & M \end{bmatrix}$$

and the lower right block is given by

$$H_2 = \frac{1}{\sigma^2}\begin{bmatrix} K_b & -\epsilon_0\epsilon_2 K_g & 0 \\ -\epsilon_0\epsilon_2 K_g & K_g & -\epsilon_0\epsilon_3 K_g\mathbb{1} \\ 0 & -\epsilon_0\epsilon_3\mathbb{1}^T K_g & k_\lambda \end{bmatrix}.$$

We will now show that there exists sufficiently small ϵ_0 such that $H_1(\varphi), H_2$ are both positive definite for all $x \in \Omega$. To this end, let us define the function

$$\mathcal{U}(\eta) = D_t^\dagger D\Gamma \cos(\eta) D^T D_t^{\dagger T} \tag{10.21}$$

and note that $\mathcal{U}(D^T D_t^{\dagger T}\varphi) = \nabla^2 U(\varphi)$, implying that $0 < \mathcal{U}(\gamma\mathbb{1}) \leq \nabla^2 U(\varphi) \leq \nabla^2 U(0) = \mathcal{U}(0)$ for all $x \in \Omega$, see (10.19). Consequently, for $D := \epsilon_0\epsilon_1 D_t^\dagger M$, we have

$$\underbrace{\begin{bmatrix} \mathcal{U}(\gamma\mathbb{1}) & D \\ D^T & M \end{bmatrix}}_{K_1} \leq H_1(\varphi) \leq \underbrace{\begin{bmatrix} \mathcal{U}(0) & D \\ D^T & M \end{bmatrix}}_{K_2}, \qquad \forall x \in \Omega.$$

By considering the Schur complements, the matrices K_1, H_2 are shown to be positive definite by choosing $\epsilon_0 > 0$ sufficiently small such that

$$\begin{aligned} \mathcal{U}(\gamma\mathbb{1}) - \epsilon_0^2\epsilon_1^2 D_t^\dagger M D_t^{\dagger T} > 0, \\ K_b - \epsilon_0^2\epsilon_2^2 K_g > 0, \\ k_\lambda - \epsilon_0^2\epsilon_3^2 \mathbb{1}^T K_b K_g (K_b - \epsilon_0^2\epsilon_2^2 K_g)^{-1}\mathbb{1} > 0. \end{aligned} \tag{10.22}$$

Next we define

$$c_1 := \min\{\lambda_{\min}(K_1), \lambda_{\min}(H_2)\}, \tag{10.23}$$

$$c_2 := \max\{\lambda_{\max}(K_2), \lambda_{\max}(H_2)\}, \tag{10.24}$$

where $\lambda_{\min}(A), \lambda_{\max}(A)$ denote the smallest and largest eigenvalue of the matrix $A \in \mathbb{R}^{n\times n}$. Note that $c_1, c_2 > 0$ and the following holds

$$0 < c_1 I \leq \nabla^2 W_\epsilon(x) \leq c_2 I, \qquad \forall x \in \Omega \tag{10.25}$$

Note that since $W_\epsilon(\bar{x}) = 0, \nabla W_\epsilon(\bar{x}) = 0$, we have

$$\begin{aligned} W_\epsilon(x) = W_\epsilon(x) - W_\epsilon(\bar{x}) &= (x-\bar{x})^T \int_0^1 \Big(\nabla W_\epsilon((x-\bar{x})\tau + \bar{x}) - \nabla W_\epsilon(\bar{x})\Big) d\tau \\ &= (x-\bar{x})^T \int_0^1 \int_0^1 \tau \nabla^2 W_\epsilon((x-\bar{x})\tau\theta + \bar{x}) d\tau d\theta (x-\bar{x}). \end{aligned}$$

Since Ω is convex, it follows that $x\tau\theta + (1-\tau\theta)\bar{x} \in \Omega$ for all $\tau, \theta \in [0,1], x \in \Omega$. Consequently, by (10.25) we have

$$c_1 I \leq \nabla^2 W_\epsilon(x\tau\theta + (1-\tau\theta)\bar{x}) \leq c_2 I, \ \forall \tau, \theta \in [0,1],$$

and $\forall x \in \Omega$. Since $\int_0^1 \int_0^1 \tau d\theta d\tau = \frac{1}{2}$, inequality (10.20a) follows.

Dissipation inequality

Here we establish the inequality (10.20b). First we consider the case without disturbance, i.e., $d = 0$. Given the equilibrium $\bar{x}$ of (10.15), we define $\tilde{x} := x - \bar{x}$ and likewise $\tilde{\varphi}, \tilde{\omega}, \tilde{b}, \tilde{P}_g, \tilde{\lambda}$. Then, the system (10.15) reads as

$$\begin{aligned}
\dot{\tilde{\varphi}} &= D_t^T \tilde{\omega}, \\
M\dot{\tilde{\omega}} &= -D_t(\nabla U(\varphi) - \nabla U(\bar{\varphi})) - A\tilde{\omega} + \tilde{P}_g, \\
K_b \dot{\tilde{b}} &= \tilde{P}_g - Q^{-1}\tilde{b}, \\
K_g \dot{\tilde{P}}_g &= \mathbb{1}\tilde{\lambda} - \tilde{b} - \rho \mathbb{1}\mathbb{1}^T \tilde{P}_g - \sigma^2 \tilde{\omega}, \\
k_\lambda \dot{\tilde{\lambda}} &= -\mathbb{1}^T \tilde{P}_g.
\end{aligned}$$

In addition, note that W_ϵ (eq. (10.18)) takes the form

$$W_\epsilon(x) = V(x) + V_\epsilon(x), \tag{10.26}$$

$$V_\epsilon(x) = \epsilon_0\epsilon_1 \tilde{\varphi}^T D_t^\dagger M\omega - \frac{\epsilon_0\epsilon_2}{\sigma^2}\tilde{b}^T K_g \tilde{P}_g - \frac{\epsilon_0\epsilon_3}{\sigma^2}\tilde{\lambda}\mathbb{1}^T K_g \tilde{P}_g. \tag{10.27}$$

Next, we determine the time-derivative of the individual terms of the candidate Lyapunov function W_ϵ.
(0): First, observe from (10.16) that

$$\dot{V} = -\omega^T A\omega - \frac{1}{\sigma^2}(b - \bar{b})^T Q^{-1}(b - \bar{b}) - \frac{\rho}{\sigma^2}(P_g - \bar{P}_g)^T \mathbb{1}\mathbb{1}^T (P_g - \bar{P}_g).$$

(1): The time-derivative of the first term of V_ϵ satisfies

$$\begin{aligned}
\frac{d}{dt}\tilde{\varphi}^T D_t^\dagger M\omega = \tilde{\omega}^T M D_t^{\dagger T} D_t^T \tilde{\omega} - \tilde{\varphi}^T D_t^\dagger D_t(\nabla U(\varphi) - \nabla U(\bar{\varphi})) \\
- \tilde{\varphi}^T D_t^\dagger A\tilde{\omega} + \tilde{\varphi}^T D_t^\dagger \tilde{P}_g.
\end{aligned}$$

By exploiting $D_t^\dagger D_t = I$, the second term is rewritten as

$$-\tilde{\varphi}^T D_t^\dagger D_t(\nabla U(\varphi) - \nabla U(\bar{\varphi})) = -\tilde{\varphi}^T \mathcal{U}(\varphi)\tilde{\varphi}^T$$

where we used that $\nabla U(\varphi) - \nabla U(\bar{\varphi}) = \mathcal{U}(\varphi)(\varphi - \bar{\varphi})$ with

$$\mathcal{U}(\varphi) = \int_0^1 \nabla^2 U((\varphi - \bar{\varphi})\theta + \bar{\varphi}) d\theta. \tag{10.28}$$

Since $\mathcal{U}(\varphi) \geq \mathfrak{U}(\mathbb{1}\gamma) = D_t^\dagger D\Gamma \cos(\mathbb{1}\gamma) D^T D_t^{\dagger T}$ (see eq. (10.21)) for all $x \in \Omega$, we obtain

$$\frac{d}{dt}\tilde{\varphi}^T D_t^\dagger M\omega \leq \tilde{\omega}^T M D_t^{\dagger T} D_t^T \tilde{\omega} - \tilde{\varphi}^T \mathfrak{U}(\mathbb{1}\gamma)\tilde{\varphi}^T - \tilde{\varphi}^T D_t^\dagger A\tilde{\omega} + \tilde{\varphi}^T D_t^\dagger \tilde{P}_g.$$

(2): For the second term of V_ϵ the following holds:

$$\frac{d}{dt}\tilde{b}^T K_g \tilde{P}_g = \tilde{P}_g^T K_{gb} \tilde{P}_g - \tilde{P}_g^T K_{gb} Q^{-1} \tilde{b} + \tilde{b}^T \mathbb{1}\tilde{\lambda} - \tilde{b}^T \tilde{b} - \rho \tilde{b}^T \mathbb{1}\mathbb{1}^T \tilde{P}_g - \sigma^2 \tilde{b}^T \tilde{\omega},$$

where we define $K_{gb} := K_g K_b^{-1}$.
(3): Similarly, by defining $K_{g\lambda} := K_g K_\lambda^{-1}$ we obtain

$$\frac{d}{dt}\tilde{\lambda}\mathbb{1}^T K_g \tilde{P}_g = -\tilde{P}_g^T K_{g\lambda} \mathbb{1}\mathbb{1}^T \tilde{P}_g + n\tilde{\lambda}^2 - \tilde{\lambda}\mathbb{1}^T \tilde{b} - \rho n \tilde{\lambda}\mathbb{1}^T \tilde{P}_g - \sigma^2 \tilde{\lambda}\mathbb{1}^T \tilde{\omega}.$$

By combining the above calculations, we can show that the time-derivative of W_ϵ satisfies

$$\dot{W}_\epsilon = \dot{V} + \dot{V}_\epsilon \leq \frac{1}{2}\epsilon_0 (x - \bar{x})^T \mathcal{P}^T \Xi_\epsilon \mathcal{P} (x - \bar{x}).$$

where Ξ_ϵ is given by the matrix illustrated below.

$$\underbrace{\begin{array}{c} \\ \omega \\ \frac{b}{\sigma} \\ \frac{P_g}{\sigma} \\ \frac{\lambda}{\sigma} \\ \varphi \end{array}\!\!\begin{array}{c} \begin{array}{ccccc} \omega & \frac{b}{\sigma} & \frac{P_g}{\sigma} & \frac{\lambda}{\sigma} & \varphi \end{array} \\ \begin{bmatrix} \frac{2}{\epsilon_0}A - \epsilon_1 \mathcal{M} & -\epsilon_2\sigma I & 0 & -\epsilon_3\sigma\mathbb{1} & \epsilon_1 A D_t^{\dagger T} \\ -\epsilon_2\sigma I & -2\epsilon_2 I + \frac{2}{\epsilon_0}Q^{-1} & -\epsilon_2(Q^{-1}K_{gb} + \rho\mathbb{1}\mathbb{1}^T) & (\epsilon_2 - \epsilon_3)\mathbb{1} & 0 \\ 0 & -\epsilon_2(K_{gb}Q^{-1} + \rho\mathbb{1}\mathbb{1}^T) & 2\epsilon_2 K_{gb} + \frac{2}{\epsilon_0}\rho\mathbb{1}\mathbb{1}^T - \epsilon_3\mathcal{T} & -\epsilon_3 n\rho\mathbb{1} & -\epsilon_1\sigma D_t^{\dagger T} \\ -\epsilon_3\sigma\mathbb{1}^T & (\epsilon_2 - \epsilon_3)\mathbb{1}^T & -\epsilon_3 n\rho\mathbb{1}^T & 2n\epsilon_3 & 0 \\ \epsilon_1 D_t^\dagger A & 0 & -\epsilon_1\sigma D_t^\dagger & 0 & 2\epsilon_1 \mathcal{U}(\mathbb{1}\gamma) \end{bmatrix} \end{array}}_{\Xi_e} \tag{10.29}$$

In addition, $\mathcal{P}$ takes the form

$$\mathcal{P} = \begin{bmatrix} 0 & I & 0 & 0 & 0 \\ 0 & 0 & \frac{1}{\sigma}I & 0 & 0 \\ 0 & 0 & 0 & \frac{1}{\sigma}I & 0 \\ 0 & 0 & 0 & 0 & \frac{1}{\sigma} \\ I & 0 & 0 & 0 & 0 \end{bmatrix},$$

and $\mathcal{M} := M D_t^{\dagger T} D_t^T + D_t D_t^\dagger M, \mathcal{T} := K_{g\lambda}\mathbb{1}\mathbb{1}^T + \mathbb{1}\mathbb{1}^T K_{g\lambda}$. Next, we will show that there exists $\epsilon_0, \epsilon_1, \epsilon_2, \epsilon_3 > 0$ such that Ξ_ϵ is positive definite. This can be done by successive use of the Schur complement. In particular, for $A \in \mathbb{R}^{n\times n}, B \in \mathbb{R}^{n\times m}, C \in \mathbb{R}^{m\times m}, \beta > 0$, recall that

$$\begin{bmatrix} \beta A & B \\ B^T & C \end{bmatrix} > 0 \quad \Longleftrightarrow \quad C > 0 \;\; \& \;\; \beta A - BC^{-1}B^T > 0.$$

For successively applying this result to Ξ_ϵ, given by (10.29), let us first fix $\epsilon_1, \epsilon_3 > 0$. Then ϵ_2 can be chosen sufficiently large such that lower-right 3×3 block submatrix of Ξ_ϵ is positive definite. Then we can choose a $\epsilon_0 > 0$ sufficiently small

such that (10.22) holds and $\Xi_\epsilon > 0$. Here, note that choosing ϵ_0 smaller does not affect the positive definiteness of the lower-right 3×3 block submatrix of Ξ_ϵ. By construction of $\epsilon_0, \epsilon_1, \epsilon_2, \epsilon_3$, there exist constants $c_1, c_2 \in \mathbb{R}_{>0}$ such that (10.20a) holds for all $x \in \Omega$, see also Section 10.4.2. In addition, for this choice of ϵ we have that $\Xi_\epsilon > 0$ and, as a result, there exists $\hat{\alpha} := \frac{1}{2}\epsilon_0 \lambda_{\min}(\mathcal{P}^T \Xi_\epsilon \mathcal{P}) > 0$ such that

$$(\nabla W_\epsilon(x))^T F(x) \leq -\hat{\alpha}\|x - \bar{x}\|^2$$

for all $x \in \Omega$. Next, we consider the case when the disturbance is present. Let ϱ satisfy $0 < \varrho < \hat{\alpha}/(L_W\|B\|)$. Then, by exploiting the Lipschitz property of ∇W_ϵ,

$$\begin{aligned}(\nabla W_\epsilon(x))^T(F(x) + Bd) &\leq -\hat{\alpha}\|x - \bar{x}\|^2 + \nabla W_\epsilon(x))^T Bd \\ &\leq -\hat{\alpha}\|x - \bar{x}\|^2 + L_W\|B\|\|x - \bar{x}\|\|d\| \\ &\leq -(\hat{\alpha} - L_W\|B\|\varrho)\|x - \bar{x}\|^2 = -\alpha\|x - \bar{x}\|^2\end{aligned}$$

with $\alpha := \hat{\alpha} - L_W\|B\|\varrho) > 0$ and thus (10.20b) holds. This concludes the proof of Theorem 10.4.1. □

10.5 Time-triggered implementation: iterative bid update and market clearing

In realistic implementations, the bidding process between the ISO and the generators is not performed continuously. Given the availability of digital communications, it is reasonable to instead model it as an iterative process. Building on the continuous-time bidding dynamics proposed in Section 10.4, here we develop a time-triggered hybrid implementation that combines the discrete nature of bidding with the continuous nature of the frequency evolution in the power network. We consider two time-scales, one (faster) for the bidding process that incorporates at each step the frequency measurements, and another one (slower) for the market clearing and updates of the power generation levels that are sent to the power network dynamics. We refer to this implementation as time-triggered because we do not necessarily prescribe the time schedules to be periodic in order to guarantee that the asymptotic stability properties are retained by the hybrid implementation.

10.5.1 Algorithm description

We start with an informal description of the iterative update scheme between the ISO and the generators, and the interconnection with the dynamics of the power network.

> *[Informal description]:* The algorithm has two time indices, k to label the iterations on the bidding process and l to label the iteration in the market clearing process that updates the power setpoints. At each iteration $l \in \mathbb{Z}_{\geq 0}$, ISO and generators are involved in an iterative process where, at each subiteration k, generators send a bid to the

ISO. Once the ISO has obtained the bids and the network frequency measurements at time t_k^l, it computes the new potential generation allocations, denoted $P_g^{k+1} \in \mathbb{R}^n$, and sends the corresponding one to each generator. At the $(k+1)$-th subiteration, each generator adjust its bid based on their previous bid and the generation allocation received from the ISO at time t_{k+1}^l. Once $k = N_l \in \mathbb{Z}_{\geq 1}$ at time $t_{N_l}^l$, the market is cleared, meaning that the bidding process is reset (i.e., $k = 0$), the power generations in the swing equations are updated according to the current setpoints $P_g^{N_l}$, and the index l moves to $l + 1$.

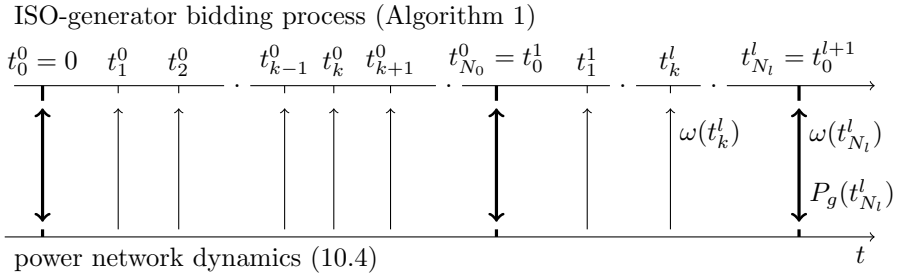

Figure 10.1: Relation between time and iteration numbers in the time-triggered system (10.31). The lower time-axis corresponds to the continuous-time physical system (10.4) while the upper one corresponds to the time sequence $\{\{t_k^l\}_{k=0}^{N_l}\}_{l=0}^{\infty}$ of the ISO-generator bidding process given in Algorithm 1. The arrows pointing up indicate the frequency updates in the bidding dynamics while the arrows pointing down correspond to update of the power generation levels in the physical system. As indicated, for each $l \in \mathbb{Z}_{\geq 0}$ the lower index k is reset once it reaches $k = N_l \in \mathbb{Z}_{\geq 1}$, i.e., $t_{N_l}^l = t_0^{l+1}$ for all $l \in \mathbb{Z}_{\geq 0}$.

Figure 10.1 shows the two iteration layers in the update scheme. The evolution of the frequency occurs in continuous time according to (10.4). To relate iteration numbers with time instances on $\mathbb{R}$, we consider time sequences of the form $\{\{t_k^l\}_{k=0}^{N_l}\}_{l=0}^{\infty}$ for $N_l \in \mathbb{Z}_{\geq 1}$ and $l \in \mathbb{Z}_{\geq 0}\}$, satisfying

$$t_k^l - t_{k-1}^l > 0, \qquad t_0^{l+1} = t_{N_l}^l \tag{10.30}$$

for all $l \in \mathbb{Z}_{\geq 0}$ and all $k \in [N_l]$. Here $N_l \in \mathbb{Z}_{\geq 1}$ is the number of bid iterates before the bidding process of market clearing instance $l \in \mathbb{Z}_{\geq 0}$ stops, see Figure 10.1. Algorithm 1 formally describes the iterative updates of the bidding process between the generators and the ISO.

For analysis purposes, we find it convenient to represent the dynamics resulting

Algorithm 1: Iterative Bid Update & Market Clearing Algorithm

Executed by: generators $i \in \mathcal{I}_n$ and ISO

Data : time sequence $\{\{t_k^l\}_{k=0}^{N_l}\}_{l=0}^{\infty}$; cost function (10.5) for each generator i; frequency deviation $\omega(t_k^l)$ at each time t_k^l and load P_d for ISO

Initialize : each generator i selects arbitrarily $b_i^0 \geq c_i$, sets $k = 0, l = 0$, and jumps to step 6; ISO selects arbitrary $P_{gi}^0 > 0, \lambda_i^0 > 0$, sets $k = 0, l = 0$ and waits for step 8

while $l \geq 0$ **do**
  while $k \geq 0, k < N_l$ **do**
    `/* For each generator i: */`
    Receive P_{gi}^k from ISO at t_k^l; Set
    $b_i^{k+1} = b_i^k + (t_{k+1}^l - t_k^l) K_{bi}^{-1} (P_{gi}^k - q_i^{-1}(b_i^k + c_i))$
    Send b_i^{k+1} to the ISO; set $k = k + 1$
    `/* For ISO: */`
    Receive $b_i^k, \omega_i(t_k^l)$ from each $i \in \mathcal{I}_n$ at t_k^l
    Set
    $P_{gi}^{k+1} = P_{gi}^k + (t_{k+1}^l - t_k^l) K_{gi}^{-1} (\lambda^k - b_i^k - \sigma^2 \omega_i(t_k^l) + \rho \sum_{i \in \mathcal{I}_n} (P_{di} - P_{gi}^k))$
    for all $i \in \mathcal{I}_n$ $\lambda^{k+1} = \lambda^k + \frac{t_{k+1}^l - t_k^l}{k_\lambda} \sum_{i \in \mathcal{I}_n} (P_{di} - P_{gi}^k)$
    Send P_{gi}^{k+1} to each $i \in \mathcal{I}_n$, set $k = k + 1$
  end
  Set $P_{gi}(t) = P_{gi}^{N_l}$ in (10.4) $\forall i \in \mathcal{I}_n, \forall t \in [t_{N_l}^l, t_{N_{l+1}}^{l+1})$
  Set $b_i^0 = b_i^{N_l}, P_{gi}^0 = P_{gi}^{N_l}, \lambda_i^0 = \lambda_i^{N_l}$ for each $i \in \mathcal{I}_n$
  Set $l = l + 1, k = 0$
end

from the combination of Algorithm 1 and the network dynamics (10.4) as the time-triggered continuous-time system

$$\begin{aligned} \dot{\varphi}(t) &= D_t^T \omega(t), \\ M\dot{\omega}(t) &= -D_t \nabla U(\varphi(t)) - A\omega(t) + P_g(t_0^l) - P_d, \\ K_b \dot{b}(t) &= P_g(t_k^l) - Q^{-1} b(t_k^l) - Q^{-1} c, \\ K_g \dot{P}_g(t) &= \mathbb{1}\lambda(t_k^l) - b(t_k^l) - \sigma^2 \omega(t_k^l) + \rho \mathbb{1}\mathbb{1}^T (P_d - P_g(t_k^l)), \\ k_\lambda \dot{\lambda}(t) &= \mathbb{1}^T (P_d - P_g(t_k^l)), \end{aligned} \tag{10.31}$$

for $t \in [t_k^l, t_{k+1}^l) \subset [t_0^l, t_0^{l+1}), l \in \mathbb{Z}_{\geq 0}, k \in \{0, \ldots, N_l - 1\}$. We write the system (10.31) compactly in the form

$$\dot{x}(t) = f(x(t)) + g(x(t_k^l)) + h(x(t_0^l)) \tag{10.32}$$

with

$$
\begin{aligned}
f(x) &= \mathrm{col}(D_t^T\omega, -M^{-1}(D_t\nabla U(\varphi) + A\omega + P_d), 0, 0, 0)\\
g(x) &= \mathrm{col}(0, 0, K_b^{-1}(P_g - Q^{-1}b - Q^{-1}c),\\
&\qquad K_g^{-1}(\mathbb{1}\lambda - b - \sigma^2\omega + \rho\mathbb{1}\mathbb{1}^T(P_d - P_g)), k_\lambda^{-1}\mathbb{1}^T(P_d - P_g))\\
h(x) &= \mathrm{col}(0, M^{-1}P_g, 0, 0, 0).
\end{aligned}
$$

With this notation, note that the continuous-time dynamics (10.15) corresponds to

$$\dot{x}(t) = f(x(t)) + g(x(t)) + h(x(t)). \tag{10.33}$$

Since $\sup_{\varphi\in\mathbb{R}^{n-1}} \|\nabla^2 U(\varphi)\| < \infty$ and g, h are linear, it follows that f, g, h are globally Lipschitz (we denote by L_f, L_g, L_h their Lipschitz constants, respectively). When viewed as a continuous-time system, the dynamics (10.31) has a discontinuous right-hand side, and therefore we consider its solutions in the Carathéodory sense, cf. [29].

10.5.2 Sufficient condition on triggering times for stability

In this section we establish conditions on the time sequence that guarantee that the solutions of (10.31) are well-defined and retain the convergence properties of (10.15). Specifically, we determine a sufficient condition on the inter-sampling times $t_{k+1}^l - t_k^l$ for bidding and $t_k^{l+1} - t_k^l$ for market clearing that ensure local asymptotic convergence of (10.32) to the equilibrium $\bar{x}$ of the continuous-time system (10.15).

Our strategy to accomplish this relies on the robustness properties of (10.15) characterized in Theorem 10.4.1 and the fact that the time-triggered implementation, represented by (10.32), can be regarded as an approximation of the continuous-time dynamics, represented by (10.33). We use the Lyapunov function W_ϵ defined by (10.18) and examine the mismatch between both dynamics to derive upper bounds on the inter-event times that guarantee that W_ϵ is strictly decreasing along the time-triggered system (10.31).

Theorem 10.5.1. *(Local asymptotic stability of time-triggered implementation): Consider the time-triggered implementation* (10.31) *of the interconnection between the ISO-generator bidding processes and the power network dynamics. With the notation of Theorem 10.4.1, let*

$$
\begin{aligned}
\bar{\xi} &:= \frac{1}{L_f + L_g}\log\Big(1 + \frac{\beta(L_f + L_g)}{L(L_W L_h + \beta)}\Big),\\
\bar{\zeta} &:= \frac{1}{L_f}\log\Big(1 + \frac{L_f(\alpha - \beta)}{L_g(LL_W + \alpha) + (\alpha - \beta)(L_f + L_g)}\Big),
\end{aligned}
\tag{10.34}
$$

where $0 < \beta < \alpha$, $L := L_f + L_g + L_h$, *and* L_W *is the Lipschitz constant of* ∇W_ϵ. *Assume the time sequence* $\{\{t_k^l\}_{k=0}^{N_l}\}_{l=0}^{\infty}$ *satisfies, for some* $\underline{\zeta} \in (0, \bar{\zeta})$ *and*

$\underline{\xi} \in (0, \overline{\xi})$,

$$\underline{\zeta} \leq t_0^{l+1} - t_0^l \leq \overline{\zeta} \quad \textit{and} \quad \underline{\xi} \leq t_k^l - t_{k-1}^l \leq \overline{\xi}, \tag{10.35}$$

for all $l \in \mathbb{Z}_{\geq 0}$ *and* $k \in \mathcal{I}_{N_l}$. *Then,* $\bar{x}$ *is locally asymptotically stable under* (10.31).

Before we go to proof of Theorem 10.5.1, we note that the uniform lower bounds $\underline{\zeta}$ and $\underline{\xi}$ in (10.35) ensure that the solutions of the time-triggered implementation (10.31) are well-defined, avoiding Zeno behavior. Theorem 10.5.1 implies that convergence is guaranteed for any constant stepsize implementation, where the sufficiently small stepsize satisfies (10.35). However, the result of Theorem 10.5.1 is more general and does not require constant stepsizes. Another interesting observation is that the upper bounds can be calculated without requiring any information about the equilibrium $\bar{x}$. This is desirable, as this equilibrium is not known beforehand and must be determined by the algorithm itself.

Proof of Theorem 10.5.1

Here we establish the proof of Theorem 10.5.1. In doing so, we rely on Gronwall's inequality, which in general allows to bound the evolution of continuous-time and discrete-time signals described by differential and difference equations, respectively. Given the hybrid nature of the time-triggered dynamics (10.31), we rely on a version of Gronwall's inequality for hybrid systems developed in [74]. Adapted for our purposes, it states the following.

Proposition 10.5.2. *(Generalized Gronwall's inequality [74]): Let* $t \mapsto y(t) \in \mathbb{R}$ *be a continuous signal,* $t \mapsto p(t) \in \mathbb{R}$ *be a continuously differentiable signal,* $r := \{r_j\}_{j=0}^{k-1}$ *be a nonnegative sequence of real numbers,* $q \geq 0$ *a constant, and* $E := \{t_j\}_{j=0}^{k+1}$, $k \in \mathbb{Z}_{\geq 0}$ *be a sequence of times satisfying* $t_j < t_{j+1}$ *for all* $j \in \{0, \ldots, k\}$. *Suppose that for all* $t \in [t_0, t_{k+1}]$, *the elements* y, p, *and* r *satisfy*

$$y(t) \leq p(t) + q \int_{t_0}^{t} y(s)ds + \sum \prod_{j=0}^{i(t)-1} r_j y(t_{j+1}) \tag{10.36}$$

with $i(t) := \max\{i \in \mathbb{Z}_{\geq 0} : t_i \leq t, t_i \in E\}$ *for* $t < t_{k+1}$ *and* $i(t_{k+1}) := k$. *Then,*

$$y(t) \leq p(t_0)h(t_0, t) + \int_{t_0}^{t} h(s, t)\dot{p}(s)ds \tag{10.37}$$

for all $t \in [t_0, t_{k+1}]$ *where for all* $t_0 \leq s \leq t \leq t_{k+1}$,

$$h(s, t) := \exp\big(q(t - s) + \sum_{j=i(s)}^{i(t)-1} \log(1 + r_j)\big). \tag{10.38}$$

We are now ready to prove the main theorem.

Proof of Theorem 10.5.1. Let $\{\{t_k^l\}_{k=0}^{N_l}\}_{l=0}^{\infty}$ be a sequence of times satisfying the hypotheses. Consider a trajectory $t \mapsto x(t)$ of (10.31) with $x(0)$ belonging to

a neighborhood of $\bar{x}$. The definition of this neighborhood will show up later. Our proof strategy involves showing the monotonic decrease of the function W_ϵ (cf. (10.18)) along this arbitrarily chosen trajectory. Consider any $t \in \mathbb{R}_{\geq 0}$ such that $t \notin \{t_k^l\}_{k=0}^{N_l}$ for any $l \in \mathbb{Z}_{\geq 0}$ and $x(t) \in \Omega$ where Ω is defined by (10.19). With a slight abuse of notation let l and $k \in \{0, \ldots, N_l - 1\}$ be fixed such that $t \in (t_k^l, t_{k+1}^l)$. Then, using the expression of $F(x) = f(x) + g(x) + h(x)$ given in (10.33), one can write the evolution of x at t for the considered trajectory as

$$\dot{x}(t) = F(x(t)) + g(x(t_k^l)) - g(x(t)) + h(x(t_0^l)) - h(x(t)).$$

(I) Dissipation inequality: Note that at t the evolution of W_ϵ is equal to the dot product between the gradient of W_ϵ and right-hand side of the above equation. Hence, we get

$$\dot{W}_\epsilon(x(t)) = \nabla W_\epsilon(x(t))^\top \Big(F(x(t)) + g(x(t_k^l)) - g(x(t)) + h(x(t_0^l)) - h(x(t)) \Big). \tag{10.39}$$

From (10.20b), we have $\nabla W_\epsilon(x(t))^\top F(x(t)) \leq -\alpha \|x(t) - \bar{x}\|^2$. Moreover, since maps ∇W_ϵ, g, and h are globally Lipschitz and $\nabla W_\epsilon(\bar{x}) = 0$, one has $\|\nabla W_\epsilon(x(t))\| \leq L_W \|x(t) - \bar{x}\|$, $\|g(x(t_k^l)) - g(x(t))\| \leq L_g \|x(t_k^l) - x(t)\|$, and $\|h(x(t_0^l)) - h(x(t))\| \leq L_h \|x(t_0^l) - x(t)\|$. Using these bounds in (10.39), we get the following.

$$\dot{W}_\epsilon(x(t)) \leq -\alpha \|x(t) - \bar{x}\|^2 + L_W \|x(t) - \bar{x}\| (L_g \|x(t) - x(t_k^l)\| + L_h \|x(t) - x(t_0^l)\|) \tag{10.40}$$

Next, we provide bounds on $\|x(t) - x(t_k^l)\|$ and $\|x(t) - x(t_0^l)\|$ in terms of $\|x(t) - \bar{x}\|$, $t - t_k^l$, and $t - t_0^l$. To reduce the notational burden, we drop the superscript l from the time instances $\{t_i^l\}_{i=1}^{N_l}$. In addition, we define

$$\begin{aligned} x_k &:= x(t_k), & \zeta_k(t) &:= t - t_k, \\ \zeta_j^k &:= \zeta_j(t_k) = t_k - t_j, & \xi^l(t) &:= \zeta_0(t) = t - t_0. \end{aligned}$$

(II) Bounds on $\|\mathbf{x(t) - x(t_k^l)}\|$: Note that $x(t)$ can be written using (10.32) as the line integral

$$\begin{aligned} x(t) - x_k &= \int_{t_k}^{t} f(x(s)) ds + \zeta_k(t) g(x_k) + \zeta_k(t) h(x_0) \\ &= \int_{t_k}^{t} (f(x(s)) - f(x_k)) ds + \zeta_k(t)(f(x_k) - f(\bar{x})) \\ &\quad + \zeta_k(t)(g(x_k) - g(\bar{x}) + h(x_0) - h(\bar{x})). \end{aligned} \tag{10.41}$$

Above, we have added and subtracted $\zeta_k(t) f(x_k)$ and subtracted $f(\bar{x}) + g(\bar{x}) + h(\bar{x})$ as $\bar{x}$ is an equilibrium. Using Lipschitz bounds and triangle inequality in (10.41)

we obtain

$$\|x(t) - x_k\| \leq L_f \int_{t_k}^{t} \|x(s) - x_k\| ds + \zeta_k(t)(L_f + L_g)\|x_k - \bar{x}\| + \zeta_k(t) L_h \|x_0 - \bar{x}\|. \tag{10.42}$$

We wish to obtain an upper bound on $\|x(t) - x_k\|$ that is independent of the state at times $s \in (t_k, t)$. To this end, we employ Gronwall's inequality as stated in its general form in Proposition 10.5.2. Drawing a parallelism between the notations, for (10.42), we consider $E = \emptyset$, $r = 0, y(t) = \|x(t) - x_k\|, q = L_f, p(t) = \zeta_k(t)(L_f + L_g)\|x_k - \bar{x}\| + \zeta_k(t) L_h \|x_0 - \bar{x}\|$ and replace t_0 by t_k. With these choices, the hypothesis (10.36) is satisfied (as it exactly corresponds to (10.42) above). Then, with the notation of Proposition 10.5.2, we have

$$\begin{aligned} h(s,t) &= e^{L_f(t-s)}, \\ \dot{p}(s) &= (L_f + L_g)\|x_k - \bar{x}\| + L_h \|x_0 - \bar{x}\|, \qquad p(t_k) = 0, \end{aligned}$$

and (10.37) reads as

$$\begin{aligned} \|x(t) - x_k\| &\leq \int_{t_k}^{t} e^{L_f(t-s)} \big((L_f + L_g)\|x_k - \bar{x}\| + L_h \|x_0 - \bar{x}\| \big) ds \\ &= \big(1 + \tfrac{L_g}{L_f}\big)\|x_k - \bar{x}\|(e^{L_f \zeta_k(t)} - 1) \\ &\quad + \tfrac{L_h}{L_f}\|x_0 - \bar{x}\|(e^{L_f \zeta_k(t)} - 1). \end{aligned} \tag{10.43}$$

Bounding the above inequality using the triangle inequality $\|x_k - \bar{x}\| \leq \|x(t) - x_k\| + \|x(t) - \bar{x}\|$, collecting coefficients of $\|x(t) - x_k\|$ on the left-hand side, and rearranging gives

$$\begin{aligned} \|x(t) - x_k\| &\leq \frac{L_h(e^{L_f \zeta_k(t)} - 1)}{L_f - (L_f + L_g)(e^{L_f \zeta_k(t)} - 1)} \|x_0 - \bar{x}\| \\ &\quad + \frac{(L_f + L_g)(e^{L_f \zeta_k(t)} - 1)}{L_f - (L_f + L_g)(e^{L_f \zeta_k(t)} - 1)} \|x(t) - \bar{x}\|. \end{aligned} \tag{10.44}$$

(III) Bounds on $\|\mathbf{x(t)} - \mathbf{x(t_0^l)}\|$: Our next step is to provide an upper bound on the term $\|x(t) - x_0\|$. Recall that the considered trajectory satisfies (10.32) and so, the line integral over the interval $[t_0, t]$ gives

$$x(t) - x_0 = \int_{t_0}^{t} f(x(s)) ds + \sum_{j=0}^{k-1} \zeta_j^{j+1} g(x_j) + \zeta_k(t) g(x_k) + \xi^l(t) h(x_0).$$

As done before, on the right-hand side, we add and subtract the terms $\xi^l(t)f(x_0)$ and $\xi^l(t)g(x_0)$ and then subtract $f(\bar{x}) + g(\bar{x}) + h(\bar{x})$. This gives us

$$\begin{aligned} x(t) - x_0 = &\int_{t_0}^{t} (f(x(s)) - f(x_0))ds \\ &+ \sum_{j=0}^{k-1} \zeta_j^{j+1}(g(x_j) - g(x_0)) + \zeta_k(t)(g(x_k) - g(x_0)) \\ &+ \xi^l(t)(f(x_0) - f(\bar{x}) + g(x_0) - g(\bar{x}) + h(x_0) - h(\bar{x})) \end{aligned}$$

By defining $L := L_f + L_g + L_h$, taking the norms, using the global Lipschitzness, we obtain from above

$$\begin{aligned} \|x(t) - x_0\| \leq L_f &\int_{t_0}^{t} \|x(s) - x_0\|ds + \xi^l(t)L\|x_0 - \bar{x}\| \\ &+ L_g \sum_{j=0}^{k-1} \zeta_j^{j+1}\|x_j - x_0\| + L_g\zeta_k(t)\|x_k - x_0\|. \end{aligned}$$

Consider any $\hat{t} \in [t, t_{k+1}]$ and note that $\zeta_k(t) \leq \zeta_k(\hat{t})$. Using this bound and the fact that the first term in the above summation is zero, we write

$$\begin{aligned} \|x(t) - x_0\| \leq L_f &\int_{t_0}^{t} \|x(s) - x_0\|ds + \xi^l(t)L\|x_0 - \bar{x}\| \\ &+ L_g \sum_{j=0}^{k-2} \zeta_{j+1}^{j+2}\|x_{j+1} - x_0\| + L_g\zeta_k(\hat{t})\|x_k - x_0\|. \end{aligned}$$

We now apply Proposition 10.5.2 to give a bound for the left-hand side independent of $x(s)$, $s \in (t_0, t]$. In order to do so, the elements corresponding to those in the Gronwall's inequality are: $E = \{t_j\}_{j=0}^{k} \cup \{\hat{t}\}$, $y(t) = \|x(t) - x_0\|, p(t) = \xi^l(t)L\|x_0 - \bar{x}\|, q = L_f, r_j = L_g\zeta_{j+1}^{j+2}$ for $j = 0, \ldots, k-2$, and $r_{k-1} = \hat{t} - t_k$. From Proposition 10.5.2, we get

$$\|x(t) - x_0\| \leq L\|x_0 - \bar{x}\| \int_{t_0}^{t} h(s,t)ds, \tag{10.45}$$

where $h(s,t) = \exp\big(\int_s^t L_f dK + \sum_{j=i(s)}^{k-2} \log(1 + \zeta_{j+1}^{j+2}L_g) + \log(1 + L_g\zeta_k(\hat{t}))\big)$ and $i(s)$ is as defined in Proposition 10.5.2. Using $\log(1+x) \leq x$ for $x \geq 0$ and the fact that the exponential is a monotonically increasing function, we get

$$h(s,t) \leq \exp\Big(L_f(t-s) + L_g \sum_{j=i(s)}^{k-2} \zeta_{j+1}^{j+1} + L_g\zeta_k(\hat{t})\Big).$$

By noting that $s \leq i(s) + 1$ and $t \leq \hat{t}$, we can upper bound the right-hand side as

$h(s,t) \leq \exp\big(L_f(t-s) + L_g(\hat{t}-s)\big)$. Since $\hat{t}$ was chosen arbitrarily in the interval $[t, t_{k+1}]$, we pick it equal to t. Thus, $h(s,t) \leq \exp\left((L_g+L_f)(t-s)\right)$. Substituting this inequality in (10.45) yields

$$\|x(t)-x_0\| \leq L\|x_0-\bar{x}\| \int_{t_0}^{t} e^{(L_f+L_g)(t-s)}ds = \tfrac{L}{L_f+L_g}(e^{(L_f+L_g)\xi^l(t)}-1)\|x_0-\bar{x}\|. \tag{10.46}$$

This inequality when used in the right-hand side of the triangle inequality $\|x_0 - \bar{x}\| \leq \|x(t)-x_0\| + \|x(t)-\bar{x}\|$ yields after rearrangement the following

$$\|x_0-\bar{x}\| \leq \frac{L_f+L_g}{L_f+L_g-L(e^{(L_f+L_g)\xi^l(t)}-1)}\|x(t)-\bar{x}\|. \tag{10.47}$$

Subsequently, using the above bound in (10.46) gives

$$\|x(t)-x_0\| \leq \frac{L(e^{(L_f+L_g)\xi^l(t)}-1)}{L_f+L_g-L(e^{(L_f+L_g)\xi^l(t)}-1)}\|x(t)-\bar{x}\|. \tag{10.48}$$

Combining inequalities (10.44) and (10.47) we obtain

$$\begin{aligned}\|x(t)-x_k\| \leq{}& \frac{L_h(e^{L_f\zeta_k(t)}-1)}{L_f-(L_f+L_g)(e^{L_f\zeta_k(t)}-1)}\cdot \\ & \frac{L_f+L_g}{L_f+L_g-L(e^{(L_f+L_g)\xi^l(t)}-1)}\|x(t)-\bar{x}\| \\ & + \frac{(L_f+L_g)(e^{L_f\zeta_k(t)}-1)}{L_f-(L_f+L_g)(e^{L_f\zeta_k(t)}-1)}\|x(t)-\bar{x}\|\end{aligned} \tag{10.49}$$

(IV) Monotonic decrease of $\mathbf{W}_\epsilon$: Note first that following (10.48) and using the bound $\xi^l(t) \leq \bar{\xi}$ yields

$$\|x(t)-x_0\| \leq \frac{L(e^{(L_f+L_g)\bar{\xi}}-1)}{L_f+L_g-L(e^{(L_f+L_g)\bar{\xi}}-1)}\|x(t)-\bar{x}\|.$$

Using the definition of $\bar{\xi}$, one gets $e^{(L_f+L_g)\bar{\xi}}-1 = \frac{\beta(L_f+L_g)}{L(L_W L_h+\beta)}$. Substituting this value in the above inequality and simplifying the expression provides us

$$\|x(t)-x_0\| \leq (\beta/(L_W L_h))\|x(t)-\bar{x}\|. \tag{10.50}$$

In a similar way, using the bound on $\xi^l(t)$ and substituting the value of $e^{(L_f+L_g)\bar{\xi}}-1$ in (10.49) and simplifying yields

$$\|x(t)-x_k\| \leq \frac{(e^{L_f\zeta_k(t)}-1)(L+\beta/L_W)}{L_f-(L_f+L_g)(e^{L_f\zeta_k(t)}-1)}\|x(t)-\bar{x}\|.$$

Note that $\zeta_k(t) \leq \bar{\zeta}$. Using this bound and the definition of $\bar{\zeta}$ in the above inequality gives

$$\|x(t) - x_k\| \leq \tfrac{\alpha-\beta}{L_W L_g}\|x(t) - \bar{x}\|. \tag{10.51}$$

Finally, substituting (10.50) and (10.51) in (10.40) and using the fact that $\beta < \alpha$, we obtain $\dot{W}_\epsilon(x(t)) < 0$. Recall that $t \in \mathbb{R}_{\geq 0}$ was chosen arbitrarily satisfying $t \notin \{t_k^l\}_{k=1}^{N_l}$ for any $l \in \mathbb{Z}_{\geq 0}$. Therefore, W_ϵ monotonically decreases at all times along the trajectory except for a countable number of points. Further, the map $t \mapsto W_\epsilon(x(t))$ is continuous. Therefore, we conclude that the trajectory initialized in a compact level set of W_ϵ contained in Ω converges asymptotically to the equilibrium point $\bar{x}$. This completes the proof. □

Remark 10.5.3. *(General cost functions, generator box constraints, and elastic demand):* We briefly discuss here the feasibility and challenges involved in extending the present treatment along different directions.

General cost functions: The results presented above also hold for general convex (instead of quadratic) cost functions. Specifically, if there exist $c_1, c_2 \in \mathbb{R}_{>0}$ such that $0 \prec c_1 I \preceq \nabla^2 C(P_g) \preceq c_2 I$ for all $P_g \in \mathbb{R}^n$, then one can establish LISS of the closed-loop system and compute bounds on the inter-event times to guarantee local asymptotic stability. However, this setting requires a significant more technical derivation and therefore it is omitted in the present work.

Generator box constraints: An interesting extension would be the inclusion in (10.7) of box constraints on power generation. Such extension would require the re-examination of the existence and uniqueness of Nash equilibria, as generators may take advantage of them to arbitrarily increase their individual profit, and the modification of the proposed algorithm to accommodate these constraints, e.g., by using projections in the dynamics. The latter makes it difficult to asses LISS as the characterization of the input-to-state stability properties of projected dynamics systems is still open.

Elastic demand: Our treatment here has considered inelastic loads. If instead loads are flexible, i.e., the demand is elastic, then consumers would also react to prices, possibly in a price-taking manner as in a Cournot-type of competitive market. This implies that the game-theoretic model has to be revised to accommodate loads that change with generator bids/prices. The investigation of how to carry this out is an interesting topic for future research. •

10.6 Simulations

In this section we illustrate the convergence properties of the interconnected time-triggered system (10.31). We consider the IEEE 14-bus power network depicted in Figure 10.2, where each node has one generator and one load according to model (10.2). We assume that the costs at each node $i \in \{1, \ldots, 14\}$ are of the

form

$$C_i(P_{gi}) = \frac{1}{2} q_i P_{gi}^2 + c_i P_{gi}$$

with $q_i > 0$ and $c_i \geq 0$. In the original IEEE 14-bus benchmark model, nodes $1, 2, 3, 6, 8$ have synchronous generators while the other nodes are load nodes and have no power generation. We replicate this by suitably choosing the cost at the load nodes such that the optimizer of the economic dispatch problem (10.7) is zero at them. In addition, we choose $M_i \in [4, 5.5]$ for generator nodes $i \in \{1, 2, 3, 6, 8\}$ and $M_i \ll 1$ for the load nodes. We set $A_i \in [1.5, 2.5], V_i \in [1, 1.06], K_{bi} \in [0.0005, 0.001], K_{gi} = 13.5$ for all $i \in \mathcal{I}_{14}$ and $\rho = 900$. The other parameter values for the ISO dynamics (10.12b) are $k_\lambda = 0.0004$, $\rho = 3$, $\sigma = 17$.

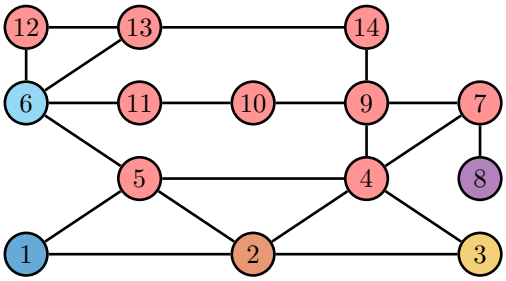

Figure 10.2: Schematic of the modified IEEE 14-bus benchmark. Each edge represents a transmission line. Red nodes represent loads. All the other nodes represent synchronous generators, with different colors that match the ones used in Figures 10.3 and 10.5. The physical dynamics are modeled by (10.2).

At time $t = 0\,\text{s}$, the inelastic load (in MW's) is given by

$$P_d = (0, 20, 86, 43, 7, 10, 0, 0, 27, 8, 3, 6, 12, 14).$$

Initially, we set $(q_1, q_2, q_3, q_6, q_8) = (22, 128, 45, 60, 30)$, $c_i = 7.5$ for $i \in \{1, 2, 3, 6, 8\}$ and $q_i = 1500, c_i = 26$ for the remaining nodes. The time-triggered system (10.31) is initialized at steady state at the optimal generation level

$$(P_{g1}, P_{g2}, P_{g3}, P_{g6}, P_{g8}) = (85, 15, 42, 31, 63)$$

and with $P_{gi} = 0$ for all other nodes. Figures 10.3-10.5 on pages 212-214 depict the simulation of the time-triggered system for different triggering times. At $t = 1\,\text{s}$ all the loads are increased by 10% and we set $c_i = 28$ for the load nodes. As observed in all figures, the trajectories converge to a new efficient equilibrium with optimal power generation level

$$(P_{g1}, P_{g2}, P_{g3}, P_{g6}, P_{g8}) = (94, 16, 46, 34, 69)$$

and $P_{gi} = 0$ for all other nodes. Furthermore, at steady state the generators all bid equal to the Lagrange multiplier which, by Proposition 10.3.1, corresponds to

an efficient Nash equilibrium.

At $t = 15\,\mathrm{s}$ the cost functions of the generators are changed to $(q_1, q_2, q_3, q_6, q_8) = (23, 116, 48, 63, 38)$, $(c_1, c_2, c_3, c_6, c_8) = (7.5, 6, 13.5, 15, 10.5)$ and $q_i = 1500, c_i = 33$ for the remaining nodes. As a result, the optimal dispatch of power changes. Due to the changes of the power generation, a temporary frequency imbalance occurs. As illustrated in Figures 10.3-10.5, the power generations converge to the new optimal steady state given by

$$(P_{g1}, P_{g2}, P_{g3}, P_{g6}, P_{g8}) = (108, 23, 40, 28, 60).$$

In addition, we observe that after each change of either the load or the cost function, the frequency is stabilized and the bids converge to a new efficient Nash equilibrium. The fact that the frequency transients are better in Figures 10.3-10.4 (with inter-event times of maximal 2 ms for bidding and on average respectively 50 ms, 62.5 ms for market clearing) than in Figure 10.5 (with inter-event times of 2 ms for bidding and 160 ms for market clearing) is to be expected given the longer inter-event times in the second case. A slight increase in the inter-event times for Figure 10.5 in either bid updating or market clearing time result in an unstable system. Figure 10.6 illustrates the evolution of the interconnected system with the primary/secondary and tertiary control layers separated and its loss of efficiency compared to the proposed integrated design.

10.7 Conclusions

This chapter has studied the joint operation of the economic dispatch and frequency regulation layers, which are traditionally separated in the control of power networks. The starting point of our design was a continuous-time bid update scheme coupled with the frequency dynamics whose equilibrium corresponds to an efficient Nash equilibrium and zero frequency deviation. Building on the identification of a novel LISS-Lyapunov function for this dynamics, we have characterized its robustness properties against additive disturbances. We have exploited the LISS-property to propose a provably correct multi-rate hybrid implementation that combines the iterative nature of the fast bid updates and the slower power setpoint updates with the continuous frequency network dynamics. Our results show that real-time iterative bidding can successfully be interconnected with frequency control to increase efficiency while retaining stability of the power system.

Future work will incorporate elastic demand, generator bounds, and power flow constraints in the formulation. We also wish to explore more general bids including piecewise constant and linear supply functions. Finally, we aim to develop distributed and opportunistic self-triggered implementations of the proposed dynamics, and characterize the convergence properties of data-driven optimization algorithms.

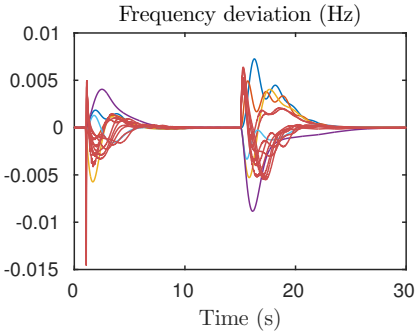

(a) Evolution of the frequency deviations. After each sudden supply-demand imbalance, frequency is restored to its nominal value.

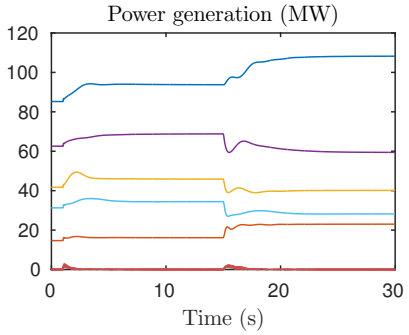

(b) Evolution of the nodal power generations. After each change in the network, the power generation quantities converge to the optimal values determined by (10.7).

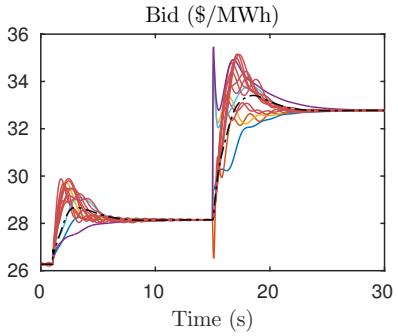

(c) Evolution of the bids and the Lagrange multiplier (dashed black line). As shown, the bids converge to the unique efficient Nash equilibrium.

Figure 10.3: Simulations of the interconnection between the iterative bidding mechanism and the power network dynamics modeled by the time-triggered system (10.31). The colors in the graph corresponds to the nodes as depicted in Figure 10.2. We choose identical inter-event times given by $t_k^l - t_{k-1}^l = 2\,\text{ms}, t_0^l - t_0^{l-1} = 50\,\text{ms}$ for all $l \in \mathbb{Z}_{\geq 1}, k \in \{1, \ldots, 25\}$. As expected, the time-triggered system is asymptotically stable for sufficiently fast updates.

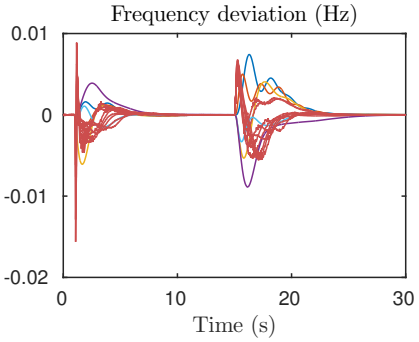

(a) Evolution of the frequency deviations.

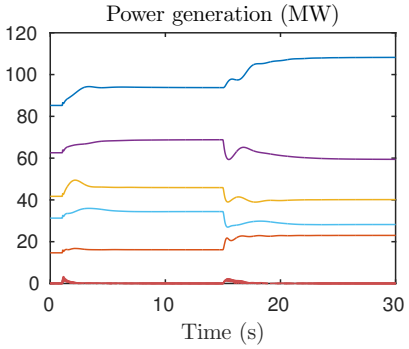

(b) Evolution of each power generation.

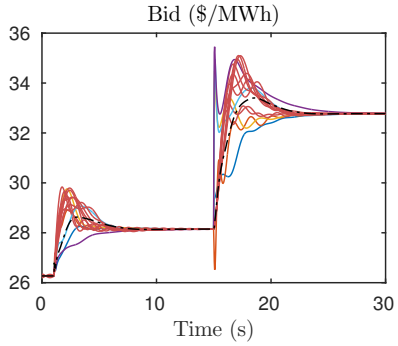

(c) Evolution of the bids and the Lagrange multiplier.

Figure 10.4: Simulations of the time-triggered system (10.31) under time-varying step sizes. We choose the time between two consecutive bid iterations randomly between $0.5\,\text{ms} \leq t_k^l - t_{k-1}^l \leq 2\,\text{ms}$, for all $l \in \mathbb{Z}_{\geq 1}, k \in [N_l]$, and we choose the number of bid iterations $N_l \in \mathbb{Z}$ before market clearing occurs randomly in the interval $[20, 80]$. Since the step sizes are sufficiently small, and therefore the mismatch of the time-triggered system with its continuous-time variant, the performance is similar compared to Figure 10.3.

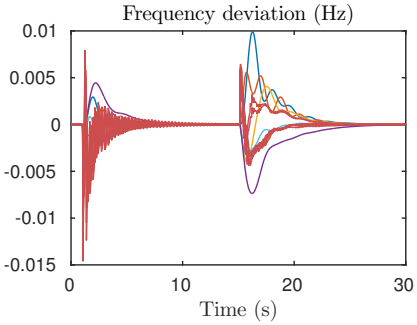

(a) Compared to Figure 10.3a, there are more oscillations and a larger overshoot of the frequency deviations.

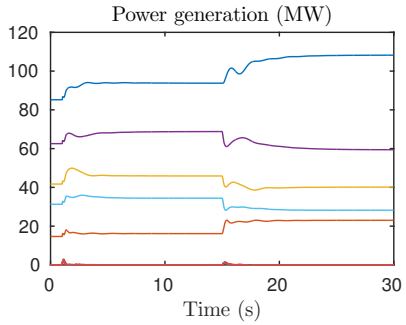

(b) Evolution of the power generations at each node.

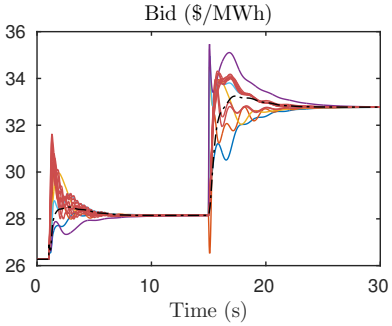

(c) Evolution of the bids and the Lagrange multiplier. Compared to Figure 10.3c, more oscillations in the bids occur.

Figure 10.5: Simulations of the time-triggered system (10.31). Here we consider the case $t_k^l - t_{k-1}^l = 2\,\text{ms}, t_0^l - t_0^{l-1} = 160\,\text{ms}$ for all $l \in \mathbb{Z}_{\geq 1}, k \in \{1, \dots, 80\}$. The scenario is the same as in Figure 10.3. In this case however, the interconnected time-triggered system is only marginally stable; a small increase in either of the inter-event times results in an unstable system.

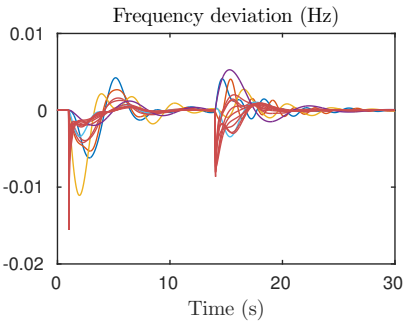

(a) Evolution of the frequency deviations. Compared to Figures 10.3a-10.4a, there are more oscillations in the frequency deviations.

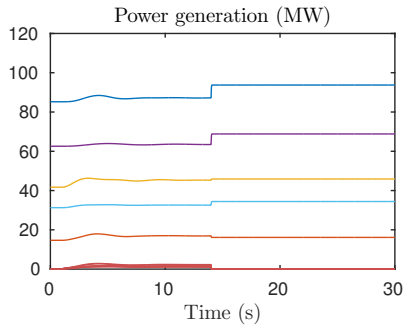

(b) Evolution of each power generation. After primary and secondary controllers are activated at $t = 1\,\mathrm{s}$, optimal power sharing is lost.

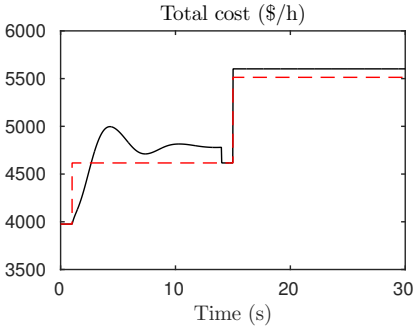

(c) Evolution of the total generation costs (in black) compared to the optimal values calculated by (10.7). Activation of primary/secondary control, and changes in the cost function result in a loss of efficiency.

Figure 10.6: Simulations of swing equations with the primary/secondary and tertiary control layers separated. At time $t = 1\,\mathrm{s}$, the load is increased as in Figure 10.3 and decentralized primary/secondary controllers are activated to regulate the frequency but, as a result, optimal power sharing is lost. At $t = 14\,\mathrm{s}$ the tertiary control layer is activated by resetting the setpoints optimally. After the change of the cost functions at $t = 15\,\mathrm{s}$, economic optimality is temporary lost again until the next time the tertiary control layer is activated (typically in the order of minutes).

Chapter 11

Conclusions

In this research, we developed a unifying energy-based approach to the modeling, analysis and control of smart grids. We have seen how the port-Hamiltonian framework lends itself not only to model and analyze the physical power network but also the real-time dynamic pricing schemes. Regarding the physical system, we have seen how power grids can be modeled as networks of synchronous machines with various accuracy and complexity. In particular, each of these systems admit a port-Hamiltonian representation which for the high-dimensional models are far from trivial. It also clearly reveals the interconnection and damping structure of such multi-machine systems. We also have shown that each of the models varying from the sixth order model till the second order swing equations are shifted passive with respect to their steady states. This property is crucial in the interconnection with passive control algorithms, including consensus-based controllers and dynamic pricing schemes introduced in part II of this thesis. There we showed that such real-time dynamic pricing algorithms can be obtained from the primal-dual gradient dynamics corresponding to a social welfare optimization problem. We have seen that the primal-dual dynamics associated to a general optimization problem can be represented as an incrementally port-Hamiltonian system, thus admitting passivity with respect shifted input/output pairs using a shifted storage function. This allows the interconnection with the physical system yielding a closed-loop (incrementally) port-Hamiltonian system. By using a shifted energy function (shifted Hamiltonian) of the interconnected system and by invoking a suitable invariance principle we have proven convergence to an optimal equilibrium. Here 'optimal' means that it corresponds to the allocation of power generation and consumption and power flow throughout the network that maximizes the social welfare, possibly also considering the generator limits and line congestion in the network.

The last part of this thesis also dealt with the game-theoretic aspects of electricity markets. We have shown how price-setting market players can reach a Nash equilibrium corresponding to cost efficiency, while also taking the network frequency into account. First, these frequency-aware market mechanisms have been realized as continuous-time systems and established their (input-to-state) stability properties. Thereafter, we considered a more realistic setting where the generators iteratively negotiate electricity prices while at the same time the physical system evolves in continuous-time, and established sufficient conditions on the time steps that guarantee stability of the hybrid system.

11.1 Discussion

In this section we briefly relate our findings with other references and discuss the meaning of our results. We also explain some unexpected results we have come across in this research. Finally, a few limitations of our approach are stated as well.

Emphasis on passivity

Compared with the existing literature, we emphasize the passivity properties of both the physical models as well as the controller/dynamic pricing dynamics. This allowed us to consider the physical dynamics and the dynamic pricing scheme on an equal footing. We believe that this passivity-based approach forms the fundamental starting point for generalizations. For example, this allowed us to exploit the modular property of these systems: e.g. we can add or remove constraints from the social welfare optimization problem while still retaining similar stability properties of the interconnected system. In addition, we have seen that many different types of physical models can be considered as long as they admit the appropriate shifted passivity properties. We believe that this idea could even be pursued further by considering a general convex optimization problem and a shifted passive (networked) physical system for which we aim to operate at an optimal (steady-)state characterized by the optimization problem. As an example, one application could be to use in machine learning techniques as in [60] and use it for control of relevant physical systems.

Market/physical demand response

Reflecting grid congestion or for example an excess supply of renewables like wind power onto the price can provoke stabilizing customer behavior. However, this does not mean that monetary incentives like real-time pricing could solve all existing problems of the energy grid. This is because limited customer elasticity and physical situations that are not mapped onto prices lead to the fact that real load shedding for grid relief cannot be done via prices alone [78]. This also requires *physical demand response* which sends out binding requests for demand management if the grid or parts of its infrastructure (e.g. power lines) are in a reduced performance due to maintenance or failure, for example by the use of frequency-aware cooperative loads [54, 78]. A good mixture of both market and physical demand response is usually necessary to run a grid optimally. In the approach adopted in this thesis we do not necessarily have to make a distinction between the physical demand response or the market demand response: both the market-based interpretation [2, 3, 112] as well as the (physical) control interpretation [69, 135, 136] (or a combination) can be adopted in our framework.

Myopic behavior of market players

In this thesis we assume some rationality of the market players and in particular that they show some myopic behavior by trying to maximize their profit in the

next step. However, it is typically difficult to characterize and prove some kind of robustness against irrational behavior although an attempt is made in for example [24].

Line resistances

In this thesis we have not considered line resistances which is a reasonable assumption for transmission networks. However, in microgrids/distribution grids this assumption is not valid anymore. One of the counter-intuitive observations in power networks is that line resistances are not easily incorporated in the energy-based analysis adopted in this thesis. This is because, for reduced-order models of the power networks the resistive elements of the lines do not enter the port-Hamiltonian representation of the AC power network as additional damping (or dissipation structure).

Nonlinear power flow equations

As Chapter 5 reveals, dealing with both line congestion and nonlinear power networks that contain cycles in the interconnection topology is particularly challenging from an analytical point of view. In fact, this forms the important domain of solving the nonlinear power flow equations. Such a problem is proven to be nonconvex and difficult to solve. Throughout the literature there is quite some work on finding suitable convexifications of the problem, including [63, 129] and the references therein.

11.2 Outlook

Power systems are amazingly complex systems and in this thesis we could only grasp a specific part of it. There are many developments going on in this field but, since we cannot discuss all of these topics in detail, we now first restrict ourselves to alternative research directions closely related to this thesis.

11.2.1 More realistic physical models

Although we considered complex models for power network dynamics, there are many extensions possible. We list just a few of them.

Turbine-governor dynamics

Another extension of the synchronous machine models is to include turbine-governor models [30, 53, 115]. We believe that this is possible for first-order turbine-governor models as appearing in [115] as they admit suitable passivity properties. However, for second-order turbine governor dynamics this does not hold and instead need to be 'passified' by some control law [114], or requires different control techniques such a sliding mode control [30].

Voltage regulation

Although we consider power network dynamics with voltage dynamics and have shown voltages stability, we did not consider regulating the voltage to a desired level. This appears to be a challenging task from a port-Hamiltonian point of view but a starting point could be to model Automatic Voltage Regulators (AVR's) from an energy-based perspective.

11.2.2 Including inflexible loads and generation

In a large part of this research we assumed that both generation and loads are controllable. However, a more realistic scenario would be that part of both generation (like solar panels) and the load is inflexible. We believe that, under the assumption that these generation and load quantities are known, this can be included in the social welfare problem and similar controllers as introduced in this thesis can be designed for that case. In addition, we assumed that the demand can be adjusted as desired and in a continuous fashion, however, an interesting extension would be to consider the discrete on-off nature of loads such as done in for example [54].

11.2.3 Robustness

In this thesis we only touched upon the topic of robustness in the last part of this thesis. A relevant direction for future research is to consider robustness analyses of the interconnected systems presented in the other parts of this thesis as well. This could be guided by the results of [27] for primal-dual general gradient dynamics and for distributed averaging integral based control of power networks by [123]. One of the challenges to the former case will be to extend the robustness results to projected dynamical systems. To the author's best knowledge there have been no results of input-to-state stability of such systems. Another research question could be what communication delays in the control schemes would be tolerated without compromising the stability of the network, see e.g. [57].

11.2.4 Region of attraction

In this thesis we were concerned with establishing asymptotic stability. When for example considering transient stability analysis, estimating the region of attraction is also important. There are various approaches for estimating the region of attraction that have been adopted in the literature, including sum of squares iterations that is for example used in [111].

11.2.5 The broader perspective

On a broader level there also many other developments in the field of power networks which where also pointed out in the last Power System Computation Conference in Dublin, 2018. One of these challenges is dealing with the low inertia in the network [72]. In particular, when the total inertia is decreased by an

increased share of renewables, there is less kinetic energy stored in the system that can be used for compensate for a power imbalance. This makes that alternative energy storage capabilities such as batteries, super-capacitors and flywheels will play a bigger role in the future, especially for frequency regulation. Not only that, also more automation is envisioned, in particular at the lower voltage levels, that demand for appropriate control strategies [124] since at this moment only at the transmission level most of the operation is automated. In particular, the operation of the inverters and interfacing them with the grid (in a grid-feeding or grid-following mode) has to be investigated further [72]. Also, with the increased communication, cyber-security plays an more critical role in power networks. This raises the need for appropriate strategies to maintain stable operation even in the presence of an attack on a certain part of the network.

Bibliography

[1] S. Ahmed-Zaid et al. "Reduced order modeling of synchronous machines using singular perturbation". In: *IEEE Transactions on Circuits and Systems* 29.11 (1982), pp. 782–786.

[2] F. Alvarado. "The Stability of Power System Markets". In: *IEEE Transactions on Power Systems* 14.2 (1999), pp. 505–511.

[3] F. L. Alvarado et al. "Stability Analysis of Interconnected Power Systems Coupled With Market Dynamics". In: *IEEE Transactions on Power Systems* 16.4 (2001), pp. 695–701.

[4] P. M. Anderson and A. A. Fouad. *Power System Control and Stability*. First. The Iowa State Univsersity Press, 1977.

[5] M. Arcak. "Passivity as a design tool for group coordination". In: *IEEE Transactions on Automatic Control* 52.8 (2007), pp. 1380–1390.

[6] J. Arrow et al. *Studies in linear and non-linear programming*. Stanford, CA: Stanford University Press, 1958.

[7] A. Arsie and C. Ebenbauer. "Locating omega-limit sets using height functions". In: *Journal of Differential Equations* 248.10 (2010), pp. 2458–2469.

[8] T. Başar and G. J. Oldser. *Dynamic Noncooperative Game Theory*. Academic Press, 1982.

[9] D. Bauso et al. "Game theory: models, numerical methods and applications". In: *Foundations and Trends® in Systems and Control* 1.4 (2014), pp. 379–522.

[10] A. R. Bergen and D. J. Hill. "Structure preserving model for power system stability analysis". In: *IEEE Transaction on Power Apparatus and Systems* PAS-100.1 (1981), pp. 25–35.

[11] S. Borenstein, M. Jaske, and A. Rosenfeld. "Dynamic pricing, advanced metering, and demand response in electricity markets". In: *Center for the Study of Energy Markets* (2002).

[12] S. Boyd and L. Vandenberghe. *Convex Optimization*. Cambridge University Press, 2004. ISBN: 0521833787.

[13] S. Boyd et al. "Distributed optimization and statistical learning via the alternating direction method of multipliers". In: *Foundations and Trends in Machine Learning* 3.1 (2011), pp. 1–122.

[14] N. G. Bretas and L. F. Alberto. "Lyapunov function for power systems with transfer conductances: extension of the invariance principle". In: *IEEE Transactions on Power Systems* 18.2 (2003), pp. 769–777.

[15] B. Brogliato et al. “On the equivalence between complementarity systems, projected systems and differential inclusions”. In: *Systems & Control Letters* 55.1 (2006), pp. 45–51.

[16] B. Brogliato and D. Goeleven. “The Krakovskii-LaSalle invariance principle for a class of unilateral dynamical systems”. In: *Mathematics of Control, Signals and Systems* 17.1 (2005), pp. 57–76.

[17] M. Bürger and C. De Persis. “Dynamic coupling design for nonlinear output agreement and time-varying flow control”. In: *Automatica* 51 (2015), pp. 210–222.

[18] M. Bürger and C. De Persis. “Internal models for nonlinear output agreement and optimal flow control”. In: *Proc. of 9th IFAC Symposium on Nonlinear Control Systems (NOLCOS))*. Toulouse, France, 2013, pp. 289–294.

[19] M. Bürger, C. De Persis, and S. Trip. “An internal model approach to (optimal) frequency regulation in power grids”. In: *Proceedings of the MTNS*. Groningen, 2014, pp. 577–583.

[20] S. T. Cady, A. D. Domínguez-García, and C. N. Hadjicostis. “A distributed generation control architecture for islanded AC microgrids”. In: *IEEE Transactions on Control Systems Technology* 23.5 (2015), pp. 1717–1735.

[21] S. Y. Caliskan and P. Tabuada. “Compositional Transient Stability Analysis of Multimachine Power Networks”. In: *IEEE Transactions on Control of Network systems* 1.1 (2014), pp. 4–14.

[22] S. Y. Caliskan and P. Tabuada. “Uses and abuses of the swing equation model”. In: *IEEE Conference on Decision and Control*. 2015, pp. 6662–6667.

[23] A. Cherukuri and J. Cortés. “Decentralized Nash equilibrium learning by strategic generators for economic dispatch”. In: *American Control Conference*. IEEE. 2016, pp. 1082–1087.

[24] A. Cherukuri and J. Cortés. “Iterative bidding in electricity markets: rationality and robustness”. In: *arXiv preprint arXiv:1702.06505* (2017). submitted to *IEEE Transactions on Control of Network Systems*.

[25] A. Cherukuri, B. Gharesifard, and J. Cortes. “Saddle-point dynamics: conditions for asymptotic stability of saddle points”. In: *SIAM Journal on Control and Optimization* 55.1 (2017), pp. 486–511.

[26] A. Cherukuri, E. Mallada, and J. Cortés. “Asymptotic convergence of constrained primal–dual dynamics”. In: *Systems & Control Letters* 87 (2016), pp. 10–15.

[27] A. Cherukuri et al. “The role of convexity on saddle-point dynamics: Lyapunov function and robustness”. In: *IEEE Transactions on Automatic Control* (2017).

[28] V. Chinde. “Modeling and control of complex building energy systems”. PhD thesis. 2018.

[29] J. Cortés. "Discontinuous dynamical systems - a tutorial on solutions, nonsmooth analysis, and stability". In: *csm* 28.3 (2008), pp. 36–73.

[30] M. Cucuzzella et al. "Distributed second order sliding modes for optimal load frequency control". In: *American Control Conference (ACC)*. IEEE. 2017, pp. 3451–3456.

[31] C. De Persis and N. Monshizadeh. "A modular design of incremental Lyapunov functions for microgrid control with power sharing". In: *European Control Conference (ECC)*. IEEE. 2016, pp. 1501–1506.

[32] C. De Persis and N. Monshizadeh. "Bregman storage functions for microgrid control". In: *IEEE Transactions on Automatic Control* 63.1 (2018), pp. 53–68.

[33] C. De Persis et al. "A Lyapunov approach to control of microgrids with a network-preserved differential-algebraic model". In: *IEEE Conference on Decision and Control*. 2016, pp. 2595–2600.

[34] F. Dörfler and F. Bullo. "Synchronization in complex networks of phase oscillators: A survey". In: *Automatica* 50.6 (2014), pp. 1539–1564.

[35] F. Dörfler, J. W. Simpson-Porco, and F. Bullo. "Breaking the hierarchy: Distributed control and economic optimality in microgrids". In: *IEEE Transactions on Control of Network Systems* 3.3 (2016), pp. 241–253.

[36] D. Feijer and F. Paganini. "Stability of primal–dual gradient dynamics and applications to network optimization". In: *Automatica* 46 (2010), pp. 1974–1981.

[37] S. Fiaz et al. "A port-Hamiltonian approach to power network modeling and analysis". In: *European Journal of Control* 19.6 (2013), pp. 477–485.

[38] A. Fouad and S. Stanton. "Transient stability of a multi-machine power system Part I: Investigation of system trajectories". In: *IEEE Transactions on Power Apparatus and Systems* 7 (1981), pp. 3408–3416.

[39] D. Fudenberg and J. Tirole. *Game Theory*. Cambridge, MA: MIT Press, 1991.

[40] R. Goebel. "Stability and robustness for saddle-point dynamics through monotone mappings". In: *Systems & Control Letters* 108 (2017), pp. 16–22.

[41] *Guidelines of Good Practice for Flexibility Use at Distribution Level: Consultation Paper*. Report Ref: C16-DS-29-03. Council of European Energy Regulators (CEER). Brussels, Belgium, 2017 (accessed on: July 23, 2018). URL: `https://www.ceer.eu/documents/104400/-/-/db9b497c-9d0f-5a38-2320-304472f122ec`.

[42] W. M. Haddad and V. Chellaboina. *Nonlinear dynamical systems and control: a Lyapunov-based approach*. Princeton University Press, 2008.

[43] T. Hatanaka et al. "An integrated design of optimization and physical dynamics for energy efficient buildings: A passivity approach". In: *Conference on Control Technology and Applications (CCTA)*. IEEE. 2017, pp. 1050–1057.

[44] D. J Hill and I. M. Mareels. "Stability theory for differential/algebraic systems with application to power systems". In: *Sadhana* 18.5 (1993), pp. 731–747.

[45] G. H. Hines, M. Arcak, and A. K. Packard. "Equilibrium-independent passivity: A new definition and numerical certification". In: *Automatica* 47.9 (2011), pp. 1949–1956.

[46] J.-B. Hiriart-Urruty and C. Lemaréchal. *Convex analysis and minimization algorithms I: Fundamentals*. Vol. 305. Springer science & business media, 2013.

[47] B.-M. Hodge and M. Milligan. "Wind power forecasting error distributions over multiple timescales". In: *Power and Energy Society General Meeting*. IEEE. 2011, pp. 1–8.

[48] S.-H. Huang et al. "Impact of wind generation on system operations in the deregulated environment: ERCOT experience". In: *Power & Energy Society General Meeting*. IEEE. 2009, pp. 1–8.

[49] D. Jeltsema and J. M. Scherpen. "A power-based description of standard mechanical systems". In: *Systems & Control Letters* 56.5 (2007), pp. 349–356.

[50] D. Jeltsema and J. M. Scherpen. "Multidomain modeling of nonlinear networks and systems". In: *IEEE Control Systems* 29.4 (2009).

[51] R. Johari and J. N. Tsitsiklis. "Efficiency loss in Cournot games". In: *Harvard University* (2005).

[52] A. Jokić, M. Lazar, and P. P. Van den Bosch. "On constrained steady-state regulation: dynamic KKT controllers". In: *IEEE Transactions on Automatic Control* 54.9 (2009), pp. 2250–2254.

[53] A. Kasis, N. Monshizadeh, and I. Lestas. "A novel distributed secondary frequency regulation scheme for power networks with high order turbine governor dynamics". In: *arXiv preprint arXiv:1806.11449* (2018).

[54] A. Kasis, N. Monshizadeh, and I. Lestas. "Secondary frequency control with on-off load side participation in power networks". In: *arXiv preprint arXiv:1708.09351* (2017).

[55] F. P. Kelly, A. K. Maulloo, and D. K. Tan. "Rate control for communication networks: shadow prices, proportional fairness and stability". In: *Journal of the Operational Research society* 49.3 (1998), pp. 237–252.

[56] H. K. Khalil. *Nonlinear systems*. Vol. 3. Prentice Hall, New Jersey, 1996.

[57] A. Kiani and A. Annaswamy. "The effect of a smart meter on congestion and stability in a power market". In: 49^{th} *IEEE Conference on Decision and Control*. Atlanta, USA, 2010.

[58] A. Kiani and A. Annaswamy. "A hierarchical transactive control architecture for renewables integration in smart grids". In: *IEEE Conference on Decision and Control*. IEEE. 2012, pp. 4985–4990.

[59] P. V. Kokotovic et al. "Singular perturbation and iterative separation of time scales". In: *Automatica* 16.1 (1980), pp. 23–33.

[60] K. C. Kosaraju, S. Mohan, and R. Pasumarthy. "On the primal-dual dynamics of Support Vector Machines". In: *arXiv preprint arXiv:1805.00699* (2018).

[61] P. Kundur. *Power System Stability and Control*. Mc-Graw-Hill Engineering, 1993.

[62] G. K. Larsen, N. D. van Foreest, and J. M. Scherpen. "Distributed control of the power supply-demand balance". In: *IEEE Transactions on Smart Grid* 4.2 (2013), pp. 828–836.

[63] J. Lavaei and S. H. Low. "Zero duality gap in optimal power flow problem". In: *IEEE Transactions on Power Systems* 27.1 (2012), p. 92.

[64] N. Li et al. "Connecting automatic generation control and economic dispatch from an optimization view". In: *American Control Conference*. IEEE. 2014, pp. 735–740.

[65] N. Li, C. Zhao, and L. Chen. "Connecting automatic generation control and economic dispatch from an optimization view". In: *IEEE Transactions on Control of Network Systems* 3.3 (2016), pp. 254–264.

[66] S. H. Low and D. E. Lapsley. "Optimization flow control—I: basic algorithm and convergence". In: *IEEE/ACM Transactions on Networking (TON)* 7.6 (1999), pp. 861–874.

[67] J. Machowski, J. W. Bialek, and J. R. Bumby. *Power System Dynamics: Stability and Control*. Second. Ltd: John Wiley & Sons, 2008.

[68] E. Mallada and S. H. Low. "Distributed frequency-preserving optimal load control". In: *IFAC World Congress*. 2014.

[69] E. Mallada, C. Zhao, and S. Low. "Optimal load-side control for frequency regulation in smart grids". In: *Annual Allerton Conference on Communication, Control, and Computing (Allerton)*. IEEE. 2014, pp. 731–738.

[70] B. Maschke, R. Ortega, and A. J. van der Schaft. "Energy-based Lyapunov functions for forced Hamiltonian systems with dissipation". In: *IEEE Transactions on Automatic Control* 45.8 (2000), pp. 1498–1502.

[71] A Michel, A Fouad, and V. Vittal. "Power system transient stability using individual machine energy functions". In: *IEEE Transactions on Circuits and Systems* 30.5 (1983), pp. 266–276.

[72] F. Milano et al. "Foundations and Challenges of Low-Inertia Systems". In: *Power System Computation Conference (PSCC)*. In press. 2018. ISBN: 978-19-109631-0-4.

[73] P. Monshizadeh et al. "Nonlinear analysis of an improved swing equation". In: *IEEE Conference on Decision and Control*. 2016, pp. 4116–4121.

[74] N. Noroozi, D. Nešić, and A. R. Teel. "Gronwall inequality for hybrid systems". In: *Automatica* 50.10 (2014), pp. 2718–2722.

[75] R. Ortega et al. “Transient stabilization of multimachine power systems with nontrivial transfer conductances”. In: *IEEE Transactions on Automatic Control* 50.1 (2005), pp. 60–75.

[76] R. Ortega and E. Garcia-Canseco. “Interconnection and damping assignment passivity-based control: A survey”. In: *European Journal of control* 10.5 (2004), pp. 432–450.

[77] M. Pai. *Energy Function Analysis for Power System Stability*. Springer Science & Business Media, 1989.

[78] P. Palensky and D. Dietrich. “Demand side management: Demand response, intelligent energy systems, and smart loads”. In: *IEEE transactions on industrial informatics* 7.3 (2011), pp. 381–388.

[79] R. H. Park. “Two-reaction theory of synchronous machines generalized method of analysis-part I”. In: *IEEE Transactions of the American Institute of Electrical Engineers* 48.3 (1929), pp. 716–727.

[80] R. Patel et al. “Optimal Automatic Generation Control of an Interconnected Power System Under Network Constraints”. In: *IEEE Transactions on Industrial Electronics* 65.9 (2018), pp. 7220–7228.

[81] D. Richert and J. Cortés. “Robust distributed linear programming”. In: *IEEE Transactions on Automatic Control* 60.10 (2015), pp. 2567–2582.

[82] R. T. Rockafellar. “The multiplier method of Hestenes and Powell applied to convex programming”. In: *Journal of Optimization Theory and applications* 12.6 (1973), pp. 555–562.

[83] M. Roozbehani, M. Dahleh, and S. Mitter. “Dynamic Pricing and Stabilization of Supply and Demand in Modern Electric Power Grids”. In: *First IEEE International Conference on Smart Grid Communications (SmartGridComm)*. 2010.

[84] M. Roozbehani, M. Dahleh, and S. Mitter. “On the stability of wholesale electricity markets under real-time pricing”. In: *IEEE Conference on Decision and Control*. 2010, pp. 1911–1918.

[85] M. Roozbehani, M. Dahleh, and S. Mitter. “Volatility of Power Grids Under Real-Time Pricing”. In: *IEEE Transactions on Power Systems* 27.4 (2012), pp. 1926–1940.

[86] M. Roozbehani et al. “Analysis of Competitive Electricity Markets under a New Model of Real-Time Retail Pricing”. In: *8th International Conference on the European Energy Market (EEM)*. Zagreb, Croatia, 2011, pp. 250–255.

[87] J. B. Rosen. “Existence and uniqueness of equilibrium points for concave n-person games”. In: *Econometrica: Journal of the Econometric Society* (1965), pp. 520–534.

[88] W. Rudin. *Principles of mathematical analysis*. Vol. 3. McGraw-Hill New York, 1964.

[89] P. W. Sauer and M. A. Pai. *Power system dynamics and stability*. Prentice-Hall, 1998.

[90] J. Schiffer et al. "A survey on modeling of microgrids-From fundamental physics to phasors and voltage sources". In: *Automatica* 74 (2016), pp. 135–150.

[91] R. Sepulchre, M. Janković, and P. Kokotović. *Constructive Nonlinear Control*. Communications and control engineering. W.H. Freeman., 1997.

[92] Y. Seungil and C. Lijun. "Reverse and forward engineering of frequency control in power networks". In: *Proc. of IEEE Conference on Decision and Control, Los Angeles, CA, USA*. 2014.

[93] D. J. Shiltz, M. Cvetković, and A. M. Annaswamy. "An Integrated Dynamic Market Mechanism for Real-Time Markets and Frequency Regulation". In: *IEEE Transactions on Sustainable Energy* 7.2 (2016), pp. 875–885.

[94] D. J. Shiltz et al. "Integration of Automatic Generation Control and Demand Response via a Dynamic Regulation Market Mechanism". In: *IEEE Transactions on Control Systems Technology* (2018). To appear.

[95] J. W. Simpson-Porco, F. Dörfler, and F. Bullo. "Synchronization and power sharing for droop-controlled inverters in islanded microgrids". In: *Automatica* 49.9 (2013), pp. 2603–2611.

[96] J. W. Simpson-Porco. "Input/output analysis of primal-dual gradient algorithms". In: *Allerton Conference on Communication, Control, and Computing*. IEEE. 2016, pp. 219–224.

[97] R. Singh, P. R. Kumar, and L. Xie. "Decentralized control via dynamic stochastic prices: The independent system operator problem". In: *IEEE Transactions on Automatic Control* (2018). Publication date: 30 January.

[98] R. Singh, P. R. Kumar, and L. Xie. "The ISO problem: Decentralized stochastic control via bidding schemes". In: *53rd Annual Allerton Conference on Communication, Control, and Computing (Allerton),* IEEE. 2015, pp. 552–559.

[99] E. D. Sontag and Y. Wang. "New characterizations of input-to-state stability". In: *IEEE Transactions on Automatic Control* 41.9 (1996), pp. 1283–1294.

[100] T. W. Stegink et al. "Hybrid interconnection of iterative bidding and power network dynamics for frequency regulation and optimal dispatch". In: *IEEE Transactions on Control of Network Systems* (2018), pp. 1–1. DOI: 10.1109/TCNS.2018.2856404.

[101] T. W. Stegink, C. De Persis, and A. J. van der Schaft. "A unifying energy-based approach to stability of power grids with market dynamics". In: *IEEE Transactions on Automatic Control* 62.6 (2017), pp. 2612–2622.

[102] T. W. Stegink et al. "Frequency-driven market mechanisms for optimal dispatch in power networks". In: *IEEE Transactions on Automatic Control* (2017). Submitted.

[103] T. W. Stegink et al. “Integrating iterative bidding in electricity markets and frequency regulation”. In: *American Control Conference*. To appear. Milwaukee, Wisconsin, USA, 2018, pp. 6182–6187.

[104] T. W. Stegink et al. “Stable interconnection of continuous-time price-bidding mechanisms with power network dynamics”. In: *Proceedings of the 20th Power Systems Computation Conference (PSCC)*. To appear. Dublin, Ireland, 2018. ISBN: 978-19-109631-0-4.

[105] T. W. Stegink, C De Persis, and A. J. van der Schaft. “Port-Hamiltonian Formulation of the Gradient Method Applied to Smart Grids”. In: *IFAC-PapersOnLine* 48.13 (2015), pp. 13–18.

[106] T. W. Stegink, C. De Persis, and A. J. van der Schaft. “A port-Hamiltonian approach to optimal frequency regulation in power grids”. In: *54th IEEE Conference on Decision and Control (CDC)*. 2015, pp. 3224–3229. ISBN: 978-1-4799-7886-1.

[107] T. W. Stegink, C. De Persis, and A. J. van der Schaft. “A unifying energy-based approach to stability of power grids with market dynamics”. In: *IEEE Transactions on Automatic Control* 62.6 (2017), pp. 2612–2622.

[108] T. W. Stegink, C. De Persis, and A. J. van der Schaft. “Optimal power dispatch in networks of high-dimensional models of synchronous machines”. In: *55th IEEE Conference on Decision and Control (CDC)*. 2016, pp. 4110–4115. ISBN: 978-1-5090-1837-6.

[109] T. W. Stegink, C. De Persis, and A. J. van der Schaft. “Stabilization of structure-preserving power networks with market dynamics”. In: *IFAC-PapersOnLine* 50.1 (2017), pp. 6737–6742.

[110] S. Stoft. “Power system economics”. In: *Journal of Energy Literature* 8 (2002), pp. 94–99.

[111] M. Tacchi et al. “Power System Transient Stability Analysis Using Sum Of Squares Programming”. In: *Power System Computation Conference (PSCC)*. In press. 2018. ISBN: 978-19-109631-0-4.

[112] C. Y. Tee and J. B. Cardell. “Market integration of distributed resources through coordinated frequency and price droop”. In: *IEEE Transactions on Smart Grid* 5.4 (2014), pp. 1556–1565.

[113] S. Trip, M. Bürger, and C. De Persis. “An internal model approach to (optimal) frequency regulation in power grids with time-varying voltages”. In: *Automatica* 64 (2016), pp. 240–253.

[114] S. Trip and C. De Persis. “Distributed optimal Load Frequency Control with non-passive dynamics”. In: *IEEE Transactions on Control of Network Systems* (2017).

[115] S. Trip and C. De Persis. “Optimal frequency regulation in nonlinear structure preserving power networks including turbine dynamics: an incremental passivity approach”. In: *American Control Conference*. IEEE. 2016, pp. 4132–4137.

[116] T. Van Damme, C. De Persis, and P. Tesi. "Optimized thermal-aware job scheduling and control of data centers". In: *IEEE Transactions on Control Systems Technology* (2018), pp. 1–12.

[117] A. J. van der Schaft and D. Jeltsema. "Port-Hamiltonian Systems Theory: An Introductory Overview". In: *Foundations and Trends in Systems and Control* 1.2-3 (2014), pp. 173–378.

[118] A. J. van der Schaft. *L_2-gain and passivity techniques in nonlinear control*. Springer, 2017.

[119] A. J. van der Schaft and T. W. Stegink. "Perspectives in modeling for control of power networks". In: *Annual Reviews in Control* 41 (2016), pp. 119–132.

[120] J. Wang and N. Elia. "A control perspective for centralized and distributed convex optimization". In: *IEEE Conference on Decision and Control and European Control Conference*. IEEE. 2011, pp. 3800–3805.

[121] Z. Wang et al. "Distributed Frequency Control with Operational Constraints, Part I: Per-Node Power Balance". In: *arXiv preprint arXiv:1702.07965* (2017).

[122] G. Weiss and E. Venezian. "Stability analysis for coupled synchronous generators with virtual friction". In: *22nd International Conference on Digital Signal Processing (DSP)*. IEEE. 2017, pp. 1–5.

[123] E. Weitenberg and C. De Persis. "Robustness to noise of distributed averaging integral controllers in power networks". In: *Systems & Control Letters* 119 (2018), pp. 1–7.

[124] W. H. Wellssow et al. "Situational awareness and control of distribution systems and interaction with transmission systems". In: *Power System Computation Conference (PSCC)*. In press. 2018. ISBN: 978-19-109631-0-4.

[125] J. T. Wen and M. Arcak. "A unifying passivity framework for network flow control". In: *INFOCOM 2003. Twenty-Second Annual Joint Conference of the IEEE Computer and Communications. IEEE Societies*. Vol. 2. 2003, pp. 1156–1166. DOI: 10.1109/INFCOM.2003.1208952.

[126] J. T. Wen and M. Arcak. "A unifying passivity framework for network flow control". In: *IEEE Transactions on Automatic Control* 49.2 (2004), pp. 162–174.

[127] J Willems. "Direct method for transient stability studies in power system analysis". In: *IEEE Transactions on Automatic Control* 16.4 (1971), pp. 332–341.

[128] P. Yi, Y. Hong, and F. Liu. "Initialization-free distributed algorithms for optimal resource allocation with feasibility constraints and application to economic dispatch of power systems". In: *Automatica* 74 (2016), pp. 259–269.

[129] R. Y. Zhang, C. Josz, and S. Sojoudi. "Conic optimization theory: Convexification techniques and numerical algorithms". In: (2018). In press.

[130] X. Zhang, N. Li, and A. Papachristodoulou. "Achieving real-time economic dispatch in power networks via a saddle point design approach". In: *Power & Energy Society General Meeting*. IEEE. 2015, pp. 1–5.

[131] X. Zhang and A. Papachristodoulou. "A real-time control framework for smart power networks: Design methodology and stability". In: *Automatica* 58 (2015), pp. 43–50.

[132] X. Zhang and A. Papachristodoulou. "A real-time control framework for smart power networks with star topology". In: *American Control Conference*. IEEE, 2013, pp. 5062–5067.

[133] X. Zhang and A. Papachristodoulou. "Distributed dynamic feedback control for smart power networks with tree topology". In: *American Control Conference*. 2014, pp. 1156–1161.

[134] Y. Zhang et al. "Distributed controllers seeking AC optimal power flow solutions using ADMM". In: *IEEE Transactions on Smart Grid* (2018). To appear.

[135] C. Zhao, E. Mallada, and S. H. Low. "Distributed generator and load-side secondary frequency control in power networks". In: *49th Annual Conference on Information Sciences and Systems (CISS)*. IEEE. 2015, pp. 1–6.

[136] C. Zhao et al. "A Unified Framework for Frequency Control and Congestion Management". In: *Power Systems Computation Conference*. 2016.

[137] C. Zhao et al. "Design and stability of load-side primary frequency control in power systems". In: *IEEE Transactions on Automatic Control* 59.5 (2014), pp. 1177–1189.

Summary

Maintaining a stable an reliable electricity grid has become increasingly challenging due to several reasons, including the shift from conventional generation towards the integration of renewable energy resources such as wind and solar energy. The main challenge is to deal with their intermittency which causes unexpected power imbalances in the network. In addition, with the ever increasing demand of electricity the power network is operating closer to its capacity limits. As a result, the (frequency) stability of the system is compromised and therefore not only the flexibility of conventional generation but also flexibility of the demand is required. This raises the need for sophisticated control strategies to deal with such potential instabilities and to appropriately (and efficiently) allocate power generation and demand throughout the network.

One possible approach to alleviate some of these challenges is by the use of real-time dynamic pricing as a control method. This allows to make incentives to change consumer behavior when the generator limits are reached or line congestion occurs. Moreover, it allows to incorporate economical considerations that enable producers and consumers to fairly share cost and utilities associated with the generation and consumption of energy. However, little is known about the integration of dynamic pricing algorithms and the control of the physical dynamics of the network.

The aim of this thesis is to provide a unifying framework that allows us to model and analyze both the physical power network as well as the market-based control algorithms from the same perspective. The framework behind this is based on mathematical theory of port-Hamiltonian systems. This approach builds on modeling the energy flows (through 'ports') and dissipation in the system, and the stability analysis is conducted using energy functions (Hamiltonians). The first part of this thesis focuses on the modeling of power system dynamics and in particular networks of synchronous machines. We show that several multi-machine models with varying accuracy and complexity can be represented as port-Hamiltonian systems. In particular, we show that these models admit a shifted passivity property which allows them to be interconnected with (market-based) controllers.

In part II, we design such dynamic pricing mechanisms such that the coupled physical-economical system remains stable and approaches a state of maximal social welfare (characterized by a mathematical optimization problem). At the same time, we can incorporate physical constraints such as the line capacities and generator limits. For the physical dynamics, we considered several different network-reduced models, including the conventional so-called *swing equations* and the third-order model which describes both frequency and voltage dynamics, and

structure-preserving models where a distinction between generator and load nodes is made. On the economical side, we provide a general approach to the design of dynamic pricing algorithms. This is based on constructing the primal-dual dynamics of an optimization problem aiming at maximizing the social welfare. Here the primal variables correspond to the power generation, demand and transmission, and dual variables are interpreted as prices that are sent to the power producers and consumers. Moreover, the dynamic pricing scheme can be designed to be fully distributed, requiring only local exchange of information along a connected communication graph for its implementation. For the interconnected system we conduct a suitable energy-based (Lyapunov) stability analysis where we exploit both the shifted passivity properties of the physical system as well as for the primal-dual dynamics (of the social welfare problem). We also compare the resulting dynamic pricing algorithms with an alternative consensus-based controller design. The latter control method is applied to a sixth order multi-machine model and frequency regulation together with cost minimization is realized. Finally, we establish the convergence of general projected primal-dual dynamics under mild convexity assumptions of the underlying optimization problem.

In the last part of this thesis, we study the game-theoretic aspect of electricity markets. In particular, we show how real-time price-bidding mechanisms can lead to cost efficiency and while at the same time corresponds to a market (Nash) equilibrium of the underlying price competition game. Moreover, in the design, also frequency measurements are taken into account and stability of the physical power network is established. In our approach we first consider a continuous-time bidding mechanism coupled with the physical swing dynamics and establish asymptotic convergence. Thereafter, we consider a discretized bidding mechanism and provide bounds on the step-sizes for guaranteeing convergence of the resulting hybrid implementation. This is achieved by exploiting the robustness property called *input-to-state stability* of (the continuous-time version of) the closed-loop system.

Samenvatting

Het behouden van een stabiel en betrouwbaar elektriciteitsnet is, om verschillende redenen, een steeds grotere uitdaging geworden. Een van die redenen is de verschuiving van conventionele generatie naar vernieuwde energiebronnen zoals zonne- en windenergie. De voornaamste uitdaging is om goed om te gaan met de intermitterende energieproductie van deze vernieuwde energiebronnen. Dit veroorzaakt vaak onverwachte energie onbalansen in het netwerk. Daarnaast, met de steeds toenemende vraag naar elektriciteit, functioneert het stroomnetwerk dichterbij zijn capaciteitslimieten. Als gevolg is de (frequentie)stabiliteit van het systeem in het geding gekomen en daarom is niet alleen de flexibiliteit van conventionele generators nodig maar ook de flexibiliteit aan de vraagzijde. Dit verhoogt de noodzaak naar geavanceerde regeltechnische strategieën om beter om te gaan met dit soort potentiële instabiliteiten en om op de juiste (en meest efficiënte) wijze stroomgeneratie en stroomverbruik toe te wijzen door het netwerk heen.

Een mogelijke benadering om een aantal van deze uitdagingen aan te pakken, is door het gebruik van dynamische elektriciteitsprijzen als regelmethode. Op deze manier is het mogelijk om consumenten aan te sporen om hun verbruik te veranderen als de generatoren hun limieten hebben bereikt of er sprake is van lijncongestie. Bovendien staat dit toe om economische overwegingen mee te nemen en maakt dit het mogelijk om een eerlijke verdeling te creëren van kosten en utiliteiten geassocieerd met de generatie en consumptie van energie. Echter is er maar weinig bekend over de integratie van dynamische prijsalgoritmes en het regelen van de fysische dynamica van het netwerk.

Het doel van deze thesis is om een geünificeerd framework tot stand te brengen dat het mogelijk maakt om het fysische stroomnetwerk en de marktgebaseerde regelalgoritmes te benaderen vanuit hetzelfde perspectief. Het achterliggende kader is gebaseerd op de wiskundige theorie van poort-Hamiltonse systemen. Deze benadering bouwt op het modelleren van de energiestromen (door 'poorten') en de dissipatie in het systeem, en de stabiliteitsanalyse wordt door middel van energiefuncties (Hamiltonians) uitgevoerd.

Het eerste deel van deze thesis focust op het modelleren van de dynamica van stroomnetwerken en met name netwerken met synchrone machines. We laten zien dat verscheidende multi-machine modellen met variërende nauwkeurigheid en complexiteit gerepresenteerd kunnen worden als poort-Hamiltonse systemen. In het bijzonder, laten we zien dat deze modellen een verschoven passiviteitseigenschap hebben wat het mogelijk maakt om ze te koppelen met (marktgebaseerde) regelaars.

In deel II ontwerpen we zulke dynamische prijsmechanismen zodat het gekoppelde fysisch-economische systeem stabiel blijft en een toestand van maximale sociale welvaart (gekarakteriseerd door een wiskundig optimalisatieprobleem) bereikt. Tegelijkertijd, kunnen we fysische restricties incorporeren zoals lijncapaciteiten en generatielimieten. Voor de fysische dynamica beschouwen we verscheidene netwerkgereduceerde modellen waaronder de conventionele zogenoemde *schommelvergelijkingen* en het derde-orde model dat frequentie én voltage dynamica beschrijft, en structuurbehoudende modellen. Aan de economische kant, verstrekken we een algemene benadering voor het ontwerp van dynamische prijsalgoritmes. Dit is gebaseerd op het construeren van de zogenaamde *primal-dual dynamica* van een optimizatieprobleem gericht op het maximaliseren van de sociale welvaart. Hierbij corresponderen de *primal* variabelen met de stroomgeneratie, -verbruik en -transmissie, en de *dual* variabelen worden geïnterpreteerd als prijzen voor de producenten en consumenten van energie. Bovendien kunnen de dynamische prijsalgoritmes ontworpen worden op een volledig gedistribueerde manier, waarbij alleen lokale informatie-uitwisseling in een verbonden communicatienetwerk vereist is voor de implementatie. Voor het gekoppelde systeem voeren we een energiegebaseerde (Lyapunov) stabiliteitsanalyse uit waarbij we gebruik maken van de verschoven passiviteitseigenschappen van het fysische systeem maar ook van de primal-dual dynamica (van het welvaart maximalisatieprobleem). Ook vergelijken we de resulterende dynamische prijsalgoritmes met een alternatief regelaarontwerp gebaseerd op consensus dynamica. Deze laatste regelmethode wordt toegepast op een zesde orde multi-machine model waarbij frequentieregulatie en kostenminimalisatie wordt gerealiseerd. Tenslotte, bewijzen we convergentie voor een algemene geprojecteerde primal-dual dynamica onder milde aannames op het onderliggende optimalisatieprobleem.

In het laatste deel van deze thesis, beschouwen we de speltheoretische aspecten van elektriciteitsmarkten. In het bijzonder laten we zien hoe real-time prijsbiedmechanismen leiden tot kostenefficiëntie en tegelijkertijd tot een (Nash) marktevenwicht van het onderliggende prijs-competitie spel. Bovendien worden in het ontwerp ook frequentiemetingen meegenomen en wordt de stabiliteit van het fysische netwerk tot stand gebracht. In onze benadering beschouwen we eerst een continue-tijd biedmechanisme gekoppeld met de fysische schommelvergelijkingen en bewijzen we asymptotische convergentie. Daarna discretiseren we het biedmechanisme en geven we limieten voor de stapgroottes waarvoor convergentie voor het resulterende hybride systeem gegarandeerd is. Dit wordt tot stand gebracht door gebruik te maken van de robuuste eigenschap genaamd *input-naar-toestand stabiliteit* van (de continue-tijd versie van) het geïnterconnecteerde systeem.